International Energy Agency
Photovoltaic Power Systems Programme

UNDERPERFORMING PV ARRAY

Analysis of Monitoring Data

On-site Inspection with Mobile Test Equipment

Visual Inspection of PV Array

Electrical Inspection Techniques

Imaging Techniques

Spectroscopic Methods

BENEFIT:
- Quality and Lifetime of PV Array
- Trouble-Shooting & Warranty Claims

Task 13 Performance, Operation and Reliability of Photovoltaic Systems

PVPS

Qualification of Photovoltaic (PV) Power Plants using Mobile Test Equipment
2021

What is IEA PVPS TCP?

The International Energy Agency (IEA), founded in 1974, is an autonomous body within the framework of the Organization for Economic Cooperation and Development (OECD). The Technology Collaboration Programme (TCP) was created with a belief that the future of energy security and sustainability starts with global collaboration. The programme is made up of 6.000 experts across government, academia, and industry dedicated to advancing common research and the application of specific energy technologies.

The IEA Photovoltaic Power Systems Programme (IEA PVPS) is one of the TCP's within the IEA and was established in 1993. The mission of the programme is to "enhance the international collaborative efforts which facilitate the role of photovoltaic solar energy as a cornerstone in the transition to sustainable energy systems." In order to achieve this, the Programme's participants have undertaken a variety of joint research projects in PV power systems applications. The overall programme is headed by an Executive Committee, comprised of one delegate from each country or organisation member, which designates distinct 'Tasks,' that may be research projects or activity areas.

The IEA PVPS participating countries are Australia, Austria, Belgium, Canada, Chile, China, Denmark, Finland, France, Germany, Israel, Italy, Japan, Korea, Malaysia, Mexico, Morocco, the Netherlands, Norway, Portugal, South Africa, Spain, Sweden, Switzerland, Thailand, Turkey, and the United States of America. The European Commission, Solar Power Europe, the Smart Electric Power Alliance (SEPA), the Solar Energy Industries Association and the Copper Alliance are also members.

Visit us at: www.iea-pvps.org

What is IEA PVPS Task 13?

Within the framework of IEA PVPS, Task 13 aims to provide support to market actors working to improve the operation, the reliability and the quality of PV components and systems. Operational data from PV systems in different climate zones compiled within the project will help provide the basis for estimates of the current situation regarding PV reliability and performance.

The general setting of Task 13 provides a common platform to summarize and report on technical aspects affecting the quality, performance, reliability and lifetime of PV systems in a wide variety of environments and applications. By working together across national boundaries we can all take advantage of research and experience from each member country and combine and integrate this knowledge into valuable summaries of best practices and methods for ensuring PV systems perform at their optimum and continue to provide competitive return on investment.

Task 13 has so far managed to create the right framework for the calculations of various parameters that can give an indication of the quality of PV components and systems. The framework is now there and can be used by the industry who has expressed appreciation towards the results included in the high-quality reports.

The IEA PVPS countries participating in Task 13 are Australia, Austria, Belgium, Canada, Chile, China, Denmark, Finland, France, Germany, Israel, Italy, Japan, the Netherlands, Norway, Spain, Sweden, Switzerland, Thailand, and the United States of America.

Further information and results of Task 13 can be found at: https://iea-pvps.org/research-tasks/performance-operation-and-reliability-of-photovoltaic-systems/.

INTERNATIONAL ENERGY AGENCY

PHOTOVOLTAIC POWER SYSTEMS PROGRAMME

IEA PVPS Task 13

Performance, Operation and Reliability of Photovoltaic Systems

Qualification of Photovoltaic (PV) Power Plants using Mobile Test Equipment

Report IEA-PVPS T13-24:2021

April 2021

AUTHORS

Main Authors

Werner Herrmann, TÜV Rheinland, Cologne, Germany

Gabriele Eder, Österreichisches Forschungsinstitut für Chemie und Technik, Vienna, Austria

Boris Farnung, Fraunhofer-Institut für Solare Energiesysteme ISE, Freiburg, Germany

Gabi Friesen, University of Applied Sciences and Arts of Southern Switzerland (SUPSI), Mendrisio, Switzerland

Marc Köntges, Institut für Solarenergieforschung GmbH Hameln/Emmerthal, Hamelin, Germany

Bernhard Kubicek, Austrian Institute of Technology, Vienna, Austria

Oliver Kunz, University of New South Wales, Sydney, Australia

Haitao Liu, Electrical Engineering Institute/Chinese Academy of Sciences, Beijing, China

David Parlevliet, Murdoch University, Western Australia, Australia

Ioannis Tsanakas, CEA INES – Institut National de l'Energie Solaire, Le Bourget-du-Lac, France

Jan Vedde, European Energy, Birkerød, Denmark

Contributing Authors

Mohammadreza Aghaei, TU Eindhoven, Netherlands

Anne Andersson, RISE Research Institutes of Sweden AB, Borås, Sweden

Alexander Astigarraga, European Academy Bozen/Bolzano, Italy

Evelyn Bamberger, SPF Institut für Solartechnik, Rapperswil-Jona, Switzerland

Franz Baumgartner, ZHAW School of Engineering, Zurich University of Applied Sciences, Winterthur, Switzerland

Gisele Alves dos Reis Benatto, DTU Fotonik, Technical University of Denmark, Lyngby, Denmark

Karl Berger, Austrian Institute of Technology, Vienna, Austria

Christof Biba, SPF Institut für Solartechnik, Rapperswil-Jona, Switzerland

Raghavi Bhoopathy, University of New South Wales, Sydney, Australia

Laura Bruckman, SDLE, Case Western Reserve University, Cleveland, USA

Sebastian Dittmann, Fraunhofer-CSP, Halle (Saale), Germany

Roger French, SDLE, Case Western Reserve University, Cleveland, USA

Mattias Juhl, University of New South Wales, Sydney, Australia

Ahmad M. Karimi, Case Western Reserve University, Cleveland, USA

Lukas Koester, Eurac Research, Bozen, Itally

Jay Lin, PV Guider Consultancy, Taipei, Taiwan

JiQi Liu, Case Western Reserve University, Cleveland, USA

Matthias Littwin, Institut für Solarenergieforschung GmbH Hameln/Emmerthal, Hamelin, Germany

David Moser, EURAC Research, Bozen/Bolzano, Italy

Urs Muntwyler, Berner Fachhochschule, Burgdorf, Switzerland

Gernot Oreski, Polymer Competence Center Leoben GmbH, Leoben, Austria

Marco Paggi, IMT School for Advanced Studies, Lucca, Italy

Samuli Ranta, Turku University of Applied Sciences, Turku, Finland

Germain Rey, University of New South Wales, Sydney, Australia

Sergiu Spataru, Technical University of Denmark, Lyngby, Denmark

Sandor Stecklum, Fraunhofer-Institut für Solare Energiesysteme ISE, Freiburg, Germany

Joshua S. Stein, Sandia National Laboratory, New Mexico, USA

Liviu Stoicescu, Solarzentrum Stuttgart, Stuttgart, Germany

Tadanori Tanahashi, Fukushima Renewable Energy Institute, AIST, Fukushima, Japan

Editors

Werner Herrmann, TÜV Rheinland, Cologne, Germany

Ulrike Jahn, TÜV Rheinland, Cologne, Germany

TABLE OF CONTENTS

ACKNOWLEDGEMENTS

LIST OF ABBREVIATIONS

ADC	Analog to Digital Converter
AC	Alternating Current
AGL	Altitude over Ground Level
AI	Artificial Intelligence
AL	Aluminium
AM	Air Mass
ATR	Attenuated Total Reflection
BBCR	BusBar Corrosion Ratio
BBW	Normalized Busbar Width
BOM	Bill-of-Materials
BSF	Back Surface Field
BYD	BYpass Diode
CCD	Charge-Coupled Device
CMOS	Complementary Metal-Oxide-Semiconductor
CNN	Convolutional Neural Network
c-Si	Crystalline Silicon
CWL	Center Wavelength
DC	Direct Current
DIN EN	Deutsche Industrie-Norm Euro Norm
DUT	Device Under Test
ECT	Equivalent Cell Temperature
EIS	Electrical Impedence Spectrum
EL	ElectroLuminescence
EM	Electrical String Modulation
EUR	Euro
EVA	Ethylene Vinyl Acetate
FFDP	Fraction of Dark Pixels in Binary EL Image
FL	Falling Leg
Fmed	Median Intensity of EL Image
FoV	Field of View
FTIR	Fourier-Transform-Infrared
G	Global irradiance
GCS	Ground Control Station
Ge	Germanium

GHI	Global Horizontal Irradiance
GPS	Global Positioning System
GS	Ground Station
GSM	Global System for Mobile Communications
GUM	Guide to the Expression of Uncertainty in Measurement
HJT	HeteroJuction
HL	Horizontal Leg
IATA	Internaltional Air Transportation Authority
ICNIRP	International Commission on Non-Ionizing Radiation Protection
I/O	Input/Output
I-V	Current-Voltage
Isc	Short Circuit Current
IEA	International Energy Agency
IEC	International Electrotechnical Commission
IMT	Image Mosaicing Technique
InGaAs	Indium Gallium Arsenide
INS	INSulation
IR	InfraRed
ISO	International Organization for Standardization
JCGM	Joint Committee for Guides in Metrology
LCOE	Levelized Cost of Electricity
LED	Light Emitting Diode
LeTID	Light and elevated Temperature Induced Degradation
Li	Lithium
MIR	Mid-InfraRed
ML	Machine Learning
MPP	Maximum Power Point
MPPT	Maximum Power Point Tracking
MST	Module Safety Test
MWP	Mega Watt Peak
NETD	Noise Equivalent Temperature Difference
NIR	Near InfraRed
OM	Optical Modulation
O&M	Operation and Maintenance
OTR	Oxygen Transmission Rate
PC	Personal Computer
PERC	Passivated Emitter Rear Contact

PET	Polyethylenterephthalat
PFA	Focal Plane Array
PID	Potential-Induced Degradation
PL	PhotoLuminescence
PMAX	Maximum Power
PO	Polyofin
PoA	Plane of Array
PR	Performance Ratio
PVPS	Photovoltaic Power Systems Programme
PWM	Pulse-Width Modulation
QA	Quality Assurance
QE	Quantum Efficiency
RGB	Red Green Blue
RISO	Insulation Resistance
RoI	Return of Interest
RPAS	Remotely Piloted Aircraft Systems
Rs	Series Resistance
RTC	Reflected Temperature Compensation
RTD	Resistance Temperature Detector
SCADA	Supervisory Control and Data Acquisition
TS	Technical Specification
SEMI	Semiconductor Equipment and Materials International
SNR	Signal-to-Noise-Ratio
SWIR	Short- Wavelength InfraRed
UAV	Unmanned Aerial Vehicle
USB	Universal Serial Bus
USD	US Dollar
UV	UltraViolet
UVF(L)	UltraViolet Fluorescence
VIS	Visual
Voc	Open Circuit Voltage
VSYS	System Voltage
WIFI	Wireless Fidelity
WLAN	Wireless Local Area Network
Wp	Watt Peak
WPVS	World PhotoVoltaic Scale
XRF	X-Ray Fluorescence

EXECUTIVE SUMMARY

The energy production of a PV power plant plays a significant role in the market evaluation of a project, as it is a key input into the financial models of the profitability of a solar project [1]. In this regard, the technical conditions of the PV array and of the PV modules have a great impact on the systems performance and the value of assets (assets' performance).

To give plant operators or asset managers confidence that PV power plants perform at current standards and provide the promised yield, on-site inspection methods with portable test equipment (mobile PV test centres) are commonly used. There are various fields of application for mobile PV test centres at different project phases:

a) Acceptance testing before commissioning;
b) Fault detection and identification of defective or degraded PV modules in PV arrays;
c) Inspection of PV power plants prior to change of ownership;
d) Periodical inspections to document the technical conditions of PV arrays regarding long-term reliability and durability of components.

It is worth mentioning that it is advisable to analyze historic performance data (if available or accessible) prior to on-site inspection. For example, the daytime dependent or seasonal variation of DC and AC performance ratios (PR) can already provide indications of potential problems and identify parts of the PV array for follow-up inspection.

On-site inspection of a PV array shall start with a visual inspection of the cabling and the PV modules. This initial diagnosis can already give indications whether PV modules are the origin of power loss or whether site-specific factors such as soiling or shading are relevant. Observed visual defects of PV modules such as glass breakage, burn marks, delamination, browning or damaged backsheets can already explain the power loss of a given PV system and facilitate the decision on the best choice of characterization methods to give the requested answers.

In practice, a 100% technical inspection of a multi-megawatt PV power plant will not be feasible. But rapid advances in infrared (IR) inspection with drones make it possible to obtain an overall picture of the status of an operational PV array. Such information can be also used to identify candidate PV strings or PV modules for further analysis using mobile PV test centres.

In this report various on-site inspection techniques using portable test equipment are presented. These are ranging from PV output power characterization, to imaging techniques and spectroscopic methods for materials analysis. Besides technical information and existing field experience, also good practice recommendations for field use and uncertainties compared to laboratory inspection methods are covered. A brief summary of ten inspection methods covered in this report is given below. From here the reader can jump directly into the relevant chapter of this report, where detailed information on the inspection method is given.

The presented on-site inspection methods are helpful tools to identify drivers for underperforming PV power plants. Their particular strength lies in the fact that the tests are carried without dismantling and shipping the PV modules to a laboratory, which often means long transport routes, transport risks and a long down time of the PV strings. Furthermore, on-site inspection allow a more targeted failure analysis, as PV modules are not blindly selected. The quality and significance of the inspection results are comparable to that of lab tests. On the

other hand, on-site inspections are dependent on the weather conditions, which is a disadvantage compared to work under controlled conditions in a laboratory. Thus, on-site inspections require a higher organizational effort and a careful planning.

A single inspection method mainly deals with a specific type of PV module defect and cannot deliver a comprehensive failure analysis. For example, electroluminescence (EL) or photoluminescence (PL) imaging can reveal cell cracks in a PV module or can give an indication for PID. But no conclusions can be made concerning the output power of the PV module. Accordingly, it makes sense to combine imaging inspection techniques with output power measurements. In this sense, the objectives of on-site inspection must be specified in advance. If applicable, the most appropriate combination of inspection methods must be considered in order to obtain meaningful results.

Electrical inspection on PV string level provides indications of defective or degraded PV modules and only conclusions for the average PV module performance can be made. This may not be sufficient for warranty claims, which usually require an individual proof that the PV module performance is outside the manufacturers' specification. To overcome this, additional inspection of PV modules with a mobile PV test centre may become necessary.

Except the application of drone flying and of a mobile PV test centre, the presented on-site inspection methods are applied to installed PV modules or PV strings. In these cases, the test equipment must be moved in the field and operation will require a power supply. This may lead to restrictions in work, as the necessary infrastructure such as paved paths may not be available.

In the case that the inspection method requires a disconnection of PV modules or PV strings, it is essential to observe that the maximum system voltage of PV strings can reach up to 1500 V. Working under high electrical voltage requires that the safety regulations of the country are respected and that work is only be performed by a qualified electrician with appropriate training. Furthermore, personal protective equipment is required and qualified tools must be used.

Because a 100% inspection of PV modules is not feasible, specific sampling methodologies and statistical evaluation methods need to be concidered, which shall assure that a representative amount of PV modules will be inspected. However, such statistical methods are not internationally harmonized and are often decided on a case-by-case basis.

Drone-mounted electroluminescence & thermal infrared inspection of PV arrays

Optical methods of fault detection in PV power plants have been commonly used in the PV industry for many years. These methods are usually conducted manually and are time consuming, limiting their uptake. With the advent of light weight non-contact imaging techniques, Remotely Piloted Aircraft Systems (RPAS) are becoming increasingly popular in commercial and research applications. These systems can have significant time and cost savings compared to traditional manual measurements. Chapter 2 outlines the current standards and opportunities for using drones for field measurements of PV systems. We discuss the types of defects identifiable from drone based measurements and identify key uncertainties or challenges with the measurements. This section provides a recommendation on best practice for drone based measurements of PV systems.

Daylight I-V measurement of PV strings and PV modules

The electrical performance of a PV array results from its current-voltage characteristic (I-V curve). The shape of the I-V curve determines the position of the maximum power point (M_{PP}),

which corresponds to the working point of the inverter. I-V curve measurement is performed with an I-V curve analyzer, which is connected to the PV string terminals inside the field combiner boxes or at the DC cables entering the inverter. I-V inspection is performed in conjunction with solar irradiance and module temperature measurements. Once measurement is completed, the PV string I-V curve is translated to standard test conditions (STC), which then allows an assessment of the average PV module output power. In Chapter 3 a failure catalogue is presented for deviations between the STC translated measured I-V curve and the calculated nominal I-V curve of the PV string.

PV module characterization with mobile PV test centres

Mobile PV test centres with integrated solar simulators allow testing of a large number of PV modules in the field. The test is highly reproducible as being almost independent of the weather conditions. A test sequence of a PV module can combine electrical output power measurements with electroluminescence imaging and safety relevant tests like bypass diode functionality and insulation resistance. Sequential testing with a high level of automation permits to obtain a complete quality picture of a statistical relevant number of PV modules. The solar simulator makes the equipment very expensive and large compared to the other field inspection methods described in this report. The complexity of the equipment requires well trained personnel and adequate quality assurance measures to guarantee a low measurement uncertainty, which is the base for warranty claims.

Dark I-V measurement of PV strings and PV modules

Dark current-voltage (I-V) characteristics measurement means I-V measurement of PV strings at nighttime. The relationship and differences between dark I-V and daylight I-V measurements are explained, and the measurement accuracy requirements are discussed. A short comparison of available measuring systems is given. Additionally, it is explained how damaged or degraded PV modules influence the shape of dark I-V curves. Multiple effects and defects are discussed, such as series or parallel resistance issues, cell cracks, and PID. Finally, best practice of performing on-site dark I-V measurements is discussed.

PV plant testing vehicle for PV strings

PV power plants can be classified into grid-connected and stand-alone systems. No matter how the design and type of the PV power plant is, the performance parameters basically include the current-voltage characteristics of PV arrays and efficiencies of inverters. The performance of a PV power plant can be measured by PV testing vehicle reconstructed from a delivery van or box truck. The testing vehicle consists of meteorological monitoring system, DC and AC combiner box testing devices, PV string and centralized inverter testing facilities. Instead of portable test instruments, the PV plant testing vehicle has a multi-functional design and can perform testing, analyzing performance parameters of all kinds of PV power plants.

Electrical impedance spectroscopy of PV strings

Electrical impedance spectroscopy represents a methodology to collect information on the characteristics and performance of PV modules within a PV string by analyzing the systems linear voltage response to an input sinusoidal oscillating (harmonic) current perturbation over a range of frequencies. This measurement provides a frequency-dependent impedance consisting of a real and an imaginary part, which can be further analyzed to extract information on specific features within the PV string such as non-operative PV modules, by-pass diode failures, performance loss due to PID or ground faults.

Daylight electroluminescence (EL) imaging

EL is the emission of optical radiation resulting from the application of electrical energy to the solar cells. A defect or inefficient area in the cell generating less irradiation will be darker in the EL image. Therefore, we can detect defects of the cells such as busbar corrosion, cracks and other defects in PV modules and extrapolate the quality of a PV Power Plant. The major challenge for outdoor EL inspection in the daytime is the near infrared (NIR) emission from the sunlight, which is higher than the emission from the solar cell. Thus, performing outdoor EL inspection requires a special setup to filter the signal irradiated from the cells. Different technologies and inspection methods are discussed in Chapter 8 with regard to their impact to the quality of the result, as well as feasibility to perform the measurements in the field.

UV fluorescence imaging

The UV fluorescence method measures the UV fluorescence of the polymer in the PV module to draw indirect conclusion on the PV module' health state or on the bill of materials used in the module. The method allows to detect cell cracks and temperature related defects, like hot spots, cell interconnect ribbon breakage and detection of hot cells with inactive cell parts. Furthermore, the method reveals if more than one type of encapsulation or backsheet material is used in PV modules. Especially for cell cracks, it is the only method to identify the timely order of cell crack occurrence. For example, this is useful to distinguish between cell cracks caused during installation or by a hail storm. For field application an UV source and a photo camera are needed. No disconnection of PV modules in the PV system is required. The method is very fast when searching for cell cracks or heat related defects in PV modules.

Outdoor photoluminescence imaging of field-deployed PV modules

Outdoor photoluminescence imaging is a new approach for finding electronically active faults and degradation effects in solar PV modules deployed in the field. This approach has the advantages that it can both provide more detail than thermal infrared imaging and has the potential to be significantly faster than the routinely used electroluminescence imaging. The core concept behind this technique is to use the sun as an illumination source, and via altering of the operating point of the modules being imagined to allow extraction of the weak luminescence signal. The use of adequate optical filtering is mandatory. The output data of this technique is almost identical to that of electroluminescence imaging but it can be performed without electrical changes to the PV system. Chapter 10 covers the current approaches being used as well as their respective advantages and disadvantages.

Spectroscopic methods for polymeric materials

The application of spectroscopic characterization techniques allows for direct material analysis in the field without dismantling PV modules, transporting them to the laboratory, cutting them in smaller pieces and analyzing them with conventional spectrometers. Spectroscopic methods can be used to identify the polymeric compounds of PV modules (encapsulants, backsheets), which is important when degradation and/or failures occur. NIR and Raman spectroscopy are suitable to identify the encapsulant within the PV module. With FTIR-spectroscopy the outer layer of the polymeric backsheet can easily be identified and surface degradation effects (e.g. oxidation, hydrolysis) can be detected. NIR spectroscopy allows for the non-destructive determination of the entire composition of the multilayer backsheet composite.

1 INTRODUCTION

According to IEA global power generation from PV has increased by 22% in 2019, to 720 TWh [2]. With this increase, the solar PV share in global electricity generation has reached almost 3%. The IEA Solar PV tracking report 2020 also states that solar PV is still on track to reach the Sustainable Development Scenario (SDS) by 2030, which will require an average annual growth rate of 15% from 720 TWh in 2019 to almost 3300 TWh in 2030. These figures indicate that significant investments will be made in PV power plants in the near future.

Due to falling prices for PV modules, progress in plant engineering and construction as well as effective O&M strategies, the competitiveness of PV projects measured by the Levelized Cost of Electricity (LCOE) has continuously improved in recent years. In this context, the energy generation of a PV power plant plays a significant role in the market assessment of a project, as it is a key input to the financial models of the profitability of the solar project. In the fact sheets about Photovoltaics, IEA has announced that "PV is the cheapest electricity source almost everywhere" [1] [3].

With this background, asset owners of utility-scale PV power plants are analyzing the historic in-field performance relative to production forecasts, so that underperforming projects are detected at an early stage. An on-site performance assessment may be required to identify and correct potential problems. Such measures contribute to a good understanding of the operating conditions and enable more accurate production forecasts.

Diagnosing drivers for underperforming PV power plants in relation to their yield expectation is a complex task. Besides the inverter performance, the inaccuracy of the measuring systems, or site-related uncertainties such as weather variability, soiling or shading, the causes can also lie in wiring issues in the PV array or in underperforming of PV modules.

The focus of this report lies (i) in fault detection of PV arrays and (ii) in identifying defective or degraded PV modules as origin of underperforming PV power plants. Various on-site inspection techniques using portable test equipment will be presented ranging from PV output power characterization, to imaging techniques for localizing cell cracks or open-circuit failures to spectroscopic methods for materials analysis. Two groups of methods can be differentiated: a) inspection methods for PV strings and b) inspection methods for single PV modules.

In this report knowledge and expertise of inspection methods is presented in ten chapters:

- Drone-mounted electroluminescence & thermal infrared imaging of PV arrays
- Daylight I-V measurement of PV strings and PV modules
- PV module characterization with mobile PV test centres
- Dark I-V measurement of PV strings and PV modules
- PV plant testing vehicle for PV strings
- Electrical impedance spectroscopy of PV strings
- Daylight electroluminescence imaging
- UV fluorescence imaging
- Outdoor photoluminescence imaging of field-deployed PV modules
- Spectroscopic methods for polymeric materials

All chapters are structured in the same way to facilitate comparison of methods. Besides technical information and field experience, they also provide good practice recommendations for field use and evaluate uncertainties compared to laboratory inspection methods.

2 DRONE-MOUNTED EL & IR INSPECTION OF PV ARRAYS

2.1 Description of inspection method

Most of the field measurement systems discussed in this document are completed manually or using ground-based measurements. While these are effective methodologies, some measurement techniques lend themselves to large scale aerial deployment. Infrared imaging is becoming very popular in surveying and monitoring PV plants. However, measuring a large-scale PV plant is time and labour intensive. To improve this, infrared imaging and surveys of PV plants have been completed by full-scale airplanes and helicopters. More recently with the advent of light weight non-contact imaging techniques, drones or Remotely Piloted Aircraft Systems (RPAS) are becoming increasingly popular in commercial and research applications. With recent advances in aerial technology and control electronics [4], RPAS have become very affordable and accessible to small businesses or independent contractors. While a few years ago this was the realm of small businesses and research organizations, now large engineering companies such as Honeywell, offer commercial services on measuring PV plants via RPAS [5]. These systems can be used for a range of optical inspection techniques including but not limited to visual inspection, infrared imaging and electroluminescence imaging. Essentially, any non-contact measurement technique that can be applied to a PV system by hand, can be done from the air.

A typical RPAS inspection of a PV plant would involve both optical and infrared measurements [6]. These can be completed simultaneously if multiple cameras are mounted on the RPAS. While RPAS systems speed up data collection, there are some challenges with identifying defects from altitude [7]. Some defects are easier to spot at low altitudes as outlined in the table below.

Table 1: Impact of altitude on the detection of PV module defects [8].

PV Module Component	Defects – Failures or Characteristic	Maximum altitude (AGL) for Visual Detection by RPAS
Cell/Encapsulant	Snail Trails	0 m to 5 m
Cover Glass	Soiling	10 m to 15 m
PV Module	White Spots	15 m to 20 m
Encapsulant	Encapsulant Discoloration (EVA)	15 m to 20 m
Cover Glass	Different Cover Glass	15 m to 20 m
Cell, Soldering Joints	Hot Spots	15 m to 20 m
Cell	Number of Cell Interconnect Ribbons	10 m to 20 m

The main benefits of using RPAS for PV inspection are the inspection speed, increased cost-effectiveness [4] and increased safety. For many measurement techniques, when surveying large PV plants manually or on ground level, it can take a long time to finish the inspection of

all panels. With a RPAS, the inspection time can be greatly reduced, and fewer human resources are required for the inspection. For roof-top PV systems, it can be dangerous for inspectors to climb up to the roof-top, and many safety accessories and permits are required for the inspection job. Furthermore, for roof PV systems without a walkway, the UAV inspection helps prevent the risk of module damage which results from the inspectors walking on the panels or dropping instruments on the panel. With the use of RPAS, the inspectors do not need to get on the roof, and the test time is also greatly reduced.

The RPAS are essentially an airborne platform for camera-based measurement systems which can increase the speed and safety of measurement. These aircraft range in size and capability, but with the reduction in size of imaging systems, they can fly several different cameras, sensitive to different spectra of light. In the early days of RPAS based PV measurements custom designed or augmented RPAS were required and were often quite large and expensive. More recently, modified consumer RPAS have been used for surveying PV plants [9].

RPAS can be classified into several categories based on weight. The weight of the aircraft often influences the regulations that apply to the aircraft. While these vary from country to country, generally lighter RPAS have less stringent regulatory requirements than heavy RPAS. This makes it easy for plant operators or service companies to use RPAS based measurements and encourages the uptake of this technique. These low entry requirements as well as many commercial providers is increasing the popularity of airborne optical measurements for PV Plant O&M.

2.1.1 IR inspection with UAV

The most common UAV application in PV is IR inspection. There are already many commercial UAV types with various IR cameras on the market. It is widely used because the inspection is easy to go with UAV and the benefits of the UAV are highly presented. The UAV with IR camera can easily take thermal image whenever there is sufficient sunlight, and the image can be taken at any distance. Most of the defects in the PV module generate heat under sunlight, and the thermal image helps to identify these defects. However, for certain defects, we can only identify the existence of the temperature difference, but we cannot determine what exactly the defect root cause is. For example, serious cracked cells generate heat, and cell mismatch also generate heat, with IR image alone we cannot determine which defect it is. In this case we will need other tools like EL for further diagnosis.

2.1.2 EL inspection with UAV

EL is the abbreviation of 'electroluminescence', where we feed in reverse current to the PV cells and the cells generate near infrared (NIR) light, and we use a special camera to capture the NIR image.

EL image shows the details of the defect, so it is helpful to determine the most of cell and module defects. UAV can be used in EL inspection, but there are mainly three difficulties hinder the application of UAV. First the inspection must be done at night because the daylight contains a lot of NIR which is stronger than the NIR irradiated from the PV modules. Therefore, we can only do the inspection at night or in a darkroom and flying at night increases the difficulty and risk of UAV control. Night flights also have increased regulatory and training requirements.

Secondly, before the EL inspection, we need to connect the PV module strings to a switch device which connects to the DC power supply to feed in current to the PV cells. It makes the workload much higher than the IR inspection. If the PV module strings are connected to DC combiner boxes which are located from a distance to each other, we need to move from box to box connecting the strings at night. The work makes the UAV inspection less efficient.

The third difficulty is the limit of the camera capability. Most of the silicon sensor commercial cameras are not sensitive in the NIR wavelength range, so the exposure time is usually long (few seconds up to minutes). Then the images taken by UAV are easily blurred because of the long exposure time.

With much lower resolution sensors, some of the InGaAs cameras have very good sensitivity for NIR getting the luminescence signal of the module in some few milliseconds. The capability of video recording is the biggest added value in these kinds of cameras, making things easier to the O&M operator. Depending on the type of analysis, a compromise between UAV-panel distance and lenses should be found to get the desired image quality for the proposed analysis. From micro-cracks to submodule or string functioning study, the solution combinations can be several. The UAV-panel distances for IR and EL are not comparable due to the resolution constraints of this last one.

There are still no turnkey solutions in the market to do EL from UAVs. Wireless communication and camera control are now the biggest challenge. Fortunately, the camera technology and the inspection devices are improving, and a complete inspection device shall be commercially realized in near future. However, inspection service companies in the market and research centres are developing their own solutions with success [10].

2.1.3 UVFL inspection with UAV

Some of the additives in the encapsulation of the PV module generate fluorescence under UV exposure. Therefore, we can irradiate the module with UV light and take the fluorescence image to see some of the defects. This inspection also needs to be performed in the dark because the fluorescence is too weak to be seen under daylight.

The difficulty of applying UAV in UVFL inspection is similar to EL inspection. First the work must be done in the dark, secondly the camera exposure time influences the image quality. Another difficulty is that the UAV must carry the UV light source and additional battery for the UV light source. When the UAV flies high, the UV light is too weak, and the fluorescence image is also too weak to be taken from a distance. On the other hand, when the UAV flies close to the PV module, it is dangerous and difficult to control, and the number of modules in one image becomes very small and then increases the inspection time. Therefore, a large UAV to carry a large UV light source and battery is helpful for the work.

UVFL is an emerging inspection technology, the test method and result analysis are still under development. It has a good potential to integrate UAV as a quick scan tool to realize the condition of the PV plant.

2.1.4 Interpreting the data - qualitative or quantitative methods

Data from RPAS based measurements can be analysed and interpreted in much the same way as land-based measurements or data collected through other techniques. The primary challenge of RPAS based measurements is the quantity of data which is collected by aerial surveys. The large amounts of data and imagery to analyse makes automated analysis techniques based around machine learning and neural nets almost critical for interpreting the data.

2.2 Existing knowledge

Solutions on diagnostic UAV inspections for PV are now reaching high TRLs and compliance with technical specifications and standards, whereas the demand from PV operators and asset owners is booming. This positive context of R&D and technical maturity creates a great market potential for the few pioneering service providers of aerial PV inspections and diagnostics.

There are increasing numbers of organisations providing turnkey aerial-IR inspection services, including artificial intelligence (AI)-based data analytics, fault diagnostics and reporting as well as consulting, i.e. recommendations for corrective maintenance actions to PV asset owners and O&M engineers. In the general PV O&M context, such services typically include scans for both regular (i.e. "per-schedule") preventative maintenance and reactive troubleshooting, as well as commissioning or asset transfer. Other operators provide aerial services for the inspection of PV plants and fault identification by drone based imagery. Table 2 shows some examples of providers for aerial inspection (AI) services

Table 2: Examples of providers of drone-based PV inspections services.

Service Provider	Web site of Service Provider
Sitemark (Belgium)	https://www.sitemark.com/
Heliolytics (Canada)	https://www.heliolytics.com/
Scopito ApS (Denmark)	http://scopito.com/
AePVI (Germany)	http://www.aepvi.com/
Aeroprotechnik (Portugal)	https://www.aeroprotechnik.com/
Above (United Kingdom)	https://www.abovesurveying.com/
Aerospec Technologies (US)	https://aerospec.us/

Further, market leaders in aerial PV inspections can leverage large and consistently increasing portfolios (already beyond the GW-scale) of inspected PV plants, to offer comparisons of different PV underperformance issues and anomalies against extensive fault libraries, utilizing proprietary imagery analysis and IR/RGB mapping software. As such, the offered solutions commonly identify a large range of PV plant anomalies, from extensive string, combiner or array-level outages, to module-, submodule- and cell- level failures and subtle defects, e.g. PID, electrical mismatches and concomitant hot spots. In addition, fast return of investments (ROIs) for aerial inspections is justified by most service providers, based on both decrease of preventative O&M costs by over 10% (compared to those employing manual and ground-based inspections) and recovery of an average 1% to 2% PV power capacity losses.

From an overall market perspective, when it comes to PV O&M and asset management, system size matters, determining the suitability and extent of different PV inspection and monitoring solutions. In this sense, smaller PV systems (typically residential and commercial ones) have only small-area diagnostic requirements and relatively small budget allocated for O&M; therefore, minimal needs for aerial diagnostic inspections. On the other hand, upscaling towards industrial- and utility- scale and more complex PV systems, on-demand, periodic aerial IR imaging diagnostics become more bankable (if not essential) option, along with state-of-the-art monitoring platforms and advanced data analytics features.

Regarding the individual equipment of aerial PV inspection systems, the market landscape is dominated by established innovators and vendors of relevant hardware solutions, notably drones/UAVs and IR (or multispectral) imagers. On the former, market-leading solutions are offered by DJI, Yuneec and Parrot who often also develop and combine multispectral imagers suited for aerial inspections, such as the Zenmuse XT2 of DJI and the RedEdge-M of Parrot Group. The former was built in collaboration with the thermal imaging specialists FLIR, while the latter was developed and is offered by MicaSense.

Then, when it comes to more specific needs on aerial image data analytics for PV, Raptor Maps offers a specialized AI-driven software as a turnkey service for aerial inspections, detection and tracking of anomalies and actionable cloud-based reporting. A successful example and efficient solution in this case is the senseFly Solar 360, co-developed with the Parrot Group, integrating an eBee X fixed-wing drone with a radiometric IR/RGB imager and the image data analytics software of Raptor Maps.

In principle, the data acquisition equipment and approaches employed for aerial PV inspections can vary among the different downstream service providers. For instance, in contrast to Above and Sitemark that offer UAV/drone-based aerial IR imaging scans, Heliolytics employ IR imagers mounted on aircrafts, offering flyovers at much higher altitude and speed; thus allowing very high inspection rates (100 MW per hour), multiple times faster compared to competitors' drone-based inspections. However, such an approach can considerably limit the spatial granularity, being rather impractical to fully comply with the minimum recommended diagnostic resolution, for correct identification of certain failure modes at PV sub-module and cell level.

Yet, all aforementioned services face certain operational limitations. Their current high reliance on (semi-)manual image data processing, represents a major drawback as human-error drives down the diagnostic accuracy (and its consistency) of IR imaging for PV. In addition, such solutions are typically "restricted" to qualitative diagnosis of PV failures, being inefficient (until today) to provide reliable, quantitative and real-time assessments on the PV yield losses associated with detected failures. To be also noted that shifting from today's "per schedule" aerial-IR inspections towards data-driven ones, will have a significant impact on the technical bankability, financial feasibility and consequent long-term competitiveness of these commercial services, as reported by EPRI [11].

2.2.1 Autonomous PV plant monitoring

Increasing number of PV installations and volumes of data collected from energy meters and sensors highlight the importance of developing new monitoring technologies and procedures that can handle such large volumes of systems and data. Existing technology and techniques for controlling PV systems have not yet been centralized and monitoring and analysis procedures are performed in several separate steps. This can be achieved more efficiently and

20

intelligently. Autonomous Monitoring and Analysis, is a novel concept to integrate various techniques, devices, systems, and platforms to enhance the accuracy of PV monitoring, consequently improving the performance, reliability and service life of PV systems. By this approach, the entire services of PV monitoring will be provided by a single integrated system [12].

Aghaei has designed and developed an autonomous monitoring system for large-scale PV plants, Figure 1 [13]. This system was able to perform the visual and thermography assessment by infrared (IR) imaging sensor and high-resolution visual camera mounted on the Unmanned Aerial Vehicle (UAV). The aerial images captured are transferred to the Ground Control Station (GCS) by RF channel automatically. The classified data are sent by the GCS to the database for processing. Subsequently, signal characteristics data (e.g. current, voltage, power, temperature, irradiance, etc.) have been acquired by SCADA. After pre-processing and postprocessing of the aerial images and data, entire processed information is transferred to the decision support system and O&M operator for future actions. In this phase, the autonomous monitoring system evaluates the information in order to identify and analyse the specific failure or fault on PV systems [6].

Autonomous monitoring aims to increase the reliability and durability of PV plants since it can contribute to reducing the time of monitoring procedure and decision-making for appropriate solutions which are very important tasks especially, for large-scale PV plants. The accuracy of the system is very high in comparison with the traditional monitoring methods. Autonomous monitoring systems can identify and analyse not only defects or failures but also the location of the specifically degraded components in the PV plants [13], [7].

UAV is one of the main parts of an autonomous monitoring system which can perform aerial RGB, IR, EL and UVFL photography of PV plants. UAVs should have the following features namely, large area coverage, precise imagery cameras, high flexibility, lightweight, ability to operate in different environmental conditions and to manage data transmission.
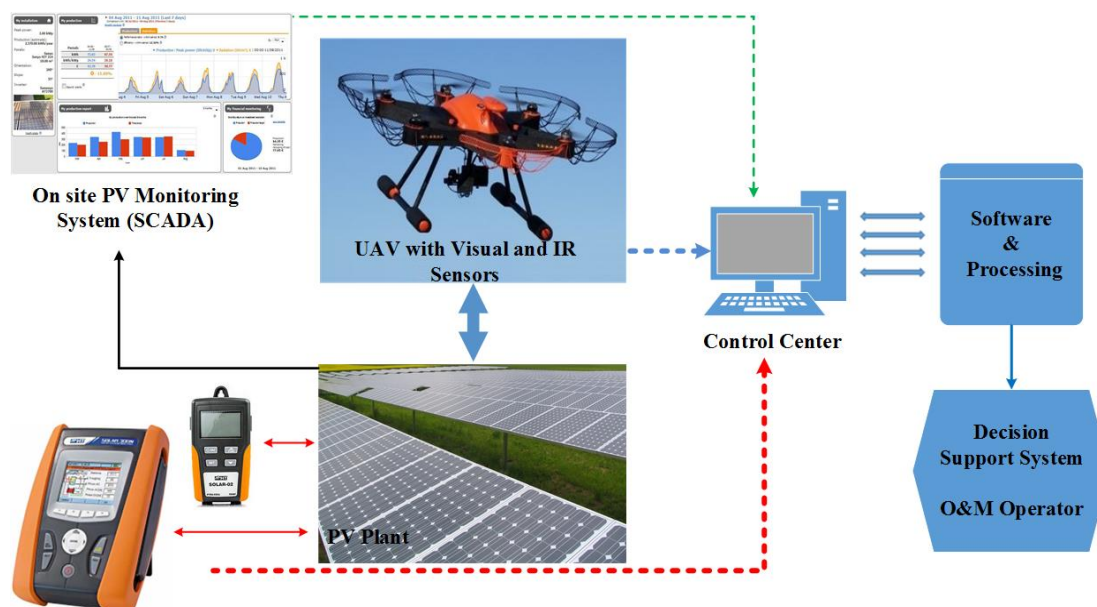

Figure 1: Schematic of the concept of autonomous monitoring system for PV plants [13], [6], [14].

In autonomous monitoring procedure by UAVs, first, the boundary of PV plants should be determined by a neural network. For this purpose, the neural network is trained by various orthophotos of PV plants. Subsequently, a static path planning algorithm should be designed in order to create an optimal path for PV plant inspection. Moreover, dynamic path planning is created based on the flight situation and checks UAV's abilities after any specific manoeuvre which means, if UAV cannot complete the initial path, dynamic path planning enters in the loop to create a new optimum path according to UAV's position and endurance [15]. The following steps are performed during autonomous monitoring of PV plants by UAVs, Figure 2 [15].

1. The processor of the Ground Station (GS) determines the boundary of the PV plant by using Convolutional Neural Network (CNN) model.

2. An optimal path is created on the PV plant by using a static path planning algorithm. Waypoints are transmitted to the UAV through a radio frequency (RF) channel.

3. The UAV takes off automatically and goes to the first point of the static path. Yellow lines show the flight path on the PV plant.

4. During the flight, at a specific point of the path, the processor detects the probability of defects or failures on the PV modules. The blue line in Figure 2 shows the transmitted aerial imageries of PV arrays to GS. If any defects or failures have been identified on the PV strings, then the UAV starts a new manoeuvre to provide a better field of view of the anomalies on the PV strings.

5. After the manoeuvring process, such as reducing the flight altitude for extended inspection of the area, the UAV continues the mission. At this stage, based on the UAV's abilities such as flight endurance, the UAV continues the current path, or a new set of waypoints is created by GS through dynamic path planning algorithm and transmitted to the UAV.

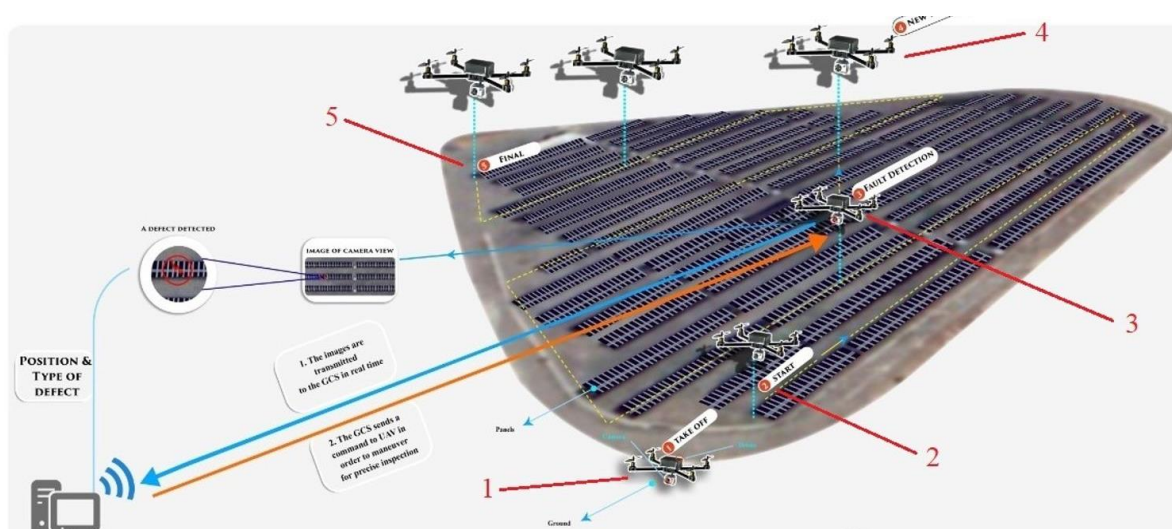6. The UAV completes the aerial inspection mission and arrives at the final point of the flight path.

Figure 2: The procedure of autonomous monitoring of PV plants by UAVs [15]. Status of standardization and licensing.

Each country has a different regulatory authority that handles RPAS operations. Regulations around RPAS operations vary and are regularly being updated or reviewed as technology and policy changes. The regulations are generally focused on safety of the public, wildlife, property, commercial and private aviation, and the drone itself. As best practice, all RPAS operations should be planned to minimise or mitigate the risks posed by the operation. For PV plant monitoring this may include a pre-flight site inspection to identify obstructions to line of sight or radio transmissions and testing of GPS reception. For RPAS flying over PV modules in the field or rooftops it is advisable to use a RPAS with six or more rotors, or a fixed wing design. This improves the redundancy and allows controlled flight if any one motor fails. This reduces the risk of the RPAS damaging the PV modules. Flights in some areas or conditions may need approval from the appropriate regulatory body. In air traffic areas, the permission for a time window can take more paperwork and a schedule can be months ahead. Finally, the scheduled time and meteorological conditions should match to work in a safe and efficient way.

As of the time of writing, there are no distinct technical specifications or standardized protocols for performing aerial IR measurements in PV plants, using e.g. UAVs or drones, with an O&M plan. Yet, it is highly recommended that such inspections are also carried out in line with the IEC TS 62446-3:2017, similarly to all general "outdoor" (field) thermographic inspections of PV systems. Compared, for instance, to lock-in thermography or other indoor PV characterization and inspection techniques that are held in controlled laboratory environment, the accuracy of field IR inspections is largely affected by diverse parameters and conditions. In this sense, it is imperative to identify, analyse and understand sources of measurement errors and uncertainties throughout aerial IR inspections, as well as to as well as to control and mitigate (or compensate) them, to the greatest extent (practically and technically) feasible.

Neither is there technical specification or standard for aerial EL inspection. IEC TS 60904-13 is the current reference for the industry which is focused on indoor environment.

2.3 Detectable failure types for PV modules and PV arrays

Most defects and failures like bubbles, delamination, yellowing, browning, bending, breakage, burning, oxidation, scratching, broken or cracked cells, corrosion, discoloration, antireflection, dirty, snail trails, detachment, open-circuited modules, bypass diode problem, internal short-circuits, potential induced degradation (PID), complete or partial shadowing, invisible cracks or microcracks, broken cell, and hot spots can be detected by various photography devices (i.e. RGB, IR, EL, UVFL) which mounted on the UAVs during inspection procedure.
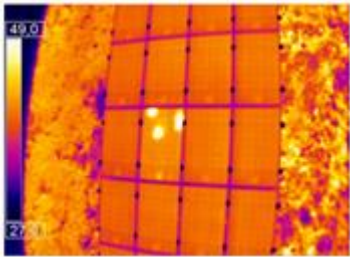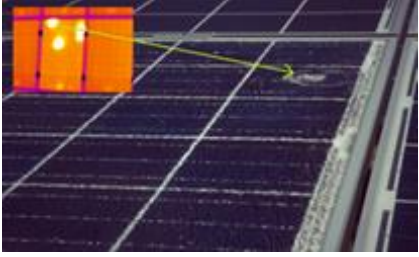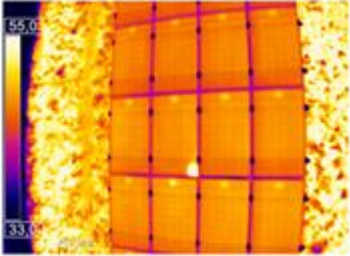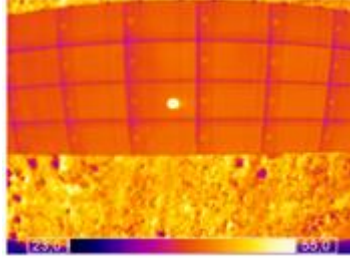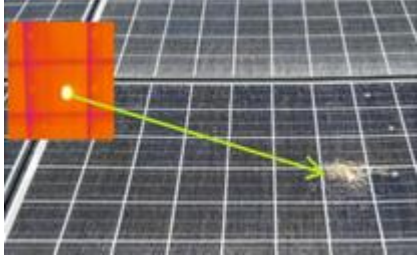
Case Study
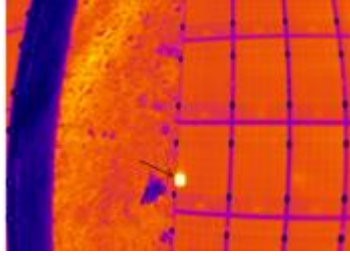
Aerial IR imagery-based inspections emerged the recent years among O&M best (corrective and partly preventive) practices for timely detection, diagnosis and classification of different failure modes in PV plants. Deploying aerial IR inspections today is a relatively inexpensive and straightforward task within a PV O&M scheme. Yet, when further combined with additional features, such as (semi)automated pattern recognition algorithms and data training/analytics, aerial IR imagery can yield to preventive, actionable PV diagnostics, at higher spatial granularity compared e.g. to standard PV monitoring systems.

Detectable and identifiable PV failures and underperformance issues include defects and failures – either permanent or temporary – from system (DC side) and string level, down to PV array, module, submodule/component or even solar cell level. These, in particular, can include

e.g. hot spots due to electrical mismatches (shading, localized soiling, cracks, shunts), fractured glass/modules or broken interconnects, as well as PID, snail trails, delamination, bypass diode failures or other electrical failures at string/system level (cabling, fuses, connectors in combiner boxes, etc).

Table 3: Examples of defects identifiable from RPAS measurements [12], [16].

Defect	Low altitude aerial image (IR)	Ground Truthing
Severe glass and cell fractures (© CEA-INES)		
Cracked cell (© CEA-INES)		
Excessive soiling and dirt, resulting in severe hot spots and power losses (© CEA-INES)		
Shading by adjacent vegetation, resulting in electrical mismatch, hot spot and power losses (© CEA-INES)		

The images above present characteristic examples of diagnostic results from campaigns of aerial IR inspections to five utility-scale PV plants of a total 29 MWp or approximately 106,000 mono-crystalline silicon PV modules, installed and operating in southern France [16]. In these cases, the employed UAV was a hexacopter drone, type Condor AY-704.

The latter was configured for orthothermographic imagery, carrying a lightweight thermal camera type Optris PI450, measuring IR radiation in the spectral range 7.5 µm to 13 µm, NETD of 0.04 K and accuracy of ±2%; along with a miniature lightweight PC, for the acquisition and processing of thermal images. The IR signatures of the inspected PV systems were obtained, analysed and used for diagnosing different failure modes on PV cell, PV submodule, PV module and PV system level. Typically, such failures are also visible by naked eye, thus can be validated with a follow-up visual inspection as shown in the right column of Table 3.

Findings during the aerial IR inspection campaign in France also highlighted the importance of following a correct O&M plan, in relation to soiling/dirt mitigation and vegetation management in PV sites. Cases shown above highlight where excessive and localized dirt or soiling, as well as unwanted shading due to vegetation on or in the proximity of PV arrays, may result in electrical mismatches and hot spots, often similarly severe as in the cases of broken PV modules and cell cracks. Different PV failures can be timely detected by means of aerial IR inspections, thus allowing human intervention (corrective maintenance), in order to recover the associated power losses.

2.4 Best practice recommendations

All flights must be planned and conducted in accordance with local aviation authority and government regulations. When mission planning, the maximum altitude should be specified in accordance with the resolution of the camera and the height at which features can be seen in Table 4. For IR inspection the flight should be planned and conducted such that a sufficient resolution (of max. 3 cm per pixel) is able to be captured by the onboard cameras.

Imaging should also take place when there is good stable illumination of a minimum 600 W/m^2 in the plane of the PV module, it is recommended that IR imagery systems, compliant with the IEC TS 62446-3:2017 and tailored for aerial PV inspections, feature lightweight imagers with:

- Optical resolution of at least 640×480 pixels
- Thermal sensitivity, NETD, lower than 0.1 K (at 30°C)
- Measurement error lower than ± 2 K (or 2%)
- Spectral response in the 2-5 µm or 8-14 µm range
- Adjustable emissivity correction and relevant temperature range

The optimal parameters and useful instructions for aerial visual and IR inspection by UAVs are summarized as the follows [8] [13].

Drone EL inspection would be effective during night time or very low light conditions. Having an InGaAs camera, a video recording would be the most comfortable solution taking into account the number of frames per second and hardware limitations. For daylight Drone EL inspection, technique explained in Daylight Electroluminiscence Imaging chapter, the drone stability plays a very important role (wind conditions should be optimal). Irradiance level does not present a constraint as PV panels are excited artificially from power supplies in both night and daylight EL inspection.

**Table 4: Summary of optimal parameters for IR inspection.**

Camera orientation angle	The visual or thermal camera should be pointed as much as possible perpendicular toward the PV strings.
Target surface emissivity	The most common emissivity setting is at 0.85 or 85%, corresponding to a (theoretical) emissivity value typically attributed to tempered soda-lime glass. However, for more accurate measurements, it is recommended that a more precise emissivity calibration is performed either using a special tape (of known, validated emissivity) or by benchmarking against a contact thermometer reading
Minimum altitude	The minimum height of flight should be more than 5m due to avoiding any self-shading of UAV during aerial inspection procedure.
Weather conditions	Aerial visual and thermal inspection should be performed on a sunny, cloudless and clear day. Also, the wind speed should not exceed 4 m/s (14.4 km/h, 3Bft). High winds can shake the UAS during the inspection.
Other external effects	Awareness of sources of shading which can affect image interpretation Reflections from PV module surfaces The best time for measurements is morning or afternoon where the angle of incidence is lower.

2.5 Measuring uncertainty aspects

We may distinguish two main sources of measurement errors or uncertainties, i.e. i) those associated with the employed thermographic/radiometric and imagery equipment and ii) those in relation to the environmental or measurement conditions.

In the former case, measurements' accuracy depends on certain features and limitations of IR sensors and imagers, notably on the optical resolution (or the size of the detector's Focal Plane Array (FPA) matrix), the thermal sensitivity (or the Noise Equivalent Temperature Difference (NETD) value), the measurement error (or uncertainty). Other IR imagery specifications to consider are the spectral and temperature ranges, i.e. the spectral response and the measured temperature range of the detector, the emissivity adjustment error and the field of view (FOV) of the thermal camera lens, see 2.4.

Real-field experiences with aerial IR inspections in PV plants have shown that – apart from the environmental parameters – the important aspects of the distance-to-target and AoV should be carefully considered, especially in aerial IR inspections for PV O&M. Indeed, the effects related to atmospheric transmission can dramatically decrease the accuracy of aerial long-distance measurements (thus, the reliability of quantitative diagnostic results), compared to ground or aerial short-distance measurements. Figure 3 (c) depicts some of these influences and Figure 3 (b) shows the optimal angle of the camera during the aerial inspection by UAVs [17].
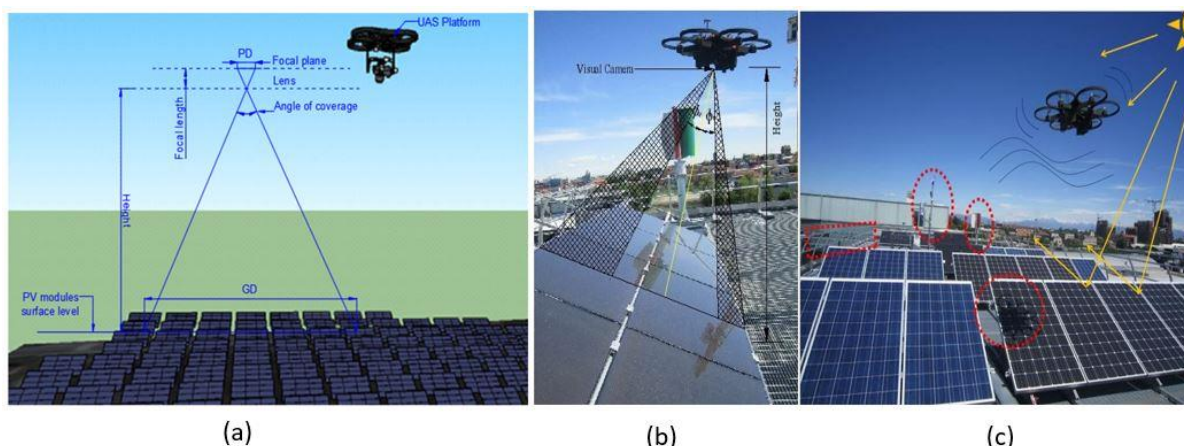
Figure 3: (a) Schematic view of aerial visual inspection over PV plant for scale determination, (b) optimal angle of camera during the aerial inspection of a PV string, (c) schematic of external effects e.g. reflection, air turbulence, irradiation and shading during the aerial inspection procedure [17].

For aerial IR inspections, a maximum altitude (d_{max}) should also be determined and respected, to enable aerial thermal imagery of sufficient spatial granularity as per the IEC TS 62446-3:2017, i.e. of at least 3×3 pixels per inspected solar cell. In order to respect this empirical rule and to find the allowed d_{max}, it is strongly recommended that a lens calculation analysis is performed, prior to aerial inspections. For doing this, key parameters to consider, are: i) the optical resolution of the output thermal image, ii) the FOV of the thermal camera, as well as the instantaneous FOV (IFOV or spatial resolution) and the measurement FOV (MFOV) and iii) the physical dimensions (surface area) of the inspected target (in this case, the PV module or array). More details on this procedure are discussed in [18]. Some indicative values of d_{max} (thus, practically, height above the inspected PV array) typically range from 7 m to 10 m to 20 m to 22 m, without excluding larger heights, when high-resolution IR cameras are employed.

Figure 4 shows examples of (a) a-Si thin film multi-junction affected by white-spot which is detectable at an altitude up to 20 m, (b) poly-cSi PV module affected by snail trail detectable at 6-7 m of altitude (red box), (c) a mono-cSi PVT module affected by bird droppings (bluebox) and a poly-cSi defected due to encapsulant discoloration (red box), both defects are detected at flight height of 20 m, (d) different Si PV modules, i.e. mono-Si PV modules with different glasses technology and poly-Si PV module can be detected up to altitude of 15 m [13], [16]. Figure 5 shows examples of (a) IRT image of damaged PV module with two hotspots and a bypassed substring, clearly visible at an altitude of 6 m. (b) IRT image of damaged PV module, with two hotspots and a bypassed sub-string, visible at an altitude of 10m. (c) IRT image of damaged PV module, with one clearly visible hotspot and one hotspot and a bypassed
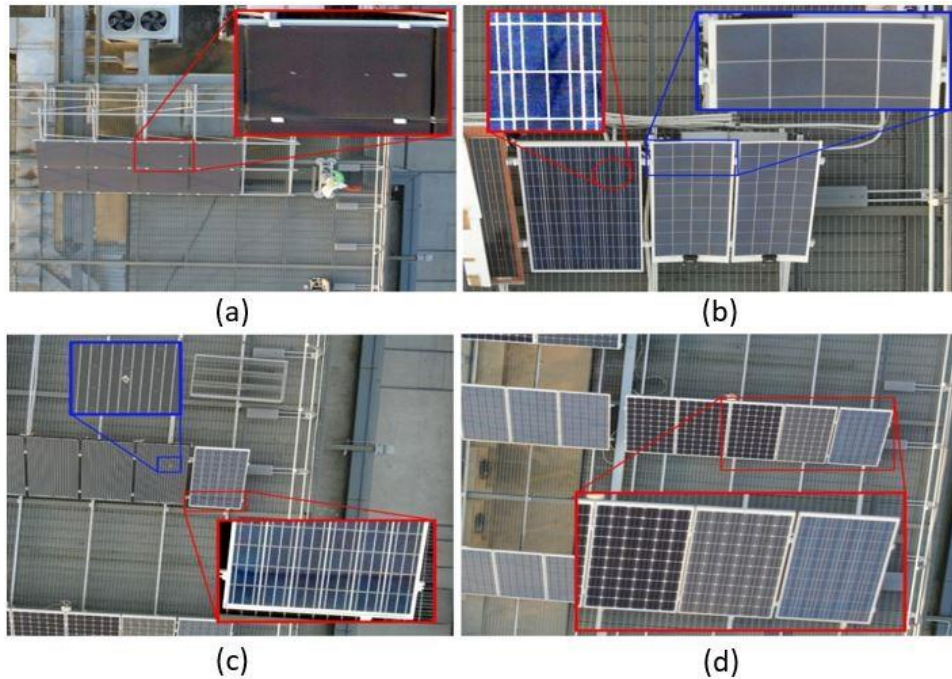
Figure 4: Examples of defects detected via aerial imagery [13], [17].
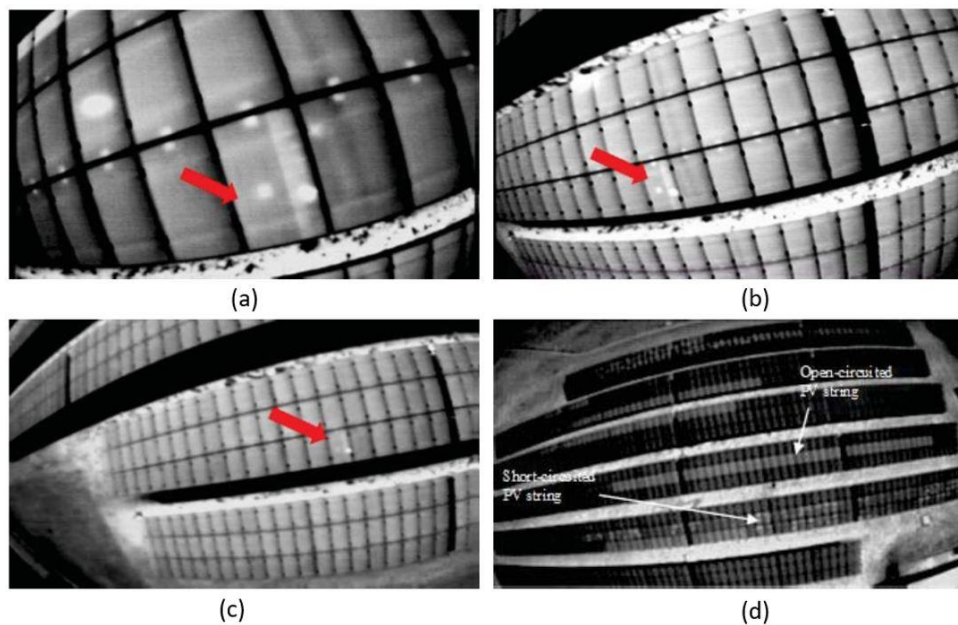
Figure 5: Examples of defects identified by drone-based infrared imagery [17].

Further considerations and (optional) corrective settings for reducing uncertainties in aerial IR measurements can include the so-called ambient compensation value (ACV) and the reflected temperature compensation (RTC) in certain IR camera types. The adjustment of the ACV is done on the basis of ambient temperature, relative humidity and distance-to-target inputs. Moreover, RTC provides the proper background correction, in order to compensate the influence of reflective/emissive objects, with known temperature, near the measured target. RTC

is typically recommended to be used when, due to significantly high uniform background temperature, IR energy is reflected off the target surface to the thermal camera (thus, increasing the measurement uncertainty). Further details on this aspect can be found in [18], [19].

2.5.1 Image mosaicing

The image mosaicing technique (IMT) is very useful for planning and mapping of large-scale PV plants. In addition, the image mosaicing provides an overview of PV modules condition in different PV strings in a faster way. IMT aims to merge several taken aerial imagery from various PV strings in order to composite a larger, integrated and consistent image of the entire PV plant.

For a better image mosaicking (IM), the flight line should be planned along a single line either overlapping or succession aerial photography which is very crucial for the quality of IM. Furthermore, the flight line could be parallel to the array structure orientation, e.g. east-west for fixed arrays or north-south for single-axis tracking arrays. It aims to maximize the amount of side-lap and end-lap based on mission purpose. The standard IM of PV plants should be 30±15 percent for side-lap and 60±5 % for end-lap to provide a higher Field of View (FoV) of the PV strings. Figure 6 shows the effect of drift and crab in aerial inspection of PV plants.
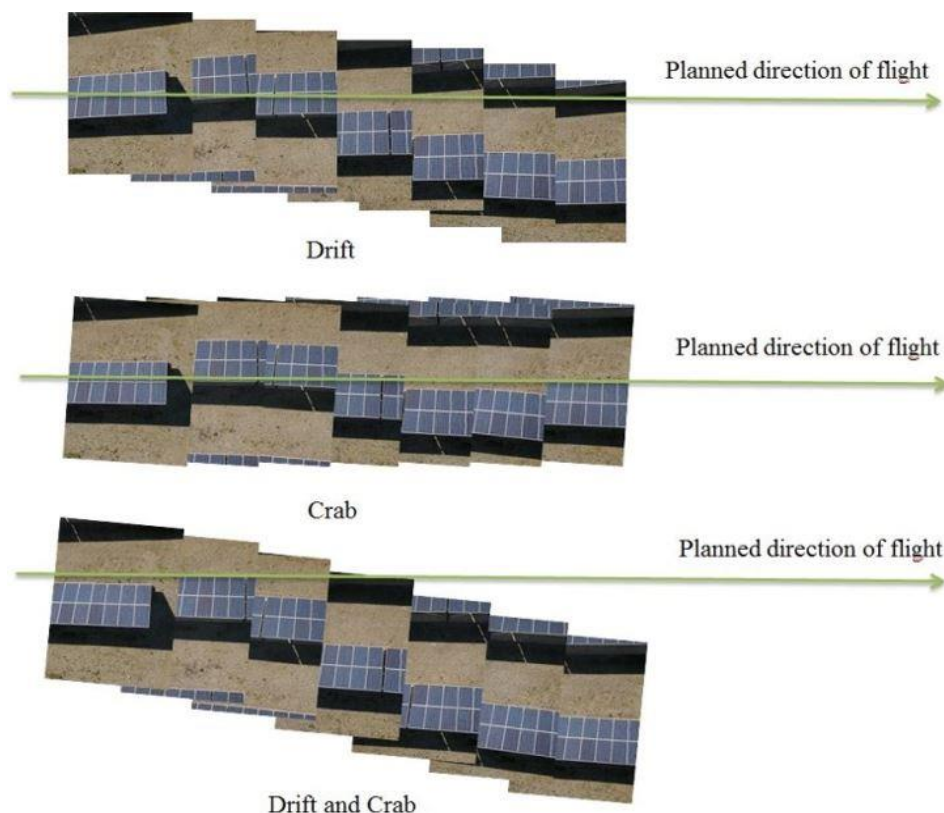
Figure 6: Drift and crab effect on aerial inspection of PV plants [13].

Drift is flying results of a UAV which may not be followed the planned flight line. Crab is created based on the result of the sensors onboard which was not oriented to the flight line planned. Typically, drift and crab are very primary reasons of unsatisfactory IM. Drift makes a displacement or lateral shift during flights due to external stresses (e.g. wind turbulence, navigation

errors rain) and other unexpected issues. The autonomous route-finding should work to minimise drift. Crab occurs when the RGB or IR imaging camera onboard is not oriented based on the planned flight line during the aerial monitoring of PV plant.

2.6 Occupational safety

All RPAS activity needs to be completed with a clear view on health and safety. Although these aircraft are relatively light (<25kg) they can do catastrophic damage to people, property or other aircraft if control is lost. The industry is much regulated and most commercial operators will need appropriate training and licenses before missions are able to be flown. In general this includes minimising risk by a regular maintenance schedule on the aircraft, pre and post flight checks and safe flying. To minimise risk, any missions should maintain a minimum separation distance from people or buildings. If the aircraft must fly over buildings or structures such as PV modules, it is recommended that an aircraft with at least 6 propellors is used to provide redundancy in the case of engine failure.

These specifics of these is contained within the aviation regulations for each country. Due to the rapidly changing nature of RPAS regulations, we suggest that the reader reviews the relevant regulations from their region. The regulator for each region is shown below in Table 5.

Table 5: Regulatory authorities in IEA countries.

Region	Regulatory Authority
Australia	Civil Aviation Safety Authority (CASA)
Austria	Austro Control
Belgium	MOBILIT
Canada	Transport Canada
Czech Republic	Civil Aviation Authority
Denmark	Civil Aviation Authority
Estonia	Civil Aviation Authority
Finland	Transport Safety Agency
France	Civil Aviation Authority
Germany	Aviation Office
Greece	Civil Aviation Authority
Hungary	General Directorate for Air Transport
Ireland	Aviation Authority
Italy	Italian Civil Aviation Authority (ENAC)
Japan	Japan Civil Aviation Bureau (JCAB)
Mexico	Directorate General of Civil Aeronautics (DGCA)
New Zealand	Civil Aviation Authority of New Zealand (CAANZ)
Norway	Civil Aviation Authority of Norway (CAAN)

Table 5: Regulatory authorities in IEA countries (continued).

Region	Regulatory Authority
Poland	Civil Aviation Authority
Portugal	National Civil Aviation Authority
Slovak Republic	Civil Aviation Division of the Transportation Office (CAD)
Spain	State Agency of Air Security
Sweden	Transport Agency of Sweden (TAS)
Switzerland	Federal Office of Civil Aviation (FOCA)
The Netherlands	Directorate of Civil Aviation (DGCA)
Turkey	States Airport Administration of Turkey (SAMA)
United Kingdom	Civil Aviation Authority
United States	Federal Aviation Authority (FAA)

2.7 Transportability

With the trend towards using small or very small RPAS for optical inspection of PV plants, most modern RPAs are easy to transport. Larger RPAs may require some disassembly before transporting by car or aircraft. Modern very small RPAS can be folded into a portable carry case and are promoted as being very easy to transport.

The main concern with transportation of RPAS are the batteries as some restrictions apply to the capacity of batteries allowable in aircraft.

For transport by air it is recommended to:

- Cover switches to avoid activation
- Pack RPAS in rigid or well-padded travel case

There are several regulations that cover the transport of batteries. Consult with your airline before flying. In general, the following regulations apply to international flights:

- Cover or protect battery terminals to prevent shorting.
- All spare (or removable) batteries must be carried in carry-on baggage
- Batteries over 100 Wh must be approved by the airline before flying
- A maximum of two batteries is allowable per person

2.8 Cost considerations

The cost of RPAS has come down rapidly over the last years. The purchases costs range from hundreds of dollars to tens of thousands. For RPAS for monitoring PV plants, the cost of the camera and sensors are a significant portion of the total system cost. Typical systems include:

- Freefly ALTA 8 UAS (aircraft only) 17,500 USD
- DJI Matrice 210 V2 (aircraft only) 12,000 USD
- Deltaquad Pro #INSPECT (with FLIR Duo Pro R) 11,000 USD
- DJI Mavic Enterprise 2 (with FLIR camera) 2,800 USD

These systems do require ongoing maintenance and inspection to ensure they are flightworthy. Additional costs may be associated with calibration of the cameras and any regions specific licensing and registration costs.

The largest impact and benefit of RPAS imaging is the time taken for the measurement. The time required for IR inspection highly depends on the criteria for the inspection, for example the resolution of the image, the limitation of the irradiance level and the influence of clouds.

With the resolution of max. 3 cm per pixel as required in IEC62446-3, generally it takes 1 hour for the IR inspection of 1 MW ground mount PV plant. If we follow the requirement of irradiance in IEC62446-3, minimum 600 W/m^2 in the plane of the PV module, the qualified inspection time per day is only around 4 hours/day or shorter in some areas. It will be the major limit for the inspection of a large PV plant.

Another factor that greatly influences the inspection time is the cloud condition. IEC62446-3 suggests a waiting time of 15 min after change in operating conditions >10% per minute, for example clouds pass by, to regain the steady state measurement conditions. It greatly influences the inspection duration because the UAV must be called back and wait for 15 minutes when clouds pass by. After 15 min waiting time the UAV must fly back to the same location which is usually difficult to identify in a large PV park. The waiting time is sometimes more than the actual inspection time and consumes a lot of spared batteries. Therefore it is better to choose a very sunny day with no clouds to do the IR inspection, however practically it is difficult to predict whether there is cloud and it is also difficult to cancel the inspection after traveling all the way to the PV plant from a long distance. Therefore, weather condition is the key factor for IR inspection time.

InGaAs cameras used for ground based EL inspection are in a price range of 10,000 USD to 70,000 USD. The main differences are resolution, sensor quantum efficiency and cooling system. The cost of dedicated filters and SWIR lenses could reach an amount of 3000 USD depending on the dimensions and various factors. Unfortunately, it is not possible to quantify the wireless adaptation as it is not still commercially available. The price for the rest of equipment can be found in Chapter 4 Daylight Electroluminescence Imaging.

3 DAYLIGHT I-V MEASUREMENT OF PV STRINGS AND PV MODULES

The electrical performance of a PV array is described by its current-voltage characteristic (I-V curve). This characteristic is composed of the I-V curves from individual PV modules as illustrated in Figure 7. In this example, all PV modules are assumed to have the same I-V curve (ideal case). The number of serially connected PV modules to a PV string determines the PV systems voltage and the number of parallel connected PV strings its current. The resulting PV array I-V curve is the outer enclosure of the set of PV module I-V curves. This construction principle explains that any spread in PV module I-V curves, which indicate differences in their electrical performances, will affect the shape of the resulting array I-V curve.
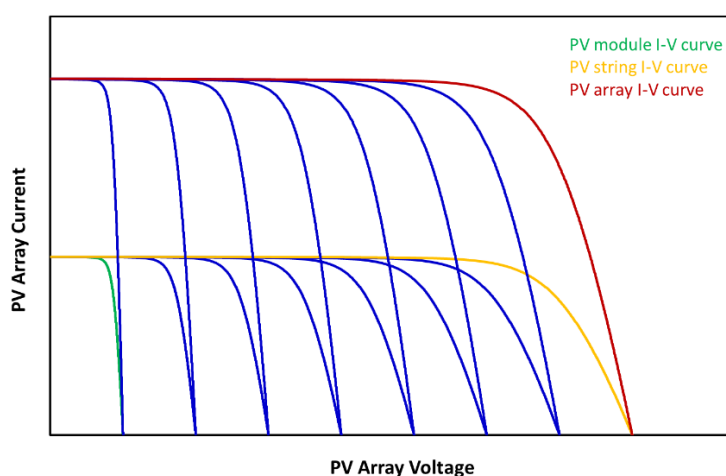
Figure 7: Composition of the PV array I-V curve from individual PV module I-V curves.

Accordingly, I-V curve measurement of a PV string or a PV array under natural sunlight is an electrical test for verifying the PV module performance. Compared to the output power measurement in specialized PV test laboratories, the on-site measurement has various advantages. Firstly, the PV modules do not need to be dismantled so that long downtimes of the PV system are avoided. Furthermore, risks and costs associated with dismantling the PV modules and transporting them to the PV test laboratory are avoided. On the other hand, on-site I-V measurements are affected with a higher measurement uncertainty, which results from the fact that the I-V measurement depends on the weather and installation conditions and cannot be carried out at standard test conditions (STC). These STC are commonly referenced for the nominal output power as stated by the PV module manufacturer.

Measurement of the array I-V curve requires a high experimental effort. Therefore, it should be clarified in advance whether the I-V curve analyzer is suitable for the intended measuring task. Two requirements are:

- The I-V tracing method and equipment shall be capable of I-V measurement of PV strings with high capacitance PV modules. In such case, a short I-V data acquisition time can lead to artefacts in the M_{PP} range of the I-V curve.
- Voltage and current measurement ranges shall conform with the systems conditions. For example, PV systems can have a maximum systems voltage up to 1500 V.

The performance analysis of a PV array is based on the comparison of the measured I-V curve and the predicted I-V curve, which is calculated from the PV module data sheet information according to the construction principle described above. Installation failures and PV module defects will then result from differences in shape between both I-V curves. The type of deviation reveals deficiencies in the PV array and gives valuable hints for troubleshooting (Section 0).

Figure 8 shows the PV array I-V curve with the main I-V performance parameters. In view of the interpretation, the I-V curve can be separated into two parts:

a) Horizontal leg (HL):   Section between short circuit current and M_{PP}
b) Falling leg (LF):   Section between M_{PP} and open circuit voltage
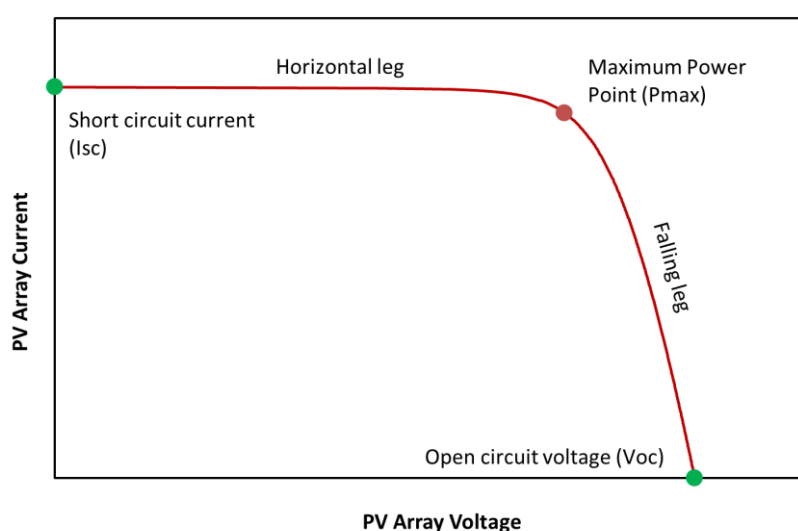
Figure 8: Characteristic sections of a PV array I-V curve with technical parameters.

I-V curve analysis helps to support manufacturer warranty claims and to decide whether PV modules shall be dismounted and subjected to further inspection. It should be noted that PV array I-V curves only allow statements to be made about the average performance of the PV modules, which results from the measured quantities of PMAX, VOC and Isc divided by the number of serially or parallel connected PV modules. If necessary, output power characterization of dismantled PV modules can be carried out on site with mobile PV test centres (see Chapter 4). Understanding PV module failures will usually require the application of further inspection methods, such as imaging techniques (see Chapters 2, 8 9 and 10).

Often the question arises about how many PV strings should be measured (I-V coverage) to make a general statement on the PV systems performance. There is no clear rule for this, but faulty strings can be identified with the help of historical power generation monitoring data from inverters or IR recordings made during operation of the PV array. If such information is not available, measurement of PV string operating currents and voltages in the field combiner boxes can also help to select candidate PV strings.

Furthermore, manufacturers' PV module flash reports are a suitable information source. The so-called flash list summarizes the electrical performance values of PV modules as measured at the end of the production process. It provides information on the production tolerances and

allows a comparison with the nominal power. Detailed information on initial degradation and power warranty is provided in the data sheet of the PV module type.

The following chapters deal with the test equipment and the procedures for on-site I-V measurement of PV arrays, the interpretation of I-V curve shapes and the relationship with possible problems or deficiencies in the PV string or PV array.

It is worth noting, that the measurement and interpretation of PV array I-V curves with bifacial PV modules is complex and will require specific additional considerations. This is due to the fact that the rear face irradiance on bifacial PV modules is dependent on a number of factors such as ground surface albedo, bifaciality factor of the PV module type or installation conditions. Furthermore, rear face irradiance may not be uniform across PV modules and within a PV string, which makes it difficult to determine the effective irradiance. Thus, a single irradiance measurement of the rear face irradiance is not sufficient for quantification of the PV array performance.

3.1 Description of inspection method

I-V curve measurement requires specific test equipment, so-called I-V tracers or I-V curve analyzers. Besides electronic components for running through the I-V curve such devices integrate a data acquisition system. I-V curve measurement is performed in conjunction with measurement of the plane-of-array solar irradiance (G_{poa}) and PV module temperature (T_m), which both define the test conditions. To correct impacts of solar fluctuations during I-V curve measurement, solar irradiance is typically measured synchronously for each I-V data point.

After completion of an I-V measurement, the I-V curve must be converted to the commonly used Standard Test Conditions (STC) as laid down in the international standard IEC 60904-3 [20]. This STC corrected I-V curve is used for analysis purposes.

- Plane-of array solar irradiance: 1000 W/m²
- Spectral irradiance distribution: AM1.5
- Average PV module temperature: 25°C

3.1.1 I-V curve analyser

Commercially available I-V curve analyzers use various technical strategies to run through the I-V curve of a connected PV string [21] [22]. Most commonly, the capacitor charging method is applied. This allows a compact design but leads to a fast I-V data acquisition time in the range of milliseconds. In that case, special care should be taken when PV strings consisting of PV modules with high capacitance solar cells (heterojunction, back-contact, PERC etc.) shall be measured. For these cell types the junction capacity is voltage dependent, which leads to artefacts in the MPP region of the I-V curve, where the current change over time is large [23]. It is advisable to contact the manufacturer of the I-V tracer to receive information which kind of c-Si technologies are compatible with the device.

As mentioned above, the voltage range of the data acquisition unit shall cover the range of today's maximum systems voltage, which can reach values to up to 1500 V DC. The current range shall cover the maximum possible short circuit current of PV modules. For PV modules with 6-inch bifacial solar cells and ground albedo of 80% at the test site, the short circuit current of a PV string can amount up to 15 A DC.

An overview of commercially available I-V curve analyzers is shown in Table 6. The typical features of I-V curve analyzers that can be extracted from the technical data sheets include:

- Lightweight, portable, battery powered, in some cases handheld systems with a screen to display measurement results;
- Wireless connection of irradiance sensors, which can considerably reduce the cabling effort;
- Access to a PV module database: This contains information on the PV module type, which is required to calculate the predicted STC I-V curve and to translate the measured I-V curve to STC;
- Display of STC corrected I-V curve and predicted I-V curve in a diagram for immediate analysis;
- Export of I-V data to PC through USB, RS-432 or Bluetooth connection;
- Maximum PV array power: up to 18 kW.

3.1.2 Connection of the I-V curve analyser

Figure 9 shows a typical test set-up for I-V curve measurement of a PV string in the field. In case of a central inverter the I-V curve analyzer is connected to terminals, busbars or other suitable connection points inside the field combiner box or at the inverter side with separate leads for current and voltage (4-wire measurement). For safety reasons, all series fuses of PV strings must be opened first. PV strings are then measured individually by closing string fuses, one by one.

For PV string inverters, the I-V curve analyzer is directly connected to the string cables at the inverter side. This is easiest to do when the inverter is equipped with Stäubli MC4 or Sunclix connectors. If these connectors are not available, it might be necessary to connect the I-V curve analyzer directly to the first and last PV modules of the strings. For rooftop PV arrays this can be challenging and would require long extension cables for the I-V curve analyzer.

For safety reasons, a circuit breaker should be used in the 4-wire connection lines to the I-V analyser. This device shall be switched on when the connections on both sides are done.
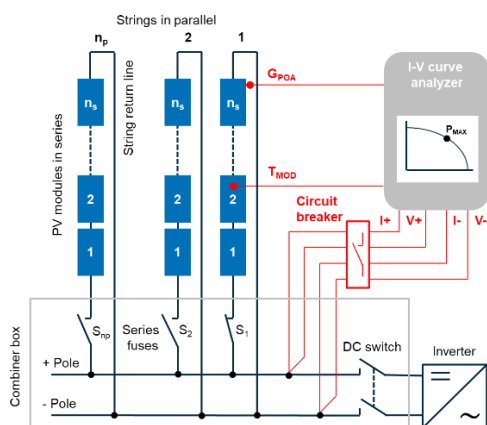
Figure 9: Typical test set up for I-V curve measurement of PV string in the presence of field combiner boxes. The DC input of the inverter and string fuses must be disconnected to make PV string terminals accessible (Photo: TÜV Rheinland).

Table 6: Commercially available I-V curve analyzer systems.

Manufacturer	Model/integrated sensors	Measurement ranges	Accuracies	I-V sweep time	Data analysis/ communication	Weight/Power supply	Website
AMPROBE	SOLAR-4000 Si-photodiode sensor Thermocouple sensor Inclination sensor	1000 V, 15 A	Voltage: ±0.5% Current: ±0.5% Temperature: ±2°C Irradiance: ±2°C	15 ms to 30 ms	Wireless communication to PC and sensors	1.16 kg Battery powered	https://www.caulfieldindus-trial.com/p/amprobe-solar-4000-solar-panel-analyser/p-k10087
Daystar	DS-1000	1000 V, 100 A	Voltage:0.2% to 0.4% Current: 0.2% to 0.9% Temperature: ±1°C	<1000 ms	USB, RS-232	14.4 kg Battery powered	http://daystarpv.com/curve-tracer.html
EKO Instruments	MP-11	1000 V, 30 A	Voltage: ±1% Current: ±1%	4 ms to 640 ms	I-V translation RS422	3 kg	https://eko-eu.com/products/
Halm Electronic	cetisPV Outdoortest	1000 V, 100 A				12 kg Battery powered	www.halm.de
HT Instruments	I-V 500W c-Si irradiance sensor	1500 V, 15 A	Voltage: ±0.5% Current: ±0.5%		I-V translation IEC 60891 WIFI connection	1.2 kg	https://www.ht-instru-ments.co.uk/en-gb/prod-ucts/photovoltaic-testers/
Kewell	IVT-200-1000	1000 V, 200 A	Voltage: ±1% Current: ±1%	<20 ms		12 kg	

Table 6: Commercially available I-V curve analyzer systems (continued).

Manufacturer	Model/integrated sensors	Measurement ranges	Accuracies	I-V sweep time	Data analysis/ communication	Weight/Power supply	Website
Photovoltaic engineering	PVPM1500X	1500 V, 20 A	Voltage: ±1% Current: ±1%	20 ms to 2000 ms	Proprietary I-V translation RS-422, USB 2.0	8.5 kg	https://www.pv-engineering.de
QUNLING	PV-8150 IR temperature sensor	1000 V, 150 A	Voltage: ±2% Current: ±2% Temperature: ±2°C	<10 ms	USB, WLAN, GSM	10 kg	https://www.bjqunling.com/h-pd-62.html?nSL=%5B1%2C2%2C3%2C4%2C9%2C10%2C8%5D#skeyword=pv+8150&_pp=0_35
Shanghai Noyo Technology Co., Ltd.	PV900 c-Si irradiance sensor Pt1000 sensor	1000 V, 12 A	Voltage: ±1% Current: ±1% Temperature: ±1°C	No information	RS485/RS232, Bluetooth (up to 100 m)	2.2 kg Battery powered	www.noyotech.com
Shanghai Noyo Technology Co., Ltd.	PV1800	1000 V, 20 A	Voltage: ±1% Current: ±1%	No information	Simultaneous I-V measurement of up to 6 PV strings		www.noyotech.com
Solmetric	PVA-1500V2 Si photodiode sensor Thermocouple sensor	1500 V, 30 A	Voltage: ±0.5% Current: ±0.5% Temperature: ±2°C	<250 ms	proprietary procedure, wireless communication to PC and sensors	Battery powered	http://www.solmetric.com

3.1.3 Solar irradiance measurement

Irradiance sensors for PV applications typically use crystalline silicon cells or a photodiode as detector. It is not recommended to use a pyranometer as an irradiance sensor. For these instruments, measurement errors are caused by the long response time to irradiance fluctuation and the broad band spectral responsivity up to 4000 nm. Solar cells (c-Si and thin-film) only utilize a limited wavelength range 300 nm to 1200 nm for photocurrent generation. Even for clear sky conditions, the associated spectral mismatch can result in measurement errors of a few percent [24].
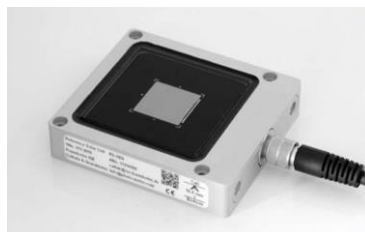
But also the use of c-Si irradiance sensors must be considered with care, because its spectral responsivity will not 100% match with the fielded PV modules, so that a spectral mismatch error cannot be fully eliminated [25]. In particular, for the inspection of PV power plants with thin-film PV modules the use of a spectrally filtered c-Si irradiance sensor should be considered to reduce the spectral mismatch error [23].As shown in Table 7 most suppliers of I-V analysers provide a specific irradiance sensor or temperature sensor with their system. This may result in disadvantage that other irradiance sensors with lower calibration uncertainty cannot be used. In any case, the requirements for use of sensors shall be clarified with the supplier.

In Table 7 companies are listed that are specialized on the manufacture of calibratable c-Si irradiance sensors for PV applications. Generally, such reference cells shall comply with the requirements of IEC 60904-2 [26]. The calibration of irradiance sensors is either performed by independent calibration laboratories or by factory calibration. Depending of the calibration methodology different levels of uncertainty are achieved (±0.5% to ±4%). Lowest calibration uncertainty is achieved if a primary calibrated cell (WPVS design) is used as reference device and if the spectral response of the irradiance sensor is available. For factory calibration the uncertainty is ±2.5% or higher. Attention should be paid that a calibration certificate is issued, which should inform on the calibration uncertainty and the validity of calibration. The Fraunhofer-ISE outdoor sensor offers the option with optical filter for measurement of thin-film PV modules or PV strings.

Table 7: Commercial irradiance sensors with c-Si cells.

Mencke & Tegtmeyer	**Fraunhofer-ISE**	**IKS Photovoltaik**
Multi-Si cell	Mono-Si cells, filter option	Mono-Si or multi-Si cell
Calibration uncert.: ±2.5%	Calibration uncert.: ±1%	Calibration uncert.: ±4%
Temp. compensation: Pt100	Temp. compensation: Pt100	Temp. compensation: Pt1000
https://www.ib-mut.de	https://www.ise.fraunhofer.de	http://www.iksphotovoltaik.de

A typical error source for performance inspection of PV power plants is the misalignment of the irradiance sensor and the PV modules in a PV string. According to the requirements of the standard IEC 60904-1 [27] the irradiance sensor should be mounted coplanar with the PV modules with accuracy better than ±2°. Therefore, it should be installed at a representative location near the PV string or array to be measured. The impact of ±2° misalignment can be illustrated with the following example. For clear sky days in summer a measured irradiance of 700 W/m² is associated with an incident angle of approx. 45°. In that case, ±2° misalignment would cause a measurement error of $[1 - \cos{(47°)}/\cos{(45°)}]$ which yields ±4%.

3.1.4 PV Module temperature measurement

PV module temperature is commonly measured with temperature sensors, which are affixed to the rear surface of a PV module. The following sensor types are used:

- Pt 100 temperature sensor: requires 4-wire connection for accurate temperature measurement, uncertainty less than 0.5°C for class A type
- Pt 1000 temperature sensor: 2-wire connection, uncertainty larger than 1°C
- Thermocouple sensor: small sensor area, uncertainty larger than 1°C

Instead of affixing sensors to the PV module rear also a handheld infrared (IR) thermometer can be used. In this case however, the temperature reading must be manually entered into the I-V curve analyzer software.

An effective method for detecting temperature inhomogeneities in PV arrays is the use of an IR camera, with which a large field of view is considered. Such cameras are mainly used for fault detection in PV systems (i.e. hot-spots, defective bypass diodes, interconnection failures). It must be noted that the camera is normally not suitable for absolute temperature measurement. If an absolute measurement is intended the operating manual shall be carefully studied.

When temperature sensors are used to determine the cell temperature under natural sunlight, three main problems arise:

A) A considerable spread of temperature can be observed over the area of the PV string. On the other hand, I-V analyzers only have a single temperature input channel. Therefore, the selection of the sensor location is of particular importance to avoid measurement errors. It is recommended to use an infrared camera or an infrared hand thermometer to scan the PV module temperature range in the array and find a suitable position for temperature measurement.

B) As the solar cells are usually not accessible, temperature measurement is performed at the back of the PV module. Thus, the measured temperature is influenced by the thermal conductivity of the encapsulant and backsheet materials. Other measurement errors may arise from a bad thermal contact of the sensor, if no conductive glue is used.

C) In the case of bifacial PV modules, the rear side must not be shaded over a large area by the temperature sensor or connecting cables. In such case a sensor with small receiver area shall be used.

These problems are avoided when the equivalent cell temperature (ECT) is used. The procedure is defined in the standard IEC 60904-5 [28]. The given formula for ECT calculation is based on the temperature and irradiance dependence of the open circuit voltage of PV devices. The model requires input of various PV module parameters and the measured values of in-

plane solar irradiance and open-circuit voltage. It should be noted that this method can only be applied if PV modules are not subject to degradation or damages that may affect open circuit voltage.

$$ECT = 25°C + \frac{1}{\beta_{rel} \cdot f^2(G)} \cdot \left(\frac{V_{OC}}{V_{OC,STC}} \cdot f(G) - 1 \right) \tag{1}$$

$$f(G) = 1 + B_1 \cdot ln\left(\frac{1000 \frac{W}{m^2}}{G} \right) + B_2 \cdot ln^2 \cdot \left(\frac{1000 \frac{W}{m^2}}{G} \right) \tag{2}$$

Table 8: Input parameters for calculation of the Equivalent Cell Temperature (ECT).

	Unit	Description
G_{POA}	W/m²	Measured plane-of-array irradiance
V_{OC}	V	Measured open circuit voltage of the PV string
$V_{OC,STC}$	V	Nominal open circuit voltage as stated in the manufacturers' data sheet or PV module label. Here is to be noted that the accuracy of the ECT method is mainly determined by the accuracy of this parameter. Care should be taken because open-circuit voltage may be subject to production tolerance. The higher the tolerance, the greater the ECT uncertainty.
β_{rel}	1/K	Voc temperature coefficient as stated in the PV module manufacturers' data sheet.
B_1		Linear irradiance correction factor of open circuit voltage.
B_2		Quadratic irradiance correction factor of open circuit voltage.

B_1/B_2 parameters are normally not provided in the manufacturers' data sheet but result from performance measurements in PV test laboratories. For crystalline silicon PV modules the following values can be used with good approximation: B_1= 0.045, B_2 = 0.

3.1.5 Translation of the measured I-V curve to STC

For analysis purposes the measured I-V curve cannot be directly compared with the predicted I-V curve of the string/array, because the PV module temperature and irradiance normally differ from the STC (25°C, 1000 W/m²). Therefore, the measured I-V curve must be translated to STC. This task is performed by the operating software of the I-V curve analyzer.

The principles for translation of I-V curves of PV devices measured at a specific solar irradiance and PV module temperature (test conditions) to the STC (target conditions) are defined in the standard IEC 60891 [29]. The conversion is based on two equations for current and voltage data pairs, of which the I-V curve is composed. The calculation requires the input of specific PV module translation parameters. Most known are the temperature coefficients (TC) of short circuit current and open circuit voltage, which are documented in PV module data sheets.

In addition, the internal series resistance (Rs) of the PV array is important for I-V translation, which is associated with power losses due to PV module wiring. Usually assumptions must be made for this value. The greater the deviation of the measured irradiance from the nominal value (1000 W/m²), the greater the impact of Rs uncertainty. In order to achieve a high translation accuracy, it is recommended to determine the "real" Rs value with two I-V curve measurements at different irradiances, which differ more than 300 W/m². The "real" Rs value results from Rs variation until the translated low irradiance I-V curve matches with the high irradiance I-V curve in the falling leg. Further details can be found in IEC 60891 [29].

The review of the operating manuals of the I-V curve analyzers (see Table 8) has shown that the translation procedure in most cases does not follow IEC 60891 [29] and the computing algorithm is in many cases not disclosed. This lack of transparency is a major deficiency because the translation accuracy of results is unclear. It would be helpful if at least the data export of the measured uncorrected I-V curve to PC is possible. This would enable the user to perform the translation calculation manually with Excel software. Only a few suppliers of I-V curve analyzers offer such data export option.

3.1.6 Predicted I-V curve of the PV string or PV array

As previously indicated the performance analysis and the identification of problems associated with the installation or PV module defects are done on the basis of two I-V curves:

A. The STC corrected measured I-V curve: The measured I-V curve of the string is translated to 25°C PV module temperature and 1000 W/m² irradiance. The required PV module parameters are taken from the PV module database provided by the supplier of the I-V curve analyzer: It contains all required PV module parameters to perform temperature and irradiance correction of I-V curves.

B. The predicted I-V curve: This curve is modelled. The calculation mainly requires the following inputs:

- Selection of the PV module type: For this purpose the supplier of the I-V analyzer provides a specific PV module database, which allows modeling of the reference I-V curve of a single PV module under STC.
- Number of PV modules connected in series and in parallel
- Estimate of additional resistive losses in the circuitry of the string, which are mainly determined by the cable length and the cable cross section.

Figure 10 illustrates the calculation of the predicted and the STC corrected I-V curves as implemented in the operating software of the I-V analyzer. They are visualized in a diagram so that deviations between both I-V curves can be identified. In the next step these deviations are interpreted and related to potential problems in the PV array or problems with PV modules (Section 3.1.3).

It must be noted that the deviation between both curves may also be the result of incorrect model parameters or incorrect values of measured temperature and irradiance. Therefore, possible sources of error in connection with the experimental setup or with the settings for modelling must be taken into account for interpretation.
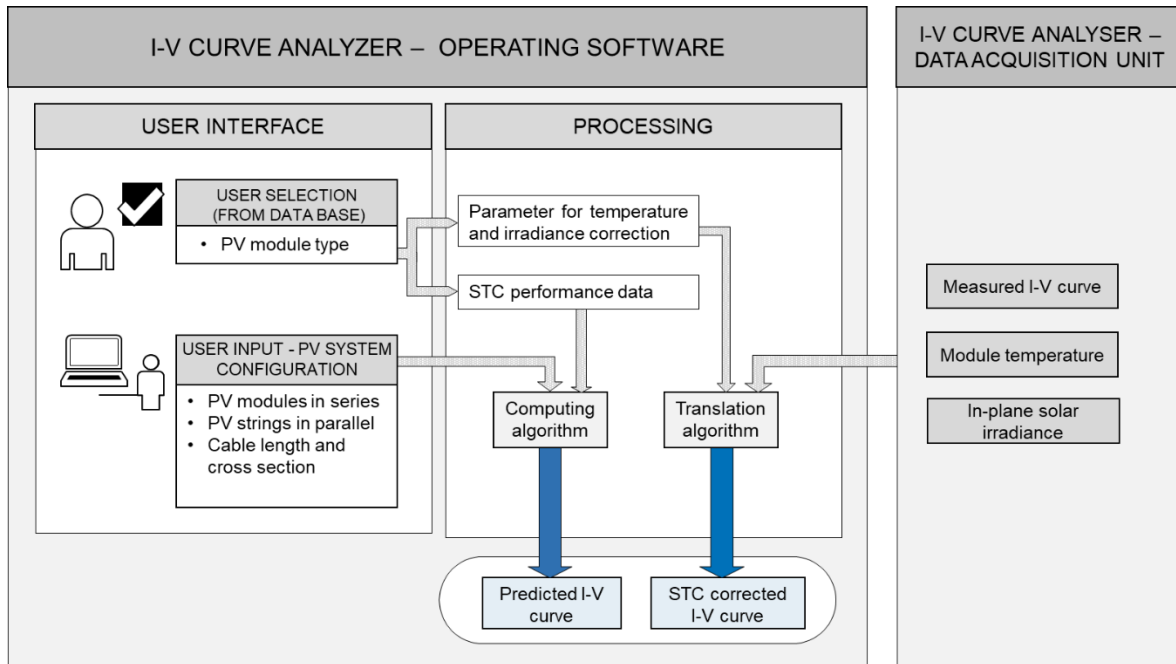
Figure 10: Functions of the I-V curve analyzer (source: TÜV Rheinland).

3.2 Existing knowledge

Measurement of array I-V curves is a well-established method for field inspection of PV systems for decades [30] [31]. Accordingly, there is a lot of measurement experience available, which were introduced in the standard IEC 61829 [32]. The measurement technology has changed considerably since the early years from heavy measurement cases to lightweight handheld instruments with a plenty of software options. A market overview of current suppliers of I-V curve analyzers is shown in Table 6.

More recently, the interpretation of array I-V curves and the relationship with system failures lies in the focus of publications. This point is covered in the next section. The importance of correct interpretation is also underlined by the fact that some suppliers of I-V curve analyzers offer comprehensive training courses for their customers.

The relevant international standard for I-V curve measurement of PV arrays is IEC 61829 [32]. The document specifies procedures for measurement of PV array I-V characteristics, the accompanying meteorological conditions and use of these for translating measured I-V curves to standard test conditions (STC).

A weak point for PV system performance assessment associated with I-V curve measurement is the non-transparent I-V curve translation to STC. The procedures implemented in I-V tracers are often not in conformance with IEC 60891 [29] or IEC 61829 [32]. In such case, the user has the only option to export raw data and perform the STC calculations manually by Excel. This demonstrates that there is still work to do to harmonize I-V measurement methods.

3.2.1 Status of standardization

IEC 60904-1 (2006): Photovoltaic devices – Part 1: Measurement of photovoltaic current-voltage characteristics [27]

> This part of IEC 60904 describes procedures for the measurement of current-voltage characteristics of photovoltaic devices in natural or simulated sunlight. These procedures are applicable to a single photovoltaic solar cell, a sub-assembly of photovoltaic solar cells, or a PV module.

IEC 60904-5 (2006): Photovoltaic devices – Part 5: Determination of the equivalent cell temperature (ECT) of photovoltaic (PV) devices by the open-circuit voltage method [28]

> The equivalent cell temperature (ECT) is the average temperature at the electronic junctions of the device (cells, PV modules, arrays of one type of PV module) which equates to the current operating temperature if the entire device were operating uniformly at this junction temperature.

IEC 60904-7 (2009): Photovoltaic devices – Part 7: Computation of the spectral mismatch correction for measurements of photovoltaic devices [23]

> This part of IEC 60904 describes the procedure for correcting the bias error introduced in the testing of a photovoltaic device, caused by the mismatch between the test spectrum and the reference spectrum and by the mismatch between the spectral responses (SR) of the reference cell and of the test specimen.

IEC 60891 (2009): Photovoltaic devices – Procedures for temperature and irradiance corrections to measured I-V characteristics [29]

> This standard defines procedures for temperature and irradiance corrections to measured I-V (current-voltage) characteristics of photovoltaic devices. It also defines the procedures used to determine factors relevant for these corrections. Requirements for I-V measurement of photovoltaic devices are laid down in IEC 60904-1.

IEC 61724-1 (2017): Photovoltaic system performance – Part 1: Monitoring [33]

> This standard outlines equipment, methods, and terminology for performance monitoring and analysis of photovoltaic (PV) systems. It addresses sensors, installation, and accuracy for monitoring equipment in addition to measured parameter data acquisition and quality checks, calculated parameters, and performance metrics.

IEC 61829 (2015): Photovoltaic (PV) array - On-site measurement of current-voltage characteristics [32]

> This standard specifies procedures for on-site measurement of flat-plate photovoltaic (PV) array characteristics, the accompanying meteorological conditions, and use of these for translating to standard test conditions (STC) or other selected conditions.

3.3 Detectable failure types for PV modules and PV arrays

The PV module circuitry of a PV array is determined by the number (Ns) of serially connected PV modules to a PV string and the number (Np) of parallel connected PV strings. Accordingly the predicted array I-V curve results from multiplication of the standard PV module I-V curve as illustrated in Figure 11. Deviations between measured and predicted I-V curves fall into various categories, which all indicate a reduction in maximum power P_{MAX} produced by the PV string or PV array [34]:

- The STC translated I-V curve shows a lower or higher short circuit current than predicted.
- The STC translated I-V curve shows a lower or higher open-circuit voltage than predicted.
- The slope of the STC translated I-V curve in the horizontal or falling leg does not match the prediction.
- The STC translated I-V curve has steps.

It must be noted that the shape of the measured I-V curve can also result from a combination of PV module defects or installation failures. This can make the interpretation very complex.

For failure analysis and troubleshooting in the field it may be also helpful to compare the results from different PV strings. This can reveal systematic or random failures.

Specific care must be taken if deviations in short circuit current or open circuit voltage are observed. These can be also caused by incorrect irradiance and temperature measurement or erroneous I-V translation. In such cases, the test setup should be carefully inspected, and I-V measurement repeated.
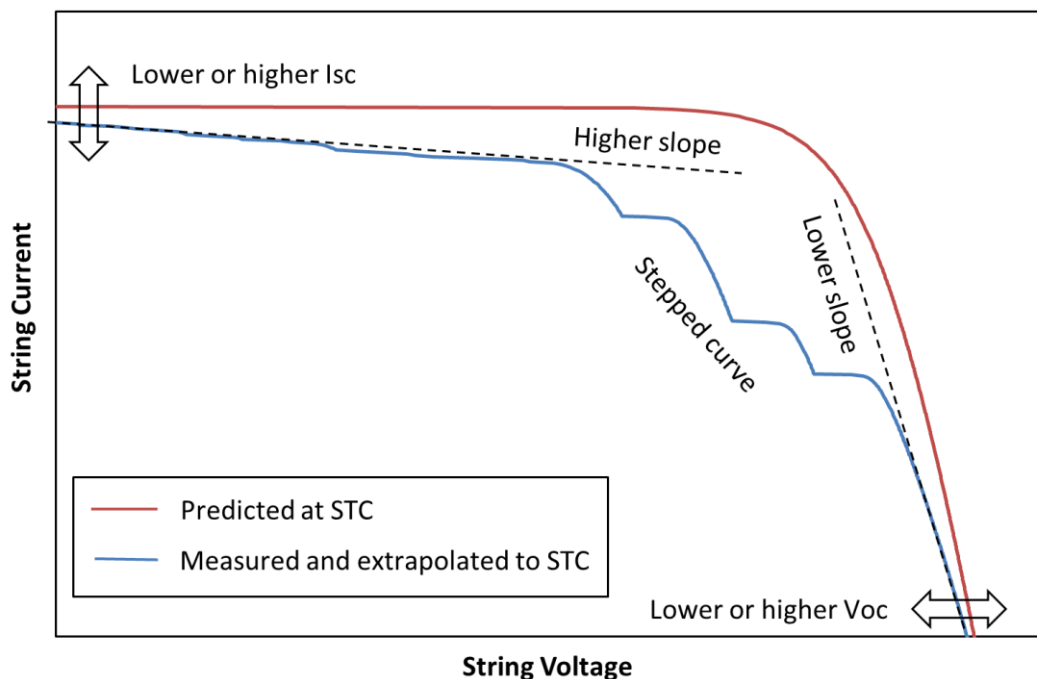

Figure 11: Possible deviations of the measured and STC corrected I-V curve to predicted I-V curve of a PV string.
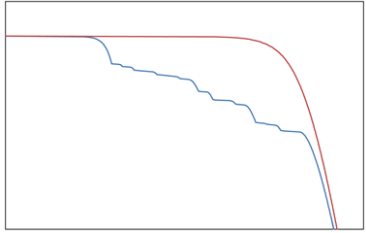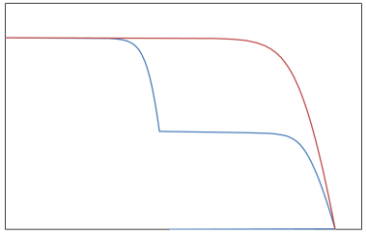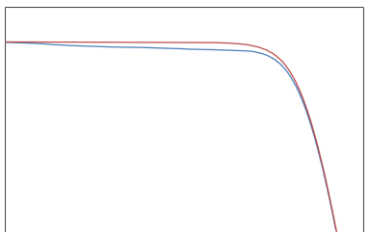
Table 9: Measurement errors associated with test environment and I-V analyzer settings.

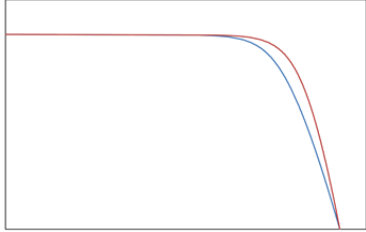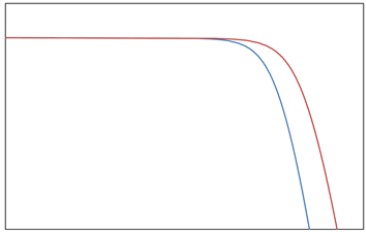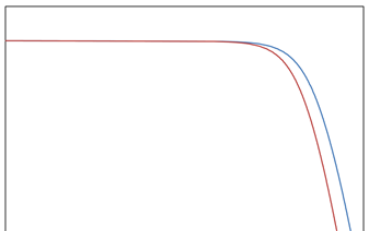| |
|---|
| **Incorrect setting of I-V curve analyser**

 • Check selected PV module type
 • Check temperature coefficients of Voc and Isc
 • Check internal series resistance of the PV module type and the number of PV modules in series and in parallel in the PV string. For non-aged c-Si PV modules a value of 5 mOhm per cell is a good estimate to calculate the PV module internal series resistance. |
| **Incorrect settings for cabling**

 The calculation of the predicted I-V curve requires assumptions for additional resistive losses in the circuitry of the PV string.

 • Check cable length, in particular for the return line of the PV module string
 • Check cable cross section |
| **Incorrect irradiance measurement**

 Erroneous irradiance measurement will cause STC translation errors. Such errors can be caused by the sensor settings, a misaligned installation or unsuitable sensor location

 • Check functionality of irradiance sensor
 • Check scaling factor and temperature coefficient (calibration protocol)
 • Check location of sensor for reflections which contribute to additional irradiance
 • Check alignment of sensor within ±1° to PV module orientation to keep the measurement error <±1%
 • High fluctuation of irradiance (if non-synchronous measurement of irradiance and I-V curve) |
| **Incorrect temperature measurement**

 • Temperature at location of the sensor may be too high/low compared to the average PV module temperature in the string, which will cause a translation error to STC.
 • Check functionality of sensor by comparing measurement with an IR thermometer
 • Find representative location for PV module temperature measurement |

Table 10: Interpretation of deviations between STC corrected I-V curve (blue lines) and predicted I-V curve (red lines).

Observed deviation of STC corrected I-V curve (blue) and predicted I-V curve (red)	Potential causes located in the PV array or associated with PV module defects or degradation
Steps in I-V curve (single I-V string) 	**Shading of PV modules** Shaded PV modules deliver a lower short circuit current. For current values higher than the PV module short circuit current the differential current is conducted via the bypass diode, which causes steps in the I-V curve. Steps occurring at different current level indicate a non-uniform shading in the area of a PV string or PV array. The deviation in V_{OC} values is caused by the lower effective irradiance in the string. ✓ Search for visible obstacles (parts of the building, trees, power line cable, grass growth, etc.) ✓ Measure I-V curve at a different time of day or day of year when PV modules are not affected by shading. **Unevenly soiled PV modules with high degree of soiling** ✓ Clean PV modules and re-measure I-V curve **Slipping snow on PV modules** ✓ Remove snow and re-measure I-V curve
Steps in I-V curve (parallel I-V strings) 	**V_{OC} mismatch of strings in parallel** When strings are connected in parallel, the currents for a certain voltage are added. If one of the parallel strings delivers a lower open circuit voltage (see section "low open-circuit voltage") a step will occur in the common I-V curve. For a large number of strings in parallel and one string operating at lower V_{oc}, the maximum power voltage of the common I-V curve may be higher than this V_{oc} value. In that case a reverse current will be injected into this faulty string, which is associated with power dissipation. The maximum reverse current is limited by the series fuse of the PV string. If the fuse trips the faulty string will be disconnected. ✓ Use IR camera to localize defective PV modules
High slope in the horizontal leg (HL) 	**Short-circuit mismatch of PV modules** This may be caused by I_{sc} production spread of PV modules. ✓ Check PV module manufacturer flash list, if available **Different orientation of PV modules in the PV string** The topography of the terrain may not assure that PV modules have the same orientation to the sun. This will lead to I_{sc} spread. **Unevenly soiled PV modules with low degree of soiling** Dust accumulation or algae growth appears along the lower PV module frame. ✓ Clean PV modules and re-measure I-V curve **PV modules highly affected by cell cracks** ✓ Use IR camera to localize PV modules with cracked cells

47

Table 10: Interpretation of deviations between STC corrected I-V curve (blue lines) and predicted I-V curve (red lines) (continued).

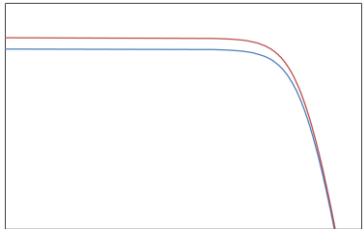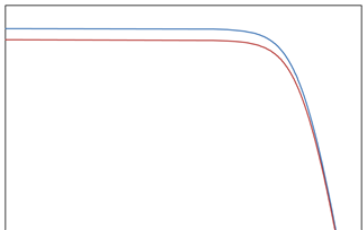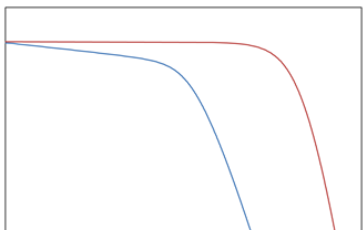| Observed deviation of STC corrected I-V curve (blue) and predicted I-V curve (red)	Potential causes located in the PV array or associated with PV module defects or degradation
Low slope in the falling leg (FL) 	**Increased series resistance in the string** The internal series resistance of a PV string causes voltage losses with increasing current. It is composed of contributions from PV modules, cabling, connectors and terminals. The series resistance of PV modules typically increases with operating time due to the corrosion of electrical contacts. Additional series resistance might also indicate deterioration of contact resistances of plugs and terminals. ✓ The exact value of overall series resistance can be determined by I-V measurement of the string at high and low irradiance with minimum 300 W/m² difference, following the procedure of IEC 60891. The use of this value will improve the translation accuracy to STC
Low open-circuit voltage 	**Installation failure** Wrong number of serially connected PV modules in the string. ✓ Check number of PV modules in series **Defective bypass diodes** Bypass diodes in PV modules may fail due to thermal overload or lightning effects during thunderstorms. Defective bypass diodes are usually shorted, so the group of cells is disconnected, resulting a lower string open circuit voltage. ✓ Use IR camera to localize PV modules with defective bypass diodes **Individual manufacturing defects of PV modules** There may be a large V_{oc} production spread for thin-film PV modules due to short circuit of individual cells. ✓ Check PV module manufacturers flash list, if available **Cells are completely shaded or inactive** ✓ Remove shade and re-measure I-V curve
High open-circuit voltage 	**Installation failure** Wrong number of serially connected PV modules in the string. ✓ Check number of PV modules in series

Table 10: Interpretation of deviations between STC corrected I-V curve (blue lines) and predicted I-V curve (red lines) (continued).

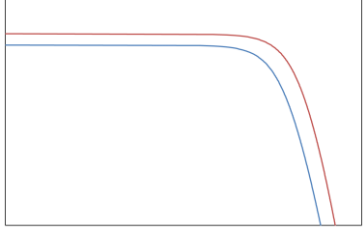| Observed deviation of STC corrected I-V curve (blue) and predicted I-V curve (red)	Potential causes located in the PV array or associated with PV module defects or degradation
Low short-circuit current 	**Light induced Degradation (LID)** LID is a performance loss of silicon PV modules arising in the very first hours of exposition to the sun. It affects the short circuit. For thin film PV modules effects from metastability must be considered. **PV Modules with lower power class installed** ✓ Check PV module labels and flash list of PV module manufacturer, if available **PV module are degraded over time** Optical transmittance loss in the light path (cover materials): Solarization of glass in the UV range, browning or delamination of encapsulation material **Uniform soiling of PV modules** ✓ Clean PV modules and re-measure I-V curve
High short-circuit current 	**PV Modules with higher power class installed** ✓ Check PV module labels and flash list of PV module manufacturer, if available
High HL slope and low Voc 	**Potential induced Degradation (PID)** PID is only observed for PID sensitive PV modules. PID is caused by leakage currents between the cells (high potential) and the PV module frame (earth potential), which cause Na+ ions to migrate from the front glass into the cells causing shunts. Because of many variables for PID (variation of PV modules, environmental and operating conditions) the array I-V curves may show different deviation from the predicted I-V curve. Long-term effect that may become apparent after several years of operation. Degradation increases with operation time of the PV power plant. ✓ Use IR or EL camera for confirmation: PV modules that are installed closer to the plus pole (n-type) or minus pole (p-type) are more affected and emit lower EL radiation. ✓ Contact the PV module supplier and discuss measures for regeneration of replacement of PV modules**.**

Table 10: Interpretation of deviations between STC corrected I-V curve (blue lines) and predicted I-V curve (red lines) (continued).

Observed deviation of STC corrected I-V curve (blue) and predicted I-V curve (red)	Potential causes located in the PV array or associated with PV module defects or degradation
Low I_{sc} and low V_{oc}	**Light enhanced temperature induced degradation (LeTID)** This type of degradation is observed for PV modules with PERC solar cells. Degradation increases with operation time until saturation is achieved and regeneration starts. Generally, the regeneration process is slower compared to degradation. Compared to LID the time frame of LeTID typically takes years. ✓ Contact the PV module supplier to receive information on expected Pmax degradation rate, max. degradation and regeneration rate.

3.4 Best practice recommendations

Based on the work presented in the previous sections, the following best practice recommendations can be given for performance analysis of a PV string/array using the I-V measurement technique.

1. The measurement shall be carried out on a sunny day and in the thermal equilibrium of the PV modules in order to avoid fluctuations in irradiation and PV module temperature during the I-V measurements. Care must be taken at high wind speed and changing wind conditions. Then a temperature equilibrium will be difficult to achieve. The irradiance shall be greater than 800 W/m² to reduce the uncertainties in translating the measured I-V curve to the STC. Irradiance fluctuation should be less than ±1% during measurement.

2. For safety reasons disconnect the DC line of the PV string/array to the inverter and switch off all series fuses in the field combiner box. If string inverters are used disconnect all strings from the input panel of the inverter.

3. Check for soiling of PV modules and shading impacts on the PV string to be measured.

4. Check if alignment of PV modules is equal within the PV string to be measured.

5. Install the irradiance sensor coplanar with the PV modules of the string within ±1°.

6. Use an IR temperature sensor or IR camera to measure the spread of rear PV module temperature in the PV string/array and select a suitable position, which corresponds to the average temperature, to attach the temperature sensor. No I-V measurement should be done until the temperature values are stabilized. A suitable criterion is less than ±1 K temperature change in the previous one-minute interval.

7. Configure the I-V analyzer and make sure that you received automatic updates of the PV module database: Select the PV module type, enter number of PV modules in series and the number of PV modules in parallel and make assumptions for additional series resistance of the cabling (usually done with cable length and diameter).

8. Perform I-V curve measurement at solar irradiance >800 W/m² (High irradiance measurement). Depending on the season, this level may not be achieved in high latitude countries. In this case, a lower irradiance can be accepted if the PV array internal series resistance is additionally measured (see step 9) and used for I-V translation to STC.

9. Optional: Measure the string/array I-V curve at low irradiance (to be done in the morning or afternoon). The irradiance difference to the high irradiance I-V measurement (step 8) shall be larger than 300 W/m². Determine the internal series resistance of the string/array. This value shall be used for I-V curve translation to STC and will yield higher translation accuracy.

10. Optional: Export measured non-corrected I-V data (raw data) to Excel and manually translate the measured I-V curve to STC, following the procedures 1 or 2 of IEC 60891 [29].

11. View the predicted I-V curve and the STC corrected measured I-V curve as calculated by the I-V curve analyzer or Excel.

12. Interpret the deviation between the predicted and the STC corrected I-V curves according to the failure catalogues of Table 10.

3.5 Measuring uncertainty aspects

The principles for measurement uncertainty assessment are defined in the guidance document JCGM 100:2008 "Evaluation of measurement – Guide to the expression of uncertainty in measurement (GUM)" [35], which was prepared by the Joint Committee for Guides in Metrology (JCGM). Annex 1 explains the proposed procedure for the calculation of the expanded measurement uncertainty.

I-V curve measurement reveals principle problems in PV arrays, which may be associated with installation failures or problems with PV modules. Quantification of PV module output power presumes that installation failures are excluded.

Warranty claims are only promising if the detected difference "measured average output power minus nominal output power of the PV module type" is larger than the overall measuring uncertainty of the I-V curve analyzer. From plant operators' point of view, a low measurement uncertainty is therefore desirable.

In view of a low measuring uncertainty, the output power characterization of PV modules in a test laboratory has clear advantages. Here reported uncertainties lie in the range ±1% to ±2.5%. But associated costs for shipping, costs for measurement of large sample sizes and risks of PV module damage during transport and handling speak for on-site measurements.

P_{MAX} uncertainty of PV strings calculated according to JCGM 100:2008 [35]

The expanded P_{MAX} uncertainty resulting from I-V curve measurements is composed of five major uncertainty contributions [36]:

- Uncertainty related to irradiance measurement: This shall cover the calibration accuracy, the estimated spectral mismatch error, the estimated misalignment between sensor and PV modules and the uncertainty of data acquisition.

- Uncertainty related to PV module temperature measurement: This shall cover the sensor accuracy, the uncertainty of data acquisition, an estimate for the temperature difference between solar cells and the PV module rear and an estimate for temperature non-uniformity in the PV string.
- Uncertainty related to I-V translation: This requires error propagation calculation with uncertainties inputs for temperature measurement, irradiance measurement and I-V correction parameters. For irradiances larger than 800 W/m² the translation uncertainty is typically less than ±1%, if procedure 2 of IEC 60891 [29] is applied and the series resistance of the PV string has been determine by multiple I-V measurement at different irradiances. The uncertainty of temperature coefficients can be assumed ±10% for ISC and ±5% for VOC [37].
- Uncertainty related to I-V data acquisition: Uncertainty budgets for current and voltage measurement are given in the technical specification of the I-V analyser.
- Uncertainty related to the repeatability of I-V measurement: Type A uncertainty should be evaluated from a minimum of 10 independent measurements.

Parameter studies with conservative assumptions have shown that the P_{MAX} uncertainty for on-site PV measurement, calculated according to JCGM 100:2008 [35], lies in the range ±3,5% to ±5% [38]. The best-case scenario with ±2.5% P_{MAX} uncertainty is achieved under conditions that:

- A primary calibrated c-Si reference cell is used (calibration accuracy ±0.5%);
- the I-V translation error is kept low due to a high irradiance value close to 1000 W/m²;
- the ECT method is used for temperature measurement and
- angular misalignment between irradiance sensor and plane of array is less than ±0.5°.

3.6 Occupational safety

For working under electrical voltage, the safety regulations of the country must be observed.

Work on a PV system may only be carried out by a qualified electrician with appropriate training. Personal protective equipment is required for working on a PV system. This includes special gloves, safety shoes and an insulating mat to protect against electric shock as well as safety eyewear to protect against electric arcs. For work under electrical voltage, qualified tools must be used.

It must be ensured that clamping work is always carried out with no electric voltage or at least without load. With that regard, it is advisable to use a circuit breaker in the test leads to the I-V tracer as shown in Figure 9.

Two application cases are to be distinguished:

A. PV system with central inverter: The power cables of the PV strings are typically assembled in the field combiner box. In this case all string series fuses and the DC switch of the inverter must be switched off (Figure 9) before any clamping work is done. After connecting the I-V analyzer, the PV string to be measured can be connected individually for the I-V measurement, whereby the circuit breaker of the measuring lines is switched off.

B. <u>PV system with string inverters:</u> The power cables of the strings are connected to the inverter. For disconnection of cables the inverter must be switched to standby. For I-V measurement the PV strings should be connected and measured individually by I-V analyzer.

3.7 Transportability

The I-V curve analyser is usually packed together with the irradiance and temperature sensor/s in a box or a case, which can be easily carried by hand. A second box may be required for cabling, cable adapters, circuit breaker, multimeters, current tongs, tools and personal protective equipment.

3.8 Cost considerations

The purchase costs of the I-V curve analyzer can vary from country. Furthermore, the cost of irradiance sensor and temperature sensor depend on the accuracy class. These are customer-specific solutions so that no global price indication can be given.

Maintenance costs arise from annual recalibration of the I-V curve analyzer and the temperature and irradiance sensor.

The number of I-V measurements per day depends on the irradiance conditions at the test site and the work infrastructure. For the following assumptions up to 1 MWp can be measured per day. The whole work can be conducted by two professionals.

- Weather conditions: Clear sky, 4 hours with irradiance higher than 800 W/m²
- PV system: 16 PV strings per combiner box, 24 PV modules per PV string
- PV module: 350 Wp
- Time required per box: 30 minutes for instrumentation and 16 I-V measurements

4 PV MODULE CHARACTERIZATION WITH MOBILE PV TEST CENTRES

Besides installation errors or incorrect planning of PV power plants, performance losses are often caused by defective or degraded PV modules. Such PV modules can sometimes be identified by visual inspection (i.e. discoloration, delamination, burn marks), but there are defects that are not visible to the naked eye and require a detailed technical inspection.

A common approach is to test a selected number of PV modules under laboratory-controlled conditions. As such, measurements can be independent of weather conditions and can be performed with high reproducibility. However, shipping PV modules to an accredited test laboratory is time consuming and potential damages generated during transportation may occur. Another way is to inspect PV modules on site with a mobile PV test centre. Such mobile PV test centres may comprise test equipment "on wheels", which is built in a trailer or truck, or dismountable test equipment, which can be packed in boxes ready to ship to the field. Table 11 gives an overview of advantages and disadvantages of an inspection done at a stationary laboratory or with a mobile PV test centre.

Mobile PV test centres can be either used for on-site pre-installation testing of PV power plants or for the detection of PV module failures in existing systems. Advantages of the mobile PV test centres over laboratory testing include the ability to characterise a representative sample of randomly selected PV modules with low disturbance of the installation process or low interruption of the PV operation when the system is already commissioned. In operational PV systems, mobile PV test centres can be used to detect common early failure modes (e.g., underperformance, cell manufacturing defects, soldering defects, cracked cells, electrical mismatch of cells etc.), but also midlife failures (e.g. bypass diode failures or power degradation due to PID or LeTID, etc.) and impacts from heavy weather events (hailstorm and wind damages), which can be used for warranty claims.

Table 11: Comparison of PV module inspection in an accredited test laboratory against mobile PV test centres.

	PV module inspection in an ISO 17025 accredited test laboratory	**PV module inspection with a mobile PV test centre**
Advantages	Output power measurement can be performed with low P_{MAX} uncertainty and high repeatability. Extended failure analyses and deeper study of degradation mechanisms will be possible.	Inspection results are immediately available and further measures can be discussed with the plant operators on site. A high number of PV modules can be inspected with or without dismounting resulting in short or even no downtime.

Table 11: *(continued).*

	PV module inspection in an ISO 17025 accredited test laboratory	PV module inspection with a mobile PV test centre
Disadvantages	Long downtime of the PV power plant or PV strings associated with revenue loss. High costs for transporting the PV modules; thus, a limited number of PV modules can be inspected. High risks of PV module damage due to transport and handling.	High equipment investment and transportation costs (long distance, customs clearance etc.). Specific infrastructure may be required (provision of power supply connection, fastening of roads). Higher P_{MAX} measurement uncertainty compared to laboratory measurement.

4.1 Description of inspection method

A mobile PV test centre makes it possible to quickly get an overview of a PV module's condition on site. It generally combines the following PV module inspection tests: maximum power determination (through I-V tracing) and electroluminescence inspection (EL). These three methods can detect the majority of PV module failures. Some manufacturers of mobile PV test centres offer additional test equipment for the inspection of bypass diodes or electrical safety. The complete test equipment is integrated into the same mobile PV test centre allowing sequential testing and automatisation of the whole inspection process. In the optimal case, the PV module should not have to be reconnected or removed from the test rack until the end of the test cycle. This reduces the time required for test execution, analysis and report preparation. The size of a mobile PV test centre is determined by the main component, the solar simulator, which is used to measure the electrical performance.

An overview of commercially available products is shown in Table 12. Beside these, there are service providers or research institutes having developed their own mobile PV test centres (e.g. BrightSpot Automation, Chemitox, Enertis, Mahindra, PVLab Germany, ZHAW/EKZ mobile Flasher, Kirchner Solar). Most of these integrate pulsed solar simulators with Xenon lamps, e.g. BERGER, ENDEAS or PASAN, which are also used in ISO 17025 accredited PV test laboratories.

Table 13 summarizes the main technical specifications of the aforementioned products subdivided into general features, I-V measurement specifications, optical inspection tests and safety test capabilities. Most of the available products require dismounting of the PV module in order to test it in the trailer or container. Other products consist of a lightweight system with an integrated light source, which can be placed over the PV module strings in the field avoiding any dismantling of the PV modules. A typical throughput for STC power measurements with mobile PV test centres is between 200 PV modules/day to 400 PV modules/day depending on the type of solar simulator, the site, logistics and skills of the technicians.

The following paragraphs give an overview of the different inspection methods.

Table 12: Overview of commercially available mobile PV test centres.

Manufacturer of mobile PV test centres	
MBJ Mobile Lab	Suncycle CTULab
Ecoprogetti ECOTruck	Wavelabs Sinus-2100 outdoor

Table 13: Technical specifications of commercially available mobile PV test centres.
Note: The list is limited to some of the last generation products available at the moment of the preparation of this report.

Product	MBJ Mobile Lab 3.0 XL	Suncycle CTULab	Ecoprogetti ECOTruck	Wavelabs SINUS-2100 outdoor
GENERAL FEATURES				
Need of dismounting PV modules	yes	yes	yes	no*
Type	trailer	container	trailer	box
Weight	1500	200	810	45
I-V MEASUREMENT				
Light source technology				
LED (colours)	13	white	6	8+1 white

* If it is not possible to move the mobile PV test centre over the string (PV modules not accessible or too steep), the PV modules will have to be dismantled and a separate measurement station has to be set-up

Table 13: *(continued).*

Product	MBJ Mobile Lab 3.0 XL	Suncycle CTULab	Ecoprogetti ECOTruck	Wavelabs SI-NUS-2100 outdoor
Simulator class according to IEC 60904-9				
Spectrum	A+	ND	A+	A+
Uniformity	A+	A	A+	A
Stability	A+	A	A+	A+
Test conditions				
Max. test area	1050x2120	1100x1700	1400x2200	1300x2300
Irradiance range [W/m²]	200 to1000	up to 1500	200 to 1200	100 to 1000
Wavelength range [nm]	350 to 1100	400 to 800	300 to 1200	400 to 1100
Temp. control	yes	yes	yes	no
Sensors (irradiance, temperature, etc)				
Irradiance	reference cell	reference cell	pyranometer	no
Temperature	IR	IR	IR	no
I-V measurement system				
I/V ranges [A/V]	20/250	32/200	120/120	14/120
I/V accuracy [%]	±0.2	±0.2	±0.2	±0.2
Max. pulse duration [ms]	200	250	5000	80
OPTICAL INSPECTION TESTS				
Visual image	-	-	(x)	-
EL image	x	x	x	-
IR image	(x)	-	-	-
ELECTRICAL SAFETY TESTS				
Hipot	(x)	-	(x)	-
Ground continuity	(x)	-	(x)	-
Bypass diode functionality	x	-	(x)	(x)
Polarisation	x	-	(x)	-

(x) optional features

4.1.1 Electrical performance inspection

Various types of solar simulators are used in mobile PV test centres to determine the current-voltage (I-V) characteristic and respective PV modules' power at STC. Figure 12 gives an overview of typical configurations. These can work as single lamp systems or multiple lamp systems, where a single lamp irradiates a part of the test area. The light source is mounted into a dark box or container. This container can be also climatized to control the PV module temperature. The light source is either Xenon based or LED based. LED simulators differs in colors and number of integrated LED's. Therefore, the spectrum of the LED simulator may not cover the total wavelength range, where the PV module under test is sensitive. In this regard, Xenon-based simulators match better the AM1.5 reference spectral irradiance (see Figure 19). On the other hand, LED type solar simulators can achieve a much higher pulse length, which is advantageous for measurement of PV modules with high-capacitance cells (Section 5.1). The performance characteristics of a solar simulator are evaluated in accordance with the test standard IEC 60904-9:2020 [39]. For each required performance indicator (spectral match, spatial non-uniformity and temporal stability) a class is specified by the manufacturers, with a specific letter grade ranging from A+ to C. Mobile PV test centres use flash-type (pulsed) solar simulators only, in which the PV module under test is exposed to a constant light intensity for fractions of a second. The typical pulse duration lies in the range of 10 ms to several hundred milliseconds. Such pulsed solar simulators are often modified stationary solar simulators, which are used in test laboratories.

Pulsed Xenon lamp system (Tunnel type)
- Operated in a test room;
- Pulse time 10 ms – 100 ms;
- Low or no diffuse light.

Pulsed Xenon lamp system (Table-top type)
- Lamps and optical system are placed in a casing;
- Reflective walls or diffuser plate used for light homogenization;
- Module sunny side down onto a glass cover plate;
- High diffuse light component.

Pulsed color LED system
- Multi-color power LEDs cover a wide wavelength range;
- High diffuse light component;
- Long pulse >100 ms time possible.

Graphics: TÜV Rheinland

Figure 12: Solar simulator designs used in mobile PV test centres.

The I-V curve is traced with an integrated electronic load, which is dimensioned for the measurement of single PV modules. The PV module is connected to the I-V data acquisition system with separate leads for current and voltage (4-wire measurement). The I-V measurement is synchronized with the ignition of the flash and recorded during the pulse with a forward sweep (short-circuit to open-circuit) and/or backward sweep (open-circuit to short-circuit). Figure 8 of Chapter 3 shows the result of an I-V measurement with the main technical parameters that are typically reported.

Some mobile PV test centres also allow I-V measurements at different irradiance levels and/or temperatures for the determination of low irradiance performance or temperature coefficients.

4.1.2 Optical inspection

Most mobile PV test centres offer EL imaging, which is included in the automated test proce-dure. For EL imaging, an independent power supply is needed to inject current in the PV mod-ule, which corresponds at least to the nominal Isc. EL imaging must be done in darkness (e.g. inside the test centre), to avoid disturbance from other light sources. EL images are taken either by several cameras at fixed positions (e.g. six) or two to four cameras on a movable axis, each taking several pictures. The final image is then merged from the individual images. These procedures lead to a higher image resolution for the PV module, but require a closer positioning of the cameras to the PV panel to save space in mobile labs. Depending on the system, the quality of the final EL image can reach laboratory standards. Typical resolutions lie in the range 200 µm/pixel to 500 µm/pixel.

Infrared imaging of PV modules is only offered as an option for MBJ mobile PV test centre (Table 12). The measurement is performed with reverse current injection (Test current = nom-inal I_{SC}) and the IR image is integrated automatically into the test report. IR imaging can detect soldering issues in the interconnection circuit of solar cells.

4.1.3 Electrical safety tests

For most mobile PV test labs, different electrical safety tests are integrated. In addition to con-nection or polarisation check, most often a bypass diode functionality test is performed. Usu-ally, the bypass diode test is done according to IEC 61215-2:2016 MQT 18.2 [40]. A reverse current is applied to the PV module by connecting the power source's positive output to the PV module's negative terminal and the power source's negative output to the PV module's positive terminal. With this configuration, the current passes through the bypass diodes in for-ward direction. Current and voltage are measured and compared to the diode forward voltage multiplied by the number of diodes. Another method is described by Baumgartner et al. [41] where all bypass diodes of a standard PV module can be tested in the field within a few milli-seconds, without opening the junction box.
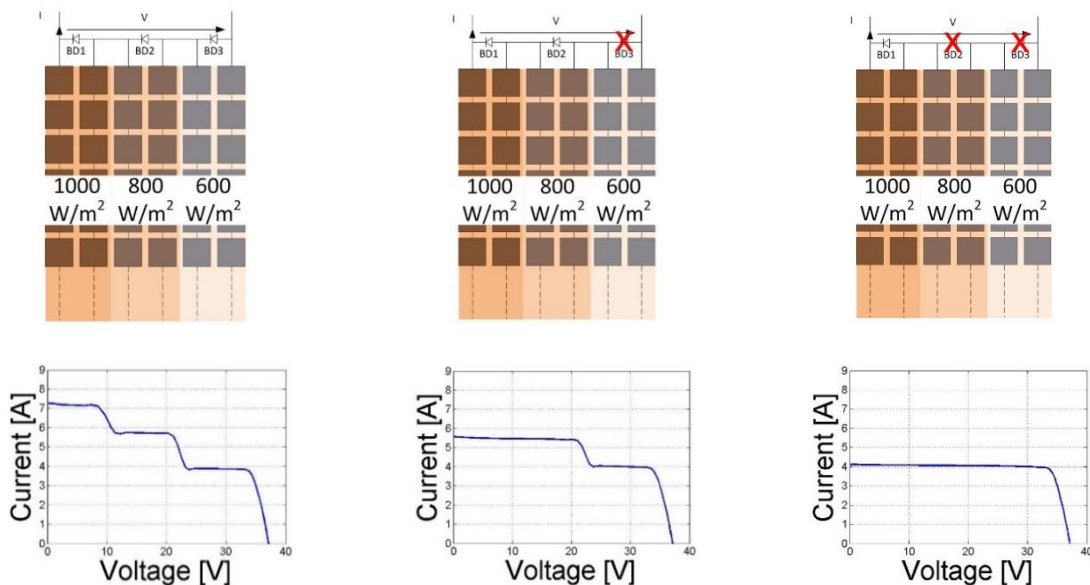

Figure 13: Field-test of bypass diode failure with an LED flasher [42].

By using an LED flasher, the three different sub-strings of the PV module, which are protected by an individual diode, are illuminated with different irradiance, resulting in different short-circuit currents. As shown in Figure 13, the shape of the I-V curve offers a different number of local maxima in power if one or more by-pass diodes fail. The analyses of these I-V characteristics can be done automatically and the LED flasher software shows the status at the end of the measurement.

In order to see whether the PV module is well insulated between current carrying parts and the frame or other outside accessible components, insulation tests are performed during production. The conformity of the installed PV modules should be verified again in the field to exclude not-conforming products or PV modules, which lost their insulation resistance due to aging. The continuity test shall verify that there is a conductive path between the exposed conductive surfaces, i.e. usually the four frame parts of the PV module, so that the exposed conductive surfaces can be adequately grounded in a PV system. A HiPot tester allowing for insulation tests according to IEC 61730-2:2016 MST 16 and continuity tests of equipotential bonding according to IEC 61730-2:2016 MST 13 [43] is mostly offered optionally. The measurements are fully integrated into the test procedure. In addition to the electric connection needed for I-V and EL imaging, all frame parts have to be connected (Figure 14). For the insulation test, the PV module is short-circuited and the insulation is measured between the short-circuit point and the PV module frame. A test voltage of 2000 V plus four times the maximum system voltage V_{SYS} is applied, for which the PV module is certified. For V_{SYS} = 1000 V the test voltage is 6 kV. The PV module passes the test if the measured leakage current is less than 50 µA. Voltage, duration, and limits can usually be configured. For the continuity test, a frame part is selected as return path and the applied current and voltage drop is then measured against all other frame parts. The PV module passes the test if the resistance between each frame part and the return path is less than 0.1Ω.
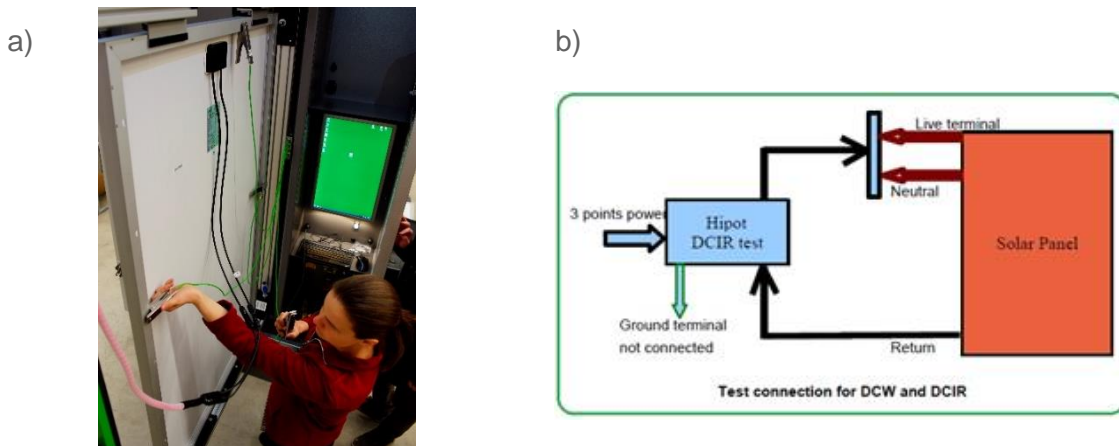
Figure 14: a) Example of PV module connection with clamps at the four frame parts for HiPot testing (insulation and continuity test) b) example of a test circuit [44].

4.2 Existing knowledge

The first mobile PV test centre was introduced in Switzerland in 2009 [45, 46, 42]. The "flasher bus" was equipped with a commercial class A pulsed solar simulator and was extended to include spectral response measuring capabilities for single- and multi-junction PV modules in order to further reduce the spectral mismatch error (Section 4.4.2). In single flash mode, a

throughput of 200 PV modules/day was achieved when limiting the measurement to STC power determination. The time effort increases for capacitive PV modules or measurements under non-STC conditions by about a factor of ten because multi-flash measurements are required. The single contributions to the STC power measurement uncertainty ($u[k=2] = \pm3\%$), as for example the impact of the required temperature correction and the irradiance non-uniformity, were analyzed in detail by the developers [41].

In the recent years, services from mobile PV test centres have been increasingly requested for the inspection of utility scale PV systems resulting in new products in the market. One of the major changes came with the introduction of LED simulators [47, 48, 49]. Over the past years great technical progress has been made to improve the repeatability of measurements and uncertainty in STC power determination, to simplify the measurement execution and to combine different inspection methods to increase the effectiveness of failure detection [50, 51, 52, 53]. To overcome the disadvantage of dismounting the PV modules from the field, a first lightweight system was developed in 2014, which can be moved over the PV system strings [50, 54, 55].

The need of statistical relevant batch testing and strategies to optimize PV module selection are discussed by different authors [51, 53, 54, 55, 56]. A statistical analysis presented by Eternalsun Spire [56] on around 6500 new PV modules imported into Europe in 2019, showed an example of how accurate power ratings can be and how important it is to have a good measurement accuracy. The study included 96 different PV module types from 29 different manufacturers which were tested between January and September 2019 in their laboratory in the Port of Rotterdam. Around 25% of the PV modules in Figure 15 exhibited a power below the rated STC power. But considering a measurement uncertainty of ±2% only 4.6% can be effectively considered to be below the rated power. Would the measurement uncertainty be ±5% none of the PV modules would fail the IV test.
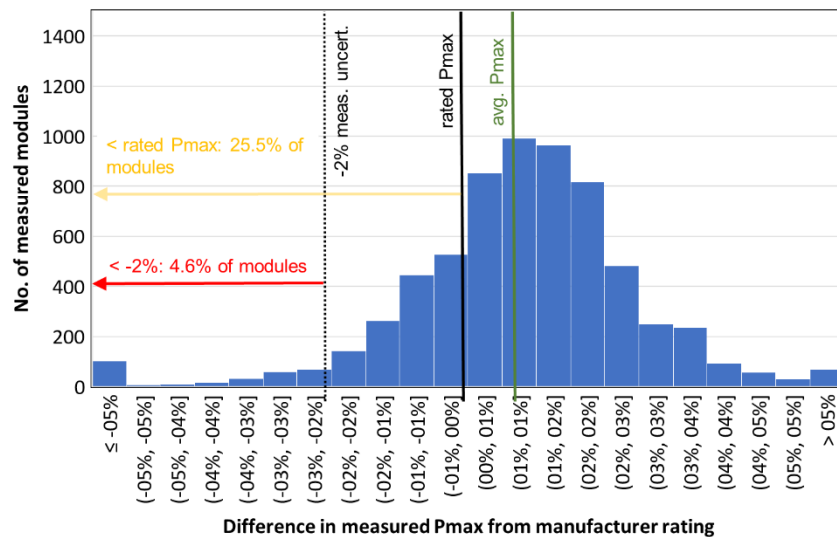

Figure 15: Measured difference from rated P_{max} of 6515 PV modules measured in 2019 [56].

Jaeckel at el. presented an approach, which combines mobile testing with stationary laboratory tests, aiming to reduce the financial risk by improving the measurement uncertainties while keeping the testing costs reasonable [51]. Furthermore, Pandey et al. of Mahindra Susten Pvt. Ltd. reported their approach for quality assurance, which combines string level inspections with measurements by means of a mobile PV test centre [53].

4.3 Detectable failure types for PV modules and PV arrays

Beside the proof of under-performance, a large number of hidden PV module failures can be detected with a mobile PV test centre. A statistically relevant number of PV modules can be selected directly from the field or from delivered pallets giving not only feedback on failure types but also on failure frequency.

The description of the different failures and detection methods can be found in various technical IEA PVPS Task 13 reports [57, 58, 18]. Table 14 gives a summary of the failures which can be detected with the inspection methods integrated into mobile PV test centres. In some cases, a combination of more methodologies is needed to get a reliable answer.

Table 14: List of failure types detectable with a mobile PV test centre (depending on integrated inspection methods). Legend: (x) detected only under certain conditions e.g. progressed failure, high measurement accuracy or in combination with other methods.

Failure types [57]	IV	EL	IR	INS	BYD	VIS
Low STC power (under-rating, degradation)	(x)					
Cracked cells or interconnects	(x)	x				(x)
Low insulation resistance				x		
Hot spots			x			
Defect bypass diode	(x)				x	
Potential induced degradation (PID)	(x)	x				
Delamination, burn marks, yellowing, defect backsheet	(x)					x

Underperforming PV modules are identified through I-V measurements. The combination with other methodologies gives answers or hints about the origin of the observed performance losses. Classifying underperformance is either based on relative deviations observed between the PV modules or in respect to the manufacturer's specifications: nominal output power for new PV modules or guaranteed output power according to warranty declarations e.g. -3% in the first year (initial degradation) and an annual degradation rate of -0.6%/year. The lowest acceptable PV module power P_{min} of a 3 years old PV module with a declared nominal power of P_{nom}= 300 Wp and a positive tolerance of t= -0/+3% would be 290.64 W minus the measurement uncertainty u(lab) of the mobile PV test centre. In the case of a measurement uncertainty of u(lab)= ±3% P_{min} would be equal to 281.9 W. In the case, of warranty claims the measurement uncertainty has to be proven and the quality control of the equipment should conform with the ISO/IEC 17025 standards. If this is not the case, additional tests by an accredited test laboratory are required.

Potential induced degradation (PID) is one of the most severe failures in respect to PV yield losses. PID appears as an increasing power loss over time, which gets visible only a few years after installation. Therefore, it cannot be detected by mobile PV test laboratories when performed on newly manufactured PV modules. On aged PV modules, the failure can be detected by combining I-V measurements with EL imaging. Figure 16 and Figure 17 show some examples of measurements of PID affected PV modules. In a progressed stage, PID can be recognized by reduced fill factor, reduced open-circuit voltage and deteriorated partial load behavior. The EL pictures show a typical PID pattern with dark cells at the border and bottom of the PV module (close to the frame). In the early stages, the power degradation effect is low at high irradiation conditions whereas it is more pronounced at low light conditions. EL pictures taken at 1/10 of the rated I_{sc} current can therefore detect PID also in an early stage, before a power loss can be noticed. When selecting the PV modules to be tested with the mobile PV test centre, it is very important to know that only a fraction of the PV modules exhibits power losses and only in strings with a distinct voltage polarity with respect to the ground. p-type or n-type solar cells will degrade when installed close to the negative or positive polarity, respectively. The power loss is more pronounced with increasing voltage potential, as compared to ground. This depends on the voltage (number of PV modules in series per string), the inverter topology (transformer) and the grounding concept.
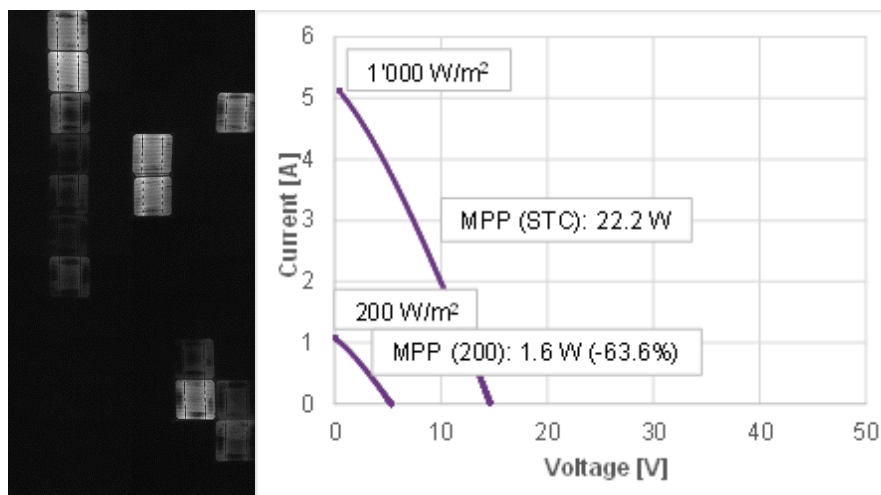
Figure 16: Example of a progressed stage PID affected PV module with power loss of 89%, left: EL at 1.5 x I_{sc}, right: I-V curve of the same PV module at 1000 and 200 W/m^2 [59].

Cell cracks is another type of failure, which is easier to evaluate by combined testing. Depending on the number of cracks, orientation and extension (Figure 18) micro cracks can have a different impact on the I-V curves or rather on the PV modules' output power. Power losses can range from no reduction to massive power losses. The severity depends on the affected area. A crack is considered as a major defect when its propagation isolates more than 10% of a cell's area. Micro cracks can be easily made visible by EL imaging. Sometimes they also show up visually as snail trails. Some manufacturers and research institutes implemented softwares and/or published guidelines for classifying micro cracks based on their severity or possible causes [60, 61].
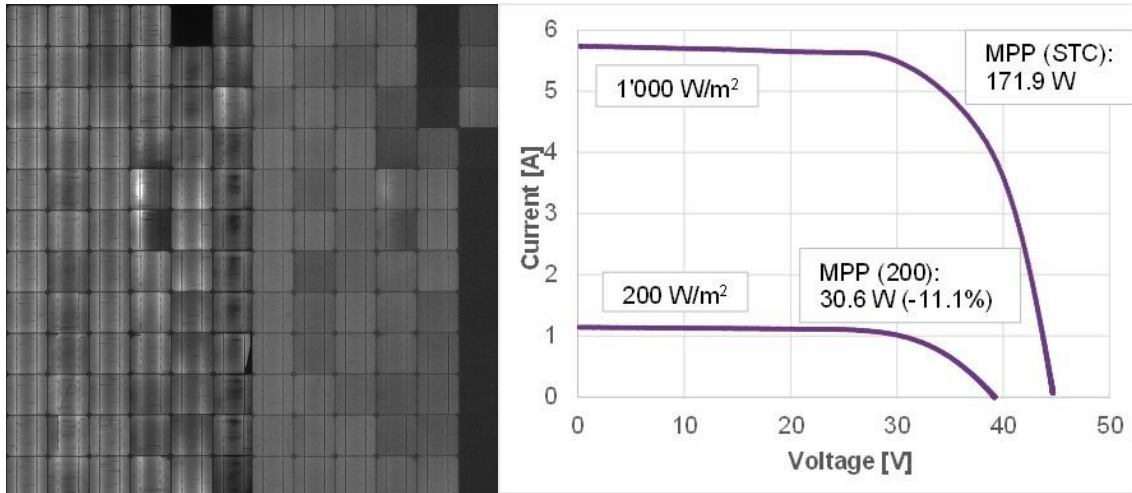
Figure 17: Example of an early stage PID affected PV module with power loss of 14%, left: EL at 1.5 x I$_{sc}$, middle: EL of the same PV module at 0.2 x I$_{sc}$, right: I-V curve at 1000 W/m² and 200 W/m² [62].
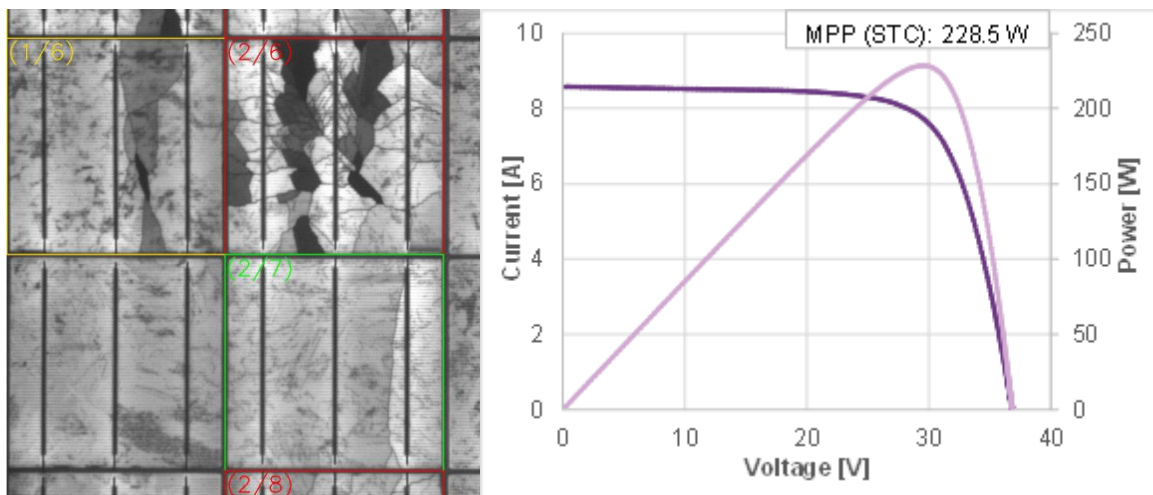
Figure 18: left: Example of different classifications of micro cracks, green: uncritical cracks with almost no cell area affected, yellow: less than 20% of cell area affected, red: massive parts of cell area are affected, already disconnected parts seen in black, right: I-V curve of the same PV module showing only a slight power loss of 3% [62].

Bypass diode failures (e.g. missing or not properly connected diodes, mounted the wrong way around or diode shortcuts) are detectable with most mobile PV test centres. Bypass diodes fail either because they are undersized or because they are exposed to high voltages due to lightning strikes or other high voltage events. The problem is that diode failures will not affect the performance until the PV module/system is exposed to a risk or bypass diodes are activated. The testing of bypass diode functionality in the field is therefore strongly recommended. The improvement in nominal output power of crystalline silicon PV modules on the market comes along with an increase of short-circuit current and number of solar cells. Thus, the rating of the bypass diodes must be taken carefully by the PV module producer to reduce bypass diode failures in the field. Defective bypass diodes could result in hot spots inside the junction box

64

causing a power loss in the affected PV module but also other PV modules within the same string by shifting their maximum power point.

Insulation failures are safety issues and might be caused by scratches on the back sheet, glass breakage, cracked insulation in wires or connectors, or production failures. With the usual insulation test provided by mobile PV test centres only severe insulation failures that show up in dry test conditions can be found. On the other hand, insulation failures often appear first in wet conditions, which are not covered by standard test procedures of mobile labs. To find these failures, additional tests like a wet leakage current test are needed or the measurement can be done in the field during wet conditions (usually in the morning) e.g. on string level. Missing continuity between conductive surfaces, e.g. because of loose frame parts, can be found with the continuity test.

4.4 Best practice recommendations

The following paragraphs provide best practices for inspecting PV modules with mobile PV test centres. The recommendations can slightly change depending on the mobile PV test centre in use.

4.4.1 Adjustment of solar simulator irradiance

The adjustment of the solar simulator light intensity is generally performed with a reference PV module or a reference cell, which is calibrated by an accredited test laboratory. The reference cell or PV module shows the traceability of the calibration and is a key element of the measurement uncertainty. Usually there is also a separate monitoring PV module that is shipped together with the mobile PV test centre. The purpose of this reference PV module is to verify the flasher's performance and detect any problems that may occurred during the transportation of the mobile PV test centre. The monitor PV module should be measured before and after each measurement session.

In order to keep the measurement uncertainty low, the reference PV module shall fulfil the following requirements:

- Size adjusted: Both reference PV module and fielded PV modules should have the same size and electrical circuitry to avoid measurement errors associated with effects of non-uniform irradiation;
- Spectrally matched: Ideally the reference PV module should be processed with the same cell type to reduce uncertainties related to spectral mismatch;
- Optically matched: The optical properties of materials (in particular front glass) should be equivalent to the fielded PV modules to guarantee comparable transmittance effects.

Because of impacts associated with non-uniform irradiation on the reference PV module, it is normally not possible to exactly reproduce both the calibrated short-circuit current and maximum output power at the same time. This offers two possibilities for adjustment of the light intensity: a) The reference PV module delivers the calibrated I_{sc} value and b) the reference PV module delivers calibrated P_{MAX} value. Table 15 summarises the advantages and disadvantages of both methods. For both Xenon- and LED-type solar simulators used in mobile PV test centres it is recommended to adjust the light intensity by referencing the calibrated P_{MAX} value of the reference PV module.

Table 15: Methodologies for adjustment of solar simulators in mobile PV test centres.

	Referencing calibrated I_{SC} of the reference PV module	Referencing calibrated P_{MAX} of the reference PV module
Advantage	Almost independent from PV module temperature and connection technique.	Better compensation of non-uniformity effects.
Disadvantage	Non-uniform illumination of a PV module will mainly affect its I_{SC}. Increase of non-uniformity will cause lower I_{SC}. Thus, a higher irradiance setting is required to deliver the calibrated I_{SC}, which results in overestimation of P_{MAX}.	Requires a careful PV module temperature measurement and PV module connection technique to the I-V load. Faulty contacts will cause a higher irradiance setting to deliver calibrated P_{MAX}. This causes overestimation of PV module I_{SC}.

4.4.2 Spectral mismatch correction

Due to the fact that the spectrum of a solar simulator is not equal to the reference spectrum AM1.5 [20] and the type of reference cell/PV module and PV module under test are not exactly the same, an error in the current measurement will be introduced. The so-called spectral mismatch is a key factor for the measurement uncertainty budget. Figure 19 shows an example of the spectrum produced by a Xenon- and LED-type solar simulator together with the reference spectrum AM1.5 and spectral response of a standard c-Si and n-type PERC module.
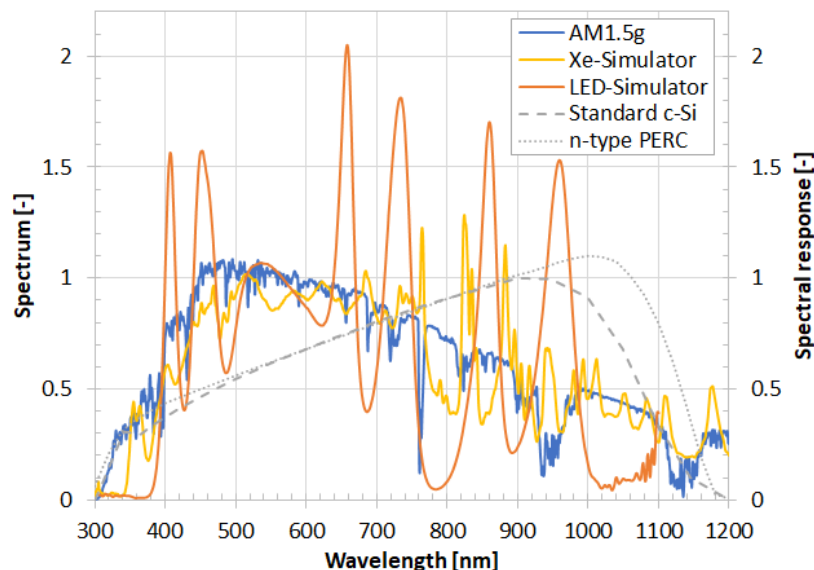
Figure 19: Comparison of the spectra from Xenon and LED flasher together with the standard spectrum AM 1.5G and spectral response data of a standard c-Si and n-type PERC module [63] [64].

The spectrum of the Xenon flasher with a class A+ is well matched to AM1.5. In case of a class A LED flasher, there is some bias compared to AM1.5. This is due to the limited number of LED colours. As explained earlier if the reference PV module or cell are well matched, i.e., the spectral response is almost similar, the spectral mismatch or the error on I_{sc} is within ±0.5%. In case the reference PV module and device under test differ a lot, as shown in Figure 19 (standard c-Si and a PERC module), the error can be up to ±4%. In this example, the reason is due to the different spectral responses and lamp spectra in the range < 400 nm and > 900 nm. In this case, however, the measurement uncertainty can be reduced by applying a spectral mismatch correction according to IEC60904-7 [23], given that the 'real' spectral response of the device under test is known. The spectral response data can be provided by the manufacturer itself or can be measured at an independent certified test laboratory.

Beside the technical requirements, dust or soil can influence the optical properties and thus has an influence on the spectral response. PV modules shall therefore be cleaned before performing any measurements [65].

4.4.3 IV-curve measurement speed

Care must be taken that the used I-V measurement unit is able to measure PV modules with high efficiency cells, such as PERC and HJT. A high cell capacitance can lead to significant measurement errors, that can be easily identified by determining the measurement differences between the forward sweep (short-circuit to open-circuit) and backward sweep (open-circuit to short-circuit) [66]. Manufacturers implement different solutions to overcome this problem, but the user has to know how to recognise capacitive PV modules and how to avoid or reduce eventual measurement errors. The sweep speed of 250 ms (possible with most systems) is sufficient to measure most of the available PV modules today. However, with the increase of PV module sizes and efficiencies, the limit could be reached, requiring further attention. Some heterojunction PV modules can lead already to 5% difference nowadays, between forward and backward sweep.

4.4.4 PV Module handling and temperature control

In general, the selected PV modules should be dry and clean for the safety and longevity of PV the equipment but also not to distort the results caused by dirt on the front glass. The PV modules should not be non-uniformly irradiated (e.g. partly shadowed) before measuring as this leads to a non-uniform temperature distribution within the PV module. If PV modules are dismounted from a PV array, they should be given sufficient time to reach ambient temperature.

The uncertainty of the power measurement is dominated by the quality of the cell temperature measurement which may deviate by several degrees from the reference 25°C. A temperature measurement uncertainty of 2°C will lead to an uncertainty in nominal power measurement of 0.5% to 1%, depending on the cell technology; e.g., when efficient PV modules are used with a lower temperature coefficient. The way that temperature is measured and stabilised depends strongly on the type of mobile PV test centre.

A.   Trailer- or container-based test centres placed close to the PV system

Best practice would be to store the PV modules before measurement without being exposed to direct irradiance or shaded under stable ambient conditions. If the storage temperature is near 25°C, temperature conditioning time can be shortened. Trailer-based mobile labs are

usually equipped with an air conditioning system to guarantee standard test conditions. Nonetheless, especially at low ambient temperatures, device temperatures can be inhomogeneous due to air flow, trailer opening and PV module loading. It is important to regularly check the device and reference cell temperature.

The higher the temperature deviation from 25°C is, the longer it takes to bring the PV module to 25°C. If there is no time to stabilise the PV module temperature or no air conditioning is available, temperature corrections have to be applied on the I-V measurements according to one of the procedures described in IEC 60891 [29].

For heating the PV module, some systems apply current to the PV module. However, this method has to be used with particular care because it can lead to other effects which could negatively impact the measurement. For newly manufactured PV modules, it should be noted that applying current to PERC modules may lead to a current induced degradation [67] whereas in aged PV modules the current flow may lead to an inhomogeneous temperature distribution in the PV module due to differences in the cells (e.g microcracks, inter-connects). The PV module should therefore have enough time to stabilise after current induced heat-up. Thin film PV modules can also be affected by current soaking after being stored in the dark [68].

B.   Lightweight flasher system on top of the PV system

With portable lightweight LED flashers measurements during the hottest time of the day should be avoided. This reduces the temperature gradient caused by the shading of the PV module by the light unit itself. Different methods for rear and front PV module temperature measurements are discussed in [55]; i.e., by calibrating with open-circuit voltage measurements [28], and by covering the PV modules for several minutes before the I-V measurement. These methods can reduce the temperature uncertainty to less than 1°C in the field test. An example on how to proceed with portable LED flasher measurement systems is described here:

- Shade the PV modules with a blanket (ten minutes before the measurement) in order to measure the electrical properties close to thermal equilibrium.
- If only a few PV modules should be tested on site, use the morning or late afternoon hours when the PV module temperatures are lower
- Optical IR sensors, mounted inside the light engine, can be used to measure the cell temperature and not only the glass temperature, which is measured with contact-based sensors are used. Using only ambient temperature sensors will lead to large uncertainty in measured STC power
- To check the quality of temperature correction over a longer period with varying ambient temperature, a reference PV module should be measured in regular intervals to verify the repeatability of the STC power measurement. Eventual deviations could be used to systematically correct the whole daily measurement run.
- The datasheet temperature coefficient used for the temperature correction of the measured power can be controlled by measuring a PV module in the morning prior total shading and during noon at highest relative constant cell temperature.

4.4.5 STC correction

The performance data of PV modules are commonly referred to the *Standard Test Conditions* (STC) that have been explained in Section 5.1. Accordingly, the output power measurement of a PV module performed with a mobile PV test centre will require the correction of a measured I-V curve from the test conditions (T1,G1) to the STC (T2 = 25°C, G2 = 1000 W/m²). The irradiance correction may not be required because irradiance setting has been performed with a reference PV module or reference cell. Temperature correction will be required if the mobile PV test centre is not equipped with controls for adjusting the PV module temperature. Procedures for the correction of measured I-V curves are defined in the IEC 60891 [29] and implemented in the operating software of the mobile PV test centre. The correction formulas for PV module current and voltage require the input of specific PV module parameters. In the case of temperature coefficients, the manufacturer's datasheet is a reliable information source. However, the irradiance coefficients such as series resistance are not provided in the datasheets and must be determined in the test laboratory. Due to the ageing of electrical contacts, the internal series resistance of fielded PV modules is not constant and will increase with exposure time due to degradation. These effects can be avoided when the I-V measurement is performed close to 1000 W/m².

4.4.6 Maintenance and calibration

Experience has shown that the classification of a solar simulator described in Section 4.1.1is not constant but subject to various factors:

Table 16: Factors to be considered for the maintenace and calibration of a Xenon or LED based solar simulator.

Xenon based flasher	LED based flasher
Ageing of lamp(s) over operation time	Ageing of single LED is negligible
Exchange of lamp(s)	Exchange of single LED boards
Lamp power settings	Light stabilization due to temperature (during long pulse flashes and operation at different temperatures)
Use of inserts in the beam of light such as optical filters or light attenuator masks	change of power of single LED channels to reduce light intensity might change uniformity and spectra
Ageing or soiling of inserts	Ageing or soiling LED boards
Reflections from the surroundings such as properties of test room walls	Reflections from the LED boards due to narrow space between board and PV module

Accordingly, the classification only refers to the actual operating conditions. Ideally, the classification as stated in the product specification or test report shall therefore cover the range of operating conditions during the practical use. It is recommended to periodically review the classification of a solar simulator against the requirements of IEC 60904-9. Onsite control of all measurement equipment, including the homogeneity of the light source and positioning of the irradiance sensors is recommended every time the test facility is moved to another location.

The following quality checks and calibration of the equipment shall be executed regularly:

- Uniformity check (Optical Misalignment due to transport), on-site
- Repeatability test (initial test with reference and/or monitoring PV module), on-site
- Spectral stability and uniformity of light source, after or before on-site use
- Calibration of I-V measurement system, yearly
- Calibration of reference PV modules or cells, yearly
- Calibration of temperature sensors, yearly

4.5 Measuring uncertainty aspects

The typically stated P_{MAX} measurement uncertainty of mobile PV test centres is around u[k=2] = ±3% [41, 52, 55, 60, 69]. This value is valid for standard crystalline silicon PV modules and under the condition that all best practice recommendations in Section 4.4 are followed. In daily practice, the uncertainty reached in the field can exceed this value due to:

- unavailability of a perfectly matched reference PV module (for size and spectral response)
- unknown spectral mismatch
- deviation of real temperature coefficient from datasheet values
- inappropriate thermal stabilization (set point and uniformity)

The solar simulator classification (letter grade) by itself does not guarantee a certain level of measurement confidence or measurement uncertainty. Specifically, the spectral classification must be carefully considered because it may not be well correlated with the spectral mismatch. For example, a class C spectrum may deliver a lower spectral mismatch for a certain PV technology compared to a higher-class spectrum. The estimation of the spectral mismatch error is therefore of primary importance.

Table 17 shows the uncertainty contributions of a high precision STC performance measurement in an ISO 17025 accredited laboratory (where a spectral mismatch correction reaches u[k=2] = ±1.6% for a crystalline silicon PV module) compared to the range of uncertainties observed in mobile PV test centres. The range is given by the level of implementation of best practices. Only temperature and optical uncertainty contributions are considered, being the main source of differences between a stationary and a mobile solar simulator.

Different intercomparisons between mobile PV test centres and stationary test laboratories accredited for STC power measurements have been published elsewhere [41, 51, 52, 55, 60, 69]. A difference lower than 3% in individual STC PV module power and lower than 1.5% in a sample of ten PV modules was found in 2017 during a comparison of outdoor power measurements with ZHAW LED prototype flasher II and indoor measurements in the certified labs of SUPSI [55]. A comparison between the portable LED flasher and the high quality JRC Labs within the same temperature-controlled laboratory facility exhibited a difference within 1% in power [54].

Table 17: Typical P_{max}@STC uncertainty contributions achievable with a mobile PV test centre compared to a high precision measurement in an accredited test laboratory.

Contributions	Example of P_{MAX}@STC uncertainty of an ISO 17025 accredited test laboratory	Typical P_{MAX}@STC uncertainty in the field with a mobile PV test centre
Temperature uncertainties		
Temperature sensor	0.18°C (RTD)	0.5°C to 1°C (IR sensor)
Temperature stability	0.5°C (climatised dark room)	1°C to 2°C
Temperature non-uni-formity	0.5°C (climatised dark room)	1°C to 2°C
Irradiance uncertainties		
Calibration of reference device	0.5% (primary ref cell)	2-3% (secondary calibration of ref. PVmodule)
Spatial non-uniformity	1% (class A+)	1% to 2%
Spectral mismatch	0.5% (spectral MM correction)	0.5% to 3%
Combined expanded P_{MAX} uncertainty (k=2, >95%)	±1.6%	±2.7% to 4.8%

4.6 Occupational safety

Besides the already described safety rules for handling PV modules or accessing PV systems, the manufacturer's safety instructions must be followed. These include general trailer safety instructions, warnings about high voltage or exposure to high radiation intensity. Entering the trailer is only allowed to authorized/trained personnel and when the equipment is disconnected.

4.7 Transportability

Mobile PV test centres comprise very often test equipment "on wheels", which is built in a trailer or truck. Depending on the type and weight of the vehicle, special driver licence could be required. In case the PV system site is not easily accessible by vehicle, a nearby location has to be selected to park the test system given that the PV modules can be easily stored and handled for testing. Trailer systems need an even, stable underground that can withstand the weight. Some manufacturers of mobile PV test centres offer dismountable test equipment, which can be packed in boxes and shipped to the field or transported in a standard station passenger car.

The system should not be placed in direct sun, to avoid overheating of the equipment. Air conditioning should be provided, if required. Appropriate power supply has to be guaranteed to allow safe operation. All moving/loose components in the vehicle (e.g., reference PV modules) should be safely stored and fixed for the transportation. After positioning the system in the field, quality control measures according to the manufacturer recommendation should be performed to assure that no misalignment of the light source has occurred due to transportation.

4.8 Cost considerations

To ensure a successful quality control measure, two main criteria should be met: 1. it should bring more value for the customer than is generates expenses, 2. results should be reliable so that decisions can be based on those.

First criterion can be met if measurement of the PV modules is made efficiently and without disturbing other site activities. Well thought workflow and semi-automatic operation of the equipment will greatly reduce the expenses and thus makes it easier to reach the first target. Typical testing costs of PV modules with mobile PV test centres are on the range of 20 to 30 €/PV module when a few hundred of PV modules are measured per day. Traveling distances and related expenses may however have great influence in case of remote locations. Second criterion is a result of the measurement uncertainty and will highlight the importance of the case specific uncertainty analysis. Measuring uncertainty will become a critical figure when warranty claims are based on measuring results.

The increase of sample numbers of electrical power test of PV modules in a plant are limited by the economics of costs of the test itself. A relevant cost share is given by the manpower of dismounting the PV module under test and again installing the PV module after the test by either a mobile test lab located elsewhere in the field or an indoor test lab. This handling costs are avoided by placing the light source of a portable LED flasher on top of the PV module in the field. There are still remaining costs given by disconnecting the PV modules in the PV string and the manpower of typical two employees operating the LED flasher which have to access the location only once.

5 DARK I-V MEASUREMENTS OF PV STRINGS AND PV MODULES

5.1 Description of inspection method

Due to its simplicity, the method of measuring unilluminated, hence "dark", voltage and current characteristics of devices was established quite early as a testing method for photovoltaic devices. It was however abandoned because of a major problem: If one were to paint a PV module fully black on each side, the dark I-V measurements would still report the same results, as any optical problems, or other effects that hinder the primary photocurrent generation, cannot be observed.

The device under test (DUT) typically has two main electrical connections (+,-), which are connected to a controlled power supply. A voltage sweep results in currents that characterize the DUT. If the voltage sweep is done under forward bias, one obtains the voltage dependent current of DUT in one quadrant of the voltage-current plot, Figure 20. In case of PV module or PV string this not only includes the current through the cells, but probably also a quite small leakage currents through the reversely biased bypass diodes. In negative voltage, the PV cells might show some leakage current, while most of the current is typically conducted through the bypass diodes. The electric interactions with the frame (additional electric connection) of PV Modules is typically ignored, as they often occur at larger AC due to capacitive effects, frequency, or require large DC offset voltages to produce small galvanic currents (i.e. through Na-ions in the case of potential induced degradation).
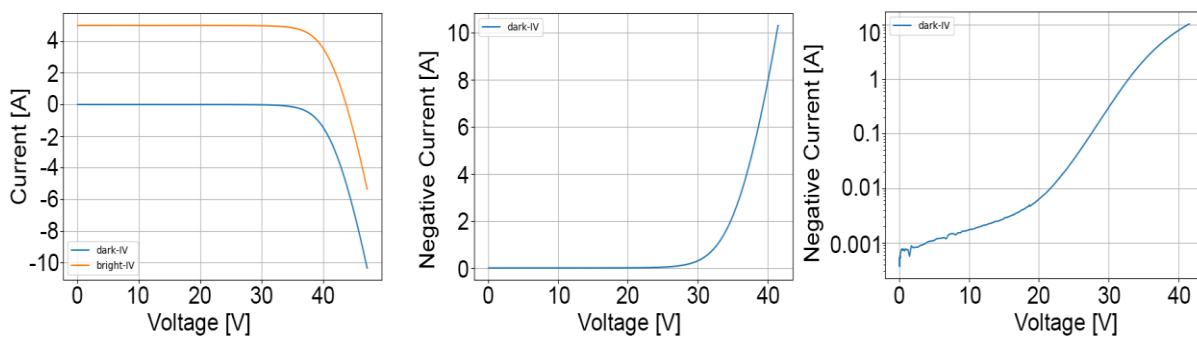
Figure 20: Left: Synthetic comparison of bright I-V to dark I-V characteristics of a PV module. As the dark I-V is only in one quadrant, it is common to inspect the negative current (middle), and the plots of the logarithmic negative current (right).

For a crystalline Si PV cell, short circuit currents (under irradiated STC conditions: I_{sc}) of up to 7 to 10 A are common. This is also a good approximation for a suitable maximum evaluated current in the dark, which is typically observed at a voltage larger than the bright STC open circuit voltage. However, also suitable data acquisition should be performed at voltages lower than that, and hence the current measurement needs to be quite accurate: The example given in Figure 20 shows a bright I_{sc} of approx. 8 A, and hence should also sample the dark I-V curve up to that current. The dark current at 10 V (approx. 20% of $V_{OC,STC}$) is approx. 2 mA, which corresponds to 0.25 permille of $I_{SC,STC}$. Actually, the better the DUT, the less current is

transmitted for lower voltages. If one were to use a measurement system that measures currents of up to 15 A using 16 bit analogue digital converters (ADCs), the theoretical resolution would be $15/2^{16}$ A=0.23 mA. As in such systems, the practical resolution (e.g. due to noise) is often less than the theoretical one, and for high performant cells leakage currents of less than 10 µA are not seldom, better ADCs are recommended. For the case of low current cells (e.g. 1 inch square lab scale), a large shunt resistor can convert the currents to similar measureable voltages. However, e.g. by using 32 bit ADCs with a voltage input of -2.5 V to 2.5 V, typically no signal amplification is required for typical 10 mOhm shunts.

The voltage measurement however is far less critical, a better than 0.5% V_{oc} resolution is only needed when evaluating characteristics with some very low irradiation, e.g. as for the case of indoor photovoltaics (e.g. on pocket calculators).

For the temporal resolution, there are two things to consider: firstly, too fast sweep times can cause problems with highly capacitive cells. PERC-cell modules in the regime of V_{mp} to V_{OC} exhibit capacity in the range of up to 400 µF. With a typical series resistance of 200 mOhm, the filter frequency is ~2 kHz for each measurement point. With the assumption of at least 512 measurements for the whole voltage range, the sweep time should be longer than 0.25 seconds. For perovskite cells, it is known that the sweep time should be much slower, e.g. in the range of mV/sec due to the so-called hysteresis effect.

On the other hand, during a dark I-V measurement, the electric energy V*I heats the PV module. In the case of a crystalline PV module, more than the M_{PP} power is dissipated in the high current regime of the dark I-V measurement. In reverse voltage, a similar measurement would cause heat up of bypass diodes. As the thermally coupled system of cells, encapsulation materials, glass, air has individual thermal masses and resistances, in most cases a local heat up of cells is unavoidable, and affects the measurements. This is clearly visible with bi-directional voltage sweeps in the form of a current hysteresis.

Dark I-V measurements need to be performed in shaded conditions. As most test systems are only able to supply energy to the DUT, the producing part of the I-V characteristic is not accessible. Practically, this means that only voltages above the irradiation dependent V_{OC} of the DUT can be measured, and at larger voltages, there exists a shift in current in the range of the irradiation dependent I_{SC}.

The method can be used qualitatively. By comparing different PV modules or PV strings, e.g. enhanced leakage current, corresponding to decreased parallel resistance, or effects of the series resistance can be found.

Additionally, one might perform analytic evaluations to estimate the series resistance, or try to fit analytic models such as the two diode model. The drawback with the latter is that a series connection of cells does not exactly behave like a two diode model. Additionally, the fitting of the secondary diode can be inconclusive if the primary leakage mechanism originates from the parallel resistance.

5.2 Existing knowledge

A major contribution about the extraction of the diode model parameters was published 1997 by King et al. [70].

In recent years, Mertens et al presented PV string dark I-V in [71]. A hardware setup development process was shown in [72]. A method to extract the series resistance in an analytic way from a single dark measurement was presented in [73].

Typically, dark I-V measurements are ideally performed at 25°C to allow comparison with STC bright I-V characteristics. However, this is not practical for outdoor applications, and hence a need for temperature compensation arises. This was approached using machine learning by [74].

5.2.1 Market overview of instruments

While measurement of dark I-V is common on cell levels, few turnkey systems for whole PV modules and PV strings exist.

Some flash based PV module testers are able to perform dark I-V measurements of PV modules and cells, e.g. the Pasan/Meyer-Burger HighLight. They are however not suited for outdoor operation.

From the original intention of performing outdoor electroluminescence, "photovoltaikbuero", situated in Germany, created a system for turnkey dark I-V measurements, Figure 21. The device is able to inject up to 5 A at up to 1 kV into the PV string, as long as the total power is below 3.3 kW, [75]. The advantage of this system is that it does not require three phase powering, while a drawback being that the current is not enough to observe a pronounced effect of the series resistance.

There exists a system to perform mobile measurements of individual PV modules developed by the Austrian Institute of Technology. The intended use is to perform a quick qualitative check before mounting PV modules in a PV plant, e.g. to detect transportation damage, Figure 22.

The direct usage of programmable power supplies is often limited by their inaccuracy of the current measurement. However, with an additional high precision current sensor a DIY solution is often feasible.
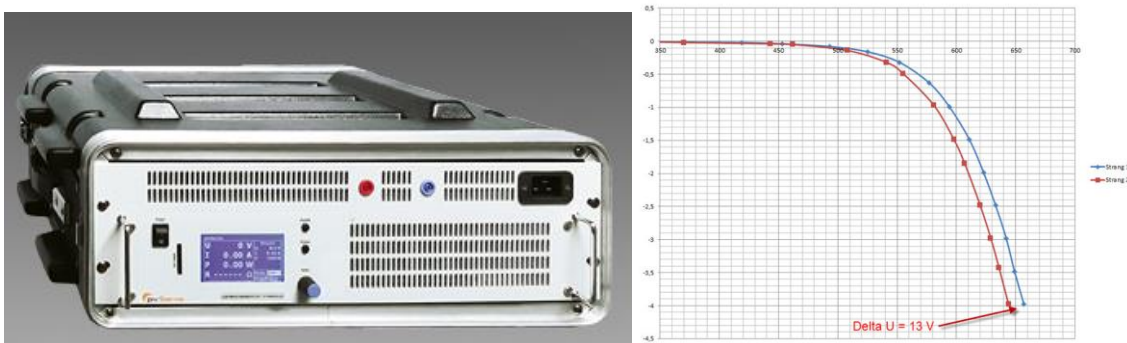

Figure 21: A dark I-V measurement system suitable for outdoor PV string and PV module evaluations produced by "photovoltaikbuero" [75].

Figure 22: A battery powered dark I-V measurement system suitable for outdoor PVmodule evaluations produced by "AIT". On the right, the previous prototype.

The method of dark I-V measurements is specified in Annex C of IEC 60904-1 Edition 3 [27].

5.3 Detectable failure types for PV modules and PV arrays

It is indisputable that some failures of PV modules cannot be investigated using dark I-V characteristics. Especially effects on the optical path, e.g. shading or browning will result in the same dark I-V characteristics. In most cases dark and bright I-V characteristics can be estimated by the one or two diode model. A PV string of PV modules can be seen as a series connection of groups ("PV sub-strings") of typically 20 cells that are each parallel to a bypass diode.

For the following simulations of failures, we assume that there are two types of cells, good ones or bad ones. They differ by their two diode modules. Then, we calculate a "good" PV sub-string and a "bad" PV sub-string, both containing an individual ratio of good and bad cells, and the effect of a bypass diode. From these two PV sub-strings, another ratio of good to bad PV sub-strings is defined. By varying the diode parameters and the ratios, many failure cases can be evaluated (Table 18).

The good cell is taken by a one diode model fit of the flash-measured bright I-V characteristics of an exemplary, anonymous PV module. Its parameters were found to be 8.94021 A for the photo current, 7.46385e-13 A saturation current, non-ideality 1.0302, series resistance 6.89436 mOhm, and a parallel resistance of 12.6047 Ohm.

These parameters are varied according to Table 18, to obtain the simulation results.

To estimate the exemplary failure case of shading, 50% shading is assumed for the affected cells. In a bad PV sub-string, half the cells are assumed shaded, while in a good PV sub-string, none are. In total, we assume to have ⅔ of the PV sub-strings unaffected, and ⅓ affected. The application of a bypass-diode is necessary, to result in realistic bright I-V curves. In darkness, these diodes only contribute by their reverse leakage currents, as determined by their Rp. This results in combined or individual dark or bright I-V characteristics, of which we normalize the voltages to an average cell. This allows for more compact visualization, Figure 23. As expected, dark I-V will not be able to detect this case.

Table 18: Modifying factors compared to the good cells' diode parameters, the ratio of good/bad cells in the "bad" PV sub-string, as well as the ratio of good PV sub-strings in the total PV sub-strings forming the "PV string".

|	Iph	j0	Rs	Rp	Ratio of "good" cells in affected PV sub-string	Ratio of "good" PV sub-strings in PV string
Shading	50%				50%	66%
Cracked cells	50%	50%	50%	200%	50%	90%
Weak PID/Rp				30%	50%	60%
Moderate PID/Rp				5%	50%	60%
Strong PID/Rp				0.5%	50%	60%
PID+Rs			150%	30%	50%	60%
Rs			300%		50%	60%

A change in total series resistance can be observed at larger currents than 25% of the I_{SC} at STC, Figure 24, although the relative effect on the PV string is the less the more undamaged cells exist in the PV string. Hence, Rs is easier observable on PV module level than on PV string level.

In the case of PID, which is caused by decreased parallel resistance of a part of the PV modules in a PV string, the observable effect depends on the advancement of the effect, Figure 25 and Figure 26. For weak PID, an increased leakage current can be observed in the kink of the characteristic, which is caused by the changing influence of the primary and secondary diode in the two diode model. The more pronounced PID gets, the larger currents are affected, finally leading even to a decrease at large currents.

Finally, the Table 19 enumerates observable effects, and their ease of observation in PV module or PV string dark I-V measurements.
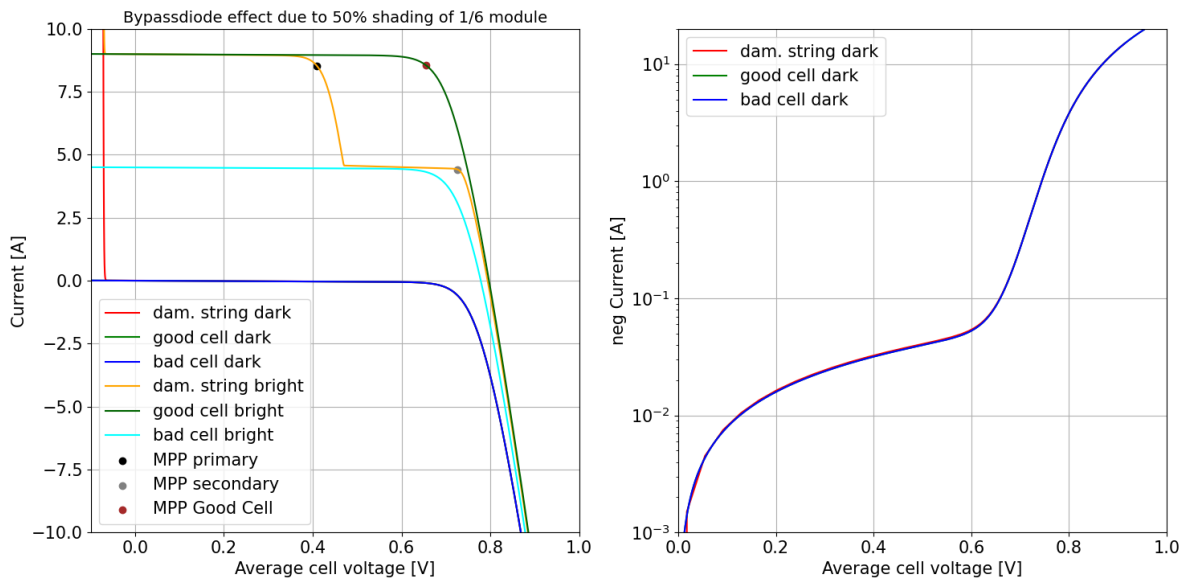
Figure 23: Left: dark and bright I-V characteristics of the shaded and unshaded cells, as well as the characteristic of the combination according to Table 18. Right, only the dark currents are plotted in logarithmic scaling. As shading has no effect on the dark currents, the damaged PV strings dark I-V is no different from the unaffected case. While measuring bright I-V, this failure could be found easily.
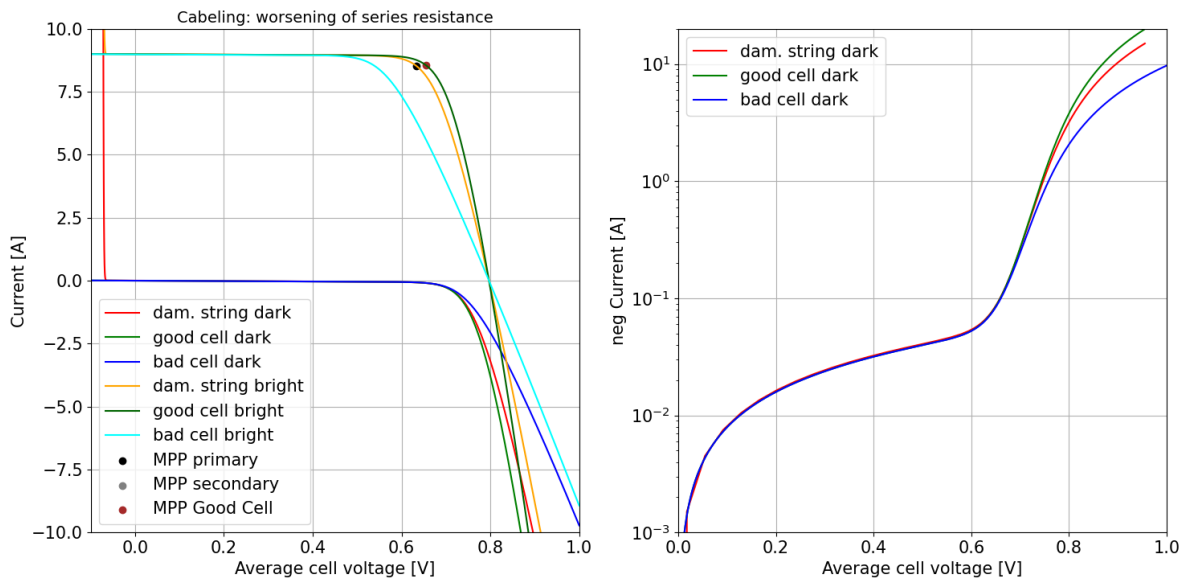

Figure 24: In case of some cells showing an increased series resistance, most often the bypass diodes do not start to carry current. Hence, all cells series resistances can be combined, and create a horizontal shift of the dark I-V by a voltage of Rs*I. This can be investigated the better, if the current measurement range is rather close to I_{SC}.
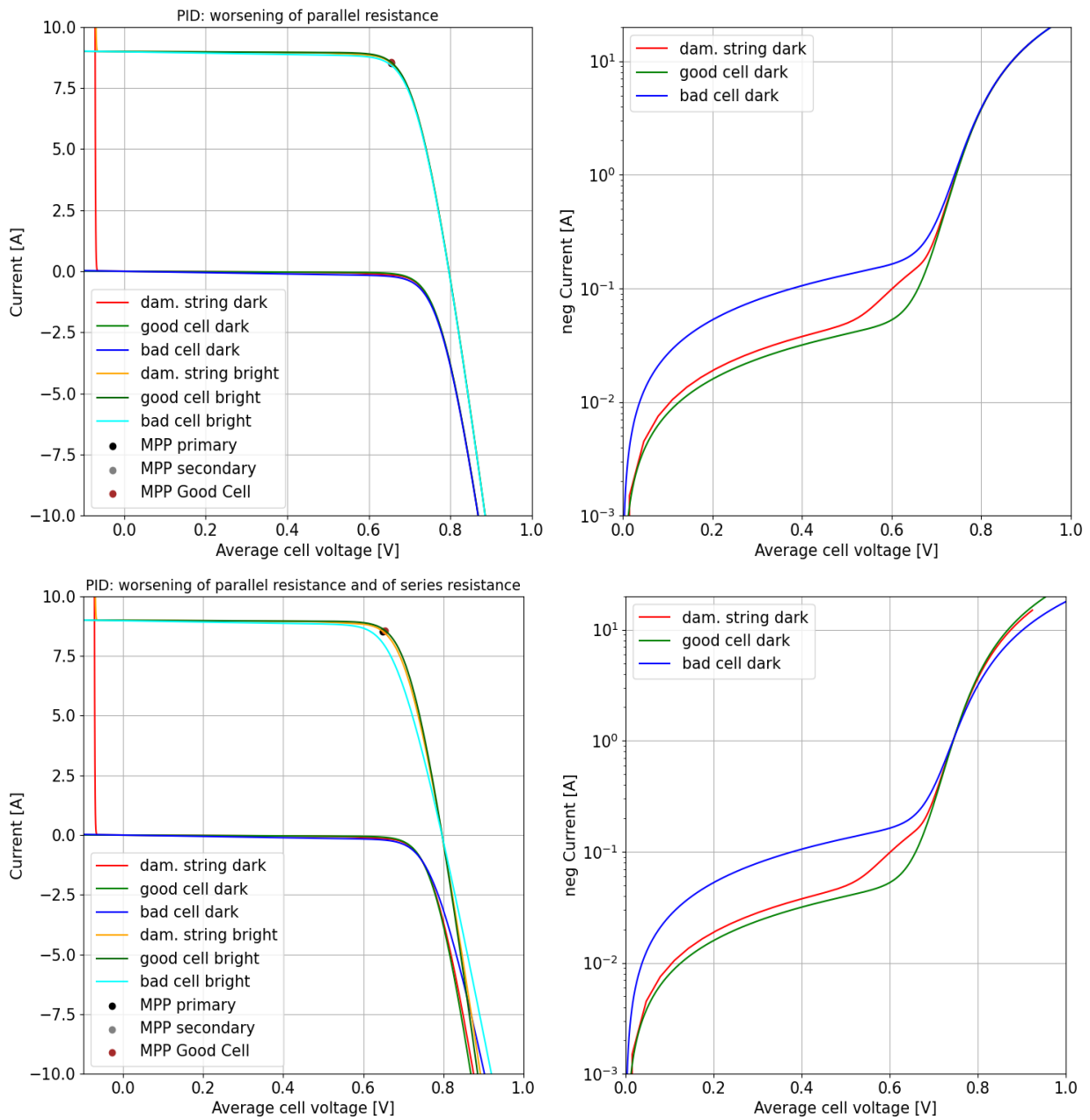
Figure 25: In case of a weak degradation of the parallel resistance, as it occurs in the initial phase of PID or LeTID, effects are very visible in the PV modules dark I-V characteristic, as the current below 50% V_{OC} is considerably larger. In case of a PV string measurement, the effect is less pronounced, but especially noticeable in the kink at ~⅔ V_{OC}.
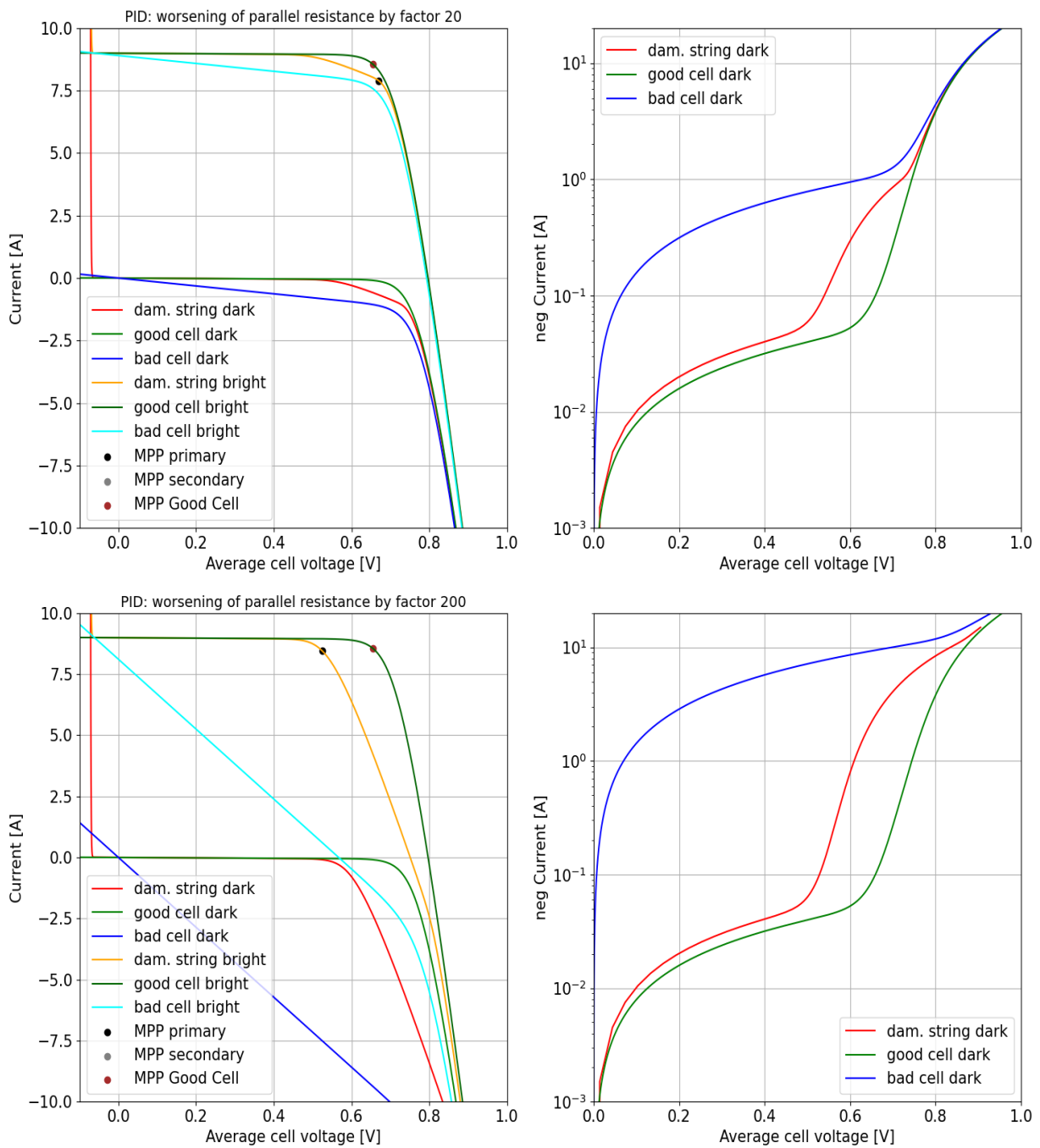
Figure 26: In case of a moderate and strong degradation of the parallel resistance, as it occurs in PID, PV module level dark I-V measurement shows clear results. On PV string level, the affected region expands towards larger voltages/currents.
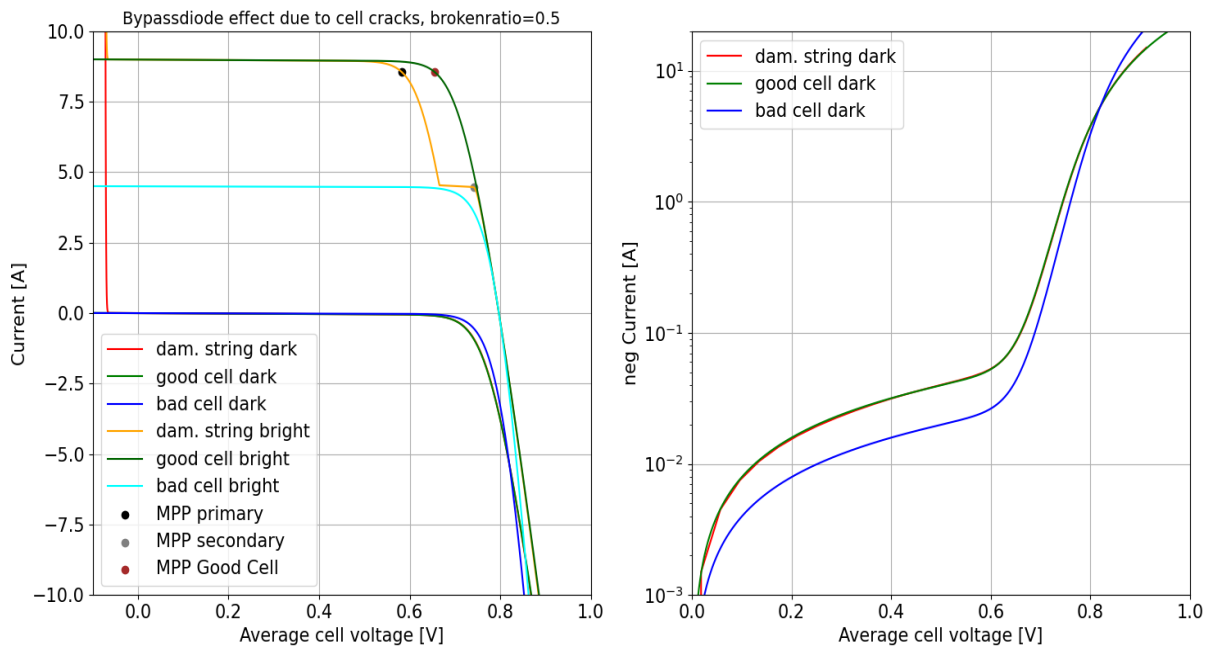
Figure 27: In case of cell cracks, the more unaffected cells exist in the measurement, the less pronounced the measured effects are. On PV string level, a detection of cracks might be quite difficult.

Table 19: Failures and ease of detection using dark I-V.

Failure	PV Module Level Dark I-V	PV String Level Dark I-V
Series Resistance	Easy (if current sufficient)	Easy(if current sufficient)
Parallel Resistance/ PID/LeTID	Easy	Easy
Cracked Cells	Possible	Difficult
Shorted Bypass Diodes	Easy	Easy
Open Bypass Diodes	Possible, reverse voltage	Possible, reverse voltage
I_{sc} Mismatch	Impossible	Impossible
Connector Resistance	Not applicable	Possible
Arcing	Voltage not sufficient	Possible

5.4 Best practice recommendations

Field measurements are often limited by the availability of power sockets. While a three phase connection is common for inverters, adding additional power sockets is seldomly considered. Some national regulations hinder the option to just connect to these phases. Power connectors typically exist in central inverters huts, but hence require long cable lengths to supply PV modules or PV strings.

The use of diesel generators is often hindered by their weight and the sometimes unsuitable terrain, as a suitable generator >5 kWp can only be lifted by more than two people.

In many climatic zones, unclouded nights cause the PV module temperature to drop below the dewing point. The wet surfaces can also appear on wires or power supplies, causing a safety risk especially when switching between PV modules. It partially helps to limit the measurement time to the early night hours, where PV modules did not cool down yet.

In terms of irradiance, a good starting time for outdoor dark measurements is to wait 1.5 h after sunset, which in summer can be quite late (e.g. 10 pm in Austria). Moonlight or street lights seem to not influence measurements.

For daytime measurements, shading needs to be applied to both the front and the backside of the PV modules, as the little light that goes through a nontransparent backsheet is sufficient to cause a notable open circuit voltage.

In case there is a total disconnection of the series connection within a PV module, the bypass diode parallel to this defective PV sub-string is blocking during a dark I-V measurement, as no reverse currents can occur. As common reverse breakdown voltages are typically 300 V, the current below this voltage limit should be compared to an expected value. If this test shows that the leakage current is far below expectation, the voltage should not be raised, as the overvoltage on the blocking diode could permanently damage it. This also applies to electroluminescence imaging. The problem is that for normal sized PV strings 300 V typically results in less current than a common power supply would display in its interface. Hence precise current measurement is important for the decision to increase the voltage further.

For free standing PV module strings, it is recommendable to only measure half of the PV modules at a time, if the circumstances allow it. This limits the required electric power. Additionally, the direct comparison between the two half PV strings can be used to pinpoint PID very clearly.

5.5 Measuring uncertainty aspects

A major uncertainty in comparison to laboratory measurements arises from temperature effects. While in the laboratory, PV modules are typically measured at 25°C, while outdoors, PV modules at nighttime typically show a temperature between ambient temperature (i.e. at cloudy nights) and up to 10°C below ambient in clear sky conditions. This arises from the thermal balance including radiative transfer from and towards the sky. While the PV module temperature can be measured, datasheet temperature correction factors for I_{SC}, P_{MAX} and V_{OC} do not apply for dark I-V. As the PV module temperature of winter measurements can deviate further than 25°C from STC, accurate corrections are quite demanding and are likely PV module type dependent, Figure 28. However, for many qualitative interpretations such a correction is not required.
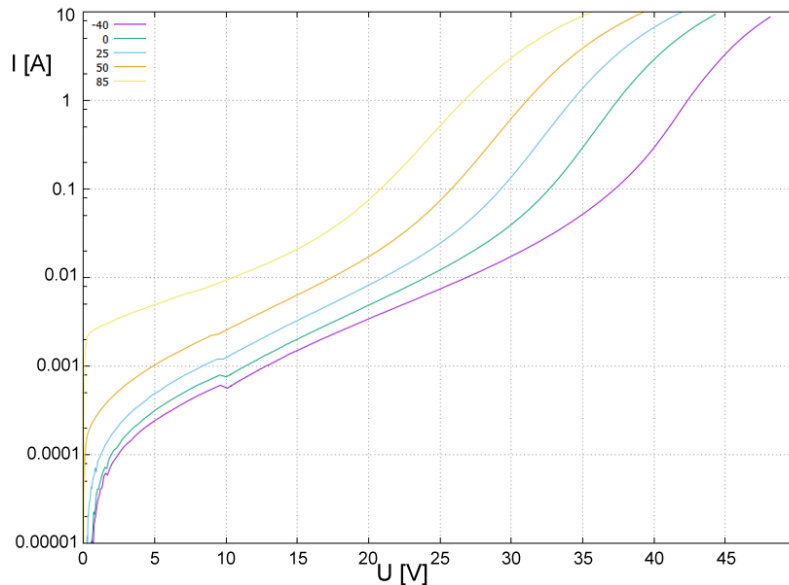
Figure 28: Temperature effects on the dark I-V characteristics. The colour indicates the temperature in Celsius.

5.6 Occupational safety

In case of PV string measurements, the applied voltages are often larger than 500 V, and requires similar safety measures as for bright I-V. As measurements are often performed at nighttime, in some climatic zones precautions need to be taken against night active animals (e.g. snakes in tropic regions). Proper grounding of the equipment should be checked, as dew might cause surface conduction. A tested residual-current circuit breaker is recommended.

5.7 Transportability

For PV string level measurements, the required power supply (ideally 1000 V, 10 A, 10 kW) can be difficult to carry by one person due to the weight of up to 30 kg. The dimensions commonly between one to four height units of 12'' industrial racks are hence easily suited for car transport. A battery powered PV module level system can be built with less than 5 kg of weight.

5.8 Cost considerations

A PV string level power supply typically cost below 2000 €. With the additional housing, control, and precise current measurement, a system should cost less than 3000 € in hardware.

The throughput is primarily limited by the time for connecting the wires. This depends on the size and structure of the investigated system. In a case where all inverters are next to each other, no PV strings are paralleled, and the inverter features connectors instead of screwed clamps, a typical PV string (up to 8 kWp) can be measured within five minutes.In the ideal case up to ~100 kWp may be measured per hour. This however is seldom true: If the operator needs to reposition the equipment, move the cables to a different location, or has to unscrew cables in combiner boxes or inverters, the measurement times can be dramatically increased.

Most often, one person is sufficient to operate dark I-V measurements, although national rules and regulations may enforce a second person being present for general work safety aspects.

6 PV PLANT TESTING VEHICLE FOR PV STRINGS

The PV plant testing vehicle is used for on-site performance testing of PV power plants, which are mainly composed of PV modules, DC or AC combiner boxes, inverters and transformers. PV power plants can be classified into grid-connected and stand-alone systems. Furthermore, PV power plants can also be classified into centralized, distributed and PV module string type in accordance with the inverter design. No matter how the design and type of the PV plant is, the main inspection and testing parameters basically include current-voltage characteristics of PV arrays, infrared imaging of PV modules and efficiency of inverters. The PV plant testing vehicle is a kind of refitted vehicle from van or box truck, and test equipment is installed inside the truck (Figure 29). Instead of individual test instruments, the PV plant testing vehicle has a multi-functional design and can perform testing, analyzing and evaluating performance parameters of PV power plants in conformance with IEC standards [33].

Figure 29: PV plant testing vehicle in China.

6.1 Description of performance test

6.1.1 Test method

In order to analyze and evaluate efficiency and energy loss of PV plant, yield of PV strings, combiner boxes and DC/AC of inverters should be measured simultaneously to avoid influence by the fluctuation of irradiance and temperature [76]. The details of the performance testing method are as follows:

Grid-connected PV systems can be divided into several sub-systems according to the quantity and sizing of transformer stations. Based on the installed capacity and historical monitoring data, candidate PV arrays for further inspection are selected from each sub-system, which refers to specific PV strings/arrays, combiner boxes, inverters and corresponding transformer stations. The test equipment is installed and connected to combiner boxes and inverters to measure real-time electrical power, DC current and DC voltage simultaneously. Based on the monitoring data of test parameters, conversion efficiency and malfunction diagnosis will be evaluated over a specific time period. The test period can be determined according to the IEC 61724-1 requirements [33]. Usually, the test period should be no less than seven days, with at least three sunny days (irradiation no less than 3 kWh/m^2/day).

The PV plant testing vehicle is suitable for monitoring of grid-connected PV power plants. It consists of meteorological monitoring equipment, DC combiner box testing equipment, PV string inverter testing equipment, centralized inverter testing equipment and AC combiner box testing equipment.

6.1.2 Measured parameters

The principle configurations of grid-connected PV plants are shown in Figure 30. Measured parameters by the testing vehicle cover each part of the PV power plant, including meteorological and electrical parameters as shown in Figure 31.
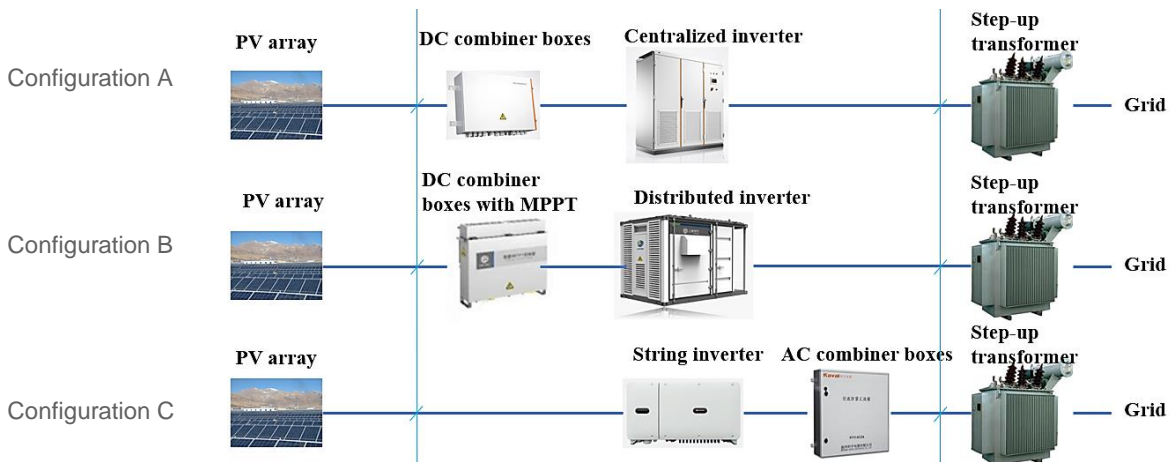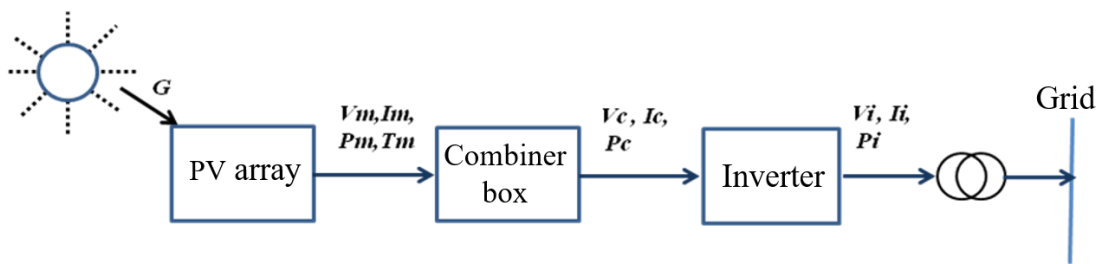

Figure 30: Principle configurations of grid-connected PV power plants.

V_m: Real-time voltage of PV string
I_m: Real-time current of PV string
P_m: Real-time power of PV string
T_m: Real-time temperature of PV string (typical PV modules temperature)
V_c: Real-time voltage of PV combiner box
I_c: Real-time current of PV combiner box
P_c: Real-time power of PV combiner box
V_i: Real-time AC voltage of PV inverter
I_i: Real-time AC current of PV inverter
P_i: Real-time AC power of PV inverter

Figure 31: Test parameters of PV plant testing vehicle.

6.1.3 Sampling

Sampling method: Candidate PV strings should be selected from several sub-systems of the PV power plant. The quantity of sub-systems is determined by the size of the PV power plant, as shown in Table 20.

Table 20: sampling requirement for quantity of sub-system.

Size of PV power plant	Quantity of sub-systems to be evaluated
<15 MW	≥2
≥ 15 MW to <45 MW	≥4
≥ 45 MW to <100 MW	≥6

6.1.4 Technical requirements

Table 21: Technical specification of the PV plant testing vehicle.

Technical specification of PV plant testing vehicle		
Functional requirements	• Meteorological monitoring equipment: No less than three total irradiation channels，one temperature and humidity channel，one wind speed and direction channel. The number of channels of the solar irradiation can be increased according to requirements • DC combiner box testing equipment: 16 PV string DC current input channels，8 PV string DC voltage input channels，1 DC current output channel • PV String inverter testing equipment：8 PV string DC current input channels，8 PV string DC voltage input channels，three-phase AC output channel (Max. PV string inverter capacity 50 kW) • Centralized inverter test equipment：4 DC input current and voltage channels，one AC output channel (Centralized inverter capacity between 500 kW and 1000 kW)		
	communication method	Ethernet，RS485，Wireless transmission and other communication methods
	Acquisition interval	1 to 1000 data points per second (optional)

Table 22: Technical specification of the PV plant testing vehicle.

Technical specification of PV plant testing vehicle		
Performance requirements	Accuracy of hall sensors	Current accuracy ±0.5% (DC:0~15 A, AC:0~80 A)
		Voltage accuracy ±0.5% (DC:0~1500 V)
	Data acquisition accuracy (PV string inverter)	Current accuracy ±0.1%;
		Voltage accuracy ±0.1%
		Power quality reaches the accuracy specified in IEC 61000-4
	Irradiance pyra-nometer	Secondary Standard
		(Class A, according to IEC 61724-1)
	Temperature and humidity sensor	Temperature accuracy ±0.2 K
		Humidity accuracy 3%
	Wind speed and direction sensor	Wind speed resolution: 0.1 m/s
		Wind direction resolution: 3°
	Synchronization	Synchronization better than 200 ms
Environmental requirements	Altitude	0 m to 5000 m

6.2 Existing knowledge

On-site testing method is a means of evaluating the performance of PV power plants. IEC 61724-1 standard have been published for performance evaluation of PV power plants including ground and roof-top PV systems, and many important parameters including the performance ratio (PR) and the energy yield are specified in the standards [33].

The testing equipment for PV systems contains the following instruments:

1. Meteorological instruments: pyranometers, ambient temperature sensors, anemometers, etc.
2. Instrument for PV module and PV arrays inspection: I-V tracers, electroluminescence (EL) and infrared (IR) cameras
3. Power analyzers and power quality analyzers
4. Current and voltage data acquisition units for combiner boxes

Due to changes of meteorological parameters under outdoor conditions, a non-synchronized data collection may lead to high uncertainties for the PV systems performance data. Therefore,

it is necessary to perform a simultaneous data acquisition of parameters and to integrate different measuring instruments into one testing unit. As a supplement of existing standards, the "Technical Specification for on-site energy efficiency testing and assessment of photovoltaic (PV) power plants" standard was released in January 2020, which was published by Chinese Society for Electrical Engineering (CSEE) [76].

6.3 Detectable failure types for PV modules and PV arrays

This section gives examples of some achieved field test results with the testing vehicle. These testing results reflect typical failures and malfunctions in PV systems such as PV module breakage, shading issues, inverter MPPT problems, and PV string connection failures.
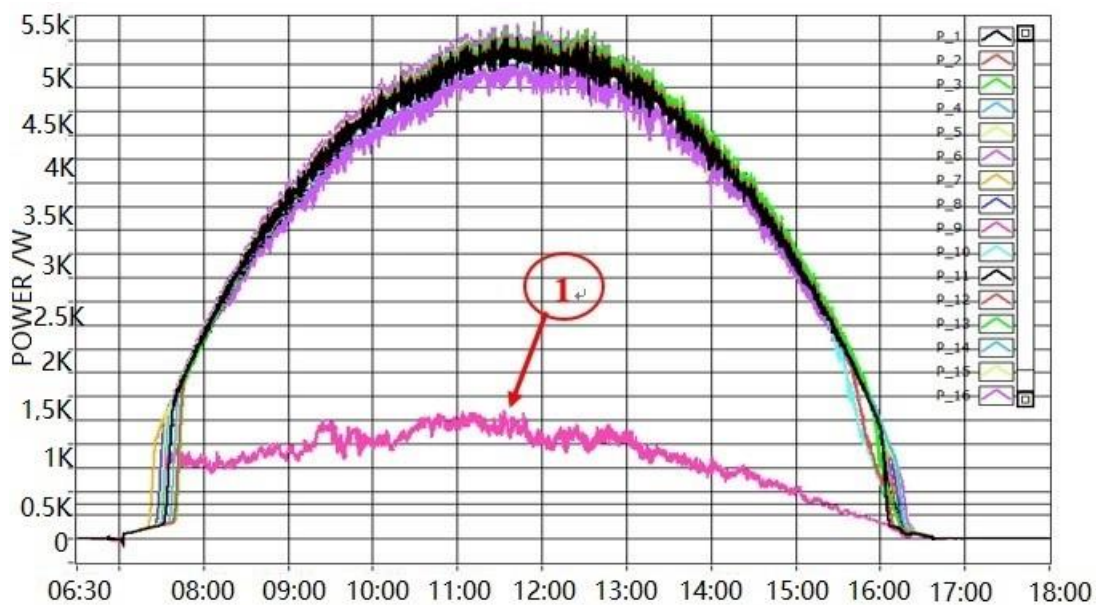
6.3.1 PV module breakage failure

Figure 32: Daily curves of elctrical power of various PV strings (mountainous landscape, PV power plant size: 20 MW, Location: Chengde, China, temperate climate).

The PV string power of curve ① in Figure 32 is significantly lower than of other PV strings over one day. It turned out that breakage of one PV module was the main reason for this failure.

6.3.2 Shading failure

A. Snow shading

The power curves of all PV strings (Figure 34) are obviously lower than daily irradiance curve (Figure 33) due to the influence of snow deposits in the morning. As the snow melts, the trend of the PV string power curves gradually becomes consistent with the trend of the irradiance curve. Figure 35 shows the picture taken during the data monitoring.
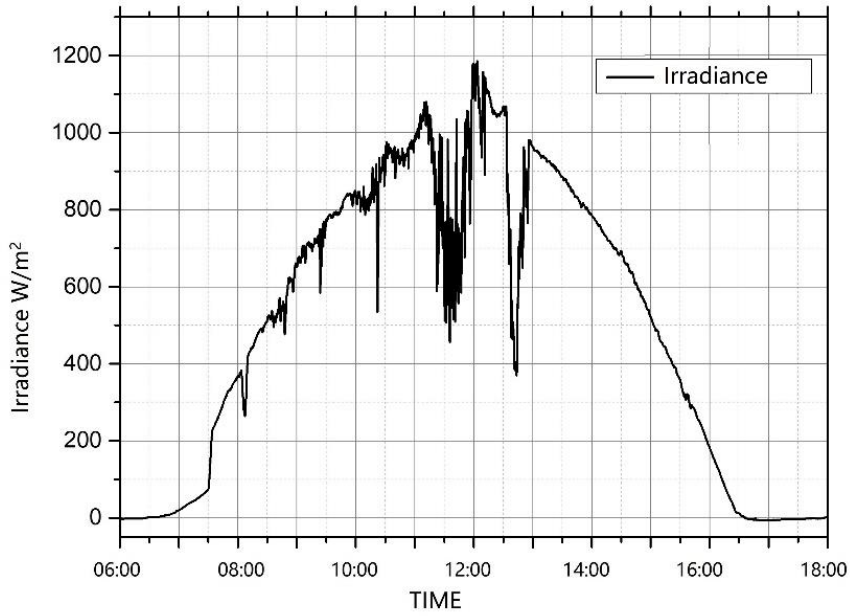
Figure 33: Daily irradiance curve.
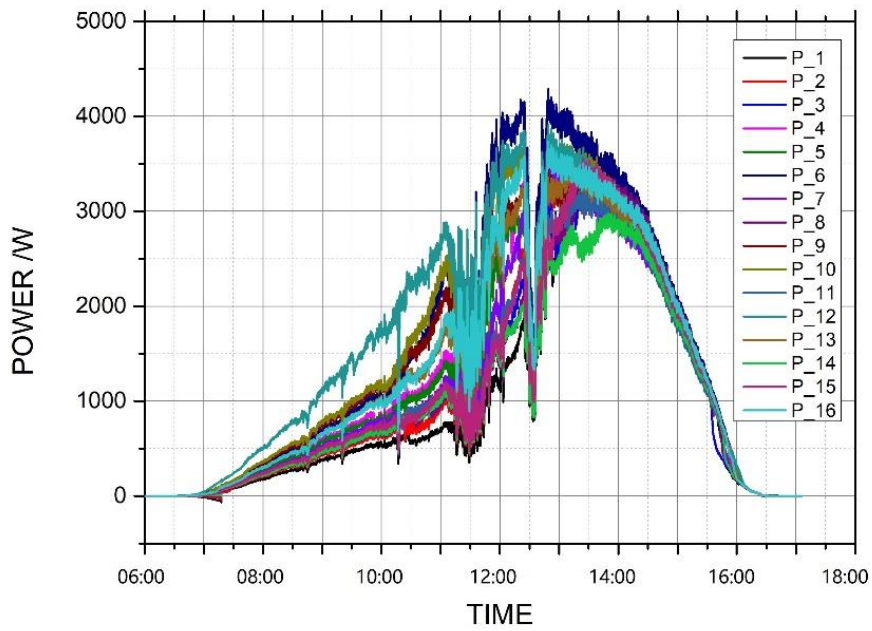
Figure 34: Daily power curve of PV strings.

Figure 35: Snow on the PV modules, mountainous landscape, PV power plant size: 20 MWp, Location: Chengde, China, temperate climate.

B.   Array shading

The output power of PV strings significantly reduces when PV modules are shaded. The power loss during the day is correlated with the size of shaded PV module area and the number of shaded PV modules.
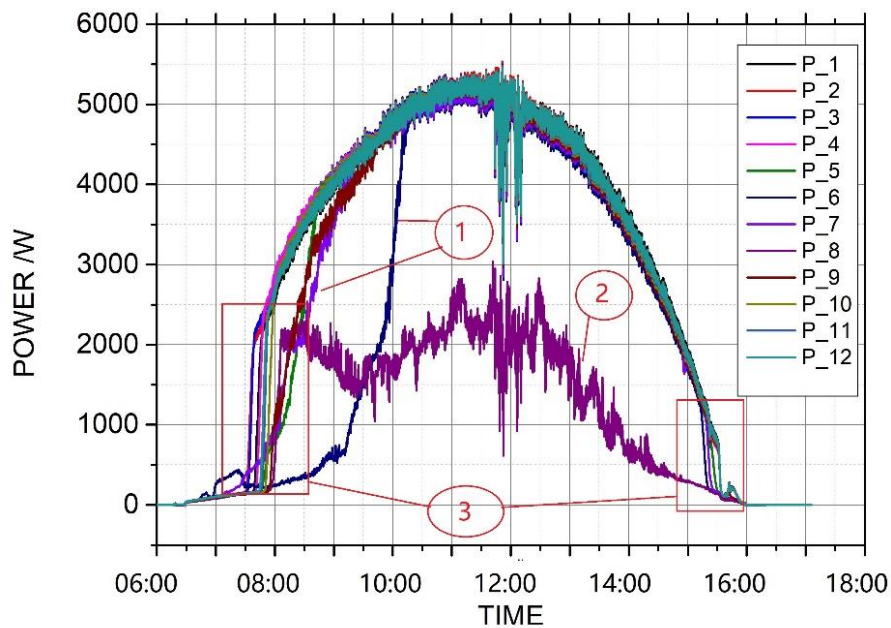
Figure 36: Daily power curves of various PV strings, mountainous landscape, PV power plant capacity: 20 MWp, Location: Chengde, China, temperate climate.

Curves indicated by "1" in Figure 36 are caused by part-time shading of PV strings by a building. Curve "2" in Figure 36 is caused by shading of the PV string during the whole day. As shown by the power curve "3" in Figure 36, there is a time delay in the PV module power change, the main reason is that the azimuth angle of each PV string installation is different. Besides, the slope of the curve "3" suddenly increases from 8 am to 9 am, and its slope suddenly drops from 4 pm to 5 pm. The main reason is that the two rows of PV strings are shaded as follows:

① 8 am to 9 am: As the area of one or more PV modules shaded gradually decreases, the internal impedance of the PV string decreases, the current of PV string increases rapidly, resulting in output power increase;

② 4 pm to 5 pm: As the area of one or more PV modules shaded gradually increases, the internal impedance of the PV string increases, the current of PV string drops rapidly, resulting in a decrease in output power.

Figure 37: PV system shading by trees.

Figure 38: Different array orientations of a PV system.

6.3.3   Misalignment of PV strings/arrays

Figure 39 shows the maximum power current curves of different PV strings in a PV arrays. The spread of curves is caused by different orientations of the PV array installation. Variable angles of incidence cause different in-plane irradiances. Figure 38 shows a view of the tested PV plant.
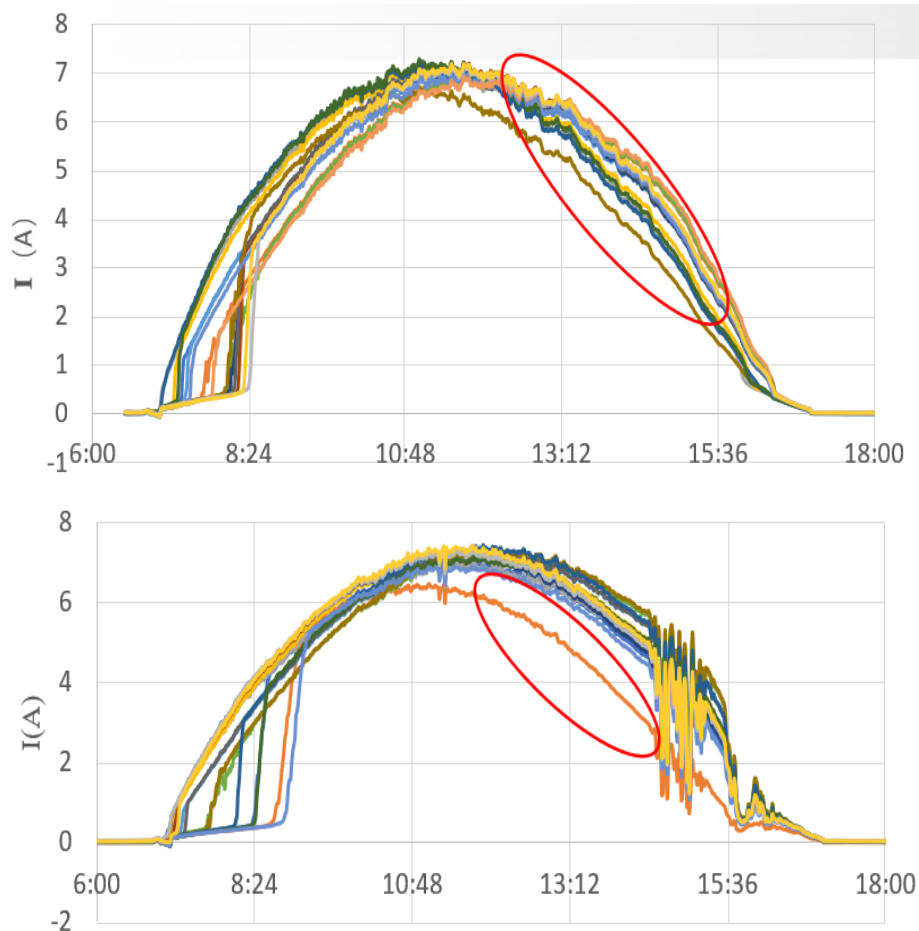
Figure 39: Daily current curve of PV strings (mountainous landscape, 20 MWp PV power plant, Location: Baoding, China, temperate climate).

6.3.4   Inverter MPPT malfunction

Figure 40 a) shows the daily curve of PV string maximum power voltage when the inverter works well. The voltage fluctuation is less than 5 V at a sunny day.

Figure 40 b) shows the daily curve when the inverter MPPT tracking does not work properly. The average voltage fluctuation range is larger than 10 V under same weather conditions.

a) normal
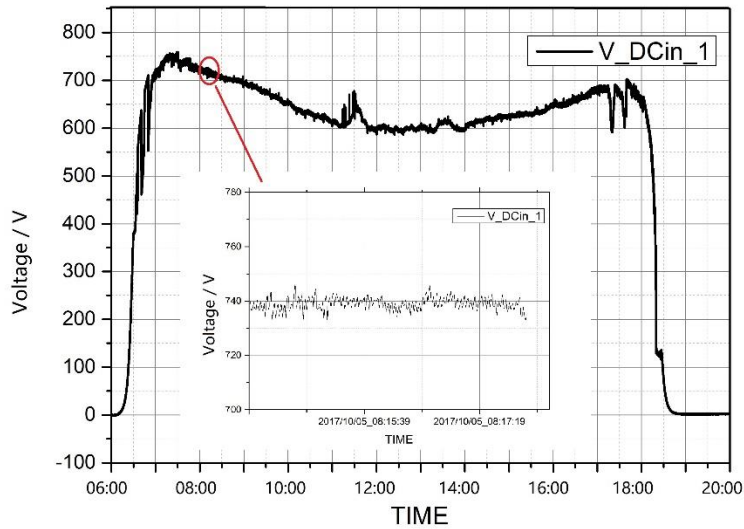
b) abnormal
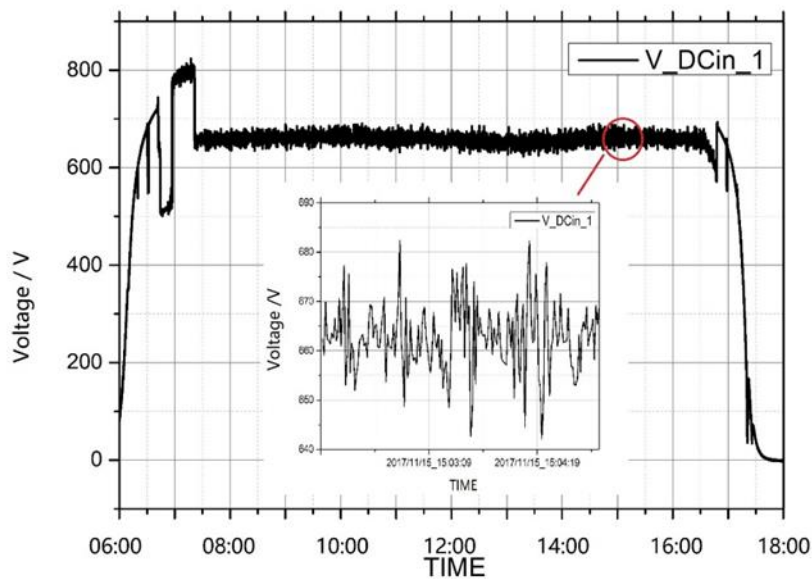
Figure 40: Daily curve of PV string maximum power voltage (desert location, PV power plant capacity: 20 MWp; Location: Qinghai, China, High elevation climate).

6.3.5 PV String connection faults/PV string mismatch

In Figure 41 the current curve of one PV string (red) is obviously higher than others and green curve is lower than others. The failure type above is mainly caused by PV module connection faults or PV modules with defect bypass diodes in PV strings.
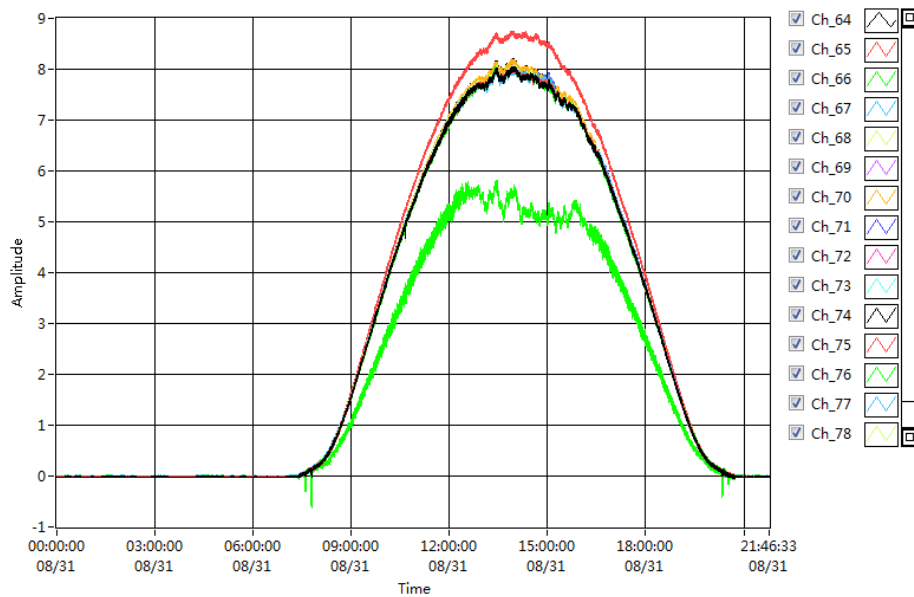
Figure 41: Daily curve of PV string current (capacity: 20 MW; Location: XinJiang, China, hot-dry climate).

6.4 Best practice recommendations

6.4.1 Test procedures

A.   The irradiance measurements shall be made using a calibrated pyranometer. The pyranometer and plane of PV array are coplanar within ±2° accuracy. Keep the surface of the sensors clean during the test period. Make sure that there is no shading around meteorological equipment.

B.   Disconnect corresponding circuit breaker on DC side and AC side of the PV string under test. Install and connect the testing equipment according to the instructions in the operating manual. The temperature of the PV module of the array under test shall be measured using thermocouple device. It is recommended to mechanically attach a flat thermocouple sensor with fine leads directly to the back-sheet in the middle of a PV module and at least 10 cm from any junction box, but opposite an active part of the PV module.

C.   Select one or more PV modules whose operating temperatures are representative of the array under test. The choice of these selected PV modules should be determined as follows: ① at minimally one centrally located PV module; ② at minimally one PV module that has been identified as one of the coolest; ③ at minimally one PV module that has been identified as one of the hottest. For each selected PV module, attach the appropriate thermocouple device in at least one location. In the event that the backs of the PV modules are not accessible, such as in some roof-mounted systems, it is acceptable to measure the temperature from the front of the PV module. More detail description is given in IEC 61829-2015 [32].

94

D.   Check functionality of each electrical connection before switch-on.

E.   Test data are acquired and transmitted to the server terminal of the test vehicle via Ethernet and wireless transmission.

For large PV installations, AC energy efficiency and performance ratio calculated on a weekly basis can provide both performance validation and diagnostic monitoring [77].

Note: It is important to check if the PV plant is restricted to generate power over the test period.

6.4.2 Data example of a typical PV plant performance

Figure 42 and Table 24 show the test results of a typical PV power plant measured using the testing vehicle [78]. The PV plant is located on a mountain at Chengde County in northern China. The details of the PV power plant are shown in Table 23.

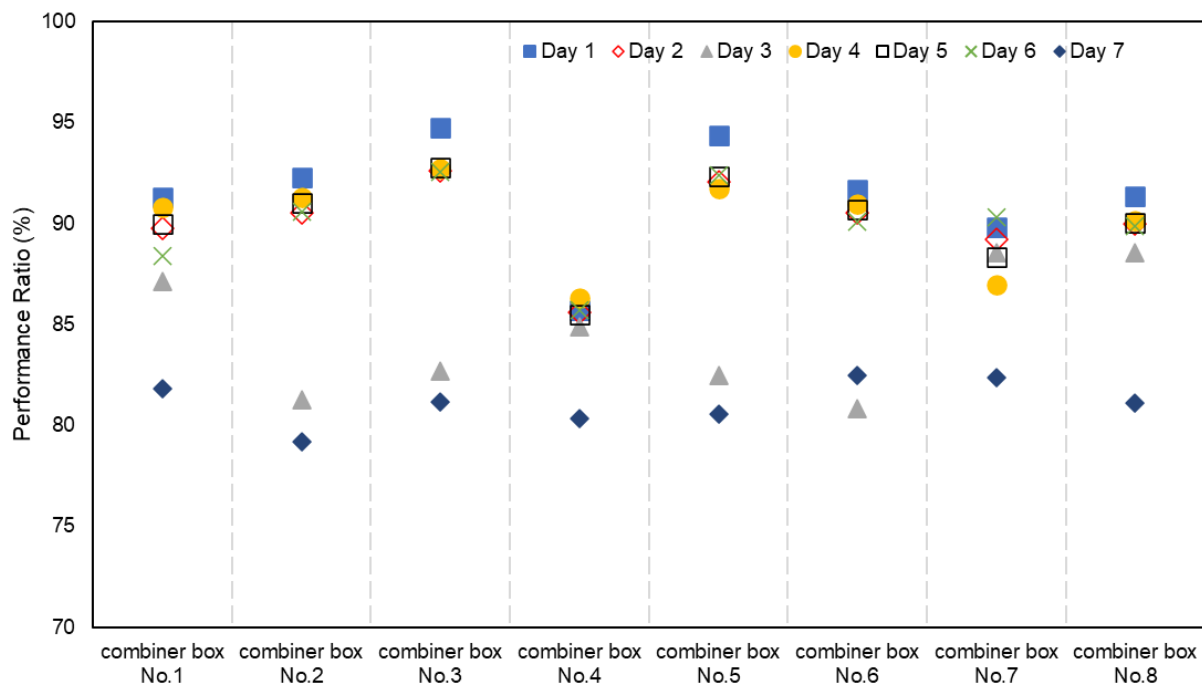**Figure 42: Combiner box performance ratio of a typical PV power plant.**

Table 23: A typical PV power plant information in northern China.

Location	Chengde county (42°N,119°E)	Power	20 MWp
Climate	Temperate continental	Date of grid-connection	Dec. 2016
PV module type	mc-Si, 265 Wp	Rack	Fixed
Inverter type	Centralized 500 kW	Inverter quantity	40

Table 24: PV power plant performance test results.

No.	Parameter	Sub-system test results（%）				Results （%）
		1	2	3	4	
1	Performance Ratio	-	-	-	-	79.81
2	η_f (Sub-system AC)	86.55	80.52	78.37	87.41	83.26
3	$\eta_{A,0}$ (Sub-system DC)	88.31	82.15	79.88	89.36	84.97
4	η_{boxes} (DC combiner box)	89.22	83.02	80.91	90.31	85.89
5	DC cable losses	0.91	0.87	1.03	0.95	0.92
6	Inverter losses	1.76	1.63	1.51	1.95	1.71
7	Other losses	10.78	16.98	19.09	9.69	14.11
8	AC losses	-	-	-	-	3.45
9	Maximum efficiency of inverter	98.38	98.56	98.53	98.31	-

Parameter definition:

η_f : AC output energy of inverter × 1000 W/m^2 /(Capacity × Irradiation)

$\eta_{A,0}$: DC input energy of inverter × 1000 W/m^2 /(Capacity × Irradiation)

η_{boxes} : Output energy of combiner box × 1000 W/m^2 /(Capacity × Irradiation)

6.5 Measuring uncertainty aspects

The uncertainty of on-site measurement of PV power plant performance is influenced by fluctuation of irradiance, ambient temperature, and other climatic parameters. Meanwhile, outdoor testing results of PV modules are related to the coplanarity between pyranometer and PV modules/string, non-uniformity of irradiance and module mismatch in PV strings simultaneously. As it is difficult to obtain good reproducibility of measurement under outdoor condition, long-term data acquisition period is needed to analyze and evaluate the uncertainty of on-site measurement.

According to the technical specification of the PV plant testing vehicle in Table 23, the typical uncertainty level of measurement is shown as follows:

Table 25: Uncertainty budgets for measurands

Test parameter	Source of uncertainty	Distribution	Typical uncertainty (range)
Irradiance	Pyranometer calibration	Gaussian	2.5%
	Solar irradiation non-uniformity	Rectangular	2.0%
	Long-term instability of pyranometer	Rectangular	1.0%
	Tilt angle difference of PV modules	Rectangular	1.0%
	Coplanarity between pyranometer and PV modules/string	Rectangular	1.0%
Temperature of PV string	Accuracy of testing equipment, mismatch of modules in PV string Temperature non-uniformity in PV strings	Rectangular	2.0%~4.0%
Voltage of PV string	Accuracy of testing equipment	Gaussian	0.5%
Current of PV string			1.0%~1.5%
Voltage of DC side of inverter			0.3%
Current of DC side of inverter			1.5%~2.5%
Power of AC side of inverter			0.5%
Performance ratio of PV plant	Accuracy of testing equipment and meteorological factors	Gaussian	5%~10%

6.6 Occupational safety

The operators/inspectors should be familiar with the performance parameters and operating specifications of the testing equipment and be able to perform various test programs of a PV power plant. Before installing and disassembling the test equipment, the operator should disconnect the DC input and then switch off the AC output. Make sure that the input and output of each channel are voltage-free. Only after the relevant components are completely powered off, subsequent related operations can be performed.

The operators must wear insulated gloves when installing and disassembling the testing equipment. The connection cables and connectors must be in good condition before and after operation. After the operator installs and disassembles the testing equipment, it is necessary to check if the connection wires and screws are secure and the grounding is reliable. If any subsystem breaks down or it show failures or malfunction occurs, the sub-system under test should be re-selected.

6.7 Transportability

The testing vehicle size is about 6.2 m×2.1 m×3.0 m. The testing equipment is mainly composed of 16 data collection boxes, a weather station which is fixed on the roof and a data processing centre in the cabin.

6.8 Cost considerations

The PV plant test vehicle costs 220,000 USD. Annual calibration costs of equipment are around 5,000 USD. The maintenance costs include:

- Sensors, cables and connectors;
- Maintenance and upgrade of test equipment;
- Daily use, maintenance of the test vehicle;
- Labour cost for two technicians to four technicians.

7 ELECTRICAL IMPEDANCE SPECTROSCOPY OF PV STRINGS

7.1 Description of the inspection method

7.1.1 Working principle

Electrical Impedance Spectroscopy is a measurement principle that can be used to extract information on the detailed electrical properties and conditions of components (e.g. PV modules) that are electrically connected into a single electrical PV string.

In contrast to the electrical resistance that can be measured by a simple multimeter, the impedance is a complex quantity, often denoted Z, consisting of a real and a imaginary part. It can be written in Cartesian form as $Z = R + jX$, where R is the Resistance and X is the Reactance, or alternative in an angular form [79].

The measurement is performed through a two-terminal (single energy band) connection where the systems linear response to an input sinusoidal oscillating (harmonic) perturbation over a range of frequencies is measured. When the input function has character as a current, the ratio of the voltage response to this current is denoted as electrical impedance. By analysing the response within different frequency ranges, information on specific features within the electrical PV string can be extracted which further - based on modelling and experience – can be converted into knowledge on individual component features like e.g. non-operative PV modules or other defects like PID within the electrical PV string.

7.1.2 Instrument type

Currently there's only one commercially available system, capable of performing Electrical Impedance Spectroscopy [80], the use of which is illustrated in Figure 43.
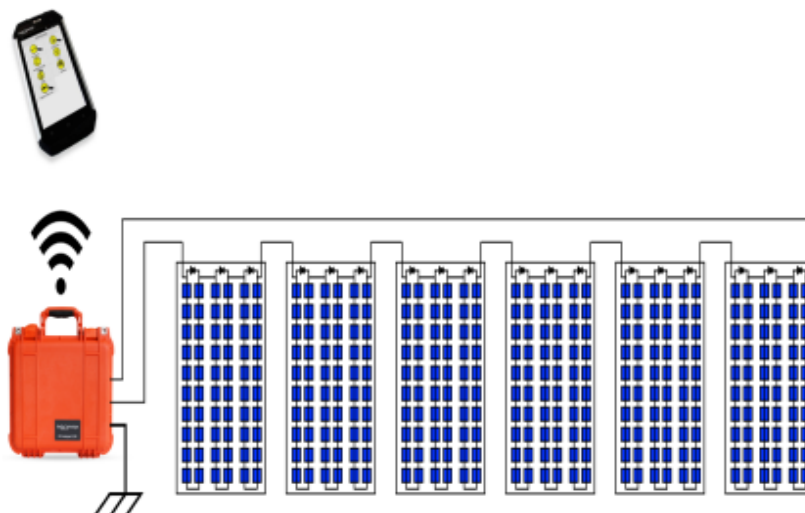

Figure 43: Experimental setup with the Electrical Impedance Analyser connected to a PV string of PV modules via the standard positive and negative PV-plugs while operated by an app installed on a smartphone or tablet via a Wi-Fi communication connection.

The instrument operates within the frequency interval from 1 Hz to 100 kHz and actually imposes an AC voltage over the terminals and measures the current response for determination of the electrical impedance.

With a browser-based interface, it's possible to initiate different testing modes and analysis algorithms covering tasks as simple live updated voltage test, to a full testing routine that will reveal the shunting resistance, level of PID, PV module voltage and bypass diode state of individual PV modules.

7.1.3 Quantitative or qualitative method

While executing a measurement, the instrument will collect the full (complex) frequency dependent impedance transfer-function. However, further elaborated analysis which involves elaborated mathematical operations and fitting of build-in network models of this function is required, in order to extract information of direct use to the operator.

Whereas the generated information by nature is quantitative and may be analysed (off-line or build-in) as such, more operational conclusions will be made based on qualitative conclusions as given by the classification of the observations in terms of typical PV module faults like defective bypass diodes, PID as well as dc-PV string/combiner box faults or ground connections [57].

7.1.4 Test requirement

When working in the field with Electrical Impedance Spectroscopy, it's required first to disconnect the dc-PV strings from the input section of the inverter, and re-connecting this PV string temporary to the analyser. Sametime also an earthing cable needs to be connected to the analyser, to ensure that the PV module frame and the ground are at equipotential.

When operated as fault detection instrumentation, the instrument and fault finding algorithms will be operative already with an irradiation level of 100 W/m^2. The same instrument may also be used in a standard testing mode as any electrical characterization instrument to collect the parameters of V_{OC}, I_{SC}, etc. When used for this purpose, it's often required to operate under Standard Test Conditions to be in conformance with the IEC 62446 conditions.

The maximum dc-voltage is currently 1000 V, which limits the number of tested PV modules to around 25. The tester can actually operate at voltages up to 1125 V, but certification is limited by the IEC 61010 directive.

7.2 Existing knowledge

7.2.1 Literature study of scientific papers

Electrical Impedance Spectroscopy analysis have become a broadly researched topic although the method were mostly used to study electrochemical issues with dye synthesized (Grätzel Cells) solar cells at the beginning of this century. Over the last years also papers on specific applications have been published addressing topics like PID detection [81] and power degradation due to microcracks [82]

7.2.2 Market overview of instruments

So far the only known supplier of instruments for this type of characterisation is the company EmaZys ApS [83]. The "Sokodes" instrument from the Japanese company System JD CO, Ltd, similar can be used to detect an open circuit in panels and connection cables as well as ground faults. This instrument is using time domain reflectometry, a method which can be considered almost equivalent to electrical impedance spectroscopy.

7.2.3 Status of standardization and licensing

Currently there's no standard in place or under development covering this measurement method.

7.3 Detectable failure types for PV modules and PV arrays

A wide range of observations, quantitative measurements and observations can in principle be made by use of Electrical Impedance Spectroscopy when inspecting a given dc-PV string [57], [81] and [82].

Among the most important faults that can be detected in a PV string is, by-pass diode failure, PID loss or ground fault.

The more specific parameters that can be extracted include:

- PV string voltage Voc
- PV string current Isc
- Voltage polarity
- PV system isolation resistance Riso
- PV string series resistance RS
- PV string impedance curves (overall degradation check)
- Position of ground (RISO) faults in PV strings
- Position of disconnect in PV strings
- Position of ground (RISO) faults in PV strings
- Position of disconnect in PV strings
- Tone generator and acoustic pickup for cable tracing
- PV Module bypass diode check (open or short diode)
- PV Module shunting resistance (PID and degradation check)
- Position of ground (RISO) faults in PV strings – monitoring mode

When analysing several PV strings in the field, it's possible to see and evaluate the measurement results directly on the controller device, but it's also an option to export data for off-line analysis. This can be accomplished by activating a dedicated cloud service where datasets can be uploaded and combined into a single spreadsheet for detailed quantitative analysis.

One aspect of the utilization of this instrument is a ground-based follow-up on suspicious PV module features identified by a fast drone-based PV plant inspection. Whereas the drone-based inspection can identify a lot of PV module features in a short period of time, it's still left for ground-based inspection to generate the final evidence and documentation of failure mode and severity. In this context it's not always possible to support the findings made by the EL camera on the drone, but still it's necessary to complement the drone maps with ground-based inspections where the Electrical Impedance Spectroscopy of the full PV strings has

proven a to be a fast and powerful method. Once e.g. a shunting resistance failure or a PID impact of a specific PV module in the PV string has been identified, this PV module may be removed and brought to the lab for further failure verification based on detailed I-V, dark I-V, and EL methods. In case the instrument identifies faults related to combiner-box ground-fault or e.g. a cable pinhole, also the exact location (position within the PV string) of these defects can be determined by the instrument whereby time-saving control measurements can be avoided and immediate actions taken in order for a ensure safe operation of the plant. This is based on the fact that this impedance spectroscopy is carried out on three (not two) terminals, which allows for determination of the positioning as illustrated in the video [84].

7.4 Best practice recommendations

The Electrical Impedance Analyser is designed for ease of use and fast fault finding, and most technicians can easily get started using the equipment after a brief training and safety instruction, in order to learn how to disconnect electrical PV strings that are under operation at high voltage.
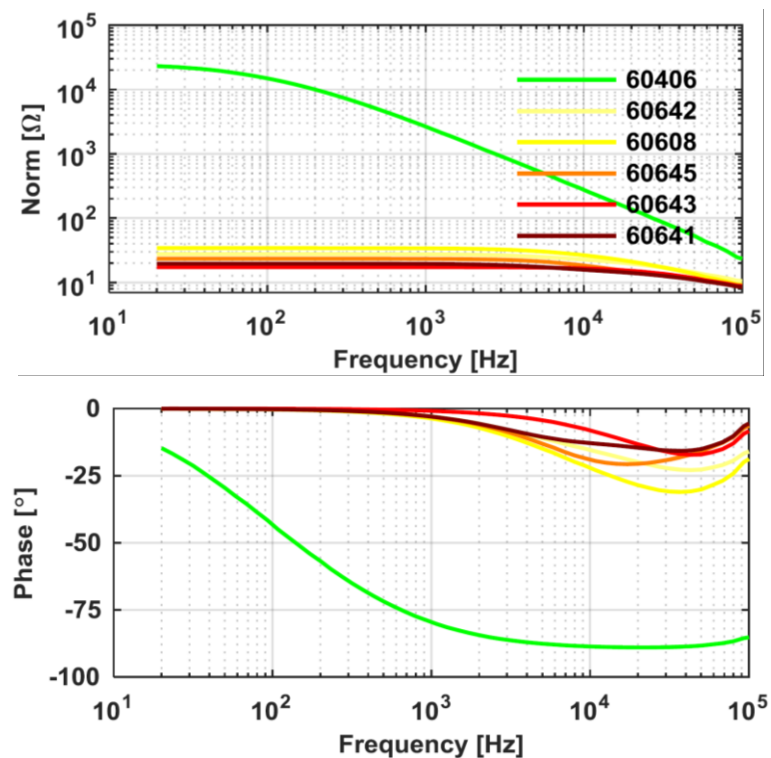
Figure 44: Electrical impedance spectre of 6 PV modules illustrated in Nyquist diagram. Only one PV module (green curves) are unaffected by PID.

An example of how to work with the instrument in the field to detect PID affected PV modules is given in [81]. A small system with 36 pcs. 260 W_p PV modules have been investigated due to suspicion of PID. EIS spectra of all PV modules were taken in Figure 44 the impedance spectra of both the best and the five worst performing PV modules are illustrated in a Nyquist plot. The differences between the curves are easily observed, but only after extraction of model parameters from fitting the measurement data with an equivalent circuit model, the conclusion

can be quantified. This extracted model parameters verifies the findings on P_{MAX} degradation (up to 80%) as measured in the lab with a standard flash tester for comparison. In terms of the extracted circuit parameters, the PID degradation can be expressed by a decrease in shunt resistance (best PV module: 30,000 Ω; worst PV modules ~20 Ω) and increase in parallel capacitance (best PV module: 0.1 µF; worst PV modules: 1 µF) respectively.

7.5 Measuring uncertainty aspects

At least four factors may influence the accuracy of the measurement result.

1. Cable capacitance estimation: The user needs to input the capacitance of the cable as a parameter to calculate the disconnection position. However, even though this input value only represents a small fraction of the total PV module string capacitance, an imprecise estimation of the cable length will impact the precision by which the exact location of the defective PV module can be identified.

2. The cable length estimation: If the measurement is performed at the DC box, the user needs to estimate the cable length from the device connection point to the plus connector of the first PV module, as well as the cable length from the device connection point to the negative connector of the last PV module. However unless detailed installation drawings are provided, it may be difficult to obtain a precise estimate of this length, especially for roof mounting systems.

3. The tightly tied cables: When the cables of different PV strings are tied together tightly, the signal generated from the analyser will be transferred to other PV strings, and result in measurement uncertainty. When tone pick up is used to locate the PV string, it is also difficult to locate the target PV string because the signal can be detected from every string.

4. Grounding: The PV modules shall be grounded and connected to the earth which is connected to the analyzer. If the grounding connection is not good, or even disconnected, the measurement result will be wrong.

The Electrical Impedance Analyser has been developed for the purpose of inspecting fully installed and electrically connected PV modules once they are installed and operative in the field. Thereby it's often not a simple task to directly compare conclusions related to a specific fielded PV string to measurements that takes place under Standard Test Conditions in the lab.

For measurement campaigns where the objective is to verify if the PV module power is in compliance with datasheet values, build-in conversion algorithms that take into account the actual measured temperature and irradiation can be applied, such that the performance can be reported under STC-equivalent conditions

7.6 Occupational safety

Working with high voltage dc can be dangerous, and shall only be performed by trained personnel as disconnection of operating PV string cables can generate arching and related personnel hazard or risk of fire.

7.7 Transportability

Electrical Impedance Spectroscopy measurement equipment is easily portable as it comes in a hard mobile case weight about 3 kg. The accessories include a Li-ion battery with charger and testing leads for MC4 connectors as well as a crocodile ground connector. The battery is safe for flights once the box has been clearly marked – safety class UN3481.

7.8 Cost considerations

The purchase cost of the Z200 PV Analyzer lies in the range 8000 USD from EmaZys resellers. The payback time can be estimated based on the time saved in the O&M fault-detection operation which has been stated as around 2.5 hours per task by the seller. Due to the low sensitivity to actual weather conditions (minimum irradiation) compared to other mobile instruments, planning of the inspection visit become easier and more flexible.

The maintenance cost is considered low and relate mostly to calibration, Calibration time is 15 minutes to 20 minutes and the cost of shipping to the test centre may be more expensive than the actual calibration.

The Z200 PV Analyzer can test up to 30 PV strings per hour using the "PV string test mode", but "solve many problems per day". The focus of this instrument is on troubleshooting faster than what is possible using alternative type of equipment.

As an example, when searching for a ground fault in a large field it may be necessary to collect data from many PV strings connected to a specific combiner. In this case the technician may be able to make a needle point operation and locate the position within ±1 PV module of the ground fault in only two minutes.

Most testing algorithms take around two minutes, so the throughput is potentially high. Testing for PID and Bypass diodes functionality takes around 10 minutes to 20 minutes per PV string. On the other hand this testing mode yields data that is normally only available after dismantling PV modules from the system and testing them in a lab. Alternatively one can use night time EL, but this again requires some more resources.

As no special safety issues are to be considered, it's possible to conduct inspection in the field by one person only.

8 DAYLIGHT ELECTROLUMINESCENCE IMAGING

8.1 Description of inspection method

8.1.1 Electroluminescence working principle

Electroluminescence (EL) is the emission of optical radiation resulting from the application of electrical energy to the solar cells. When current is fed in forward bias into the cell, the cell emits light which can be taken by a camera to generate an EL image. A defect or inefficient area in the cell generating less irradiation will be darker in the EL image. Therefore, we can detect defects of the cells such as busbar corrosion, cracks and other defects in PV modules and extrapolate the quality of a PV Power Plant.

As a baseline procedure for daylight EL, the technical specification IEC TS 60904-13 for indoor EL can be used. To generate electroluminescence, the panel must be forward biased using a DC power source. In Figure 45 a real application setup is shown and Figure 46 shows a schematic drawing for the test setup.

Figure 45: Application of daylight EL camera (copyright Fraunhofer ISE).
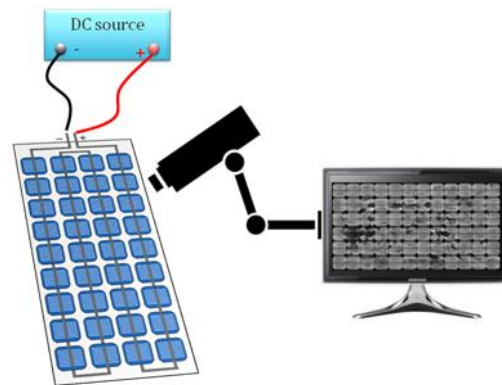
Figure 46: Schematic drawing of the EL test setup.

The major challenge for outdoor EL inspection in the daytime is the near infrared (NIR) emission from the sunlight is higher than the emission from the solar cell. Thus, performing outdoor EL inspection requires special setup to filter the signal irradiated from the cells. However, it is inconvenient and costly to work in the field at night; therefore, daylight EL technologies are developed to solve this problem [85].

8.1.2 Measurement method for daylight electroluminescence

There are several approaches for in field daylight EL inspection, which differ mainly in how the PV panels are biased during measurement, the number and timing of the luminescence measurements, and image post-processing procedures.

The most basic measurement method is to apply a constant forward bias voltage to the PV panels and measure the EL emitted by the solar cells [85], [86]. This method is sensitive to ambient light noise limited to night-time or low-light inspection ($<100W/m^2$). The inspection window can be extended by use of optical bandpass filters and noise removal by subtracting

background images, which are taken when the PV modules are not powered, from the active EL images [87].

One of the most effective methods for full daylight electroluminescence imaging was first proposed [88] and patented [89] by SolarZentrum Stuttgart (DaySy method). There are several implementations of this principle, the most common of which is the "EL lock-in", where forward bias current is modulated through the PV modules, [90], [91], [10], typically between 0 and I_{sc}, as depicted in Figure 47. One or more EL images are acquired in both the high and zero current states of the PV module. For each period of the modulation signal, the zero current images are subtracted from the high current images, resulting into a difference image [90], [91]. Thereafter, the difference images are added to a running total or averaged depending on the method used [92]. The number of image acquisition periods required can vary from a few to several hundred [90], [93], depending on the ambient noise level and the image quality requirements. A single measurement batch can take up to 60 seconds in full daylight, if using a fast InGaAs camera [88].
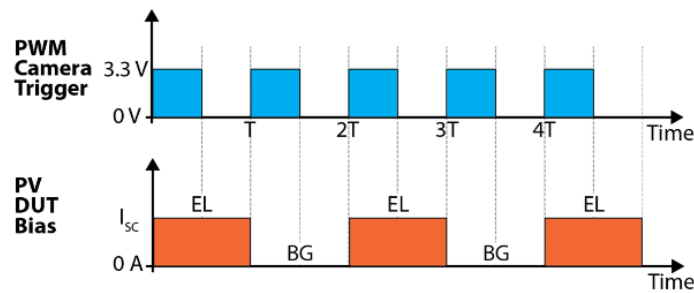
Figure 47: EL lock-in measurement principle: Synchronized Pulse Width Modulation (PWM) camera triggering and PV module (device under test – DUT) bias signal [92].

The "EL lock-in" methods can differ in terms of what hardware or procedure is used to implement the current modulation. Different EL lock-in methods can differ by using a programmable power supply [87], [85], [88], [60], [10] that can bias a single PV module or a PV string to a constant DC voltage supply in conjunction with a modulation circuit [91] depicted in Figure 48. Additionally these methods could power the PV modules from adjacent PV strings during daylight [88], [94] or temporarily store the energy produced by the panel itself, boosting it to a higher voltage, and then modulating it through the PV panel [95].
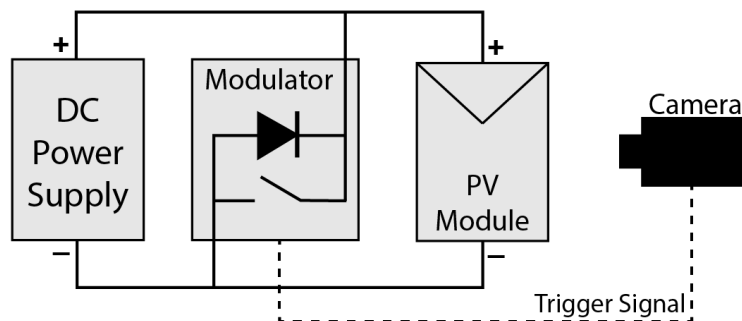
Figure 48: EL lock-in modulation hardware [91].

8.1.3 Quantitative analysis

EL images can be analyzed in qualitative and quantitative methods. With quantitative analysis, the series resistance, shunt resistance, minority carrier lifetime, and diffusion at a particular location in the cell can be determined through the signal intensity in the EL image. Areas where current flow is limited by series resistance will show a reduced EL signal because of the lack of supply of injected carriers at those regions. Conversely, for a given net current supplied to the device, areas of reduced resistance to current flow will have higher numbers of injected carriers flow there and generate a higher EL signal. If the forward bias current is not significantly limited by series resistance, the EL signal is proportional to the effective diffusion length. Shunts through the p-n junction of a cell provide alternate recombination paths to the near band edge recombination responsible for EL signal. High currents applied to the device (such as I_{sc}) may saturate leakage paths associated with shunts, thus the cells in a PV module may appear bright except at the shunt locations. When the current applied to the device is reduced (such as $0.1 \times I_{sc}$), then unsaturated shunt paths may (depending on the extent) reduce overall minority carrier density and overall cell EL intensity [96].

The quantitative analysis requires precise calibration of the signal intensity in the image, and high demand for the camera and lens specification. The analysis is helpful mainly in cell investigation, but not really necessary for PV module and PV string level analysis. Consequently, quantitative analysis is rarely used in PV module and system inspection.

With the recent rapid advances in machine learning (ML) and convolutional neural network modeling it has become possible to quantitatively analyzed hundreds of PV module EL images and tens of thousands of EL images of PV cells, to rapidly identify defects and develop predictive models of cell and PV module performance, as discussed in Section 8.2.2. And this will see increasing applications in the upcoming years.

8.1.4 Qualitative analysis

Qualitative analysis of EL images includes identifying some defects with an easily recognizable signature pattern such as cracks. It is helpful to diagnose the PV module and system problem with qualitative analysis. With the images taken at different current levels, more defect types such as Potential-induced degradation (PID) can be found. Shunts or areas of non-luminescent recombination will be seen as dark areas with higher bias currents applied, whereas whole cells will appear darker with lower bias current. The detectable defects will be addressed in Section 8.3. Traditionally EL images have only been analyzed qualitatively, but with recent advances in data science and machine learning, busbar corrosion [97] [98], cell cracking [98], [99], and seven more defects are now being quantified across tens of thousands of El images.

8.1.5 Purpose of electroluminescence inspection in the field

EL inspection in the PV module production is a standard process in most of the PV module manufacturers, where the EL image of each PV module is checked before delivery. Since most of the PV modules are supposed to pass the EL inspection at delivery, the EL inspection in the field is mainly to check the problems after the PV module is delivered, such as improper handling in transportation, installation, and reliability problems during operation. The EL inspections are performed on different occasions for different purposes and are described below.

107

Pre-installation tests are performed when the PV modules arrive at the installation site and before mounting. These tests serve to check if the PV modules are damaged during transportation and handling. It is also helpful to find the inherent defect from the PV module production and observe the quality level of the batch of PV modules [100]. For testing with normal EL setup in the daytime, a dark room or a tent (mobile darkroom) is required to keep the PV module in the dark background. If daylight EL equipment is used, the test can be done without the tent.

Post-installation tests are performed after the PV modules are fixed on the mounting structure. The purpose of the inspection is to check the defects induced during installation (e.g., improper PV module handling). The inspection is performed without dismounting the PV module to avoid the possible dispute that the PV modules were damaged during dismount for the inspection. EL inspection is also used in the operation phase of the PV plant. Regular inspection is required to see if the PV modules are damaged by maintenance work or external stress (e.g., snow, wind, hail) or deteriorate because of PV module quality issues. EL inspection could also be used to investigate the root cause of power degradation. There are many reasons that can result in power degradation and it is difficult to determine the root cause simply by voltage and current measurement or IR thermal inspection. Together with other analyzing methods EL images are a powerful additional method for determining defects.

8.2 Existing knowledge

8.2.1 Literature study of scientific papers, status of standardization and licensing

EL inspection is summarized in the previous IEA PVPS Task 13 reports in 2014 [57] and 2018 [18] where frequently observed defect types in cell and PV module levels are listed with images. IEC published IEC60904-13 in 2018, which describes the requirement of the equipment and a general description of the quantitative and qualitative analysis of EL inspection results. The technical committee of SEMI Industrial Standards is also working on a practical guideline for the application of EL inspection [101], [102]. It proposes the classification of the EL equipment so the users can identify the capability of the equipment. It also lists the defect classification which focuses more on the inherent defects that appear in the manufacturing process.

8.2.2 Inspection and measurement method

The different infield and daylight electroluminescence PV inspection methods developed can be categorized in a few main categories: i) by camera type; ii) by inspection method iii) and by failure detection method.

A.   Camera type and power supply

The wavelength of the light emitted from the PV cell depends on the cell technology. Silicon crystalline (c-Si) cells generate near infrared (NIR) light around 1100 nm which is invisible with human eyes. Thus, a camera with high sensitivity in NIR range is required.

In general, electroluminescence inspection of PV panels can be performed with low-cost consumer grade cameras, based on complementary metal-oxide-semiconductor (CMOS) or cooled Si charge-coupled device (Si-CCD) detectors, which are modified by removing their built in IR filter [87], [85] [103]. Their main advantages are low-cost and high resolution. However, CMOS and Si-CCD detectors have low sensitivity at the silicon luminesce peak at

1150 nm (about 1% [86]) thus requiring a long exposure time (0.5 s to 30 s). This makes them sensitive to ambient light noise and are only effective during night time or very low light conditions.

Daylight electroluminescence inspection of silicon-based PV modules requires faster cameras, based on InGaAs detectors [10], [57] [86], [88], [90], [91], which are significantlymore sensitive in the 1150 nm wavelength and have very short image exposure times (1 ms to 20 ms). The short exposure time is necessary in order to acquire multiple images in the same irradiance conditions, to remove ambient light noise [88], [60]. However, InGaAs cameras are more expensive (up to an order of magnitude) and lower resolution

B.   Market overview of instruments

A market overview of a selection of professional EL cameras can be found in Table 26.

Table 26: Market overview of electroluminescence cameras; * Measurement conditions not mentioned.

Brand	Model	Device	Sensor Type	Effective Number of Pixels (H) x (V)	Quantum eff @ 1100 nm*	Cooling System	Exposure Time (ms)	Approximate Weight (kg)
Solarzentrum Stuttgart	Daysy	Complete solution	InGaAs	640x512 1280x1024	-	-	-	-
Hyperion Instruments	Helios Luminescence Imaging System	Complete solution	InGaAs	640 x 512	-	Yes	-	-
Suncycle	CTU Flex EL	Complete solution with shading system	CCD	-	-	-	Measure time: 30 s	-
Xenics	Bobcat	Camera	InGaAs	640 x 512	60%	No	0.1 to 40	0.3
Xenics	Cheetah	Camera	InGaAs	640 x 512	60%	Yes	0.1 to 40	2
Hamamatsu	C12741-03	Camera	InGaAs	640 x 512	62%	Yes	16.7 ms to 1 s	0.52
Raptor	Owl 640 VIS-SWIR	Camera	InGaAs	640 x 512	87%	Yes	10 µs to 26.8 s	0.282

Table 26: Market overview of electroluminescence cameras; * Measurement conditions not mentioned (continued).

Brand	Model	Device	Sensor Type	Effective Number of Pixels (H) x (V)	Quantum eff @ 1100 nm*	Cooling System	Exposure Time (ms)	Approximate Weight (kg)
Raptor	Owl 1280 VIS-SWIR	Camera	InGaAs	1280 x 1024	~87%	Yes	up to 86.5 ms	0.247
Artray	ARTCAM-130	Camera	InGaAs	1280 x 1024	~78%	-	-	0.36
Ehd Imaging	EHD-130SWIR 1.3MP InGaAs SWIR	Camera	InGaAs	1280 x 1024	~80%	No		0.36

For a better quality, it is recommended to get the EL and background images in a very short time to avoid irradiance changes and shadow shifts due to the sun movement. To perform this technique in an automatized way, the power supply and camera could be synchronized for a fast image acquisition. Input/output (I/O) ports in both devices should be checked as well as the supported communication standards to develop the synchronization.

DC power source selection will depend on the range of electric parameters to be working with and technique deployed to get the daylight EL image. The capabilities of DC power sources are several in the market, thus, this requires a preliminary analysis of the compatibility with the considered technique and possible limitations.

C.   Inspection approach

From an inspection method perspective, there are two main approaches: ground-based and aerial inspection. Ground based EL inspection of PV plants is typically performed using tripods for stabilizing the camera during imaging [54], [85], [88]. Tripods are necessary for CMOS or Si-CCD cameras which require long exposure times [87], as well as for measurement procedures that require the acquisition of multiple images [88]. High throughput ground inspection methods can involve mobile carriers [60] such as cranes or fruit pickers [85] shown in Figure 49, or even handheld luminescence inspection tools [86] as in Figure 50. These inspection procedures need to be optimized in terms of speed to reduce motion blur [86], [60].

Ground based electoluminescence PV inspection can also be performed using mobile PV characterization labs, such as the PVMovLab [104], MELI Mobile PV Test Center [105] or the CTU Lab [106] in Figure 51, which requires PV panels to be dismounted for characterization, but can perform a multitude of measurements on the PV panels, including luminescence. Moreover, the CTU Flex EL [106] developed by SunCycle (Figure 52) can image PV modules while they are installed in the PV array, by covering an individual PV module with the tool to block sunlight, biasing it, and imaging the PV module with an EL camera integrated in the tool.

Figure 49: Mobile outdoor imaging system based on cherry picker [85].

Figure 50: Handheld EL imaging system [86].

Figure 51: CTU Lab system by SunCycle (image from suncycle.eu) [106].

Figure 52: CTU Flex EL system by SunCycle (image from suncycle.eu [106]).

There are two ways to perform the EL inspection of PV modules installed in a power plant:

1. Disconnect every PV module and then feed the forward bias current into the PV module and take EL image one by one,

2. Take an EL image of several PV modules in one PV module string. Compared to individual PV module inspection, imaging several PV modules in one PV module string is more efficient and saves time and costs. The inspection has to be done after the DC wiring of the power plant is completed, as the forward bias current is fed into all the PV modules in one PV string from the DC combiner box. The PV modules in the whole PV string will irradiate the light and the EL image of the whole PV string can be taken from a suitable distance. For better resolution, the camera is set at a closer distance to include three to 12 PV modules in one image (Figure 53). The number of PV modules to be included in one image depends on the resolution requirement and the mounting configuration of the PV module string. In this process, daylight EL equipment has a remarkable benefit compared to a normal EL setup as it has to be done at night.

Aerial luminescence inspection of PV plants has a potential to increase the inspection throughput, but is still in the development stages, facing technological and practical challenges. This method is described in detail in Chapter 2 "Drone-mounted EL & IR inspection of PV array".
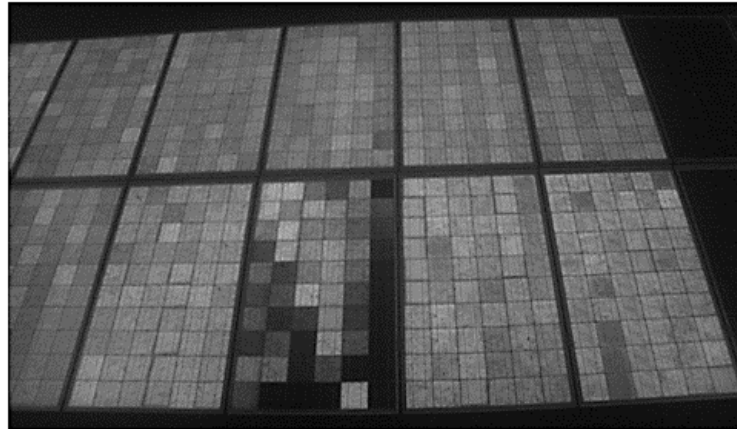
Figure 53: EL image of PV modules in one PV string.

D.   Quantitative EL image analysis & machine learning

Quantitative Image Analysis of PV module EL images is a method to analyze and quantify the degradation and failures of PV systems under environmental stressors. A data analysis pipe-line is developed which broadly includes preprocessing, segmentation, and machine learning classification or clustering of EL images into various categories depending on the degradation that the PV systems have undergone. The image processing approach provides high speed and deeper insight into characterization and degradation of solar cells and PV modules. A high resolution EL image provides millions of data points about a PV system in the form of image pixels which help us see the features like micro-cracks or initial stages of corrosion which are not even visible to eyes but affects the performance of the PV systems.

An automated EL image pipeline developed by Karimi et al. provides a machine learning model to classify PV EL images into three classes: cracked, corroded, and good (not degraded) [98] [107]. The pipeline takes a set of raw PV module EL images and in the first step preprocess these images. The major steps in the preprocessing include perspective transformation to align the images to correct for tilt and to also remove background regions as shown in Figure 54(a).
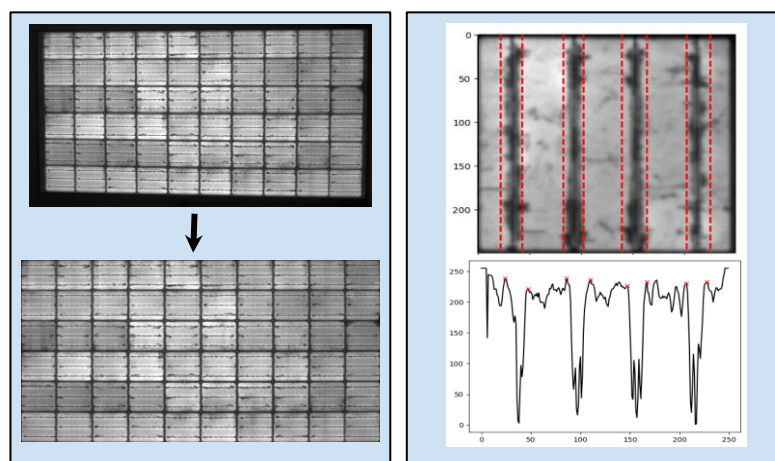

Figure 54: (a) Perspective transformation of an EL image. (b) Determination of busbar width from EL image.

112

In the image segmentation step, individual PV cells are extracted from the PV module images. In the machine learning (ML) step, convolutional neural network (CNN) models classify the cells into three classes: cracked cells, corroded cells, and good, or undegraded, cells, and this classification is accomplished with high accuracy. The process of classification can quantify the cell defects of a PV system that can contribute to underperformance or other anomalous behaviour particularly in large PV power plants where it is not possible to check manually.

Karimi et al. then demonstrated the use of other CNN models to classify the cells by their degree of corrosion, identifying five busbar corrosion levels [97]. They also demonstrated the correlation between specific I-V features and features extarcted from EL images. Maximum power (P_{mp}) and series resistance (R_s) are the two electrical features which have high correlation coefficients with EL features (except for the PV module with serious corrosion of junction boxes and/or cables and connectors, which also cause an increase of the PV module series resistance). The high correlation coefficients provide the opportunity to leverage EL features in building predictive models for the PV module power output. The drop in value of P_{mp} provides the overall evaluation of PV module degradation and the increase in R_s gives the measure of the corrosion in PV modules. The four EL features that are most significant are the *median intensity* (F_{med}), *fraction of dark pixels* (F_{FDP}), *busbar corrosion ratio* (F_{BBCR}), and *normalized busbar width* (F_{NBBW}). F_{med} is measured as the median value of pixel intensities of each cell, then the median value of all cells in a PV module is F_{med}. F_{FDP} is the fraction of dark pixels (0) over the total number of pixels when an EL image is converted into a binary image of pixel values having either zwro or one. F_{BBCR} is calculated for PV modules undergoing corrosion and it is calculated when CNN model classifies the cells into fife classes of zero to four and then the mean value of all the cells in a PV module gives F_{BBCR}. F_{NBBW} is calculated for a cell image as shown in Figure 54(b), mean pixel value in each column is calculated and then the width of the minima corresponding to the busbar is calculated, shown in the figure corresponding to the region between red dashed lines. The normalized maximum power ($P_{mp\text{-}n}$) predictive models using EL features are shown in Table 27 with metrics of Adjusted-R^2, RMSE and MAPE. Similarly Table 28 shows the model and metrics for the normalized series resistance ($R_{s\text{-}n}$) predictive models.

Table 27: Normalized P$_{mp}$ predictive models using four EL features.

$P_{mp\text{-}n} = \beta_0 + \beta_1 X + \beta_2 X^2 + \beta_3 X^3$					Adjusted-R^2		RMSE		MAPE	
X	β_0	β_1	β_2	β_3	Mean	Std. dev.	Mean	Std. dev.	Mean	Std. dev.
1-$F_{med\text{-}n}$	0.936	-1.396	-0.756	-0.039	0.88	0.025	11.87	5.57	3.46	1.58
$F_{FDP\text{-}n}$	0.936	-1.502	-0.478	-0.128	0.87	0.016	12.44	4.96	3.94	2.08
$F_{NBBW\text{-}n}$	0.935	-0.576	-0.064	-0.005	0.70	0.03	13.35	10.53	4.34	3.08
F_{BBCR}	0.932	-0.650	-0.204	0.014	0.81	0.017	9.53	4.75	2.83	1.45

Table 28: Normalized R$_s$ predictive models using two EL features.

$R_{s\text{-}n} = \beta_0 + \beta_1 X + \beta_2 X^2$				Adjusted-R^2		RMSE		MAPE	
X	β_0	β_1	β_2	Mean	Std. dev.	Mean	Std. dev.	Mean	Std. dev.
$F_{NBBW\text{-}n}$	1.192	1.992	0.360	0.61	0.057	0.049	0.034	6.88	4.50
F_{BBCR}	1.196	2.119	0.725	0.73	0.025	0.055	0.035	6.82	1.75

EL image analysis and machine learning for degradation is a promising method providing opportunities to explore, to quantify, and to understand long-term degradation and offer insights into short term operation and maintenance (O&M) of PV systems. Some challenges in EL image processing include methods to compensate for image quality, variation in camera and lens, and varying illumination conditions. The combined analysis of IR images taken under forward bias and illuminated conditions and EL images has permitted to distinguish disconnected cell interconnect, humidity corrosion, and broken fingers in highly damaged solar cells after 20 years of field exposure [108].

8.3 Detectable failure types for PV modules and PV arrays

The defect or failure types in EL image have been mentioned in earlier documents [18]. The defects are sorted into the following categories:

- Inherent defect: The defects are created during the cell or PV module manufacturing process. It exists before the PV module is delivered.
- External stress: The defects are the result of external stress like snow or hail impact.
- Degradation: The degradation is the deterioration of the material or connections.

An other possible classification of defects could be by stress factors:

- Mechanical stress factors: such as wind and snow.
- Thermomechanical stress factors: temperature difference between night and day.
- Chemical stress factors: humidity and residues from the encapsulation material which cause corrosion of metallizations.
- Others, like PID or light and temperature-induced degradation (LeTID).

8.4 Best practice recommendations

The general focus should be on taking best quality images in a fast and safe procedure with the goal to have reproducible and comparable measurement results. Thereby, the process is strongly addicted to the used measurement system and the environmental conditions in the plant. The measurement system should be the best choice for the respective plant, regarding aspects like the size of the plant, the inspection type (continuous and periodic tests or special failure detection), accessibility of the strings and modules or skills of the employees.

To detect failures in solar modules by means of electroluminescence, high-contrast sharp images must be taken with an adequate resolution. The resolution of the images is determined by the sensor size of the used camera and the field of view. Operators should try to choose the best field of view regarding the inspection type (images of the whole string, a special module and/or special parts of the module). Furthermore, the alignment of the camera should avoid geometric distortions as best as possible.

The contrast and the sharpness of the images depends on the settings of the lens, the aperture and the exposure time. Depending of the used imaging system (camera and/or software) a good way to adjust the system to the desired field of view is to apply the module current at first and adjust aperture, exposure time and focus to have images without under- and/or overexposed pixels. This procedure must be repeated several times until a sharp image with low noise and high contrast is achieved. For the best evaluation of the image settings a high-quality screen is also advisable.

Electroluminescence images in field usually are taken with a high current @1.0 x Isc. Depending on the module or string technology this assumes high output voltages. Therefore, a safe operation of the measurement system is very important. Operators always must use safe connection cables without any defects. This includes also the usage of special tools for disconnecting the cables, which are usually provided by the manufactures of the connectors. The power supply should only be used within the given safety limits and should be synchronized with the camera. Additionally, the emergency stop for the whole system must be available. Also, if not necessary, don't conduct measurements when is wet or rainy.

Conducting measurement series is a common inspection type for electroluminescence measurements in the field. Measurement series could conduct regarding several modules and/or in time. The possibility of the evaluation of such measurement series strongly depends on the comparability of the taken images. The comparability of the images will be increased by a good documentation of the used measurement setup.

8.5 Measuring uncertainty aspects

In this section, the parameters that have a major impact on EL image quality are addressed.

8.5.1 Camera detector type

The electroluminescence emission peak for silicon-based solar cells is centred at 1150 nm. EL camera detectors based on Si-CCD and Si-CMOS sensors have a low quantum efficiency (QE) in the EL emission range of crystalline silicon (c-Si) solar cells. Although a high resolution (>10MP) can easily be achieved with these detectors, they require long exposure times (of the order of seconds). This long exposure time limits inspection speed and makes them susceptible to ambient light noise. EL cameras based on InGaAs-based detectors have a better spectral response to the silicon luminescence emission and therefore require shorter integration times. An overview of the different quantum efficiencies can be found in Figure 55. From an accuracy and quality perspective, InGaAs-based detectors have better preconditions and can be used in a broader range of applications.
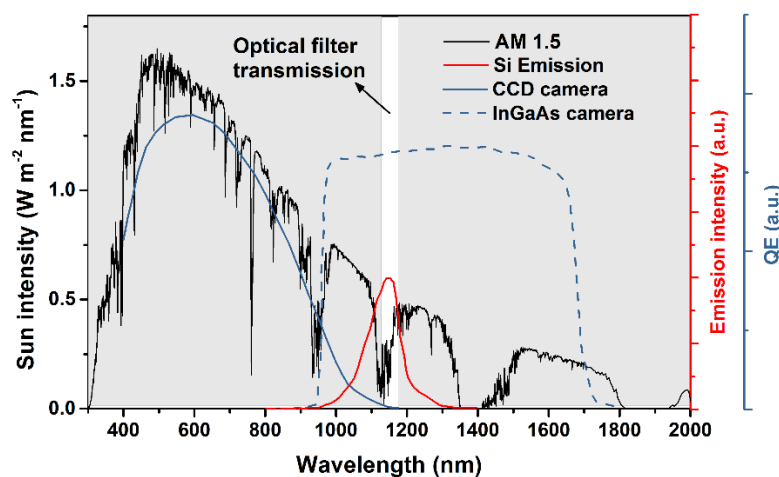

Figure 55: AM 1.5 sun spectrum (black line), CCD (solid blue line) and InGaAs (dashed blue line) camera QE curves, and silicon emission peak (red line). The grey areas show wavelengths that are cut off with the use of an optical filter.

8.5.2 Ambient light intensity and variability

The ambient light intensity has a very significant impact on the EL image quality and the useful EL signal that can be measured. The higher the ambient light intensity during the daylight EL measurement, the higher the noise level present in the EL image. This is illustrated in Figure 56 through the index of Signal-to-Noise Ratio: SNR_{50} parameter defined in IEC TS 60904-13.
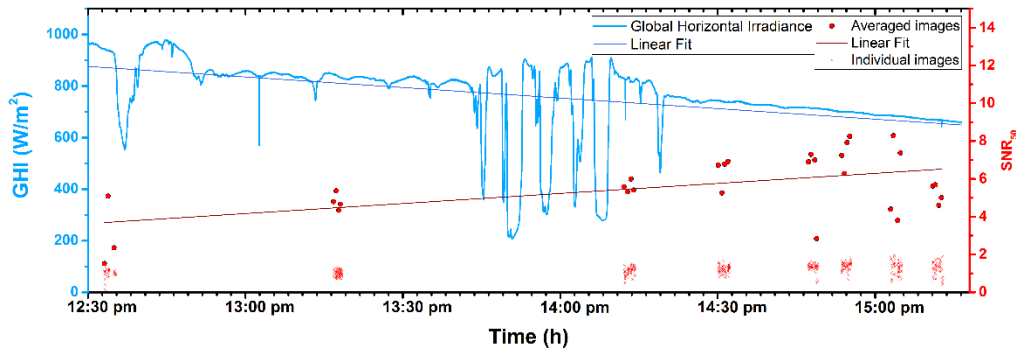

Figure 56: SNR_{50} of averaged (red dots) and individual (red crosses) EL images, from sequences acquired under the correspondent GHI (light blue line). The linear fit of the GHI (dark blue line) and the SNR_{50} of averaged images (dark red line) are also shown [94].

Some of the ambient noise present in the EL images can be reduced by repeat measurements, image averaging, and subtraction of the background EL image at 0 bias current [94]. However, high temporal variability of the ambient light, apparatus limitations and modulation character-istics can make this method less effective [94].

8.5.3 Optical filters

The intensity of the EL signal is several orders of magnitude lower than sunlight, which causes a very low signal-to-noise ratio. Therefore, optical IR bandpass filters with a centre wavelength (CWL) of 1150 nm are necessary for daylight EL measurements in order to block light outside the silicon luminescence band (Figure 57).
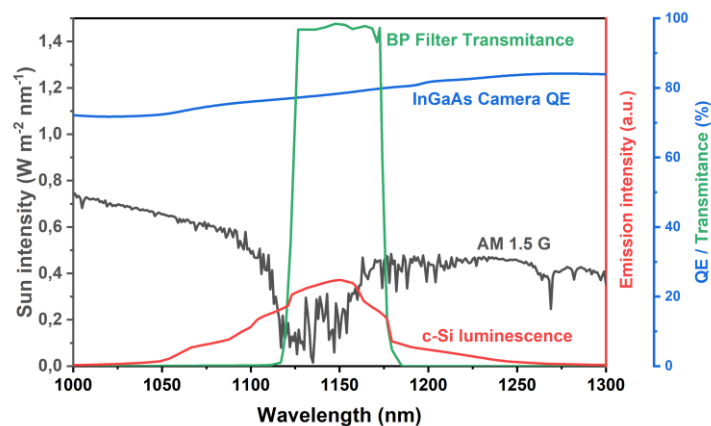

Figure 57: Solar spectrum, silicon luminescence peak, optical filter response spectrum, and EL camera detector quantum efficiency [10].

116

The optical response characteristics of the filter band transmission efficiency, transmission band width, blocking wavelength range, and optical density will determine its effectiveness in reducing the ambient light noise.

8.5.4 Measurement and image post-processing procedure

A common method to reduce noise in EL images due to ambient light is to pulse the bias current of the PV modules. Then obtain successive repeated EL measurements as the PV module is biased and unbiased. Thereafter, the unbiased (background) EL images are subtracted from the biased ones and finally averaged. The bias pulsing frequency, camera exposure time, current bias level, and number of repeats per level will influence the noise level in the processed EL image as shown in Figure 58.
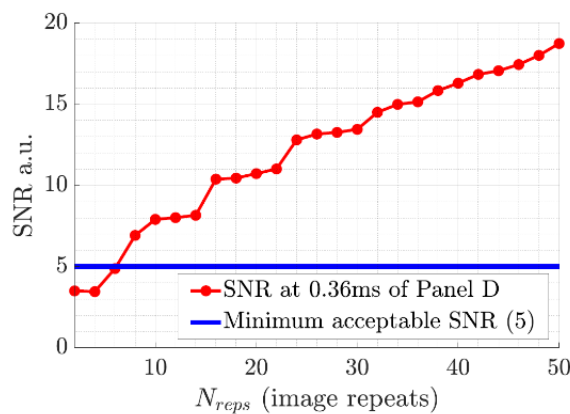

Figure 58: EL image SNR for a c-Si panel imaged as a function of repeat EL measurements [93].

8.5.5 Camera exposure time

The camera's exposure time (image integration time) is proportional with the magnitude of the EL signal, as long as the sensor is not saturated by ambient light. However, the maximum feasible exposure time is limited by the ambient light intensity during imaging and the camera movement (Figure 59).
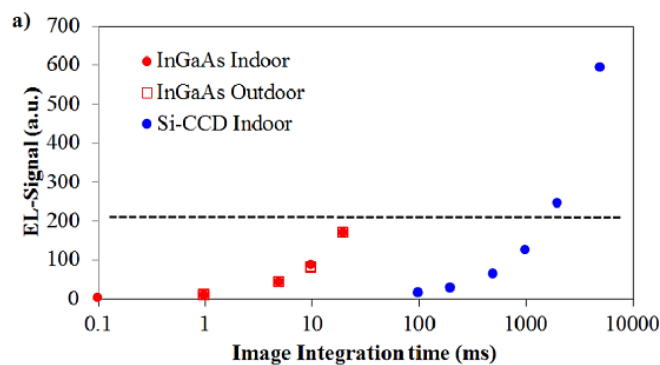

Figure 59: EL-signal of the same cell measured with both an InGaAs and a Si-CCD EL-camera as a function of the image integration time [60].

8.5.6 Bias current amplitude

Another factor directly correlated to an adequate EL signal intensity is the current amplitude used to bias the PV modules during the EL measurement as shown in Figure 60.
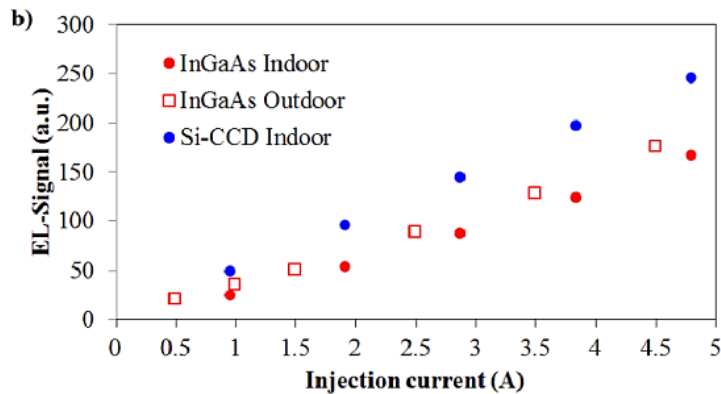

Figure 60: Increase of EL-signal as a function of different injection currents. For the InGaAs EL-measurements the image integration time was set to 20 ms whilst for Si-CCD EL-measurements the image integration time was set to 2000 ms [60].

8.5.7 Camera perspective

Daylight EL imaging is typically performed at a non-normal camera angle relative to the PV module's surface. Therefore subsequent image post-processing is necessary to correct the perspective of the images. Figure 61 shows an example of PV module EL image before and after correcting the image perspective. This perspective transformation can be performed using the Python3 package PVimage, in which this transformation is referred to as "planar indexing" of the EL image [107]. The camera's perspective angle as well as the correction procedure represent uncertainty factors for daylight EL imaging [109].
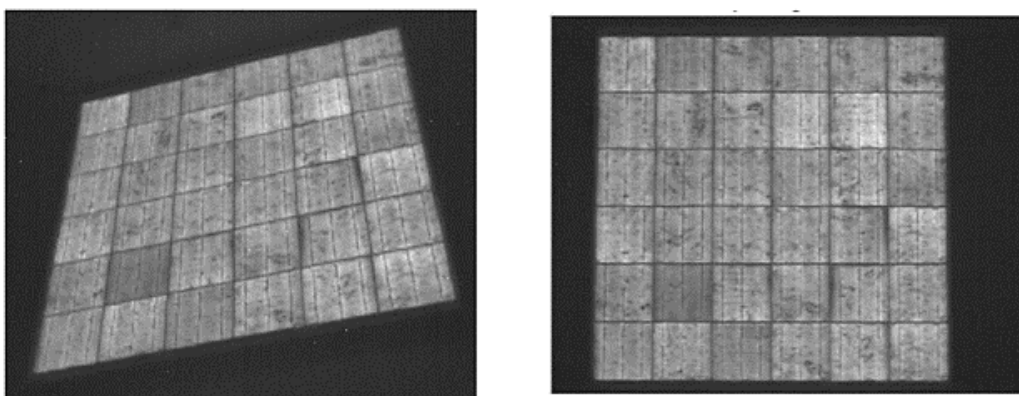

Figure 61: Example of perspective distorted (left) and not (right) EL images of a mc-Si panel, acquired with an InGAs camera [110].

8.6 Occupational Safety

The use of Personal Protective Equipment (PPE) is compulsory to perform this inspection that also includes the protection required du to the possible high irradiation by the sun-light. For preparation of the actual work and especially connection of power supply to the modules regulations for work under electrical voltage have to be followed. This may include national safety standards as well as side specific regularities defined by the operator. Most critical is the disconnection and connection of modules under sun-light, which requires qualified and trained personnel.

Performing EL in daylight adds a risk when connecting active solar panels to the power supply. Reverse current flow coming from solar panels could put in danger the power supply internal protection. The safety mechanism to prevent reverse current flow should be in accordance with the electric parameters of the string/module to be analyzed.

A careful setup design is recommended in order to avoid unexpected damages. Operation manual & safety instructions should be followed and technical support assistance requested if necessary. Considering a bidirectional power supply could be the safest option.

8.7 Transportability

The equipment for field EL inspection is different for single PV module inspection and PV module string inspection. The following examples give an impression of the weight and the dimension of outdoor EL systems. The same camera can be used, but the DC power supplies to provide forward bias current are very different. For a single standard PV module with 60 full cells inspection, the specification of the power supply is 60 V/10 A, the dimension is around 305 mm x 225 mm x 100 mm, and the weight is around 4 kg. For PV modules with more than 60 cells or with half cells, that of the power supply is 150 V/12 A. For PV module string inspection that of the power supply is above 1000 V/5 A the dimension is around 550 mm x 430 mm x 130 mm and the weight is around 25 kg.

The camera and the lens are around 0.5 kg to 2 kg depending on the technology. The mobile dark room for single PV module inspection in the daytime can be packed in a standard golf bag and the weight is around 20 kg.

If an AC power source is not available, a generator is required. For single PV module inspection, a generator with 2 kW is sufficient. In this power class, dimensions are around 500 mm x 300 mm x 450 mm and the weight is in the range of 25 kg. The generator for PV module string inspection has to provide more than 10 kW, the dimensions are 700 mm x 550 mm x 550 mm and the weight is up to 100 kg.

8.8 Cost considerations

8.8.1 Purchase costs

The cost of the camera could range from 1,000 USD to 70,000 USD, which depends on the specifications of the camera. The main differences are: resolution, sensor quantum efficiency, and cooling system. A 60 V/10 A DC power supply for single PV module inspection could be around 1,000 USD, and the 1000 V/5 A DC power supply for PV module string inspection around 6,000 USD to 10,000 USD. As explained in previous chapters, the power supply should be programmable (always depending on the deployed process to take the pictures) and prices

will depend on this option. A 2 kWp generator could be around 700 USD and a 10 kWp generator around 2,000 USD, currently.

The higher the price, the broader the range of application and the better the quality of EL images and thus the value of the inspection. In some cases, quality can be increased by lower throughput, but professional Quality Assurance (QA) and O&M providers will benefit from high cost solutions in the long term.

Table T5: Price range of the equipment for EL imaging

Device	Price range
EL camera	1 000 USD to 100 000 USD
60 V/10 A DC power supply (non programmable)	1 000 USD
1000 V/5 A DC power supply	6 000 USD to 10 000 USD
2 kWp generator	700 USD
10 kWp generator	– 2 000 USD

8.8.2 Required operating staff in the field and throughput

The number of staff required for field EL inspection is two to three. One person has to operate the power supply and connect the PV module or PV strings. The second person operates the camera and takes photos. The third person can help to move the equipment and setup along the facilities.

The throughput highly depends on the site condition, PV module orientation, PV string layout and the location of the DC combiner box and AC power source as well as the inspection method. Also the expected quality and level of detail of the EL images plays an important factor. The below estimation is based on the best condition and for average quality.

For a single PV module inspection, each PV module could take 1.5 min to 2 min if the work is done continuously with additional two persons loading and unloading the PV modules. On a working day (8 h) with one EL setup in use, the inspection of about 300 PV modules could be possible. For PV module string inspection, the throughput could be around 100 PV modules per hour, but with a lower detail level compared to single PV module inspection. With this approach, inspection of up to 800 PV modules could be possible per working day.

9   UV FLUORESCENCE IMAGING

In the following sections we introduce the basics of the Ultraviolet fluorescence (UVF) method as it is used for PV module inspection. The origin of UVF generation and photobleaching is explained for various typical PV-related examples [111], [112], [113]. Subsequently various factors influencing the formation of UVF in polymeric PV materials are presented and their impact on the quantity of fluorescent species (fluorophores), which determines the intensity of the measurable UVF of PV modules, is discussed. Furthermore, we discuss the application of the method for PV module reliability analysis.

9.1 Description of inspection method

The UVF method relies on fluorescence effects of the polymeric lamination material in a PV module. This is typically Ethylene vinyl acetate (EVA) with various additives such as oxidation stabilizers, UV absorbers and the crosslinker [114]. Fluorescence is a form of luminescence, which is the emission of light by an activated material that has absorbed light or other electromagnetic radiation. The re-emitted light (e.g., in the visible region) has a longer wavelength than the absorbed radiation (e.g., UV-light). A fluorophore is a fluorescent chemical compound that can re-emit light upon light excitation and typically contains several combined aromatic groups or other planar or cyclic molecular groups with several π bonds. Typical fluorophores are degradation products of polymers and/or additives with chromophore/fluorophore groups. The fluorescence of materials can be extinguished by "photobleaching"-effects which lead to a decrease of fluorescence due to reaction processes with e.g., oxygen [57], [115], [116], [117].

The simplest method is to irradiate the whole PV module with an excitation UV light source, and observe the fluorescence effect either with the naked eye or with a camera (UVF imaging). Both detection options operate in three spectral ranges (red, green and blue), according to the physiology of the human eye that the camera emulates. Hence, some qualitative spectral information is contained in the imaging methods. Due to the low efficiency of the UVF conversion and limited emission power of UV lights (e.g., LEDs), imaging is often performed in dark environments. Other applications are given in the literature [118], [119].

The excitation of PV modules with UV-light is commonly achieved using LEDs in the spectral range from 350 nm (glass transmission) to 380 nm (human visibility border). An additional short pass filter can be used to cut off residual visible light of the light source thus creating better contrast. For further image improvement a long pass filter in front of the camera can be used to exclude the excitation light from the image.

In general, UVF measurements are non-destructive, non-invasive, easy to handle and fast [120], [121], [122]. The UVF images presented in this work were acquired by experimental UVF imaging systems with or without filters shown in Figure 62.
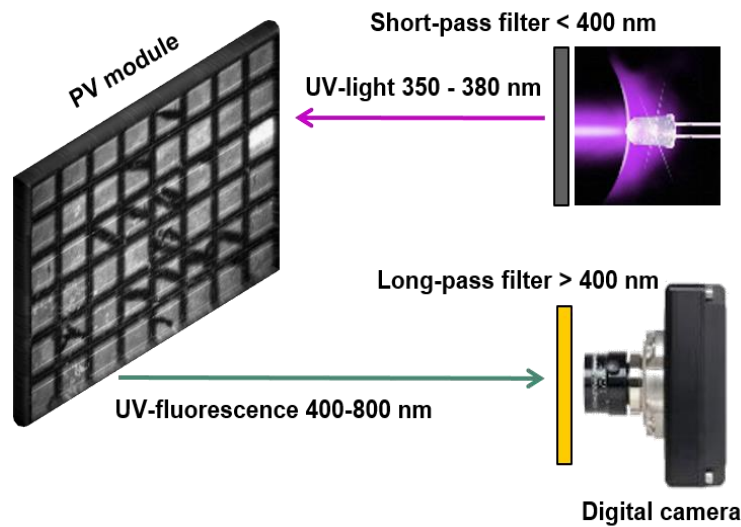
**Figure 62: Basic UVF measurement setup.**

Typical PV modules are composed of a front glass sheet, a polymeric lamination material embedding the silicon wafer based solar cells, cell interconnect ribbons and a protective polymeric backsheet. In this work we focus on this type of PVmodule design.

Some of these components contain substances with the ability to fluoresce or which develop fluorescing degradation products during their lifetime. In principle, only materials that are capable of absorbing UV photons can produce an UVF effect.

9.2 Existing knowledge

9.2.1 UVF of the encapsulation in front of a solar cell

In front of the solar cell UV radiation and high temperatures can form fluorescent groups. Due to the Lambert-Beer absorption distribution for the UV radiation in the encapsulant, the concentration of the fluorescent products is exponentially distributed between the front glass and the solar cell. The concentration is highest on the front glass and lowest on top of the solar cell of the PV module [123]. The front glass and the silicon solar cell beneath the lamination material are effective barriers for the diffusion of degradation products, leading to an accumulation in the front encapsulant and giving rise to a lateral uniform UVF. With increasing time, molecules from the rear (rear lamination material, backsheet and primarily oxygen and/or water vapour from the ambient air that diffuse through the backsheet) can diffuse into the front encapsulant via the cell gaps. The diffusion path around the edge of the solar cell is typically very long (multiple cm), thus it takes time for the oxygen to reach the front encapsulant. Figure 63 shows the UVF distribution in front of a field-aged, encapsulated, defect free solar cell of a glass/backsheet PV module being exposed in central European climate for three years.
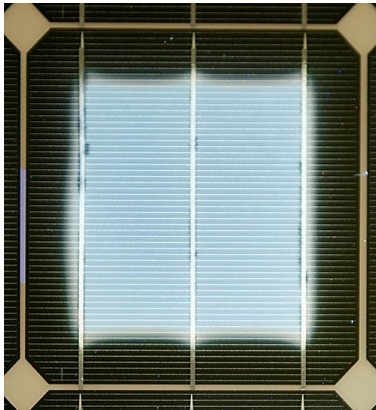
Figure 63: Build-up of UVF in the core of the encapsulation material between the front glass and cell; photobleaching takes place along the edge of the cell.
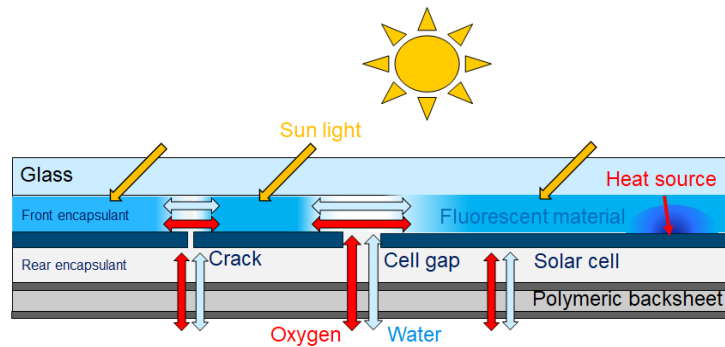
Figure 64: Schematic representation of the cross sectional view of a PV module illustrating the permeation paths within a PV module stack. The UV spectrum of the sunlight generates fluorescent material in the front encapsulant; oxygen in the presence of irradiation bleaches the UVF in the gap between the cells and above cell cracks resulting in a specific UVF pattern.

A.   UVF of the encapsulant between solar cells

In between the cells the diffusion path to and from the ambient air is maximum 1 mm for typical backsheet type PV modules. The chemical environment between cells is different from that in front of the cell, see Figure 64. Oxygen molecules can interact (e.g., energy transfer, collision, reaction) with the activated and fluorescing sites of the polymer leading to a decrease of the UVF intensity. Bleaching needs the combination of irradiation and oxygen ("photobleaching") [113].

B.   UVF in the encapsulant along the edges of the solar cells

Along the edge of the solar cells there is a region where molecules can diffuse from the cell gap into the front encapsulant above the cell. In this edge-region there is a competition between UVF generation and photobleaching. With increasing operational time of the PV module and pronounced ingress of oxygen, this effect causes a photobleached (darkend) rim along the cell edge (square pattern).

C.   UVF in the encapsulant above cell cracks

Above cell cracks similar UVF photobleaching effects are observed similar to what is seen at the edge of the solar cell. Oxygen penetrates the cell through the cell crack and, in combination with sunlight, the UVF above the crack is photobleached (Figure 65). If the cell cracks formed before the installation of the PV-module, the photobleaching pattern above a cell crack is about double as wide as the photobleaching pattern along the cell edge. This is because the oxygen spreads to the right and left of a cell crack, whereas the oxygen along the cell edge can only diffuse towards the centre of the cell.
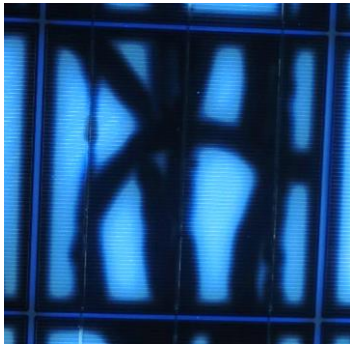
Figure 65: Photobleaching of the UVF along the edge and cracks of the solar cell. The glass/backsheet PV module was weathered in central Italy for two years.
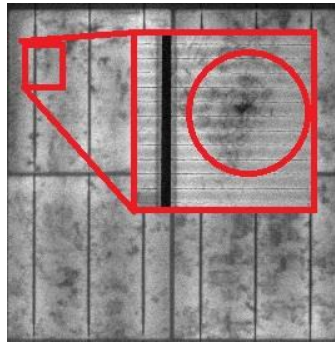
Figure 66: Left: EL image of a solar cell in a PV module with an inset of a 1-2 mm long cross crack. Right: UVF image of the same cell with a black spot at the cross crack position. The PV modules were exposed in south Germany for two years.
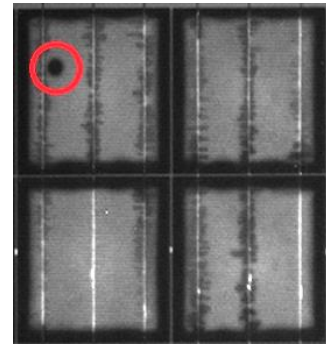
Previous work has investigated the fraction of solar cell cracks detectable with electroluminescence (EL) imaging that are also traceable with UVF [124]. Twenty fielded PV modules with cell cracks were characterized with UVF in the lab. In this experiment, all cracks seen in the EL images were also visible in the UVF images.

Cell cracks may show a grey brownish or black discoloration along the crack on top of the silver finger of the solar cells. These discolorations are called "snail tracks" and at least four different types (appearance and root cause mechanisms) have been described [125], [126], [127]. UVF images of PV modules with snail tracks show the typical black structure in the area above the cell cracks. However, to the best of our knowledge PV modules with snail tracks do not show additional UVF features compared to PV modules with only cell cracks.

D.   Effect of lamination material type and material combinations on UVF patterns

Different qualities/types of encapsulant can also cause varying UVF effects as not only the polymer itself but also impurities, cross linker decomposition products and additives (and their degradation products) can show fluorescence [128]. So far, the UVF technique has been successfully applied to PV modules encapsulated with thermoplastic silicones, crosslinking polyolefins (PO) [129] as well as with various EVA types [130], [122]. Materials with short cut-off wavelength in the UVA domain tend to develop less fluorophores than their UVA absorbing peers.

Figure 67 shows UVF images of four one-cell PV modules with different combinations of encapsulants and backsheets after artificial UV exposure. One of the PV modules is laminated with an UVA absorbing EVA. The other three PV modules are encapsulated with polyolefins (PO): one with a UVA transparent polyolefin, the other PV modules are made with a combination of UVA-absorbing (rear encapsulant) and UVA transparent (front encapsulant) polyolefins.

The EVA PV module shows the known square pattern of UVF with a dark frame along the cell edges (Figure 67 a). The PV module encapsulated with UVA transparent polyolefin does not show any UVF pattern above the cell. Nevertheless, above the backsheet around the cell UVF was observed. This shows the importance of UV absorbers in the encapsulant material to protect the backsheet from alteration through UV exposure.

The two PV modules with the different polyolefins show a UVF ring inside the usual dark frame at the cell edges (Figure 67 b and c). This ring is intensely fluorescing at the frontier with the dark frame and the intensity decreases towards the centre of the cell. As it was shown that the UVA transparent material does not lead to the enhanced formation of fluorophores under UV exposure in this experiment (Figure 67 d), the observed pattern suggests that the UV absorber from the back encapsulant diffuses into the front encapsulant and leads to an inhomogeneous distribution of UV absorber over the cell.

| a) Front: UVA abs. EVA
Rear: UVA abs. EVA
Backsheet 1 | b) Front: UVA trans. PO
Rear: UVA abs. PO
Backsheet 2 | c) Front: UVA trans. PO
Rear: UVA abs. PO
Backsheet 1 | d) Front: UVA trans. PO
Rear: UVA trans. PO
Backsheet 2 |
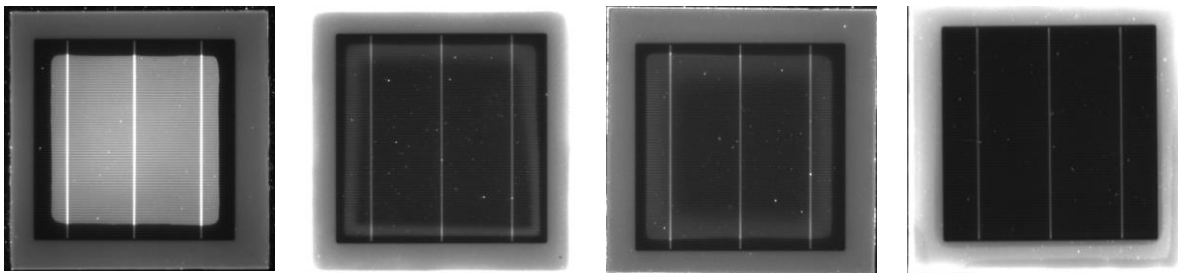
Figure 67: UVF of one-cell laminates with different materials after exposure to 172 kWh/m² UV light. The respective material combinations are given above each image.

The proposed mechanism for the formation of the ring pattern is illustrated in Figure 68, which shows a PV module that uses UVA transparent EVA on the front side and UVA absorbing EVA on the rear side. Along the cell gaps the UVA absorber molecules from the rear encapsulant diffuse into the front of the cell rim area and form fluorophores upon irradiation. The main fraction of the UVA-transparent front encapsulant does not show fluorescence. This special situation of molecular transport (UV absorber and oxygen within the encapsulant) results in the fluorescence square border in the UVF image (ring pattern). Figure 69 shows two different UVF patterns of fielded PV modules, one square pattern and a ring pattern UVF.

These two types of PV modules comprise different encapsulants. The PV module with square pattern (bottom) uses conventional UV-absorbing EVA, the PV module with the ring pattern (top) uses UVA transparent EVA on the front side and UVA absorbing EVA on the rear side of the PV module.
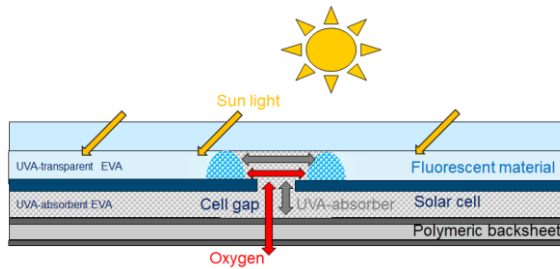
Figure 68: Fluorescence effect for UVA-transparent EVA on the front and UVA absorbing EVA on the rear. UVA absorber diffuses during the lamination process from the rear EVA to the front of the cells near the cell gap.
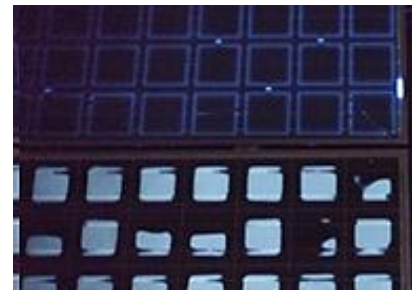
**Figure 69: Ring and square pattern in UVF of two PV modules.**

E.   Influence of backsheet type on UVF pattern

Because UVF can be extinguished or "bleached" in the presence of oxygen and irradiation, the oxygen permeation properties of the backsheet influence the UVF patterns formed, Figure 64 [131].

If polymeric backsheets are used, oxygen permeating into the encapsulant via the breathable backsheet acts as a bleaching agent for fluorescence. The steady state rate at which oxygen gas permeates through a film at specified conditions of temperature and relative humidity is called the oxygen transmission rate (OTR) and provides a measure of the oxygen permeability. The OTR (measured at 23°C and 50% r.H. according to ASTM F 1927:2005) for polymeric backsheets can vary significantly from 4.5 $cm^3/(m^2\,d\,bar)$ for typical polyester (PET)-based backsheets, to 100 $cm^3/(m^2\,d\,bar)$ for polyamid (PA) based backsheets and to 275 $cm^3/(m^2\,d\,bar)$ for polyolefin based backsheets [32]. Consequently, the broadness of the rim around the cells of extinct fluorescence is strongly dependent on the OTR of the backsheet (Figure 70).
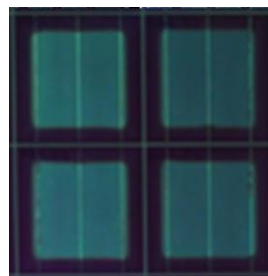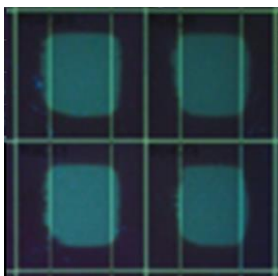
Figure 70: Fluorescence pattern of naturally aged (~5 years) PV modules with identical service life and site of installation but two backsheet types: left: Polyamid with high OTR, right: Tedlar with low OTR [3].
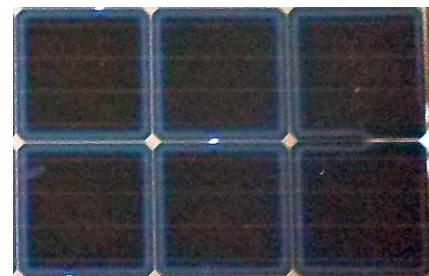
Figure 71: Zoomed UVF image of PV module using a backsheet with metal foil and a cell with a crack in the lower left corner.

Barrier materials like glass or Al-foil containing polymeric backsheet laminates block the oxygen transport and water vapour ingress into the PV module stack (except at the edges of the PV module). Thus, provided a uniform encapsulation composition, the fluorescence formed within the encapsulant upon irradiation is uniform across the whole PV module area.

Figure 71 shows an example of a PV module using a non-breathable backsheet with an integrated metal foil. Different grades of EVA were used for the encapsulation: UVA transparent for the front and UVA absorbent for the rear. As mainly the additives of the rear EVA show fluorophoric groups, enhanced UVF is detected along the gaps between cells and the cell edges as well as above cell cracks (Figure 71). In this case, the cell crack appears brighter than the other areas of the front encapsulant, because the UVA absorber of the rear EVA diffuses to the front side through the crack. The UVA absorber initiates in combination with UV radiation the generation of fluorescent groups. The photobleaching process along the crack and the cell gaps cannot take place because of the missing oxygen. It is noteworthy that if the same type of EVA is used for the front and rear side of a PV module with an impermeable backsheet, the cell cracks will not be visible in the UVF image. Most bifacial double glass PV modules use UVA transparent EVA on both the front and the rear side. For these PV modules cell crack detection via UVF inspection is not applicable. The only double glass PV module design with the material combination UVA transparent EVA in the front and UVA absorbent EVA in the rear allows crack detection with UVF. These PV modules show a similar pattern like Figure 71.

F.   Temperature history of PV module

The PV module temperature plays a considerable role in the kinetics of fluorophore formation. Under the same irradiance level and exposure time the UVF intensity increases faster in a sample held at 57°C than in an equal sample at 27°C [20]. Under natural conditions, temperature effects are also observed. Figure 72 shows the infrared image of a short-circuited PV module exposed to 800 W/m² at an ambient temperature (AT) of 28°C during a summer day. The PV module temperature was measured on the backsheet surface behind each cell.

Figure 73 shows the UV-F image of the same PV module after 77 days of outdoor exposure taken in the lab at 25°C. The UVF intensity on each cell is almost homogeneous, but there is a significant variability in UVF intensity from cell to cell. Comparing this UVF image with the cell temperature pattern (Figure 72) exhibits a strong correlation. This shows that the UVF imaging highlights the hotter parts of the PV module and that the fluorophores retain the information even after the PV module has been disconnected and dismounted. Thus, UVF imaging can be used to detect present or past heat-producing issues in the PV module without requiring the PV module to be connected and operating.

Figure 74 shows the UVF intensity measured over two selected cells as a function of the global irradiation. The initial fluorescence originates from the manufacturing [128], [129] and is fully photobleached after 10 kWh/m² of UV dose. We speculate that the rapid initial photobleaching takes place by consuming the oxygen content incorporated during the production process.

Both cells are exposed to the same dose and irradiance but their operating temperature at 800 W/m² irradiance differs by 9°C. The temperature difference leads to a significant difference in the fluorescence emission of both cells after an exposure dose of 150 kWh/m², which in this case, corresponds to three weeks in summer.
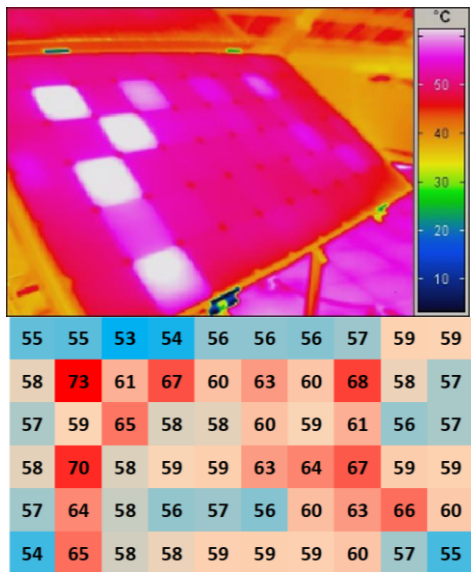
Figure 72: Infrared image (left) and backsheet temperature map in °C (right) of a short-circuited PV module under 800 W/m² sun exposure and 28°C AT.
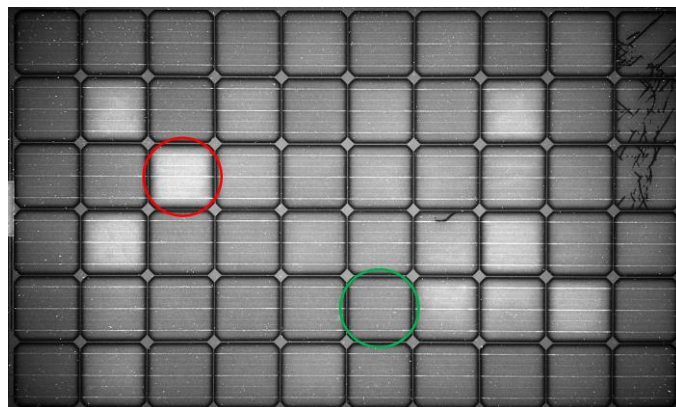
Figure 73: UVF image of a PV module with cells operating at different temperatures. The red and green circles mark cells that operate at 65°C and 56°C, respectively. Conditions: under 800 W/m² irradiance and 28°C AT.
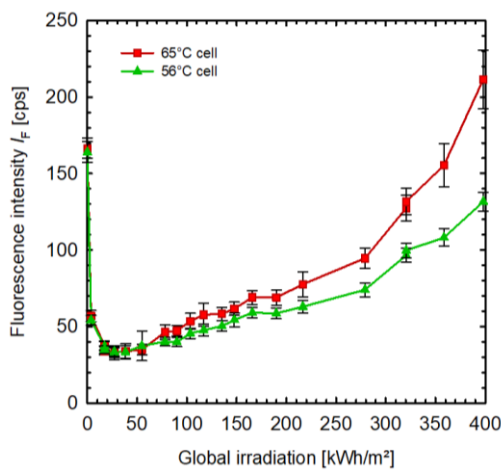
Figure 74: UVF intensity as a function of the irradiation dose measured over two cells with different operating temperatures. The lines are a guide to the eyes. The red squared and green triangle measuring points correspond to the red and green marked cells in Figure 73.
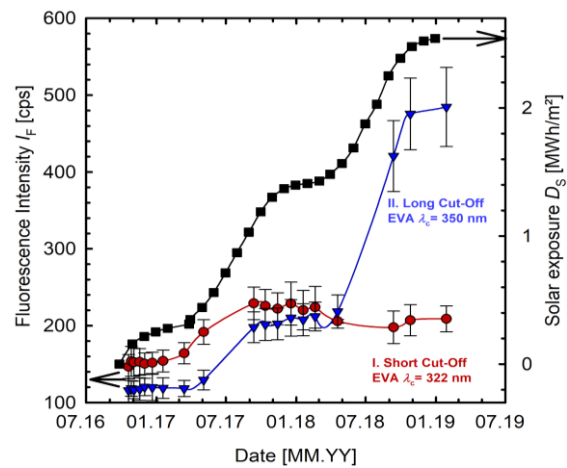
Figure 75: UVF intensity measured zones as a function of time on PV modules with encapsulation materials having cut-off wavelengths of 322nm (red dot curve) and 350 nm (blue triangle curve) exposed in Hamelin, Germany. The black square curve shows the accumulated sunlight dose since the installation.

G. UV dose of PV module

Figure 75 shows the seasonal change of the UVF intensity increase as measured on two 9-cell PV modules exposed on a roof in Hamelin, Germany. One of the PV modules contains an EVA encapsulant with a cut off wavelength of 322 nm, the other with 350 nm. Both PV modules are laminated with the same backsheet. The UVF intensity increases for both materials during the first summer and then stabilizes in the case of the short cut-off EVA. A slight decrease of the UVF intensity is observed during the winter. The EVA with the 350 nm cut-off wavelength shows an increase in both summers, the second one being higher than the first one, although the irradiation dose in the second summer was not significantly higher than in the first summer. For both EVA types only one month in the field during summertime is sufficient to observe detectable UVF. In the winter, no relevant amount of fluorophores are generated.
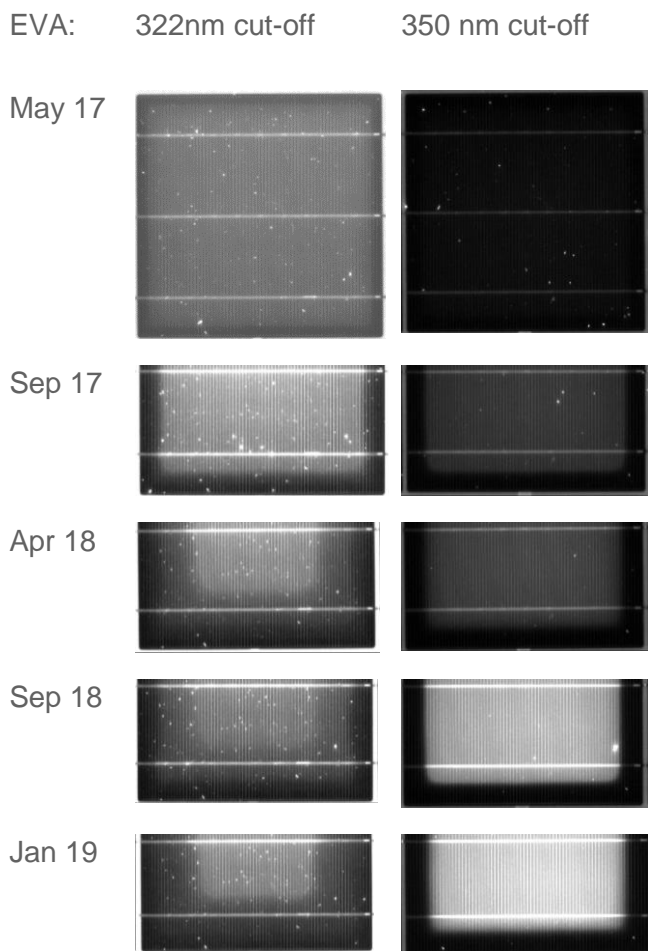

Figure 76: UVF image of a cell (half) of two out-door exposed PV modules with different EVA cut-off wavelength. Images were taken at different times in Hamelin, Germany, over two years.
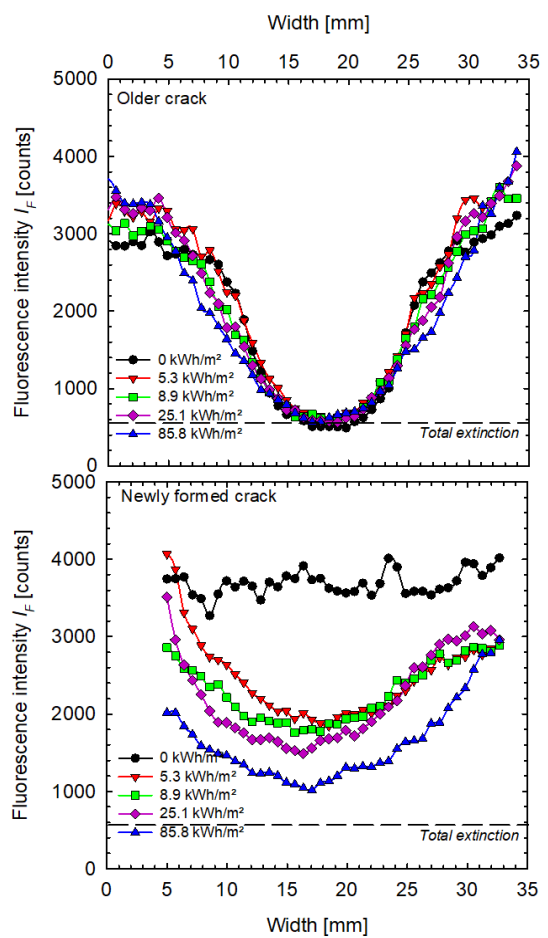
Figure 77: UVF intensity profiles measured after sequential sun exposure across two cracks in a PV module:

Figure 76 shows UVF images of the central cell of both PV modules at different dates. Besides the described UVF intensity increase in the centre of the cell a seasonally dependent contrast and framing width along the cell edge can be noted.The top diagramme is related perpendicular to an old crack and the bottom diagramme perpendicular to a crack newly formed at 0 kWh/m². The dashed line represents the UVF level of areas that have been exposed to oxygen for several years such as cell edges.

H.   Photobleaching Rate of UV Fluorescence

When a new cell crack appears in an already fluorescing glass/backsheet PV module, the photobleaching mechanism depicted in Figure 64 initiates. The UVF intensity starts to decrease along the crack, provided that the PV module is still exposed to sunlight. Figure 77 shows the UVF intensity measured across a cell crack newly formed in an already fluorescing PV module. At the same time, the UVF profile is measured across an older crack. The fluorescence profiles depicted are measured after subsequent sun exposure after the formation of a new crack in summer. The fluorescence profile across the older crack remains unchanged during the whole measurement campaign. The UVF intensity over the new crack is decreasing. But even after three months, the UVF intensity is higher over the new crack than over the older crack. This makes it possible to read the temporal sequence of the cell cracks from their UVF images. Authors have shown that UVF images of a PV module with UVA absorbing EVA can reveal transportation-induced cracks in a new PV module as soon as 11 days after installation in summer, with an equivalent sunlight dose of 55 kWh/m² [119].

I.   Other features

For the description of other known (front glass, cell fix tapes, effect of flux and cell interconnect ribbons, fluorescence strips in EVA, residual of tapes) and not yet understood (photobleaching along cell interconnect ribbons and cell metallisation finger, bright fluorescence cell cracks, strips of the size of cells across the PV module) UVF effects in PV modules we refer to the comprehensive review paper given in ref. [132].

9.3 Detectable failure types for PV modules and PV arrays

9.3.1 Cell cracks

The main application of the UVF method is the in-field detection of cell cracks in PV modules. However, one has to bear in mind that the photobleaching of the UVF along a freshly formed cell crack needs some summer days of exposure to take place and, consequently, make its detection via UVF possible. Therefore, the method cannot be applied before or directly after the installation of the PV modules. However, large PV systems are built in several months. Therefore, the UVF method should be applicable for cell crack detection after the complete installation of the system.

Freshly formed cell cracks in aged, sun exposed PV modules are up to 100 kWh of radiation dose distinguishable from older cracks. After higher radiation dose new cracks may become indistinguishable from older cracks. Therefore, the method can be used to analyse the impact of a hailstorm on the cell crack pattern of PV modules [121] several weeks after the hail-event. Figure 89 and Figure 90 show PV modules exposed to a hailstorm. The PV module in Figure 89 is hardly affected by the hailstorm, but allows a clear explanation of all phenomena that occur. An old cell crack appears broad and as dark as the UVF along the cell edge (blue mark). A freshly formed cell crack that was not exposed to the sunlight (e.g.) is not visible in the UVF

image (orange mark). In this case, the crack occurs during demounting or transport of the PV module to the lab. The cell crack caused recently by a hailstorm is brighter in the UVF image than an old cell crack (red mark). To differentiate between new and old cell cracks a logarithmic scaling of the UVF image is useful.
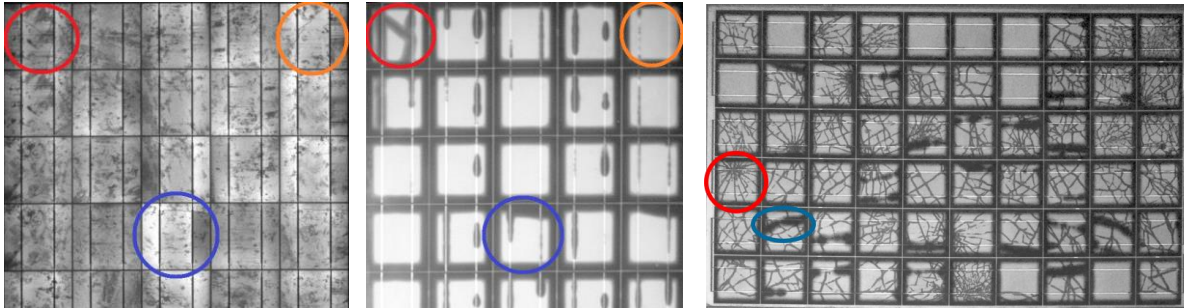
Figure 78: The left image shows an EL image of a hailstorm exposed PV module. The right image shows the corresponding UV-F image with logarithmic scale. The blue circle marks an old cell crack. The red circle marks a cell crack that occurred during the hailstorm. The orange circle marks a cell crack, which occurred during demounting or transport to the lab after the hailstorm.

Figure 79: Differentiation of old (blue marked) and new (red marked) cell cracks in a logarithmic scaled UVF image.

9.3.2 Hot spots

Hot spots can also be identified by UVF imaging. However, the UVF images have to be interpreted differently to infrared-thermographic (IR) images. While an IR image shows the current temperature distribution in an operating PV module, the UVF image indicates the thermal history of each solar cell in the PV module. This allows for the detection of hot areas during operation of PV modules during night or in the lab. Figure 80 shows two examples of PV modules parts including cells with inactive cell areas. The inactive areas are so large that these cells block the current flow through the PV module, heat up during operation and consequently result in higher UVF intensity.

Other kinds of hot spots are also visible in UVF images. Figure 81 compares the lock-in IR, EL and UVF images of a part of a PV module showing problems with contact of the cell interconnect ribbons to the solar cell. One contact area has already burned out resulting in no electrical current flow (blue marked points). These points appear dark in the IR and EL images and are visible as burn marks on the backsheet (not shown here). In the UVF image these spots are still visible as highly fluorescent spots. On the contrary, the recently formed hot spots (red marked points) are barely visible in the UVF image.
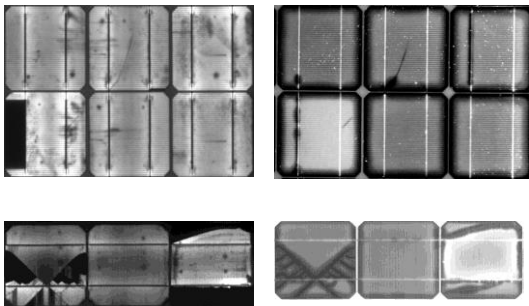
Figure 80: Left: EL images of PV module parts with inactive cell areas [20]. Right: UVF images of the same PV module parts.
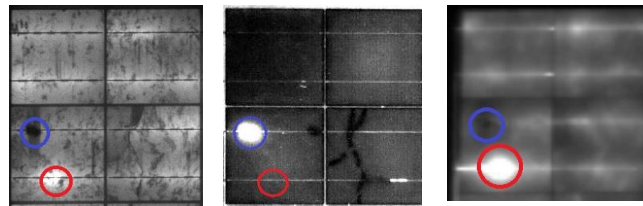
Figure 81: EL image (left) made at a current of 8.23 A; UVF image (middle) and Lock-in IR image (right) made at a current of 8.28 A. Old (blue circle) and new (red circle) hot spots are marked.

9.3.3 Hot cells

In some cases whole cells without visible cracks show fluorescence with much higher intensity than others, Figure 82. These cells most probably show a current mismatch to the other cells in the PV module and heat up.
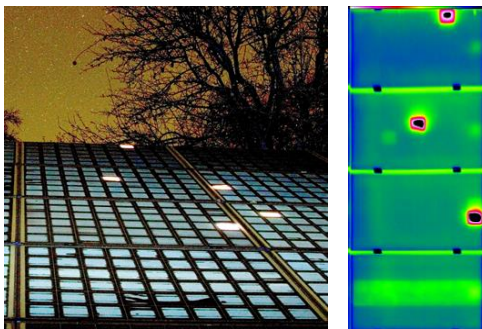
Figure 82: Left: UVF image of PV modules showing hot cells. Right: corresponding daylight IR images of the PV modules showing hot cells under working conditions.
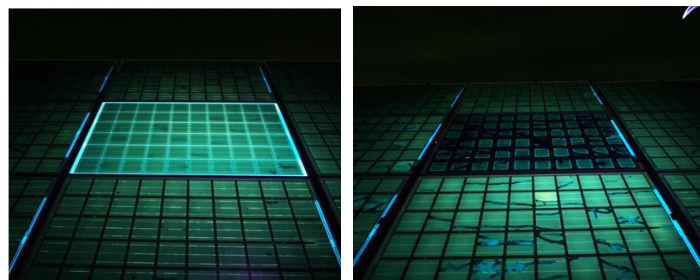
Figure 83: UVF images of PV modules with identical service life and stress impact but varying bill of materials.

9.3.4 Bill of materials differentiation

Different PV module designs in respect to varying types and/or qualities of encapsulants and backsheets cause varying fluorescence effects induced by (i) their permeation properties (mainly OTR), (ii) chemical composition including additives (and their degradation products), (iii) impurities and (iv) aging induced reaction or decomposition products. UVF images taken in the field from the same installation site (identical stress factors and also identical exposure times) can reveal unequivocally if all PVmodules exhibit the same bill of materials or not. The example given in Figure 83 shows UVF images that prove that different types of backsheets

(Polyamid, PET-based, PET+Al, Tedlar) result in different extinction patterns of the UVF [133]. Besides, also different EVA-types with varying formulation result in clearly specifiable fluorescence behavior. The resulting UVF spectra clearly show a distinguishable shape, which can mainly be explained by differences in the additive mix of the EVA films used.

Especially for large PV systems the compliance of the BOM of the PV modules with the data sheet is part of the sales contract. UVF imaging allows for fast and non destructive detection of different BOMs installed. The identification of different BOMs is also useful for the choice of sets of PV modules to be analyzed, because different BOMs may show up different degradation modes.

9.4 Best practice recommendations

9.4.1 Manual setup

The UV light source for the excitation of the UVF should be easily portable, preferably lightweight and battery-powered. It should offer a high intensity of UVA, almost no visible blue light (> 400 nm) and a high radiant flux at low electrical power requirements. Low cost UV LED torchlights often emit a higher portion of blue light (>400 nm), which may require additional filtering. In the end, the light has a lower UV conversion efficiency, which may require additional cooling and reduces battery life.

A simple UVA torch is useful for strategic sampling of test candidates for the more elaborate EL-imaging. The overall presence and qualitative distribution of cell cracks is easily visible with the bare eye under UV-light. Commercially available UVA torches with a single high efficiency UV-LED typically emit a beam angle of 20° and offer a UV irradiance of about 3 W/m² at a distance of 1 m. This torch type allows for a sufficient UVF signal also suitable for close up photography of single cells with a standard digital camera or with a smartphone. The use of a tripod is recommended for good image sharpness. The required darkness is achieved at irradiation below 0.1 W/m² light intensity. This condition is typically achieved one to two hours after sunset. Moon light or urban street light often poses only small imaging limitations, Figure 95.

Figure 84: UVF image, left with urban stray light in a large city and right with good contrast in a darker environment.
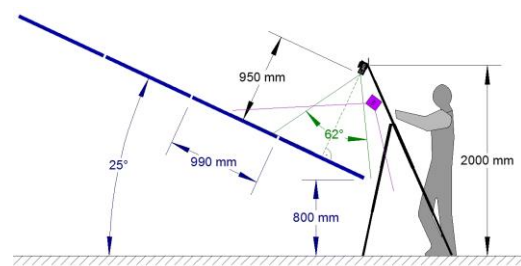
Figure 85: Schematic setup in a PV-park.

In utility-scale systems (PV parks), the rows of mounting tables incorporating several rows of PV modules normally allow for close access and viewing distances of at most a few meters.

For the PV modules above the first row, a flatter viewing angle must be accepted or a specialized high rise camera stand can be used, as depicted in Figure 96. In any case, a more distant setup from the object of interest is needed. Thus, the UV irradiance is considerably lowered and the UVF appears less distinct.

For the PV modules in higher rows, a flatter viewing angle must be accepted or a specialized high rise camera stand can be used. In any case of a more distant setup from the object of interest, the UV irradiance is considerably lowered and the fluorescence appears less distinct.

With an increased exposure time, it is still possible to depict less detailed and more general features, such as different fluorescence from PV modules with obviously different BOM, as seen in Figure 97.

Figure 86: The image stitched from 10 single images taken at ISO3200, 1/5s, f2.0 from a distance of 5 m in the centre to 8 m to the farthest PV module. Note the fainting fluorescence due to less excitation at greater distances and flatter radiating angle.

The main restriction of a manual based inspection is the necessity of direct access to the PV modules, at least within a range of a few meters, as the viewing angle becomes adverse with the distance. Typically, two rows of vertical PV modules can be analysed from the edge of a rooftop with a hand-held UV lamp. With a long tripod expander for cameras about three to four rows can be documented. Especially in PV systems with extended PV module arrays without service alleys, it can be challenging to reach the inner areas without further means like a lifting platform, as stepping onto the PV modules is not recommended.

With good accessibility to the PV modules and suitable ground and weather conditions, about 250 PV modules per hour can be processed on site, assuming one PV module per image, which provides the highest possible resolution of features.

9.4.2 Day time setup

Recently, a measurement setup consisting of a hood in which UV LED arrays and a camera are integrated has been built to allow for day time measurements. The hood is designed to be laid on the PV module to be examined with the size of the hood adjustable to the size of the PV modules. The length and width are adjustable from 98 cm to 115 cm and 165 cm to 175 cm, respectively with 1 cm increments. The hood weighs around 8.5 kg for a typical 60 cell PV module size. The operator triggers and controls the capture by means of a smartphone connected through WLAN with a small computer mounted on the hood. The UV LEDs deliver UV-light in the range of 3 W/m² to 5 W/m² at the surface of the PV module. The camera employed has a resolution of 24 Mpixel and ISO 1600. Typical exposure times are between 1 s and 3 s. The whole system is powered by a 10 Ah (128 Wh) Li iron phosphate battery. One battery lasts for 4 h in the field. So two batteries are sufficient for using and recharging them alternately.

The hood provides easy positioning of the system including the positioning of the camera in the centre of the PV module with a perpendicular view axis to the surface of the PV module. The hood stays stable during the whole exposure time. The light coming from the rear side of the PV modules through the cell gaps can be eliminated by a dark field correction, meaning a picture without UV illumination is subtracted from the UVF image. With a 1 s or 2 s exposure time, up to 200 PV modules per hour can be captured by a single person under daylight. The hood based setup can be used for one to two rows from an accessible PV system area and is recommended for PV plants or well accessible flat rooftops.

The same system can be extended to perform electroluminescence measurements. For this, the visible wavelength band pass filters on the camera need to be exchanged for IR long pass filters. The current can be applied to the PV modules with the Li-ion battery of the set up.

9.4.3 Drone based setup

In order to make the UVF inspection with a drone easy and affordable, the requirements for selecting the drone are: (1) a commercialized, inexpensive drone, (2) low skill demand for the pilot, (3) stable enough to take images in the dark with exposure time of about 0.1 s, (4) needs to carry a low noise camera and an additional UV lamp.

With the above considerations, a commercially available drone with a payload weight capacity of 2935 g, max ascent speed of 5 m/s, max speed of 22 m/s, a max. wind speed resistance of 10 m/s, and a max. flight time of 18 minutes is chosen for the UVF inspections. The camera resolution is 9 Mpixel, ISO range 100 to 25600 and exposure time 8~1/8000 s. Two remote controls are used for the inspection. One is for the pilot to control the drone, and the other one is for the photographer to take pictures. Therefore, two persons are required for the inspection job.

Battery capacity is a major constraint for the drone inspection, because the drone has to carry an additional UV lamp that seriously increases the weight of the whole setup. Furthermore, the battery also needs to supply power to the UV lamp which further reduces the flight duration. A battery package of 4.5 Ah allows a flight time of 8 minutes to 10 minutes for still air conditions. For longer flying time, drone types with two batteries can be used to almost double the flying time.

Three 20 W UV LED chips are used as excitation light sources for the UVF lamp. An additional lens (to concentrate the cone of light to a beam angle of 51°), and a low pass filter are added on top of the LED chips. The UVF inspection with a drone is more limited than the IR inspection as the distance to the PV module surface strongly influences the detectable UVF signal intensity. The higher the drone flies, the weaker is the UV intensity at PV module level. As weaker intensities require longer exposure time for taking a picture. However, the drone is always moving and vibrating, the exposure time must be as short as possible. According to our experience, if the exposure time is above 0.1 seconds, the image becomes increasingly blurred.

In order to maintain the image quality, the drone is supposed to fly as low as possible. However, flying low increases the inspection time, consumes more power, and complicates the control of the drone. With the two contradictory height demands, we have to compromise to have acceptable image quality and inspection time.

Figure 98 shows the UVF images taken at flight heights of 1.5 m, 4.5 m, 6 m, and 9 m with an exposure time of 0.16 s. At 1.5 m height, the image is clear, but there is only one PV module in the image. The inspection time will be very long, and it is difficult to locate the defect PV

module afterwards. At a height of 9 m, the UVF is too weak and the resolution is too low to identify defects. At the height between 4.5 m and 6 m, 12 PV modules to 16 PV modules can be seen in one image, respectively.

In the case that the PV modules show a 'ring pattern' UVF with low intensity, the drone has to fly with low height to be able to catch one PV module in each image, the average time required is 4 s/PV module. The time for changing battery is not included, and it depends on the drone type and battery capacity. For PV modules showing 'square pattern' UVF, the drone can fly at elevated heights of 4.5 m and take 12 PV modules in one image, the average time required is 0.5 s/PV module. Including the time for changing batteries, it is possible to inspect 720 PV modules per hour assuming battery exchange for 6 times. However, the inspection speed highly depends on the project design and weather conditions. The drone saves the inspectors from getting on the roof, and the test time is greatly reduced.

There are still some difficulties to perform the UVF inspection with a drone. First, the work has to be done in the dark, and flying in the dark increases the difficulty and risk to the drone. Second, most people are not willing to work at night, and it may increase the cost as well.

New PV module technologies applying UVA transparent EVA are detrimental to UVF inspection with drones. It makes UVF with drones much more time consuming. Therefore manual or hood based UVF inspection is recommended for this type of PV module.
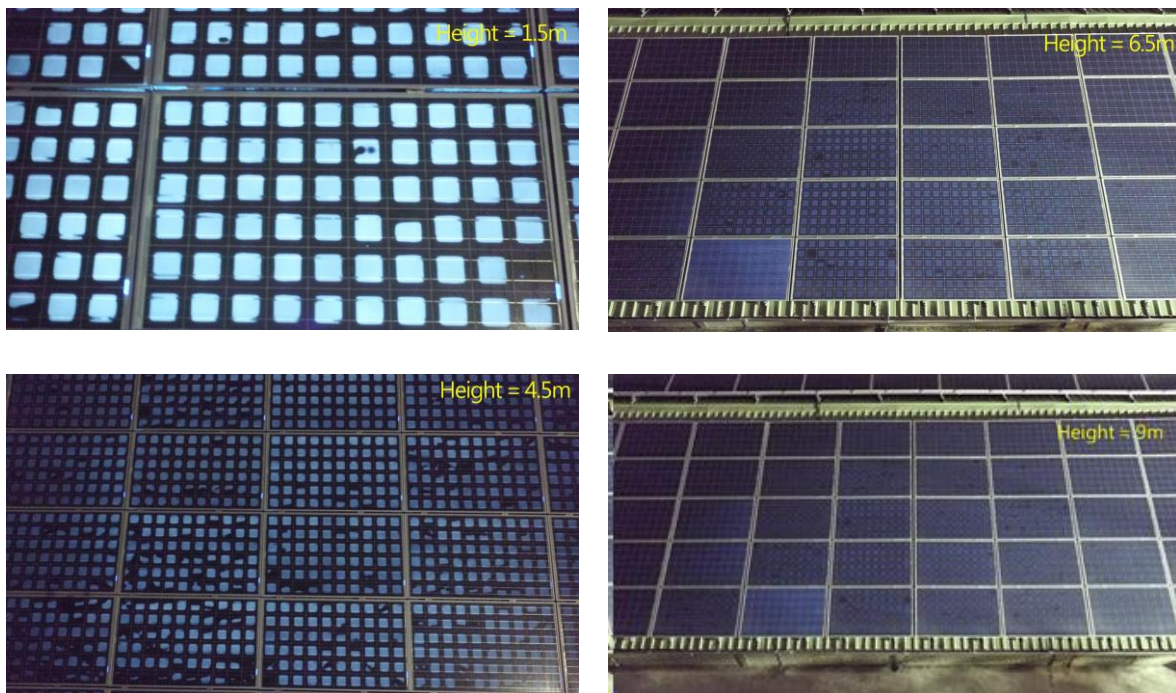

Figure 87: UVF images taken at various flight heights.

9.5 Measuring uncertainty aspects

The UV fluorescence intensity and image contrast are influenced by the temperature of the PV PV module during the measurement [134], the temperature of the UV LED source [135] used to induce the UV-fluorescence and by the temperature of the camera system used to take the images. Basically the contrast of the UV fluorescence images gets lower if the temperature of one or some of the components rises. The temperature of the UV LED has by far the highest impact on the UV image quality, e.g. the UVF intensity is almost three times more decreased if the LED source is heated compared to the PV module alone.

9.6 Occupational safety

For good visibility and for photographic documentation of the fluorescent effects, a dark environment is favourable. As the human vision is not sensitive to light at wavelengths below 380 nm, the eye will not adapt to a brightness stimulus at lower wavelengths, i.e., the iris remains wide open in assumed darkness so the UV-radiation can enter the eye and severely damage the fully exposed retina (photic retinopathy). Furthermore, painful sunburn-like effects can occur in the cornea and conjunctiva (photokeratitis) and on exposed areas of skin. It is therefore mandatory that protective measures for operating personnel as well as casual bystanders are implemented.

The safety standards for radiation exposure in most global regions are typically defined by ensuring the "state of the art". This is typically regarded to be the scientific publications of the "International Commission on non-ionizing Radiation Protection" (ICNIRP). For UV-radiation, the currently relevant document is "ICNIRP GUIDELINES on limits of exposure to ultraviolet radiation of wavelengths between 180 nm and 400 nm" [44]. It discriminates between the risks of exposure of the eyes, and the exposure of the skin. To evaluate the radiation safety of a UV lamp, it is necessary to measure the spectral intensity distribution of the emission at a distance where exposure might happen, Figure 99. This spectrum is convoluted with a weighting function given in [136] that describes the relative harmfulness of individual spectral ranges. The convolution must stay below 30 J/m² for the skin and eye and the total Energy must not exceed 104 J/m² for the eye in order to preclude thermal effects.

For a hand held UV torch UV-400 protection goggles with uncoloured glasses according to DIN EN 170 are recommended. Interestingly, wearing safety glasses in some cases also improved the visual contrast of the UVF observations. If the UV light cone of the lamp is close to the holding hand, it is advisable to wear UV protecting gloves. For a hood based UVF system transparent UV protection glasses are not required since the UV-light source is blocked by the hood. However, the eyes and skin must be protected against sunlight by sun protection glasses, clothes or sun milk if one works under sunny daylight conditions. To protect the eyes from direct UV exposure for drone setups, the inspectors must wear transparent UV protection glasses. However, the drone is most of the time quite a distance away from the inspectors so with our setup no protective measures have to be taken for the skin.

In any case, the UV irradiation exposure limits must be estimated for each individual setup. Access of unprotected persons to the examination area must be managed to avoid unprotected eye exposure of uninvolved persons. As in all situations on site, two persons are necessary for safety reasons.
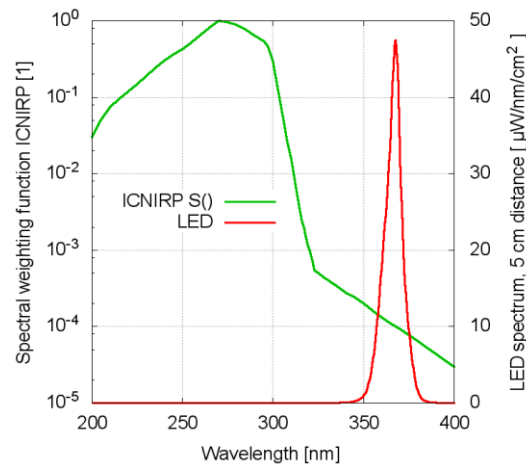
Figure 88: The spectral weighting function S(λ) (green) taken from [44], and a measured 10 W UV LED spectrum at a distance of 5 cm in µW/cm² (red).

9.7 Transportability

The basic setup for manual based inspection consisting of the camera and light source both attached to a tripod has a weight of less than 10kg and can be carried from place to place with little effort by one person.

The hood based system can be transported in an airplane by a transport box with a total weight of approximately 30 kg. According to the international air transportation authority (IATA) the lithium batteries for the system (100 Wh to 160 Wh) ought to be transported exclusively in the carry-on baggage [137]. Batteries with watt-hour ratings comprised between 100 Wh and 160 Wh a specific clearance has to be asked for before boarding. In this case, the maximal allowance per passenger is two batteries transported in a fire safety bag.

9.8 Cost considerations

The most simple application of the discussed method is using a 365 nm UV torch light to illuminate single cells and taking pictures with a low-cost compact camera, preferably featuring good light sensitivity. Suitable UV torch lights are offered for under 100 € and the costs for the complete equipment with safety goggles and small tripod may be well below 500 €. This can be regarded as a good starter package to gain experience with the method.

For higher volume inspection, the described setup using a multi-LED floodlight requires the battery-powered UV-source itself, a highly sensitive full frame camera with a high quality wide angle lens, filter and a professional tripod with extension accessories. Headlamps, safety goggles and -gloves for two persons are mandatory. This equipment is available by 5 T€ to 6 T€. The cost for a hood based system are about 25 T€.

For a drone based setup we estimate nearly the same costs as for a drone equipped with a photo camera. Additional cost will add for an additional UV-source and a second battery needed to power the UV-lamp. The authors are not aware of a commercial system.

138

10 OUTDOOR PHOTOLUMINESCENCE IMAGING OF FIELD-DEPLOYED PV MODULES

10.1 Description of inspection method

### 10.1.1 History and principle

Luminescence refers to photons (light) emitted by material that is not related to the material temperature. In a semiconductor, the intensity of the emitted luminescence is directly related to the semiconductor quality. The luminescence intensity can thus be used as a very sensitive, temperature stable proxy for the maximum voltage that can be obtained from a solar cell. Luminescence images are taken with a camera, with the images allowing direct assessment of the quality of the solar cell, revealing any imperfections or defects that affect the voltage of the cell. Photoluminescence (PL) imaging is a type of luminescence imaging where the electron-hole pairs are created by photon absorption, i.e. shining a light onto the sample. Upon absorption of a suitable photon, a charge carrier is excited from a lower energy electronic state into a higher energy electronic state. In contrast, in electroluminescence (EL) the electron-hole pair is generated by electric carriers (electrons) injected into the device. Advantages of PL imaging include:

- (i) it is *spatially resolved.* This allows both the location and identification of electronic defects.
- (ii) it *does not require contact to the sample*, i.e. it is a contactless technique. This quality has resulted in PL imaging being used throughout the entire photovoltaic (PV) value chain from measuring the quality of silicon (Si) ingots to PV modules deployed in the field.

PL imaging was invented in 1987 [138] and used to characterise direct band-gap substrates and epitaxial layers [139]. The method was then extended to silicon in 2005, a notable challenge as silicon has a luminescence efficiency several orders of magnitude lower than the previous materials measured [140]. PL imaging has been widely adopted in silicon PV manufacturing due to its versatility, speed, and high throughput. The extremely rapid technological progress that we have witnessed over the last 15 years in the PV industry was intimately linked to the capability to instantly detect quality and production issues in solar cells and solar materials at any process stage, from starting material to installed PV modules.

A PL imaging setup typically consists of an excitation light source, usually a laser or high-power LED, and the camera used to record the PL image, as shown in Figure 89. The technical challenge is making sure that the excitation light used, often 1,000 times to 10,000 times brighter than the light emitted by the sample, does not get captured by the camera. It is noteworthy to mention that typical indoor PL systems are placed in boxes to (i) protect the user from hazardous excitation light and (ii) to prevent room light, from interfering with the measurement.
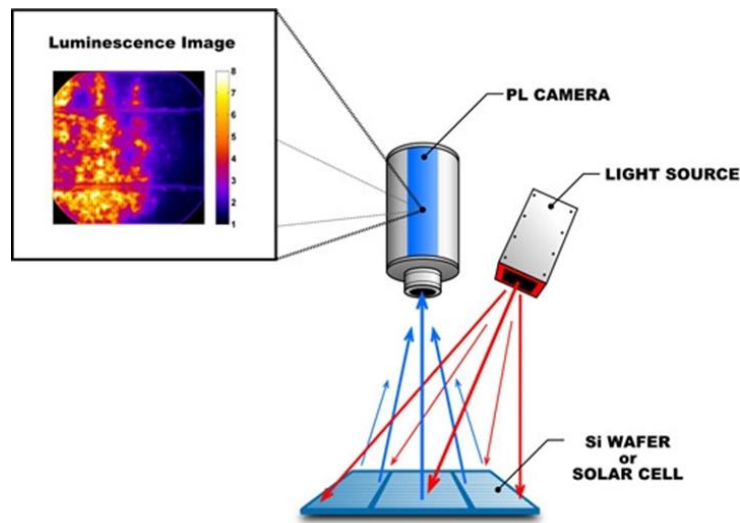
Figure 89: Schematic of a typical PL measurement set-up where a light source (laser or high-power LED) illuminates a device or material under test and a suitable camera detects the photons emitted from the sample. The resulting PL image is a direct measure of material quality [141].
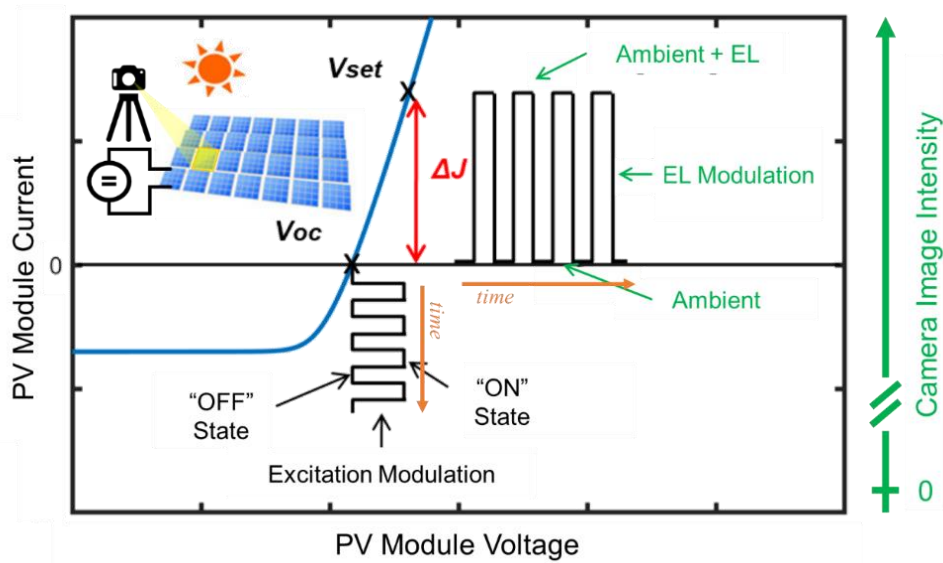
10.1.2 Lock – In Principle for daylight luminescence imaging

A PV module always emits near infrared bandgap luminescence. Depending on the working point of the PV module I-V curve and the form of excitation, the luminescence is called electroluminescence (EL) for electrical excitation and photoluminescence (PL) for optical excitation.

For a PV module which is located outdoors under sunlight illumination an InGaAs camera with suitable optical filtering detects the near-infrared light that is emitted and the reflected (sunlight) from the PV module. The camera is ideally positioned to avoid casting a shadow on the PV module under test and to avoid specular reflection of the sunlight from that same PV module as it detrimentally decreases the ratio between the luminescence over sunlight seen by the camera.

Since the luminescence radiation is several orders of magnitude lower than the reflected sunlight the Lock-In (amplification) technique is used, where the PV module is periodically excited with a known constant frequency while the camera collects a steady stream of images.

Figure 90 below sketches the excitation principle based on the patented DaySy EL Method from Solarzentrum Stuttgart GmbH. While the PV module is periodically electrically modulated between an "OFF" and an "ON" state, it reacts by emitting luminescence radiation with the same modulation frequency. The camera captures in the "OFF" state only the reflected ambient sunlight, while images of the "ON" state contain EL information on top of the ambient light.

Figure 90: Lock-In excitation principle for daylight luminescence based on the patented DaySy EL Method.

The Figure 91 below displays the average brightness of multiple camera frames captured during a Daylight EL Lock-In imaging sequence. Under good conditions, the "ON" and "OFF" state can be well distinguished for each frame, but the signal of a single pixel would fill the whole figure with noise.
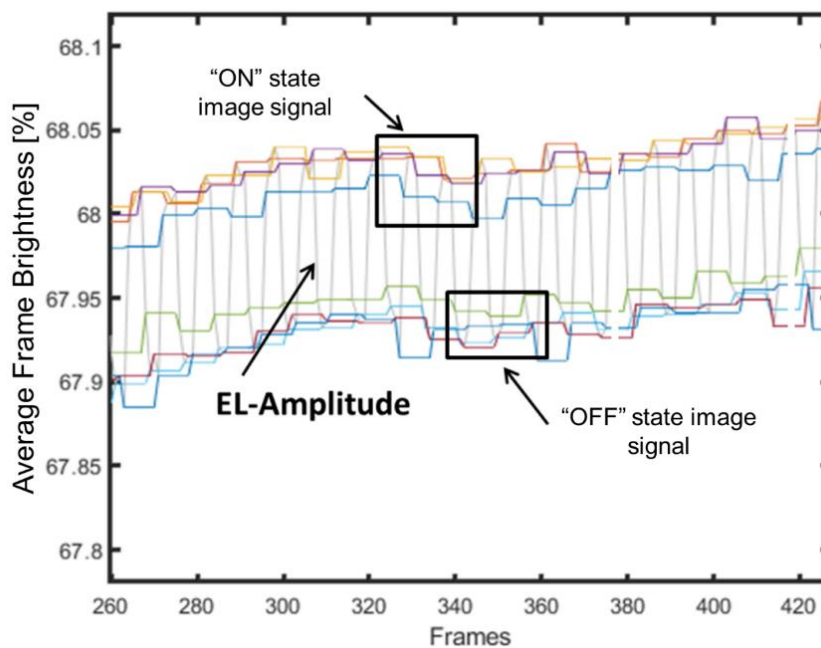
Figure 91: Camera signal acquired during periodical Lock-In excitation.

The camera is connected to a computer which performs all the required image processing. This processing is basically a digital bandgap filter positioned at the exact excitation frequency of the PV module. This way the periodically switched luminescence signal is filtered from the static reflected sunlight.

The "ON" and "OFF" states do not need to be located around the open circuit voltage V_{OC}. They can be arbitrarily chosen to gain different luminescence information from the PV module. For example, DaySy employs V_{OC} and a forward voltage V_{set} for its EL method and Voc and 0 V for its PL method. Other means of excitation are also possible e.g. optical LED based excitation as described by the OM-PL Method in Section 10.1.4.

10.1.3 Outdoor Photoluminescence Imaging

Outdoor PL imaging faces some of the same challenges as indoor PL imaging. However, Outdoor PL is not performed within a controlled environment (a dark box in a lab, high-power and well-controlled illumination). The main approach used to overcome this is to use the strong sunlight as the excitation source. Additionally, suitable optical filtering and clever uses of modulation of the PV module's operating point with signal processing to separate the luminescence intensity from the sunlight needs to be utilised. The equipment required to implement this approach is lightweight and can, in the simplest implementation, even be fitted in one suitcase, which makes it well-suited for large field inspection where mobility and ease of use are of paramount importance. This method works due to the fortunate coincidence, that silicon's PL band nearly perfectly overlaps with a significant drop in the sunlight that reaches the surface of the earth. Specifically, this occurs at a wavelength around 1130 nm and is a result of sunlight being strongly absorbed by water vapour as it passes through the Earth's atmosphere, as highlighted in Figure 92(A) (labelled H_2O). Using appropriate camera filters, it is then possible to limit the camera's detection to this range greatly improving the ratio of desirable PL emission (signal) to unwanted sunlight (noise). A typical filter for this application would be centred around 1130 nm and have a spectral bandwidth of about 25 nm to 50 nm as depicted by the purple shaded rectangle in Figure 92(B). With such filtering in place, the detected PL from a silicon PV module at open circuit is on the order of 1% of the detected sunlight, of course, depending on outdoor conditions and the specific PV module type and quality. Unfortunately, this wavelength range, corresponding to the dip in the solar spectrum, occurs beyond standard Si camera sensitivity (quantum efficiency) as shown in Figure 92(B), meaning a more expensive and lower sensor resolution InGaAs cameras are required for outdoor PL imaging under ambient sunlight.

To further separate between the strong signal from the sunlight and the weak luminesce, the PV module's electrical operating point is modulated, resulting in a significant change in the PL intensity. This must be done fast enough such that the intensity of the sunlight can be considered constant between two subsequent images. Image processing is then used to accurately extract the weaker PL signal from the dominating reflected sunlight signal. This modulated operating point approach has the additional benefit of providing PL images that show almost identical results to EL imaging which is currently the most widely accepted luminescence imaging method on solar farms.
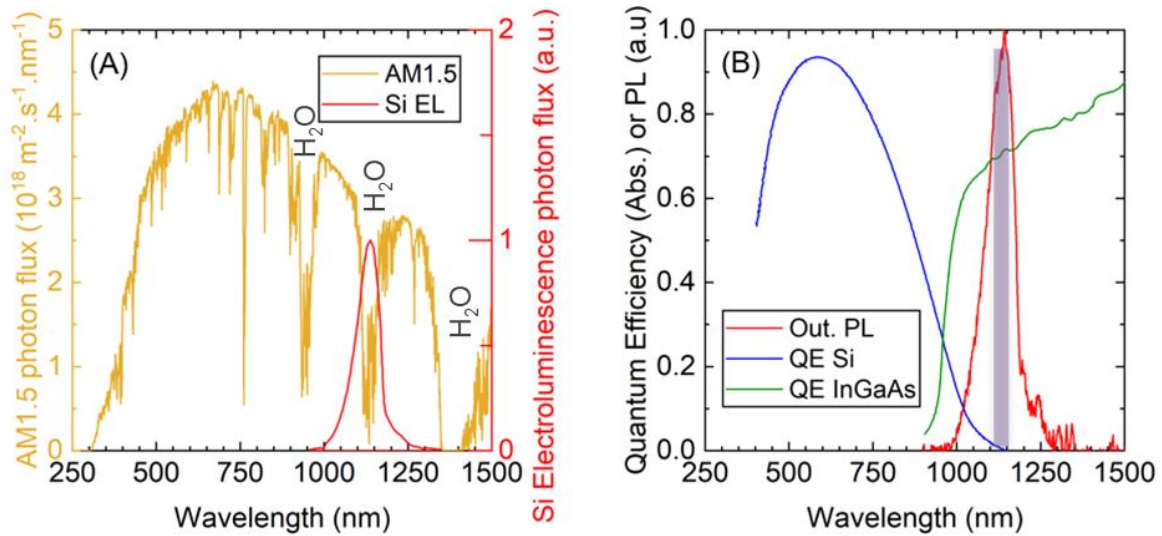
Figure 92: (A) Terrestrial AM1.5 solar spectrum (yellow line) with the absorption bands due to water vapor, and luminescence spectrum (red line) of crystalline silicon; (B) Typical quantum efficiency (QE) curves for a Si (blue line) and an InGaAs (green line) camera sensor, as well as the luminescence spectrum of silicon (red line). A typical wavelength range for a suitable optical bandpass filter is displayed as a purple shaded rectangle (UNSW original image).

Table 29: Comparing outdoor PL imaging with indoor PL and outdoor EL imaging.

	Can be performed under sunlight	Performed at night or in the lab	Does not require contact to the PV module or test sample	Can see disconnected cell areas or PV sub-strings
Standard indoor PL		✓	✓	
Outdoor EL (dark EL or daylight EL)	✓	✓		✓
PL with electrical modulation (EM-PL)	✓			✓
PL with optical modulation (OM-PL)	✓		✓	✓

Modulation of the PV modules operating condition has been demonstrated by two methods (see also Section 10.1.4):

A. The first, implemented by Solarzentrum Stuttgart is called DaySy [142]. It involves the installation of specific hardware into the system to sink or source current into the PV module/PV string being measured. Since this method requires an electrical connection to the PV module strings it is in this report termed *Photoluminescence by Electrical Modulation (EM-PL)*.

B. A second approach is to change the operating point of a PV module by intentionally and rapidly creating partial shading to a solar PV module. The shaded cell(s) in the PV module prevent current flowing through the remaining series connected cells, moving their operating condition from maximum power point to open circuit [143]. In practice this can be achieved by placing a high-powered LED onto a PV module, preventing sunlight from reaching the covered cells. The LED is then turned on and off in rapid succession, effectively simulating the missing sunlight (if LED is on). In this report this method is termed *Photoluminescence by Optical Modulation* (OM-PL).
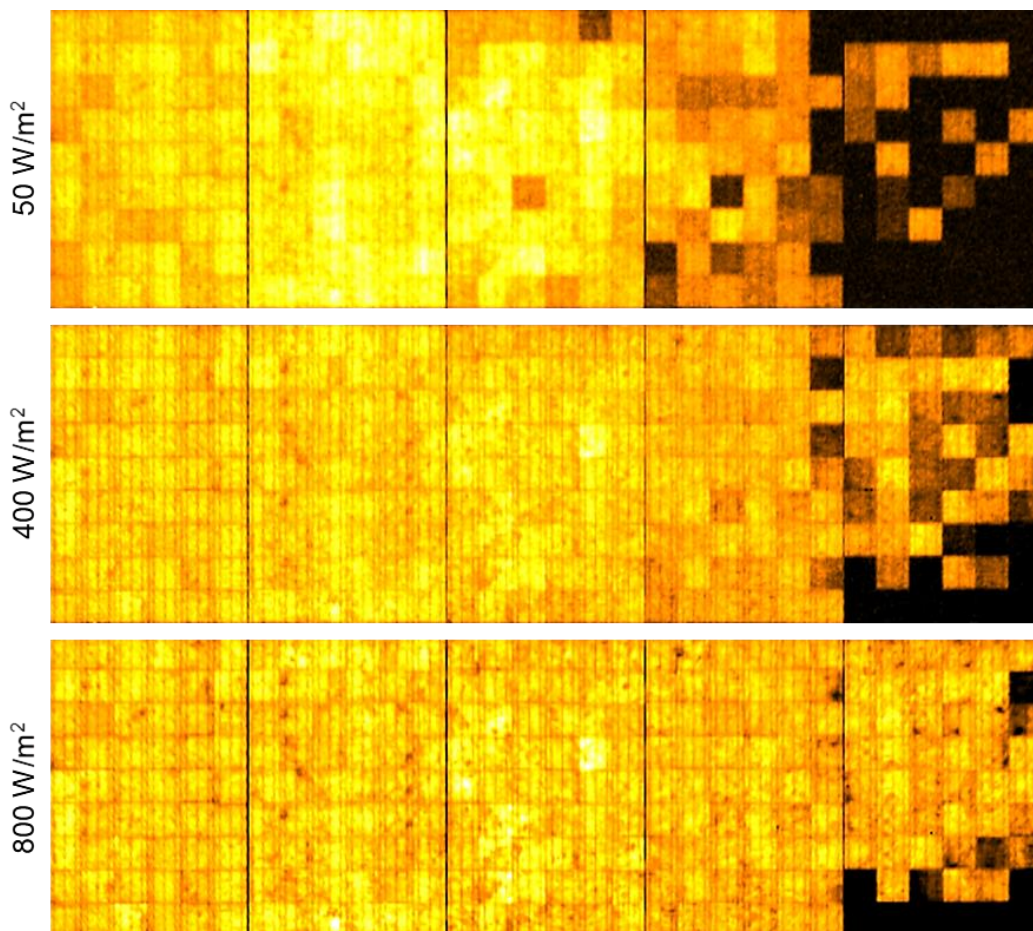

Figure 93: EM-PL image of 5 PID affected PV modules inspected under different insolation conditions. Affected cells/PV modules appear darker at low irradiance due to the stronger effect of the reduced shunt resistance [144].

144

Uses for outdoor PL imaging:

1. Inspect PV modules after installation and prior to solar plant commissioning. This enables finding faults that have been introduced by manual handling during installation and serves as a benchmark for later inspections. Pre-commissioning PL screening can also increase the bankability of solar projects since it guarantees the highest possible installation standard.
2. Inspecting solar farms that are suffering from underperformance to identify the cause of underperformance and to replace faulty PV modules.
3. To gain better insights into PV module failures on solar farms that have been inspected by thermal infrared thermography and found to have high numbers of faults.
4. Inspecting solar farms after severe weather events (wind loading and hail) to inspect damage and for insurance claims.
5. Inspecting solar farms prior to a change of ownership to ensure that installed PV modules are still of sufficient quality and that the farm can be expected to have a long life.

10.1.4 DaySy Daylight Luminescence System with electrical PV string modulation (EM-PL)

Solarzentrum Stuttgart is currently the only sizable company performing commercial outdoor PL, with a system called DaySy [142], [88]. Figure 94, Figure 95 and Figure 96 explain the working principle of electrical PV string modulation.

Other approaches of outdoor PL are described in references [145] and [146].
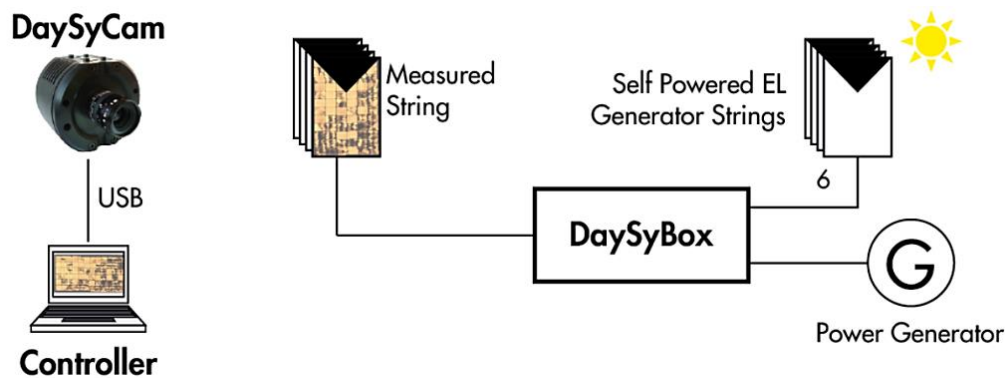
Figure 94: Schematic of the DaySy system and its components: (left) The camera (DaySyCam) and Controller unit; and (right) the DaySyBox which allows biasing of the PV module string which can be powered by other PV generator strings or a power generator [142].

The DaySy system (see schematic in Figure 94) electrically modulates the operating point of the PV modules, allowing separation between the weak PL and strong sunlight. It is capable of measuring PL during the day as well as EL during the day and at night. During the daytime, the power used to modulate a PV string is taken from adjacent PV strings. At night-time or low sunlight condition, a generator is used to provide the necessary biasing condition for the PV modules i.e. to inject current into the PV modules via electrical connections. This can be done on a PV module string basis (typically around 25 PV modules to 30 PV modules for a 1500 V system), which greatly accelerates the measurement process (as shown in Figure 95 and Figure 96).

Figure 95: Field application of the DaySy system with full PV string biasing: Top: Multiple cameras inspect the same PV string at the same time for increased throughput (Source: Solarzentrum Stuttgart GmbH). Bottom: Hail-screening from an aerial platform [147].

Measurement times to take PL images with the DaySy system are between 1 s to 120 s depending on the open circuit voltage of the solar cell technology employed. With HIT, IBC and PERC modules image acquisition times are in the 1 s to 10 s range and increase for older multicrystalline PV modules from prior to 2010 to about 60 s to 120 s. Each image has a resolution of 1280 x 1024 pixels (generated with subpixel interpolation from a 640 x 512 camera) and since the entire PV module string is modulated it is possible to take images of several PV modules in a PV module string as in Figure 96. The most suitable approach is chosen based on the resolution and throughput requirements and it can be beneficial to perform multiple PV module images first and then closeup images that feature obvious performance degrading defects.
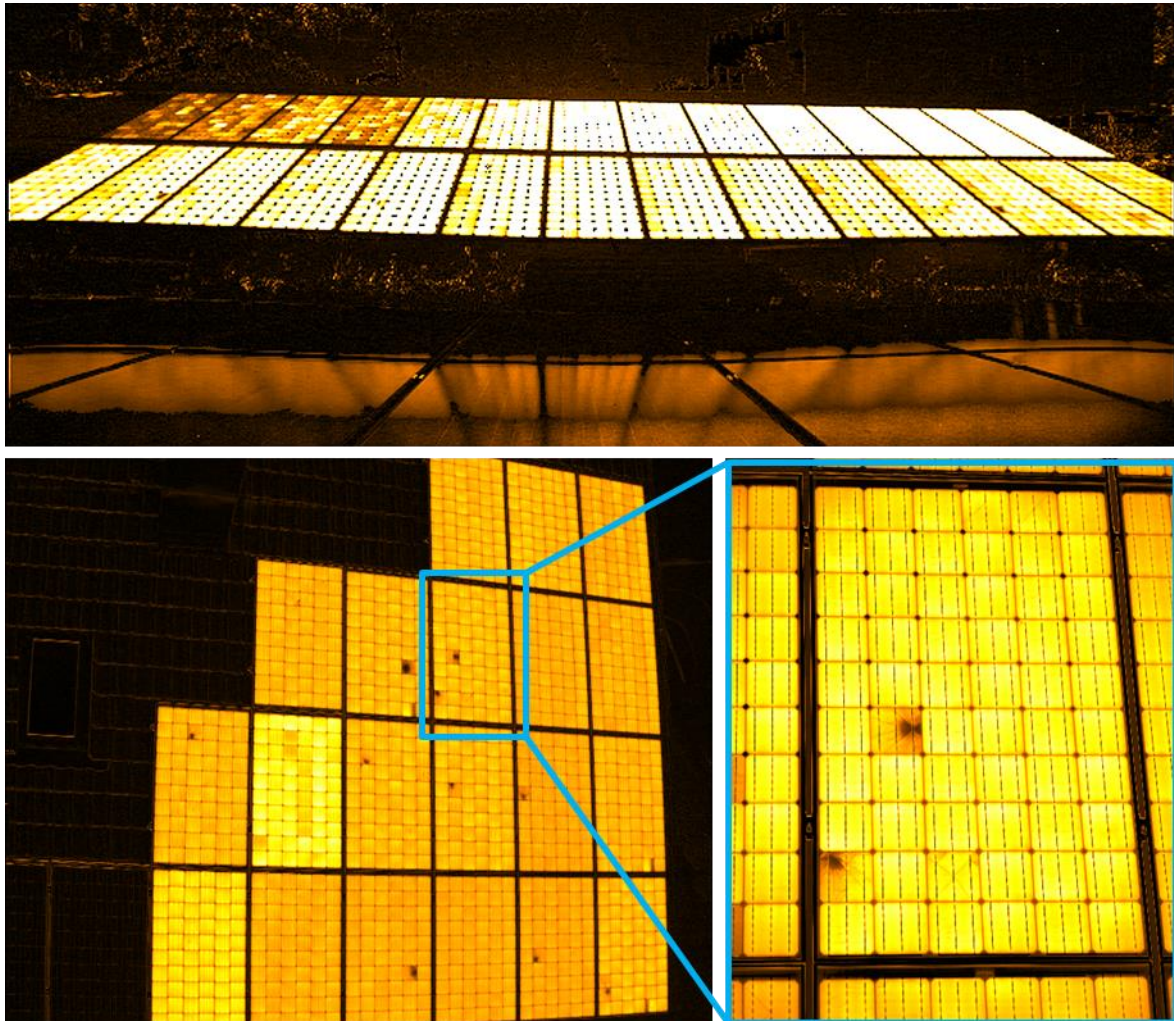
Figure 96: Depending on throughput and resolution requirements the DaySy system can image up to a full PV string at once (Top, bottom left, Source: Solarzentrum Stuttgart GmbH); or a single PV module (bottom right) [147]. Full PV string images reveal major defects like extreme cell breakage or PID, while single PV module images allow automatic image processing and crack-counting. The shown images are from daylight EL inspections, but the same statements hold true for EM-PL as well.

Throughput:

A   Cracks: In order to count single cracks or to apply software assisted damage evaluation one PV module/image has shown the best trade-off between speed and resolution. A DaySy-Team consisting of one electrician and two camera operators is able to inspect ca. 500 kWp to 750 kWp (1500 PV modules to 2000 PV modules @ 1 PV module/image) in a single working-day.

B   PID: For PID inspections it is most useful to image full PV strings. One DaySy-Team consisting of one electrician and **one camera operator** is able to inspect more than 1 MW_p (> 4000 PV modules @ 1 PV string/image) in a single working-day.

Shading and Bypass Diode failure

Figure 97 shows the effect of full/partial shading in case of the DaySy EM-PL method. DaySy modulates the working point between open circuit and short circuit electrically. In the case of a fully shaded solar cell the bypass diode keeps the PV sub-string in open-circuit conditions at all times and thus no PL signal can be extracted, and the PL image appears dark. If a cell is only partially shaded the bypass diode allows only part of the current to be modulated and the PL image appears "half-bright". The amount of modulated current is proportional to the bright-ness of the PL image if all other factors are kept constant. In Figure 97 the light was not com-pletely blocked in the rightmost PV sub-string so there is still some weak PL signal visible in the image.
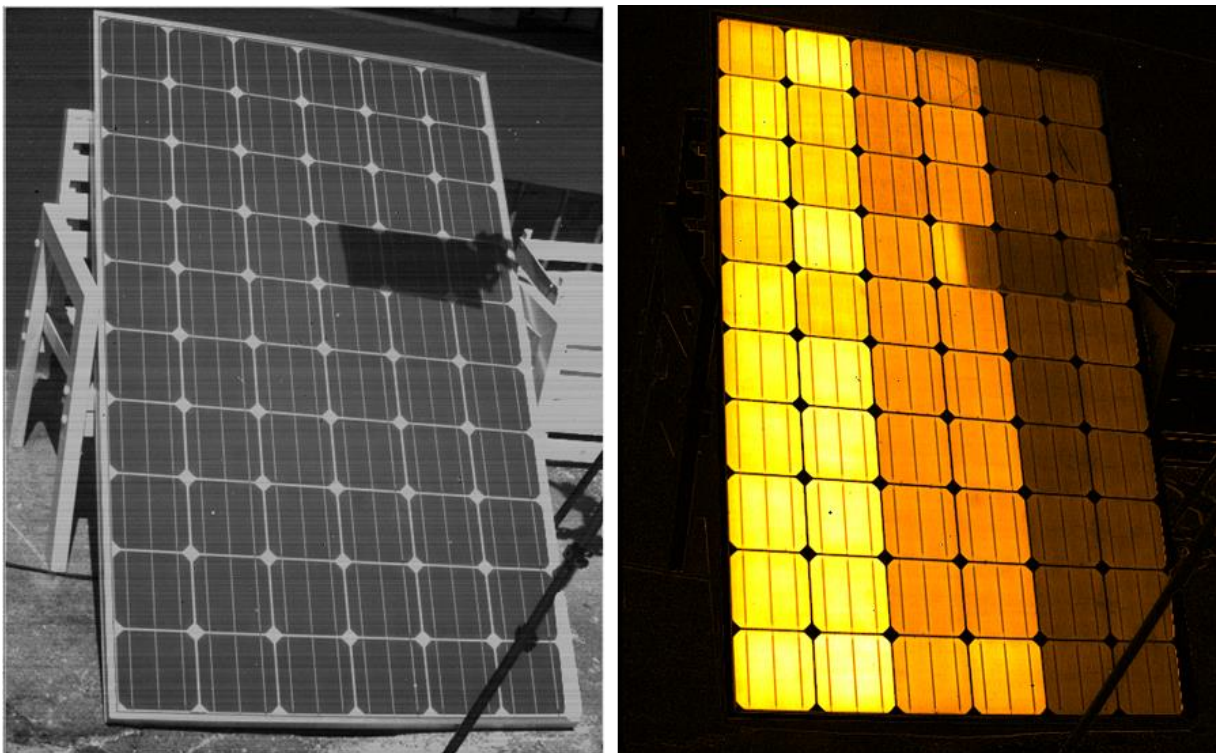
Figure 97: Controlled shading setup (left: camera image, right: EM-PL image): An object shades a cell in each the module sub-string to a different degree (left 0%, middle 50% and right 100%). With more "effective shading" the right PV sub-string appears darker than the middle one, which is in turn darker than the leftmost [147].

In case of a short-circuited bypass diode the DaySy EM-PL method cannot modulate the af-fected PV cell-sub-string and it appears completely black in the EM-PL image as shown in Figure 98.
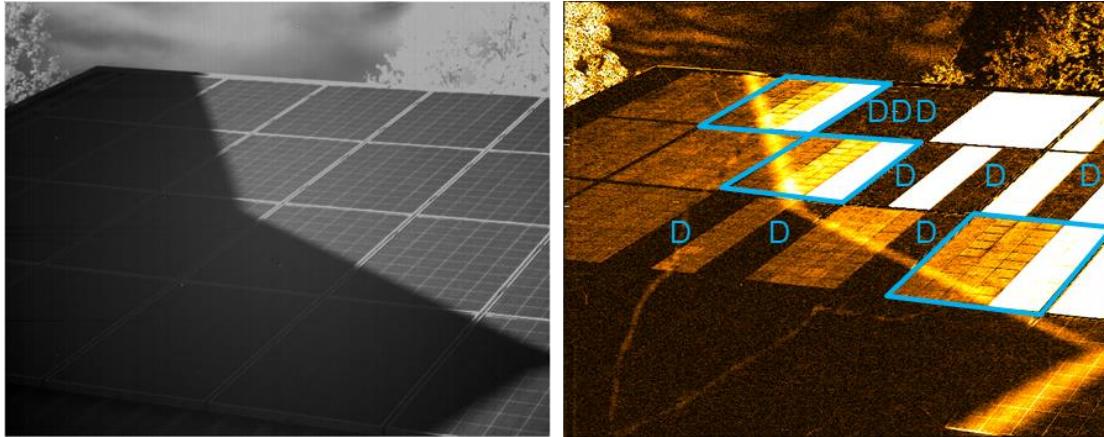
Figure 98: Real life shading and defective bypass diodes: Left image shows a live camera picture while the right picture is an EM-PL image acquired with DaySy. A neighbouring roof casts a shadow on a PV installation. Highlighted PV modules with fully/partially shaded cells show the same behaviour as in Figure 97, while completely dark substrings (marked D) have a defective bypass diode with short-circuit character [147].

10.1.5 Typical outdoor photoluminescence set-up using optical modulator switching (OM-PL)

A basic set-up that can be used for outdoor PL imaging where the operating point of the PV modules is altered using an optical modulator is schematically displayed in Figure 99(a) [148]. The PV module under test is placed outdoors under sunlight illumination. An InGaAs camera with suitable optical filtering detects the near-infrared light that is emitted (PL) and that reflected (sunlight) from the PV module. The camera is positioned to avoid casting a shadow on the PV module under test and to avoid specular reflection of the sunlight from that same PV module as it detrimentally decreases the ratio between PL over sunlight seen by the camera. The camera is connected to a computer which performs all the required image processing. The switching of the PV module operating point is performed by optical modulation of individual PV sub-strings of the PV module as depicted in Figure 99(a), i.e. no access to the PV module terminal is required.

The optical modulation is performed using a suitable high power LED array on top of one or more cells in a PV sub-string (the "control cells") and by switching this LED between different light intensities – in the simplest implementation this is between fully *On* and fully *Off*. In Figure 99(b) the workflow for this scenario is illustrated. When the LED is turned *On*, the PV substring current is maximised, and an image captured by the camera will contain ambient reflected sunlight but almost no PL signal (since almost all photogenerated charge carriers are extracted from the PV module). When the LED is subsequently turned *Off*, the PV sub-string current is minimised which results in an image containing both, ambient reflected light, and maximum PL emission (since the photogenerated charge carriers are now available in the test cells for recombination). The process of LED switching and image captured is repeated several times and the final PL image is computed as the difference of the average images for both switching states, as illustrated in Figure 99(b; right).
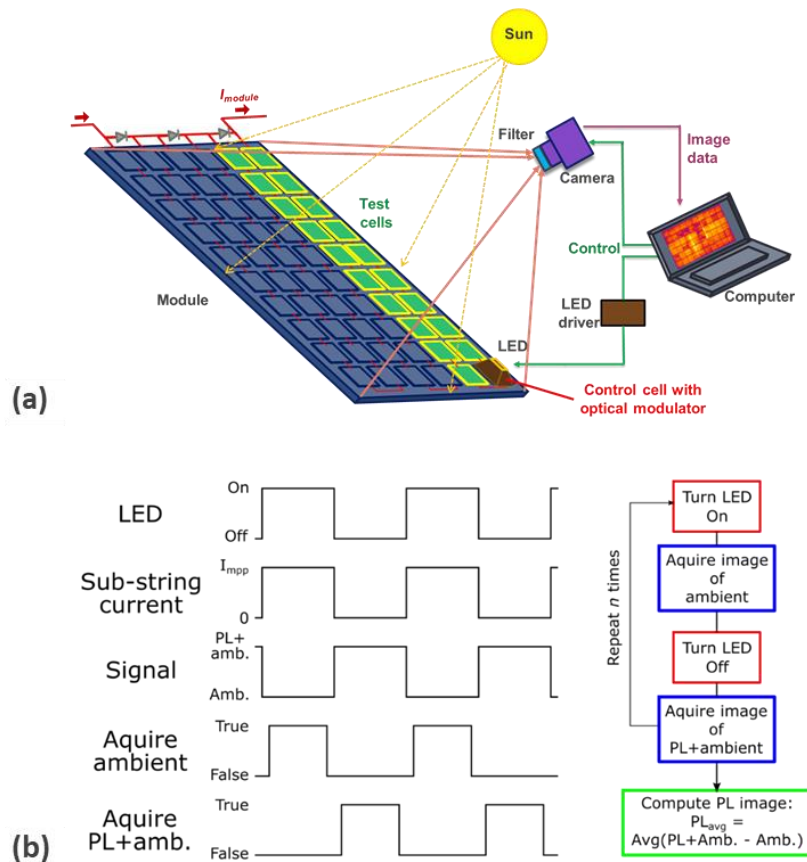
Figure 99: (a) Schematic of an outdoor PL set-up where optical modulation is used to toggle part of the PV module via a control cell between open-circuit and short-circuit conditions [148]. (b) System timing (left) and workflow (right) of outdoor PL imaging (Source: UNSW original image).

To image all three PV sub-strings simultaneously at least three control cells and the respective optical modulators are required. Note that hence, for the approach to work, at least two images are needed if the entire PV module requires imaging since the control cells cannot be imaged. In this case, the optical modulator needs to be moved from its original position onto a second position to image the cells that were previously covered by the optical modulators in the first PL image.

A fully functioning alpha-prototype tool is displayed in Figure 100(a). It features the custom-designed tripod that can withstand high winds and carries the near-infrared camera with optical filters, the laptop with control software and the battery and electronics needed to power laptop, camera and optical modulator. The optical modulator is placed onto the bottom most row of the PV module under test and a first image is taken (Figure 100(b)). Then the modulator is moved to a cell row in the top half of the PV module and a second image is taken. This procedure ensures that an entire module can be measured, and it can double the final image resolution. A resulting PV module PL image is assembled from both partial images. With this current procedure, about 100 solar PV modules can be imaged per hour. The image acquisition time for a single image is about 1 sec for PERC modules which are now the most widely installed PV modules.

150

Throughput:

Given a typical working day, it is possible to image about 1600 PV modules (around 640 kWp per day) with one measurement system (two operators) on a sunny day. Note that OM-PL is a very young technique and significant throughput improvement is expected in the near future.
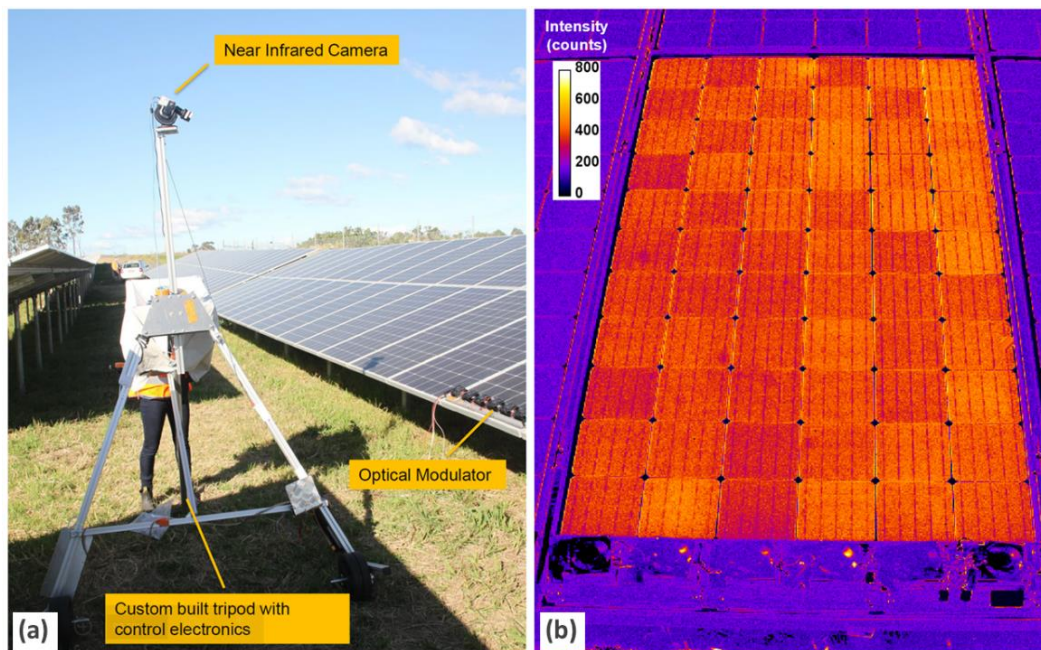
Figure 100: (a) Alpha-prototype outdoor PL tool consisting of custom tripod on wheels with battery, drive electronics, laptop and optical modulator; (b) the resultant outdoor PL image obtained from 100 image-pairs (image displays a fault free PV module) (Source: UNSW original image).

10.1.6 Ability to detect bypass diode failure [149]:

A.   Failure in open-circuit condition

If a bypass diode fails in open-circuit condition and the control cell is shaded, then the control cell will be reverse biased until it reaches a reverse current equivalent to approximately the M_{PP} current of the solar array. As a result, the maximum power point (M_{PP}) current will flow in the test cells even if the LED is turned full *Off*. Thus, a bypass diode failing in open circuit (or missing completely) will not allow switching of the PV sub-string operating point and no outdoor PL signal will be detected in the affected PV sub-string. It is important to note that shading of solar cells under such circumstances MUST STRICTLY BE AVOIDED since it can result in cell overheating and can cause severe damage to the shaded PV module. Nonetheless, such shading may occur under normal operation conditions (eg. bird droppings, grass, trees, etc.) as well and OM-PL is the only contactless method able to detect this type of defect.

In order to prevent PV module damage and the associated hazard, the prototype shown in Figure 100(a) features a *live PL mode* which displays the PL image "on the fly". After adjusting the camera field of view, the imaging system is used in *live PL mode* before placing the modulator on the PV module. When placing the modulator on the PV module, the operator looks at the live view image, if no PL signal is detected from one PV sub-string or more (the PV sub-string will appear black), the modulator needs to be removed from the PV module immediately. Current prototype improvement includes automatic detection of this failure resulting in turning *On* all LEDs to prevent further shading after fast fault detection.

B.   Failure in short-circuit condition

In contrast, a bypass diode that has failed in short-circuit will permanently short-circuit the corresponding PV sub-string and hence the difference between both modulation states will be larger as for the other PV sub-strings. As a result, the outdoor PL signal from the affected PV sub-string is about 5-10% higher than that of a PV sub-string with a fully working bypass diode. A short-circuited bypass diode thus manifests itself in a corresponding PV sub-string that is brighter compared to the other PV sub-strings in the same PV module.

10.1.7 Quantitative or qualitative method

Outdoor PL imaging can detect a broad range of defects related to (i) manufacturing, (ii) installation, and (iii) degradation. The decrease in PL intensity represents a loss in local voltage (a decrease by a factor of two corresponds to approx. 18 mV voltage loss in the affected region). Comparison from PV module to PV module in absolute quantitative terms might be challenging in variable sunlight intensity (cloudy condition, time of the day) as the excitation is not well controlled for outdoor PL imaging and also the arrangement of camera, sunlight and PV module are varied over different times of the day. However, detection, identification, and count of relevant electronic defects is still possible under those conditions if the PL image quality is sufficiently high. In Figure 101 and Figure 102 we show a comparison between an outdoor PL image taken with the OM-PL method (InGaAs camera with 640 x 512 pixels) on the left and an EL image of the same solar PV module in the middle. Closeup sections of two heavily defective regions that have resulted from very rough manual handling are displayed on the right. Essentially, the outdoor PL image looks very similar to the EL image and shows all the crack like defects (as evident from the close-up inserts on the right) and also the isolated regions. In order to obtain sufficient image quality, it is critical to have sufficient sunlight (see Figure 103 for details) and also to use appropriate exposure time and image averaging. In Figure 103 an example is presented of outdoor PL images (based on OM-PL) of a mono-crystalline PERC solar PV module with varying number of image pairs (V_{OC} and M_{PP}) used to produce the averaged output PL image. With the current system the acquisition of one image pair takes about 20 ms. For one image pair (Figure 103 (a)) a PL image with very grainy structure is apparent. The image resulting from five image pairs (middle) already shows the cracks and strong features but is difficult to analyse due to the still grainy image. In contrast, the PL image in Figure 103(c) resulting from 50 image pairs (corresponding to about 1 s total image acquisition time) is of high quality and suitable for visual and computer-based image analysis.

It can be expected that future PV module technologies with higher cell open-circuit voltage (V_{OC}) values will relax the image capture requirements significantly further.
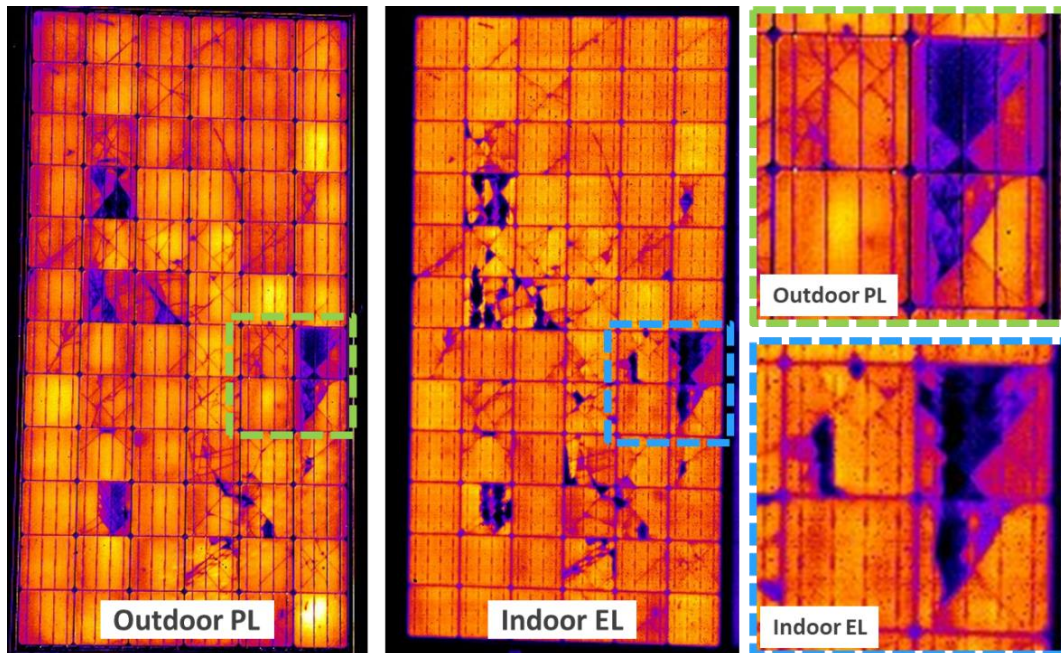
Figure 101: Comparison between outdoor PL (with optical filter) and indoor EL image acquired with the same InGaAs camera (640 pixels x 512 pixels). The inserts on the right show close-ups of a PV module area featuring many cracks and isolated regions. It is evident that the PV module has suffered from serious manual handling and both EL and PL show all the essential faults in the PV module equally well (Source: UNSW original image).
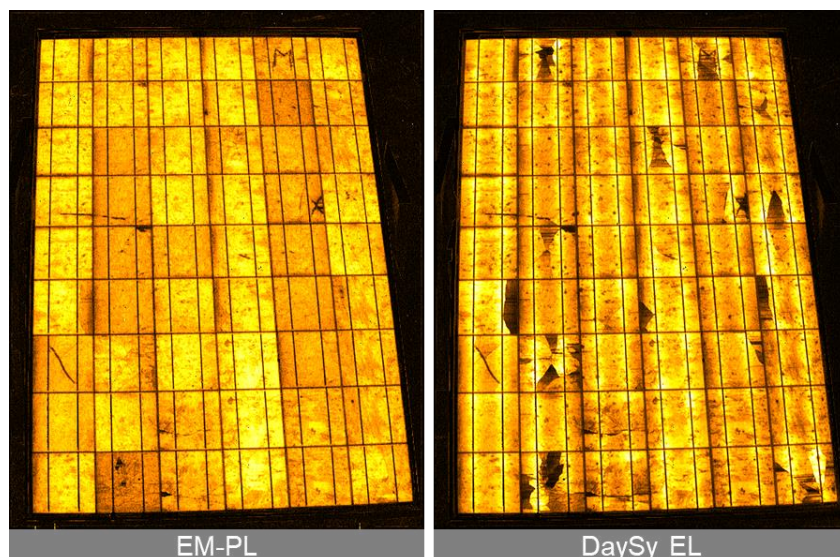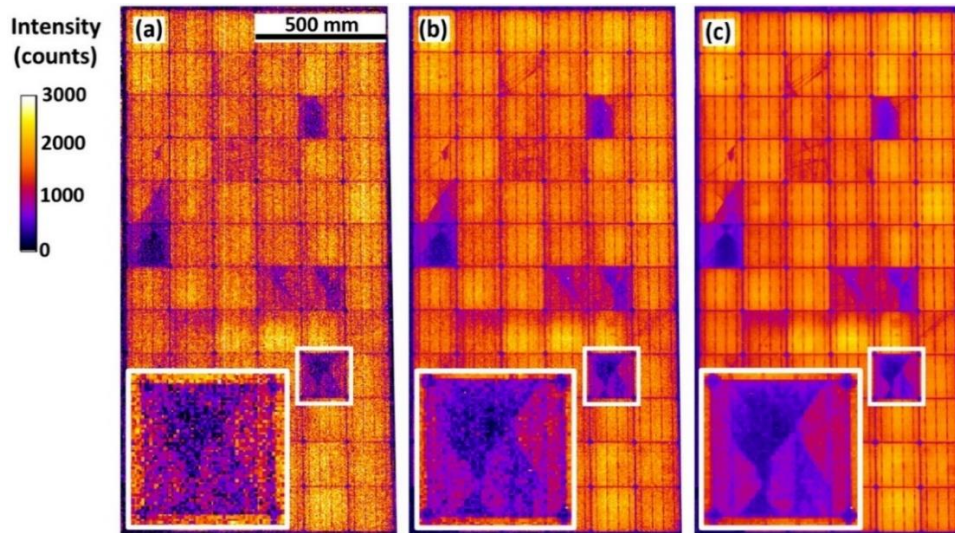

Figure 102: Comparison between outdoor DaySy EM-PL and outdoor DaySy EL image acquired with the same InGaAs camera under the same conditions. Both EL and PL show all the essential faults in the PV module, while the outdoor EL image displays a much higher contrast in regions with series resistance issues like partially isolated cracks [147].

Figure 103: Resulting average PL image of a mono-Si PERC module averaging (a) 1, (b) 5 and (c) 50 individual raw image pairs, each requiring about 20 ms acquisition time. The image height is about 620 pixels for each image.

10.1.8 Test requirement

As sunlight is used as excitation source, the measurement must be performed under ideally relatively stable sunlight conditions compared to the change of PL intensity achieved by modulation. Conditions that give the highest PV module voltage are most suitable as this translates to stronger PL emission. For this reason, older PV modules with low solar cell open-circuit voltage with additionally significant degradation can be challenging to image. The total imaging time is related to the incident sunlight intensity in approximately a square relationship, *i.e.* for a reduction in sunlight intensity by a factor of 1.4 the measurement time needs to be doubled to get approximately the same resulting image quality (signal-to-noise ratio; SNR).

Suitable sunlight conditions are those with low diffuse light and a high light intensity.

The image quality is also affected by the concentration of atmospheric water vapor, with higher atmospheric water vapor concentration leading to better image quality or shorter measurement time. On average, locations with latitude closer to the poles or with high elevation tend to have a dryer atmosphere and would require longer measurement to reach a suitable image quality.

The impact of both the water vapour concentration and time of the day and seasons on the SNR (a measure of the image quality) is illustrated in Figure 104. The exposure time is adjusted to produce the same brightness (pixel well filling (wf) = 80%) but total measurement time is kept below 2 s. The atmospheric water vapour concentration used for this calculation is derived from the Moderate Resolution Imaging Spectroradiometer MODIS monthly averaged data from 01/2003 to 11/2019. Clear sky is assumed for all calculations [148].

In this example, we see that even if the season and time of the day have a significant impact, the signal-to-noise ratio stays above five which is the minimum required for outdoor EL (as per IEC TS 60904-13 (DTS)), while keeping the total acquisition time below 2 s.
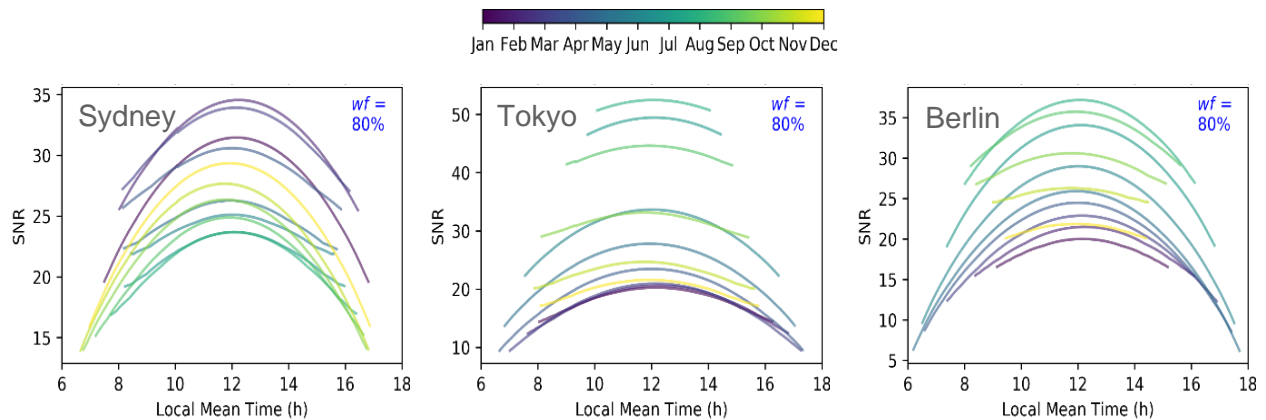
Figure 104: Simulated signal-to-noise ratio for the same PV module (standard PERC, fixed tilt mount) and fixed image brightness versus time of the day and month for different locations [148].

Other conditions that affect the acquisition time needed to obtain PL images of a sufficient quality (high SNR):

- Strong winds as they can shift the camera (and PV modules) preventing accurate image alignment of the images taken under different PV modulate operating conditions. A gimbal image stabiliser can be preferable to minimise image shaking.
- PV Module temperature. The image quality is only minimally affected by PV module temperature thanks to the weak PL thermal dependency, see Table 30 for details.
- Imaging angle. A PL image appears different depending on the angle at which it is taken. Shallower angles result in the PV module taking up a lower fraction of the image, and hence lower resolution of the PV module. The PL intensity emitted by a PV module also decreases from normal incidence. Care must be taken when comparing PL images taken at significantly different angles, although these impacts can be accounted for [150].

Table 30: Temperature coefficient of the PL intensity for different solar cell technologies [151].

Cell Technology	AL-BSF	PERC	mc-HIT	c-HIT
STC	-0.51%/K	-0.28%/K	-0.87%/K	-0.47%/K
NOCT	-0.48%/K	-0.26%/K	-0.82%/K	-0.44%/K

10.2 Existing knowledge

Positive features of outdoor PL imaging of fielded based PV modules:

- It can detect performance degrading PV module faults within such as cracks, and all forms of degradation that impact PV module performance, most notably Potential Induced Degradation (PID).

- It can detect electrical disconnects and other resistance faults within and between cells, including a short-circuited bypass diode failure. Additionally, OM-PL is the only method which is able to detect open-circuited bypass diode failure.
- It can be performed on PV modules *after* installation, i.e. faults that were introduced during the installation of the PV modules or due to ageing or external stresses (extreme weather events) can be identified.
- Unlike I-V curves, luminescence based measurements are fundamentally robust to temperature differences as the PL intensity weakly depends on the temperature [151].
- No large generator or power supply need to be carried into the field, as the sunlight is used as a high-power excitation source. However, a power source (e.g. battery) is required to operate the camera, computer and modulation electronics or LED.
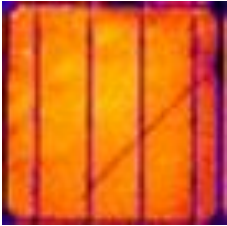
Fundamental challenges of the method:

- The method requires specific outdoor conditions. Cloudy cover can result in more diffuse sunlight getting into the camera and increasing the measurement time.
- Since sunlight is used to excite the PV modules, care needs to be taken that undesired shadows are not cast onto the PV module/PV string being imaged.
- Insolation affects the "working point" of the imaged PV module and thus some defects (e.g. Potential Induced Degradation) may appear different under different insolation conditions (noon, cloudy, dusk/dawn) as shown in Figure 93.
- Applying this technique to older PV modules with lower open circuit voltages (V_{OC}) is challenging as luminescence intensity emitted will be significantly lower. Note that a 18 mV (60 mV) decrease in the cell V_{OC} will result in a PL emission decrease by a factor of two (ten).

10.3 Detectable failure types for PV modules and PV arrays

Due to the fundamental nature of PL imaging, whereby the local voltage distribution across a solar material is measured, it is, in principle, possible to detect all failure types that are related to the electrical performance of a solar PV module, refer to Table 31 for details.
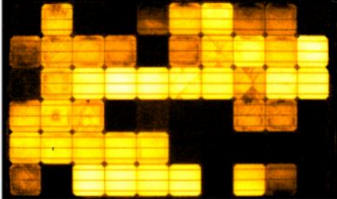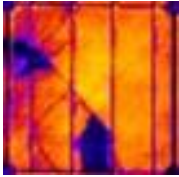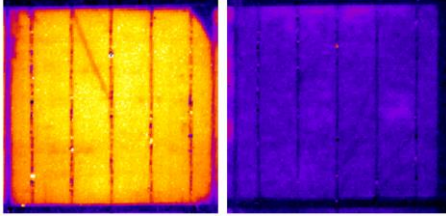
Table 31: Failure types detectable by outdoor PL imaging.

Failure	Description
(i) Cracks and micro-cracks (EM-PL and OM-PL)	Dark line: (close up or high-resolution image might be required for micro-cracks) (Source: UNSW original image).
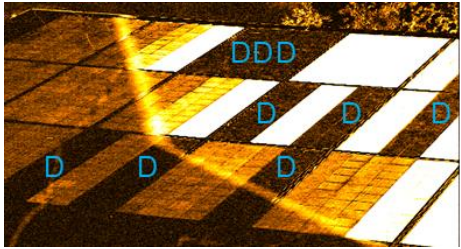
Table 31: Failure types detectable by outdoor PL imaging (continued).

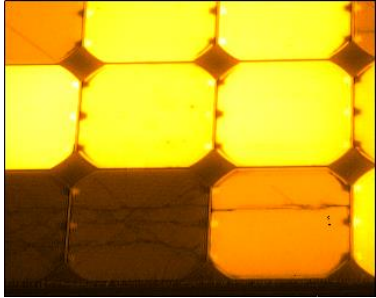| Failure	Description
(ii) Low shunt resistance (EM-PL and OM-PL)	Dark dot or area on one cell, the edge effect is gradual. May affect the entire cell area if severe (Source: Solarzentrum Stuttgart GmbH). These cracks have a shunting behaviour which reduces the EM-PL brightness of the whole cell.
(iii) potential-induced degradation (PID) (EM-PL and OM-PL)	PID example from [142], [144]:
(iv) inactive cell areas or disconnected PV sub-string (EM-PL and OM-PL)	Dark area on one cell, the edge effect is sharp if due to crack [147].
(v) LID, LeTID or any material degradation or defect affecting the voltage (EM-PL and OM-PL)	Reduced PL intensity in the affected cell (Source: UNSW original imag). Not degraded Degraded

Table 31: Failure types detectable by outdoor PL imaging (continued).

Failure	Description
(vi) bypass diode failure in short-circuit	
OM-PL	5-10% brighter PV sub-string compared to neighbour PV sub-strings.
EM-PL	 Dark sub-string
(vi) bypass diode failure in open circuit (OM-PL only)	Dark PV sub-string, similar to PV sub-string disconnection. Warning: Proper procedure needs to be followed (see 10.1.4).

10.4 Best practice recommendations

The measurement throughput of this technology depends highly on the image resolution needed. For OM-PL, throughput is about 100 PV modules per hour with the current imaging procedure. Given a typical working day, it is possible to image about 800 PV modules (around 320 kWp per day) with one measurement system on a sunny day. This estimate is similar to the 450 kWp per day quoted in the DaySy measurement guide (EM-PL). Note that OM-PL is a very new technique and significant throughput improvement is expected in the near future. Given the high cost of labour and low cost of installations, it is doubtful that this technique will be used on rooftop systems or to routinely measure every PV module in an installation.

Images should be taken such that they are comparable within a system. This means that either a fixed PV module angle relative to the camera is used, or appropriate image correction is performed to adjust the images to the same perspective. Additionally, direct reflection of sunlight onto the camera should be avoided. Given that sunlight is much stronger than the luminescence intensity, avoiding the specular reflection of sunlight from the PV module greatly increasing imaging quality and reduces imaging time.

Some form of electrical power is required on-site, no matter the form of PL imaging used. All systems require a computer and a camera, which can be powered from a battery, allowing flexibility to easily move the imaging system. Depending on the modulation technique, a generator may also be required. DaySy approach of electrical modulation a PV strings operating point is powered by adjacent PV strings, requiring no generator but a licenced electrician with the required certifications. Optical modulation, as it only requires a fraction of a PV module to be illuminated, can be powered from a reasonable sized battery.

10.5 Measuring uncertainty aspects

The fact that an outdoor PL image is done during daylight prevents the possibility of fixed imaging conditions. Thus, environmental conditions during imaging should always be noted and their impact, as far as possible, calculated and removed from the image. This can be irradiance, cell temperature and PV module conditions, as mentioned above.

To achieve best image results, averaging over several images is almost always necessary. This results typically in an image acquisition time of about one to few seconds. For modern PV modules with high open-circuit voltages significantly shorter image acquisition time is also possible. This depends on specific equipment used, the image capturing method, the amount of image pairs acquired and exposure time. Measurement duration can also be limited by the maximum frame rate of the camera or by the related hardware components in use. Even in this comparatively short measurement time, irradiance conditions can change due to the presence of fast-moving clouds. This has the potential to affect the image result in different manners: Firstly, the M_{PP} voltage depends on irradiance and may differ due to changes in irradiance, affecting the maximum power point voltage V_{MPP} and thereby the luminescence intensity. Secondly, the luminescence intensity at open circuit may change as well. In essence, variation in irradiance influences the number of excited carriers which can participate in radiative recombination. Thirdly, if the unwanted radiation change happens within one imaging cycle (i.e very fast) then subtracting images will not result in a pure PL image as the reflected sunlight intensity is different for both images.

It is important to note that failure detection and identification rely on image quality (contrast, resolution, focus etc.), rather than the measurement of the absolute intensity of the luminescence signal – which is quite challenging due to the changing time of the day and sunlight variability. Therefore, is not necessary to perform an intensity correction.

10.6 Occupational Safety

Because outdoor PL imaging is best performed under high solar irradiance, suitable protection against the sun's UV radiation is needed (sunscreen, sunglasses, hat) and care needs to be taken to avoid dehydration. As an outdoor measurement, meteorological warning should be considered beforehand. Besides representing hazards, heavy weather, or high wind both can yield poor measurement conditions due to reduced sunlight or vibration of the PV module and/or the camera.

Precautions also need to be taken against typical mechanical hazards on solar power plants via personal protective equipment such as safety boots, high visibility vest and other precautions as required by the site management. Additional requirements might exist as per national regulations.

10.6.1 Specific to DaySy system (EM-PL)

For the DaySy EM-PL system, a qualified electrician with a licence to work on solar farms is required and care needs to be taken of electrical DC high voltage electrocution since electrical contact to the high voltage DC PV strings needs to be made.

10.6.2 Specific to system using an optical modulator (OM-PL)

The equipment for outdoor PL imaging using the OM-PL method is based on extra-low-voltage equipment and no risk of electrocution exists. The use of an optical modulator relying on shading to modulate the operating point of the PV module can cause catastrophic damage to the PV module in the case following conditions are met, (i) excessive shading, as well as (ii) bypass diode failure in open-circuit or missing bypass diode. Control measures to detect bypass diode failure and reduce shading time must be put in place (as described in Section 10.1.6). As the optical modulator is placed on the PV module's surface, the modulator backside needs to be properly padded and the modulator properly handled when it is placed on the PV module to avoid damaging the PV module front side. This is generally easy to achieve.

10.7 Transportability

Since in the presented outdoor PL imaging methods take advantage of the sun as light source, the overall setup is lightweight and mobile and can in the simplest implementation even be carried in a suitcase. This facilitates greatly the transportation from site to site. The equipment described in this report can easily be carried to different locations of a solar power plant. A custom-built tripod solution can additionally help transporting all required components and will make moving the equipment between different PV modules and different locations on the solar farm much more convenient (Figure 100). The systems can also be attached to a suitable (electric) vehicle which further increases mobility.

Note that restrictions apply to transporting of large batteries on airplanes and that to do so typically a goods flight service needs to be used and special protocols apply. These restrictions are identical to those that apply to batteries for aerial vehicles that are commonly used for drone IR inspection. Usually the equipment used is transported to site by car but if transport by air is required a way around this restriction is to only use batteries that are easily sourced at the measurement site (for instance car batteries).

10.8 Cost considerations

The cost of an outdoor PL system is comparatively high, and a major cost driver is the comparatively expensive InGaAs camera in use (EUR 20-30 k). Significant additional costs are related to camera lenses and optical filters (EUR 2 to 10 k) and the required electronic components such as a suitable battery and power supplies. A computer (typically a rugged laptop with outdoor readable display EUR 3 to 4 k) is needed for data capture and analysis. The OM-PL system requires the optical modulator + control electronic and the DaySy system requires the DaySy box, all of which are custom built. The DaySy system may also require a power generator.

Currently the only commercially available system capable of taking outdoor PL images is the DaySy system [142].

However, a prototype system based on optical modulation is currently in operation and testing at the University of New South Wales and it is expected to be commercially available in the near future.

11 SPECTROSCOPIC METHODS FOR POLYMERIC MATERIALS

Performance, quality and reliability of photovoltaic (PV) modules are key factors for the favourable development of emerging photovoltaic markets worldwide. During their lifetime in the field, PV modules have to withstand environmental influences which may vary drastically depending on the surrounding climate [57], [152], [153], [154], [155], [156]. Thus, the weathering stability of the protective polymeric materials (backsheets, encapsulates) used in the multilayer laminates is crucial for the reliability of the active PV components over the whole life cycle of a PV module [157], [158], [159], [160], [161].

The role of the backsheet within the multi material composite of a PV module is to provide protection for the PV active layer and the polymeric encapsulation against environmental, mechanical and chemical influences and to ensure electrical insulation. Thus, it is decisive which type of backsheet (chemical composition, barrier properties, structure) is used, especially as the chemical and physical properties of the backsheet (and thus its ageing behaviour) can have a strong influence on cell corrosion and/or encapsulant degradation – which both are known to be important factors for the reliability of a PV module over its intended service life time of up to 25 years.

Thus, material identification of the polymeric compounds incorporated in the multi-material composite PV module is often an important task, especially when failures appear. While the knowledge of the bill of materials is one challenge, the detection of material degradation effects - especially at the material interfaces (e.g. solar cell/encapsulant or encapsulant/backsheet) is another important issue. Both tasks can be solved non-destructively by the application of mobile spectroscopic methods [162].

The following chapter will describe the usability and transferability of the well-established analytical characterisation techniques:

- Infrared (IR) - spectroscopy: Mid (MIR) and Near (NIR) infrared
- Raman - spectroscopy
- UV-VIS - spectroscopy

as mobile PV test centres for in-field characterisation of PV modules.

11.1 Description of inspection method

Spectroscopy can be defined as the interaction between matter and radiation. The different types of interaction, as well as the affected modes (e.g., molecular vibrations, rotations) or elementary particles (e.g., core-level electrons, valence electrons) of the molecule, are given in Figure 105.

Vibrational spectroscopy includes several different techniques, the most important of which are mid-infrared (MIR) and Raman spectroscopy which are mainly used for identification of organic (e.g. polymeric) and inorganic (minerals and semiconductors) materials, respectively.
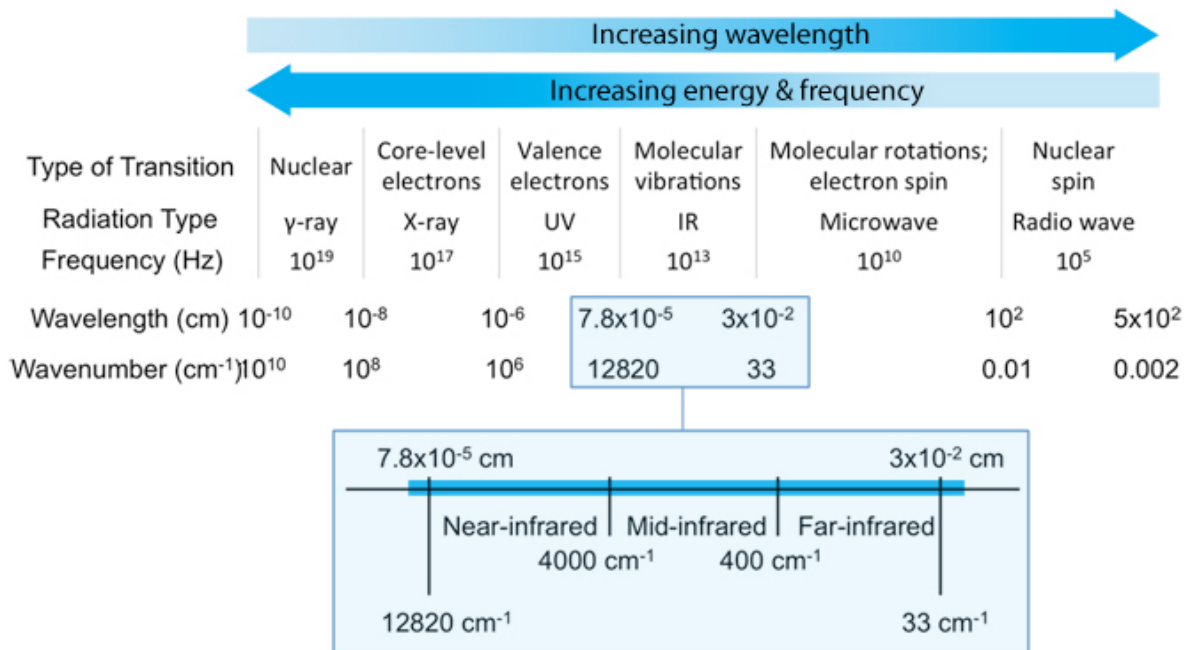
Figure 105: Electromagnetic spectrum, IR region enlarged [163]

IR and Raman spectroscopy are based on the excitation and detection of characteristic fundamental vibrations that can be used to elucidate molecular structures (material identification) [164]. Although some vibrations may be active in both, Raman and IR spectroscopy are complementary techniques as these two forms of vibrational spectroscopy arise from different processes and obey different selection rules [165]:

- IR-spectroscopy is based on the direct absorption of photons in the MIR region (2.5 µm to 25 µm wavelength corresponding to 400 cm^{-1} to 4000 cm^{-1} wavenumbers)
- Raman spectroscopy is based on inelastic scattering of photons (excitation with monochromatic laser light in the VIS-region)

While both methods are probing molecular vibrations in general, with Raman spectroscopy symmetric vibrations of non-polar groups can be detected with high intensity, while IR spectroscopy is very sensitive to asymmetric vibrations of polar groups [164].

UV-VIS spectroscopy is a spectroscopic technique that relies on the interaction of UV- and/or visible (VIS) light with matter (in specific with the valence electrons of atoms). When the sample containing species absorbs light in the UV to VIS range (200 nm to 780 nm), the absorption relates to the excitation of the species from a ground state to an excited state.

This method is less useful for material identification, but can be used e.g. to determine degradation induced colour changes, specific absorbance (quantification of additive concentrations) or - when applied in the fluorescence mode with a monochromatic excitation light source - the presence of fluorophores (often precursors to polymer degradation e.g. the encapsulant) [132].

The measurements can be performed in transmission/absorbance, reflectance or fluorescence mode which yield different information on a given substance.

NIR spectroscopy: while absorption of UV and VIS electromagnetic waves (200 nm to 780 nm) excites electrons to higher lying states, MIR radiation spanning 2500 nm to 25000 nm stimulates vibrational motion in molecules. At first sight, NIR radiation (800 nm to 2500 nm) seems to be stuck in the middle: not energetic enough to cause electronic excitation and too high in frequency for fundamental vibrational motions. However, vibrational motions involving hydrogen bound to a heavy atom - usually carbon, oxygen or nitrogen - can also be excited via so-called overtones or combination bands. These higher-energy transitions fall in the NIR range of the electromagnetic spectrum (wavelengths of 800 nm to 2500 nm, corresponding to wavelengths of 4000 cm-1 to 12500 cm-1) [166]
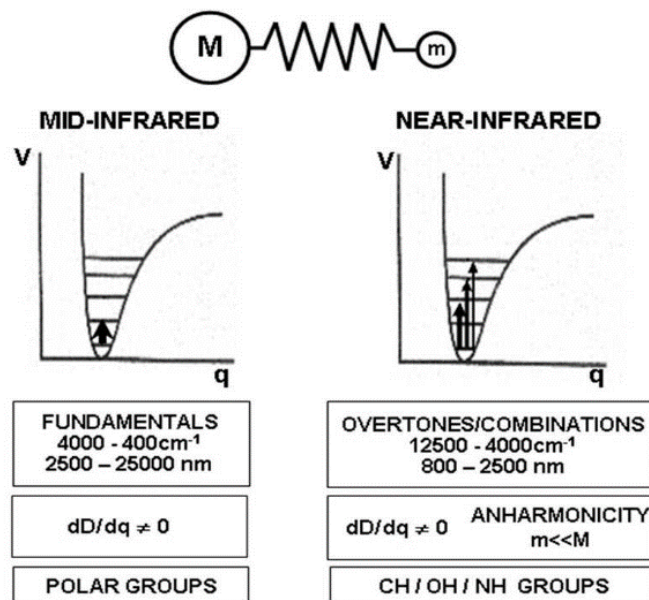
Figure 106: Physical principles of MIR and NIR spectroscopy (© Heinz Siesler, Department of Physical Chemistry, University of Duisburg-Essen, Germany); dD=change in the dipolmoment D, dq= change in the atomic distance (q) [167].

NIR vibration bands are more than 100x weaker than fundamental (MIR) bands, they are rather unspecific, wide and overlapping. Since there are no unique, easily attributable single vibration absorption bands, a multi- wavelength approach is required to unlock the information contained in the overlapping bands of the NIR and chemometrics is one key to it [166]. Based on multivariate statistics, chemometrics borrows heavily from linear algebra techniques - such as principal component analysis - to allow for qualitative and quantitative predictions of concentration, identity and quality [166], [167]. However, if solely qualitative information on the identity of the material (or material stack as in the case of a multilayer polymeric backsheet) is needed, the build-up of a spectra-library of known samples can be done. Identification of an unknown sample by an automated comparison of its NIR-spectrum with spectra stored in the database is possible.

11.2 Existing knowledge

Until very recently, handheld spectrometers were the domain of major analytical and security instrument companies, with turnkey analyzers using spectroscopic techniques like X-ray fluorescence (XRF) for elemental analysis (metals), and Raman, MIR and NIR for molecular analysis (mostly organics) [168]. The introduction of specific fibre-optic probes allows a separation of the spectrometer and the location of sample measurement (suitable for in-field measurements; used for Raman, UV-Vis and NIR). [167]

Although mobile PV test centres are already in use for fast material identification in safety and security applications (immediate application in emergency response for hazardous materials), non-destructive material analysis of large construction parts (e.g. sealing, coating or fitting on a huge production machine) or precious samples (identification of paint on ancient canvas), the application of such devices in PV is rather new [169], [132]. If we talk of "Spectral Characterisation of Photovoltaic Devices", spectral characterisation techniques used in the evaluation of their efficacy in the goal of harnessing a maximum of energy from the sun and artificial sources of light is meant.

But - as described in detail in the IEA PVPS Task 13 report on "Assessment of Photovoltaic Module Failures in the Field" [58] - many PV module failure modes are related to material interactions. Thus, recently several groups of researches active in failure analysis of PV modules (e.g [156], [170], [171], [172]) started transferring the technically mature portable spectrometers (IR, Raman) to this different field of application and applied them for

- determining the chemical identity of polymeric materials incorporated in PV modules
- validating the bill of materials (BOM) of PV-devices
- documenting ageing effects of polymeric materials (i.e. encapsulation, backsheet)

In this respect it should be emphasized that the non-destructive in-field IR measurements always are performed in reflectance mode requiring direct contact of the measuring head, the Attenuated Total Reflection (ATR) crystal, with the sample surface. Consequently, IR-spectra can only be recorded of accessible materials like e.g. surfaces of backsheets, frontsheets, junction box or adhesive. Furthermore, the ATR-measurements in the MIR region are surface sensitive: at a 45 degrees angle of incidence and a sample refractive index of 1.5 (as for most polymers), the depth of penetration of the IR beam into the sample varies from 0.5 µm for germanium (Ge) ATR crystal to 2.0 µm for diamond crystals as measured at 1000 cm^{-1} [172].

For NIR-Spectroscopy several applications exist, as it is both non-destructive and noninvasive. The method has found numerous uses in the food and agricultural sector, including quality control, ripeness measurement, soil testing and precision agriculture [132, 173, 173, 173], [167]. Up to now, NIR-spectroscopy is not frequently used for material analysis of PV modules in the field. But as its penetration depth is several mm (= whole backsheet laminate + encapsulant) [166] [169], [174] , supplementary information to the surface sensitive MIR-spectroscopy can be obtained. NIR spectra of different backsheet laminates and co-extrudates are clearly distinguishable (Figure 108) allowing for non-destructive determination of the backsheet type of fielded PV modules by mobile NIR-measurements [174]. Also, the degree of deterioration of a PV backsheet could be non-destructively and easily determined via NIR spectroscopy [174].
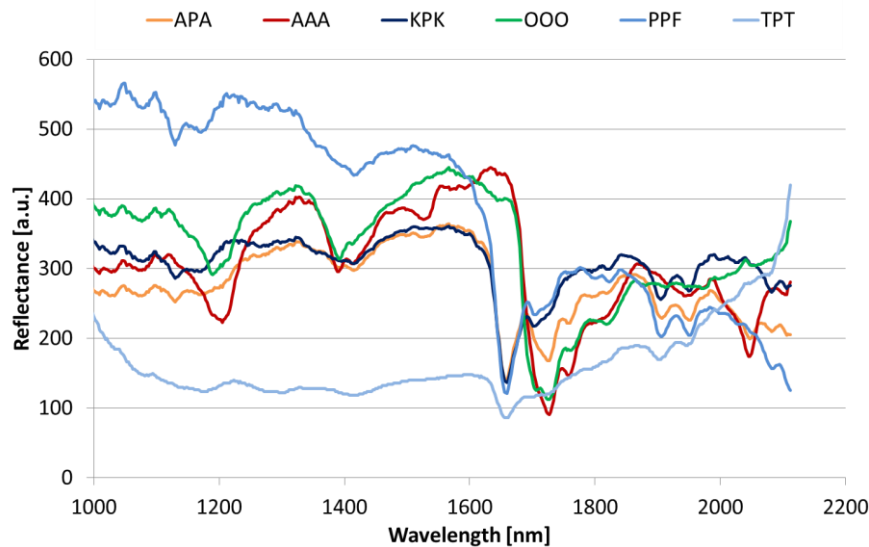
Figure 107: NIR spectra of different polymeric multilayer films used as PV-backsheets; A=Polyamide, K= PVDF, P= PET, O=Polyolefin, T= PVF [175].

Raman measurements can be performed contact-free and, a suitable probe provided, polymeric material located behind a transparent frontsheet (glass) can be identified (e.g. the encapsulant in a PV module) [171], [172], [175] or spectra of the interface solar cell/encapsulant can be recorded (confocal measurement method [175]). However, there is one major drawback with this technique: the potential formation of ageing induced fluorescence. Broad, intense and non-specific fluorescence bands can mask the specific Raman bands of the polymer [132].

11.2.1 Market overview of mobile/portable spectroscopic instruments:

Portable and handheld spectrometers can be taken to the sample [168], meaning fast and non-destructive analysis of operating PV-devices in the field. For this task small, compact, robust and easy-to-use measurement systems working with accumulators as power supply are needed. Portability, combined with algorithms and libraries for identification and quantification enables on-site analyses and allows for informed fast decision making [168].

FTIR spectrometer: In 2008, A2 Technologies, now Agilent Technologies (Danbury, CT), developed the first handheld FTIR spectrometer targeted at materials applications in the aerospace industry [175]. The first application to be studied was a non-destructive method for analyzing the surfaces of thermally induced stresses in epoxy–carbon composites. This led to the development of the Exoscan FTIR spectrometer, which over the past several years has evolved into a complete system for the analysis of materials (ATR-technology; surface sensitive, penetration depth @1000 cm^{-1} of 2 µm), Figure 108. Agilent technologies is one main provider for handheld, mobile FTIR spectrometers [176], [177]. Portable instruments (compact spectrometers with probes) are also offered by several providers but not intended to be used outdoors.

NIR spectrometers: Portable NIR-spectrometers equipped with fibre–optic probes are provided by ocean optics [178], HDTS [179] or LabSpec4 [180].
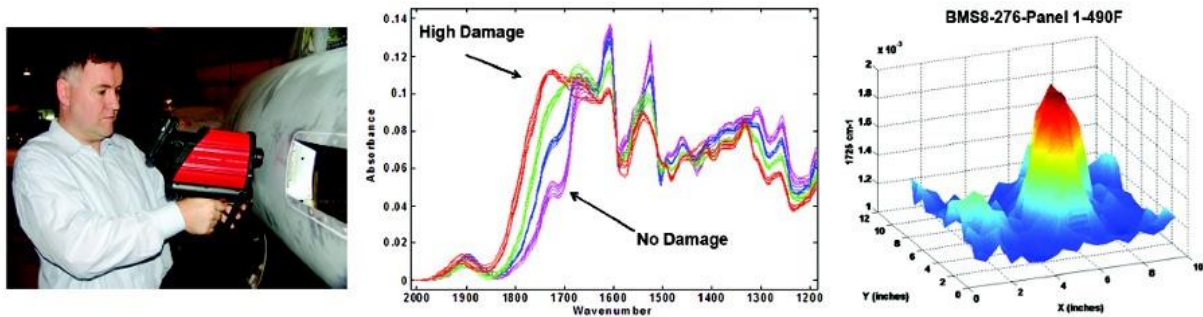
Figure 108: Left: Handheld FTIR is used to measure regions of composite-based aircraft; Middle: The carbonyl region of the IR spectrum was used as an indicator of oxidation caused by thermal overexposure; Right: Mapping intensity of the 1725 cm^{-1} carbonyl band as a function of position [175].

Raman spectrometers: The development of handheld Raman spectrometers has drastically changed the way quality control for incoming raw materials can be performed in industry. It provides advantages over other methods in that it does not require sample pre-treatment or direct contact with the sample, and has the unique capability of being able to test a sample directly through a transparent packing material like glass or plastic [181].

The main companies offering several types of portable and/or handheld Raman devices are BWTEC [182], Ocean Optics [183] (Figure 109) and Bruker [184].
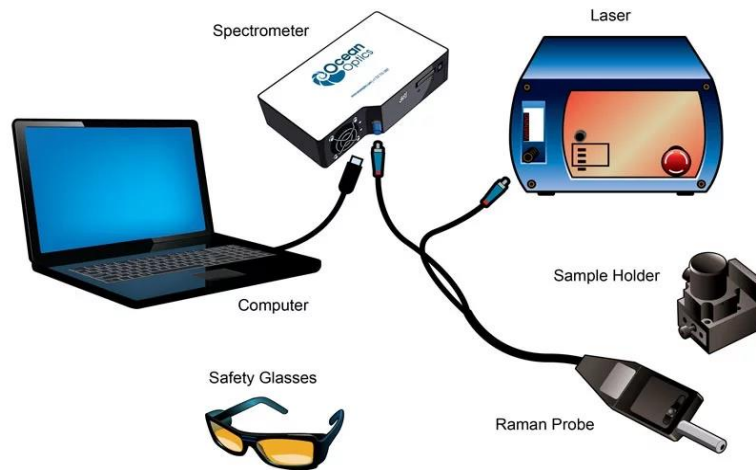
Figure 109: Example Setup: Raman Analysis of Polymers and Other Materials [183].

Status of standardization and licensing:

As mobile/portable spectroscopic devices have been in the market in different application areas since years, standardized instruments are available for each type (MIR, Raman, NIR, UV-VIS) of spectroscopy.

11.3 Detectable failure types for PV modules and PV arrays

Besides an identification of polymeric materials built-in PV-modules, also the detection of material degradation effects is possible with spectroscopic methods.

Raman and IR-Spectra of several backsheets taken by a portable spectrometer (and stored in a database) are shown in Figure 110.
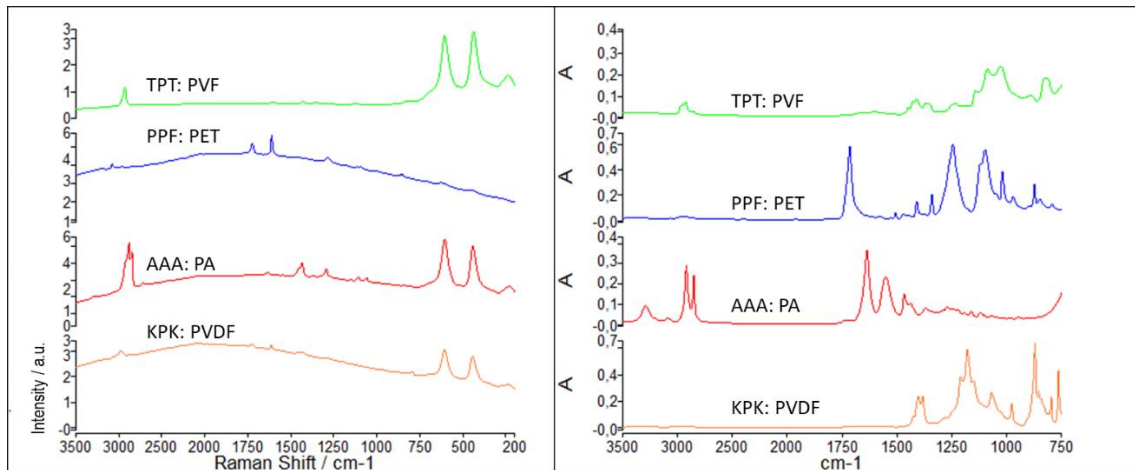
Figure 110: Raman spectra (left) and IR-spectra (right) of typical PV-backsheets (outer surfaces); TPT (PVF-surface), PPF (PET surface), AAA (polyamide surface), FPA (Polyamide), KPK (PVDF surface) recorded by mobile PV test centres [169].

The ultimate challenge, however, is to non-destructively identify the bill of materials of multi-annual field-aged PV modules. One important issue is the fact that the surface layers of polymeric films degrade under the influence of environmental stress impact and, thus, the oxidation, hydrolysis, and/or degradation of the polymer chains might occur and change the spectra obtained. These effects can best be registered with IR spectroscopy, as this method is very sensitive for the detection of polar groups like carbonyl and hydroxyl groups [169].
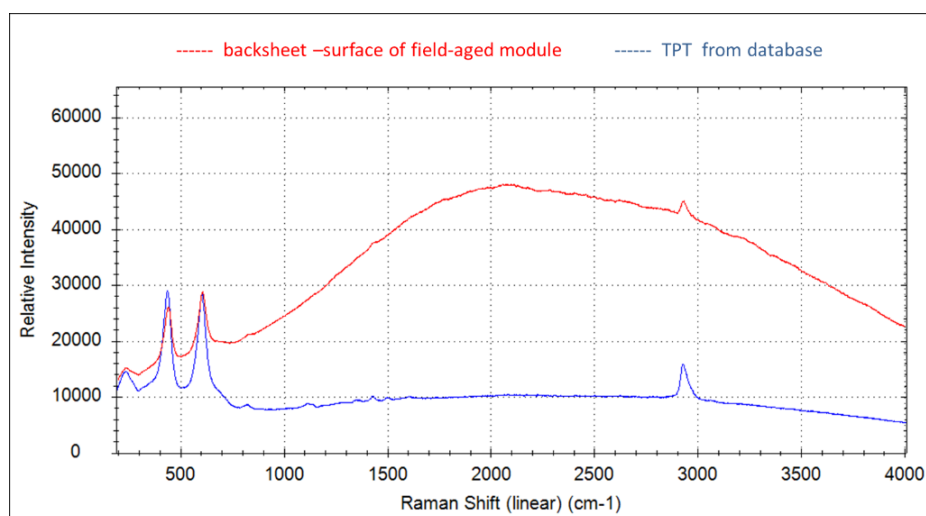
Figure 111: Raman spectra of the backsheet-surface of a field-aged PV module and best hit from database [169].
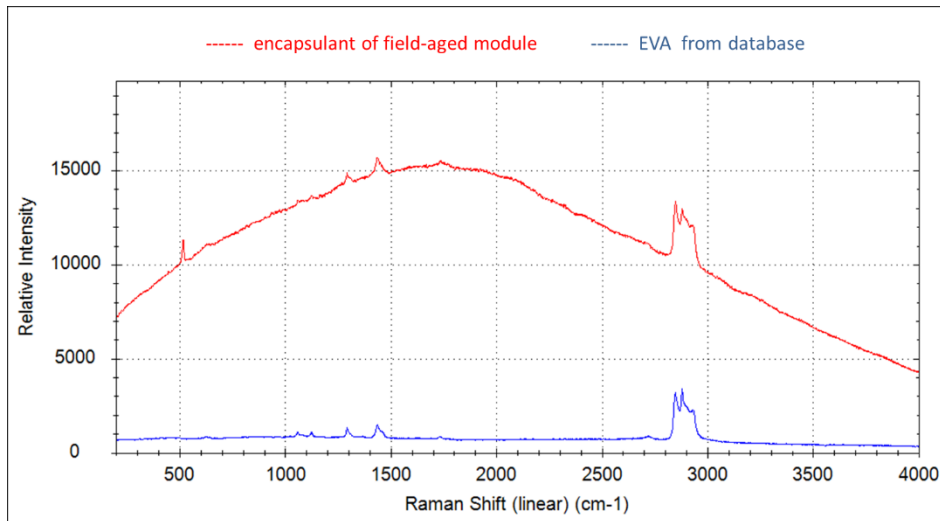
Figure 112: Raman spectra of the encapsulant of a field-aged PV module and best hit from database.

The second problem is the appearance of ageing-induced fluorescence of the weathered polymers in the Raman spectra (Figure 111 and Figure 112). This can strongly affect the detectability of specific absorptions and, thus, impede the assignment of the measured spectrum to the reference spectra stored in the database. As example, the Raman spectra of the backsheet and encapsulant of a 30-year field-aged PV module and the corresponding hit from the database are shown in Figure 111 and Figure 112, respectively. The increasing fluorescence was caused by increasing concentration of fluorophores upon ageing and originated from degradation products of the polymer and/or the additives within the polymer (see [132, 173, 173, 173] and the references given therein).

A beginning degradation of the environmental side of the backsheet is often only limited to the outer surface 1 µm to 10 µm and has no effect on (i) the integrity of the PV module laminate or (ii) the electrical performance of the PV modules. This is the case in the example of the 30-year field-aged PV module with TPT (Tedlar) backsheets and EVA encapsulants as given in Figure 111 and Figure 112.

On the other side, material degradation effects can also have severe impact on the performance of a PV plant. One well-known example is the formation of different types of cracks in Polyamide (PA)-based backsheets observed in several PV plants within the last years. One type of cracking (micro-cracks) [185], [186] showed beginning material degradation (oxidative degradation) on the environmental side of the PA-backsheet and has not been correlated with a loss in electrical performance so far. Another type of cracking (squared cracks) [35], however, exhibited first material degradation effects at the interface between EVA encapsulant and PA backsheet in the intercellular spaces. This degradation then propagated through the core and outer layer, causing a crack through the whole backsheet, leading to water ingress followed by backsheet delamination and corrosion effects, and, consequently, electrical performance loss and safety problems [185], [186].

Spectroscopic detectable chemical encapsulant degradation, e.g., the raise of carbonyl bonds, hydroxyl absorptions, or changes in the CH absorption pattern, is often paired with polymer chain splitting, leading to embrittlement and cracking of the polymer, thus facilitating delamination and corrosion effects induced by penetrating substances (water vapor, oxygen) [187].

168

11.4 Best practice recommendations

Spectroscopic measurements on PV-modules in the field can be performed without dismantling the modules and without electrically disconnecting the modules. The measurements should be carried out on dry and cleaned surfaces, especially for the ATR-FTIR measurements and Raman-measurements of the surface of the backsheet, dirt, dust or sand should be removes as they could give additional absorption features in the spectra. NIR and Raman-measurements of the encapsulant are less sensitive to soiling of the glass.

11.5 Measuring uncertainty aspects

As spectra of a given compound are independent of the location where they are recorded, good transferability of the fielded measured spectra to laboratory measurements is given. MIR and NIR radiation pose no danger to the personnel and do not induce any damage to PV modules/systems.

However, the laser radiation used for excitation in Raman spectroscopy can be harmful to the operator of the spectrometer if the laser light is directed into the eyes. Therefore, safety glasses are needed.

11.6 Occupational Safety

Infrared light used as radiation source in NIR and MIR spectroscopy is incoherent, polychromatic and is scattered in all directions. It is not hazardous for the human eyes or skin.

Laser light, however, as being a highly aligned (minimum divergence of the beam), coherent, monochromatic radiation can be hazardous to human eyesight when the beam hits the eye directly or after reflection from a shiny surface. Therefore eye protection (laser protection goggles) must be worn when the laser of the Raman spectrometer is switched on.

11.7 Transportability

Handheld and portable spectrometers are easily transportable in an equipment case. The dimensions are of the order of 50 cm x 50 cm x 20 cm.

11.8 Cost considerations

The investment costs for handheld or portable spectrometers lie in the range from 20 Euro/spectrometer to 40.000 Euro/spectrometer. Maintenance and calibration is easy and inexpensive. The time required for the measurement of an IR or Raman spectrum is in the low-minutes range allowing for a high throughput (number of inspected PV modules per day). Measurements can be performed by one operator, fast handling and data management is provided by working in teams of two persons in the field.

12 CONCLUSIONS

Qualification of PV power plants in the field is crucial to understand performance and degradation mechanisms to improve reliability and lifetime. On-site inspection methods with portable test equipment are helpful tools to diagnose drivers for underperforming PV power plants. The particular strength is that the tests are carried out in the field and that the PV modules do not have to be shipped to the laboratory, which often means long transport routes, transport risks and a long down time of the PV strings. Furthermore, on-site inspection methods allow a more targeted failure analysis, as PV modules are not blindly selected. Test experience has shown that the significance of the results is comparable to laboratory tests.

On-site inspection is dependent on the weather conditions, which is a clear disadvantage compared to laboratory work, where inspection can be performed at almost constant conditions. In this context, on-site inspection requires more organizational effort and careful planning.

There are several applications for the use of portable test equipment:

a) Quality assurance of PV module shipments: Brand-new PV modules are inspected prior to installation. This can be done at the production site before shipment, in the warehouse or at the site of the PV power plant (out-of-box measurement).

b) Inspection of PV power plants prior to change of ownership: Investors can gain confidence in the technical condition of the PV power plant.

c) Failure analysis of underperforming PV power plants: Information from a visual inspection or operational data of the PV power plant should be available in order to select the appropriate inspection method.

d) Monitoring of degradation processes: This requires periodic measurement of the same fielded PV modules or PV strings.

Before technical inspection with mobile PV test centres is started, a global visual inspection of the PV power plant shall be performed. This measure can already give hints on potential origins for performance losses, such as issues with cabling or combiner boxes, soiling or shading due to due plant growth. A specific visual inspection of PV modules can also reveal whether failures are due to weather impact or due to degradation issues such as corrosion of contacts, browning or cracking of polymeric materials, delamination, or burn marks.

Table 32 gives an overview which type of defect or failure in PV arrays or PV modules can be detected with primary inspection methods. In addition to the inspection methods covered in this report, also the infrared imaging and nighttime electroluminescence imaging are included in the table. Technical details of these two methods have already been given in a previous IEA PVPS Task 13 report [18]. The table makes clear that a single inspection method usually deals with a specific type of defect or failure and cannot deliver a comprehensive failure analysis. For example, EL or PL imaging can reveal cell cracks in a PV module or can give an indication for PID. But no conclusions can be made for the output power of the PV module. This proof must be provided with an additional output power measurement. Therefore, a combination of different inspection methods must also be considered in order to achieve robust results with the aim of clearly documenting damages or degradation phenomena for use in warranty claims.

The primary inspection methods of Table 32 are performed on PV modules as installed on the mounting racks. This makes it necessary to move the test equipment through the PV power

plant and to provide an electrical power supply. There may be restrictions in the execution of inspection work due to this, as necessary infrastructure such as paved paths may not be large scale available. Depending on the size of the mounting rack, you also have to expect that PV modules installed in upper rows may not be accessible.

Other aspects for the comparison of inspection methods concern the practical use in the field. The details of this are given in Table 33. First, it is specified whether the inspection method provides a fault diagnosis of PV strings or of PV modules. Then it is shown whether the execution must be carried out during the day or at night. Depending on local conditions and infrastructure, special challenges may arise for night work. Finally, it is important to know whether the application requires an electrical disconnection of PV strings or PV modules to connect the terminals to measuring instruments or power supply units.

For inspection methods that require disconnections in the electrical circuit of the PV array, attention must be paid as the maximum systems voltage of PV strings can reach up to 1500 VDC. In these cases all precautions must be taken against electric shock, the safety regulations of the country must be observed and work must only be carried out by qualified electricians with appropriate training.

Table 33 also provides specific requirements for carrying out the inspection work and possible limitations for the use of results. All methods have in common that good weather conditions are required. In addition, infrared imaging and output power determination of PV strings require high irradiance conditions.

It must be noted that inspection results on PV string level can only provide an indication of defects or degradations issues of PV modules. For example, for PV module output power only one statement can be made with regard to the mean value. This may restrict the use of the measurement results because warranty claims may require an individual proof that the PV module performance is outside the manufacturers' specification. Subsequently, this can be done on-site with a mobile PV test centre or by shipping PV modules to a test laboratory.

Besides the primary inspection methods of Table 32, which can be applied independently in the field, there are two applications that allow a combination of these: a) Drone-mounted electroluminescence & infrared inspection of PV array, b) PV module inspection with mobile PV test centre. In the case of drone inspection, various imaging techniques can be used. The PV test centre combines imaging techniques and electrical performance measurement for PV modules. Table 34 provides information on the applicability as well as on the specific requirements and potential limitations in the field. From all field inspection methods described in this report only the use of a mobile PV test centre requires to dismount and reinstall PV modules, which makes it necessary to move these through the plant. In all other cases, PV modules can be inspected on the mounting rack.

A 100% in-depth inspection of all PV modules in a larger PV power plant is not economically feasible. This circumstance shows the need for specific sampling plans and statistical evaluation methods, which shall assure that a representative number of PV modules is inspected. Today, statistical methods are not internationally harmonized and are often decided on a case-by-case basis. To be on the safe side, the standard ISO 2859-1 [188] can be used for the definition of the sampling rate. In any case, however, it is advisable to discuss sampling schemes at an early stage when the details of the inspection measure are determined. This is to avoid disappointing the expectations of the inspection.

Table 32: Overview of detectable defects and failures with primary inspection methods.

Legend: 1 – Can be only detected if failure causes overheating 2 – Only indicative result 3 – Partially covered in this report in chapter "Drone-mounted EL & IR inspection of PV array". For more details see [18] 4 – Dependent on encapsulant of PV module 5 – Only SC failure mode detectable	Performance variation of PV strings	Cabling or combiner box issues (i.e. open circuit failure, resistive losses)	Insulation failures (ground faults)	Induced degradation (PID, LeTID)	Electrical mismatch of PV modules	Bypass diode failure	Underperforming PV modules	Localized heating due to PV module failure	Cell cracks	Interruptions in the cell interconnection circuit	Degradation effects (Crack propagation, Polymer degradation)	BOM issues of PV module (polymeric footprint)
Daylight I-V measurement	X	X		X^2	X	X	X^2					
Dark I-V measurement	X	X		X^2		X						
PV plant testing vehicle	X	X			X		X^2					
Electrical impedance spectroscopy			X			X						
Thermal infrared imaging[3]				X^2		X		X	X^1	X^1		
Nighttime electroluminescence imaging[3]		X		X^2		X			X	X		
Daylight electroluminescence imaging		X		X^2					X	X		
UV fluorescence imaging		X							X^4		X	X
Outdoor photoluminescence imaging				X		X^5			X	X		
Spectroscopic methods for polymeric materials											X	X

Table 33: Comparison of inspection methods.

Inspection method	Application						Specific requirements and limitations in the field
	Inspection focus		Ambient requirement		Electrical disconnection of PV string or PV module		
	PV string	PV module	Day-time	Night-time	YES	NO	
Daylight I-V measurement	X	(X)	X		X		• Measurement shall be performed at high irradiance >800 W/m² and low wind speed. • Results are sensitive to I-V translation to STC. This requires accurate measurement of irradiance and PV module temperature as well as knowledge of translation parameters. • The average output power of PV modules may not be sufficient for warranty claims, so that power measurement of single PV modules may be required.
Dark I-V measurement	X			X	X		• High effort to transport equipment through the PV power plant • No conclusions on PV module output power can be made.
PV plant testing vehicle	X		X		X		• Testing vehicle must be parked close to PV strings to be monitored. • Paved roads may be required.
Electrical impedance spectroscopy	X		X		X		• Impact of detected failures on PV module output power may be unclear (if cell cracks).
Thermal infrared imaging[1]	X	X	X		X		• PV system must be operational. • Measurement shall be performed at high irradiance >800 W/m² to get meaningful results. • Impact of detected failures on PV module output power may be unclear (if cell cracks).

Table 33: Comparison of inspection methods (continued).

Inspection method	Application						Specific requirements and limitations in the field
	Inspection focus		Ambient require-ment		Electrical discon-nection of PV string or PV module		
	PV string	PV module	Day-time	Night-time	YES	NO	
Nighttime electroluminescence imaging[1]	X	X		X	X		• Impact of detected failures on PV module output power is unclear.
Daylight electroluminescence imaging	X	X	X	X	X		• High experimental effort to carry equipment through the PV power plant Power supply with high DC voltage required • Low resolution of InGaAs camera (512 x 620 pixels)
UV fluorescence imaging		X	X	X		X	• High experimental effort to carry equipment through the PV power plant • PV module in upper rows in a PV array are difficult to reach.
Advanced outdoor photoluminescence imaging		X	X			X	• High experimental effort to carry equipment through the PV array • Low resolution of InGaAs camera (512 x 620 pixels) • Operational PV system required
Spectroscopic methods for polymeric materials		X	X	X		X	

Table 34: Other application of inspection methods.

	Application range	Requirements and limitations in the field
Drone-mounted electroluminescence & infrared inspection of PV array	- Visual inspection to detect PV module damages, soiling issues or shading issues - IR inspection: Flight at high altitude gives quick overview of the operating status of a PV power plant - Nighttime EL inspection - Nighttime UV fluorescence inspection - Low flight height makes inspection of single PV module possible.	- Meaningful IR inspection requires high solar irradiance: usually 500W/m^2 is sufficient. IEC62446-3 request 600W/m^2, while IEC62446-1 request 400W/m^2. - Experienced drone operator with permission to fly - Permission to fly varies from country to country
PV module inspection with mobile PV test centre	- Accurate output power measurement of PV modules at STC - IR inspection and/or EL inspection of PV module with high resolution - Meaningful results for warranty claims	- Time consuming dismounting and reinstallation of PV modules - Good infrastructure in the field required (power supply, paved roads) - Long time required to bring the module temperature close to 25℃

REFERENCES

[1] "ETIP Fact Sheets: PV the cheapest electricity source almost everywhere," [Online]. Available: https://etip-pv.eu/publications/fact-sheets/, update of September 2020. [Accessed 07 12 2020].

[2] "IEA Solar PV tracking report 2020," [Online]. Available: https://www.iea.org/reports/solar-pv. [Accessed 07 12 2020].

[3] "https://reneweconomy.com.au/solar-power-is-now-cheapest-electricity-in-history-says-iea-39195/," [Online]. [Accessed 07 12 2020].

[4] F. Grimaccia, M. Aghaei, M. Mussetta, S. Leva, and P. B. Quater, Planning for PV plant performance monitoring by means of unmanned aerial systems (UAS), International Journal of Energy and Environmental Engineering, 6(1) pp 47-54, doi:10.1007/s40095-014, 2015.

[5] D. McGrory, "HONEYWELL LAUNCHES COMMERCIAL UNMANNED AERIAL VEHICLE INSPECTION AND DATA ANALYTICS SERVICE IN INDIA," 2018. [Online]. [Accessed 16 12 2020].

[6] F. Grimaccia, S. Leva, A. Dolara, and M. Aghaei, Survey on PV Modules' Common Faults After an O M Flight Extensive Campaign Over Different Plants in Italy, IEEE Journal of Photovoltaics, vol 4(3), pp 810-816, 2017.

[7] S. S. Leva, and M. Aghaei, "Failures and Defects in PV Systems: Review and Methods of Analysis," no. Power Engineering: Advances and Challenges Part B: Electrical Power, CRC Press, pp.56–84, ISBN 9781138319875, 12. 2018.

[8] S. Leva, M. Aghaei, and F. Grimaccia, PV power plant inspection by UAS: Correlation between altitude and detection of defects on PV modules, IEEE 15th International Conference on Environment and Electrical Engineering (EEEIC), 2015.

[9] A. de Oliveira, M. Aghaei, U. Madukanya, L. Nascimento, and R. Ruther, Aerial Infrared Thermography of a Utility-Scale PV Plant After a Meteorological Tsunami in Brazil, IEEE 7th World Conference on Photovoltaic Energy Conversion (WCPEC) (A Joint Conference of 45th IEEE PVSC, 28th PVSEC 34th EU PVSEC), 2018.

[10] G. A. dos Reis Benatto, C. Mantel, S. V. Spataru, A. A. S. Lancia, N. Riedel, S. Thorsteinsson, P. B. Poulsen, H. R. Parikh, S. Forchhammer, and D. Séra, Drone-Based Daylight Electroluminescence Imaging of PV Modules, IEEE Journal of Photovoltaics, Volume 10, Issue 3, Article number 9042865, Pages 872-877, May 2020.

[11] D. Weng, N. Enbar, and S. Rosinski, Utilizing Unmanned Aircraft Systems as a Solar Photovoltaics Operations and Maintenance Tool, The Electric Power Research Institute (EPRI), Inc., Report ID: 3002006216, Solar Generation Program 193c, 2015.

[12]   J. A. Tsanakas, L. Ha, and C. Buerhop, Faults and infrared thermographic diagnosis in operating c-Si photovoltaic modules: A review of research and future challenges, Renewable and Sustainable Energy Reviews, vol. 62, pp. 695-709, 2016.

[13]   M. Aghaei, Novel methods in control and monitoring of photovoltaic systems, Politecnico di Milano, 2016.

[14]   M. Aghaei, A. Eskandari, S. Vaezi, S. S. Chopra, "Photovoltaic Solar Energy Conversion, Chapter 10 - Solar PV Power Plants, pp. 313-348," 2020. [Online]. Available: https://doi.org/10.1016/B978-0-12-819610-6.00010-7. [Accessed 10 05 2020].

[15]   A. M. M. Sizkouhi, S. M. Esmailifar, M. Aghaei, A. K. Vidal de Oliveira, and R. Rüther, Autonomous Path Planning by Unmanned Aerial Vehicle (UAV) for Precise Monitoring of Large-Scale PV plants, 46th IEEE PVSC, 2019.

[16]   J. A. Tsanakas, L. Ha, and F. Al Shakarchi, Early Casualties in Five PV Plants in France: A Sustainability Perspective on Complete PV Fault Diagnostics for Revamping, 37th European Photovoltaic Solar Energy Conference and Exhibition (EU PVSEC), pp. 1396 -1400, 2020.

[17]   M. Aghaei, A. Dolara, S. Leva, and F. Grimaccia, Image resolution and defects detection in PV inspection by unmanned technologies, IEEE Power Energy Soc. Gen. Meet., IEEE, 2016.

[18]   U. Jahn, M. Herz, M. Köntges, D. Parlevliet, M. Paggi, I. Tsanakas, J. S. Stein, K. A. Berger, S. Ranti, R. H. French, M. Richter and T. Tanahashi, "Review on Infrared and Electroluminescence Imaging for PV Field Applications: Report IEA-PVPS T13-10:2018," ISBN 978-3-906042-53-4, 2018.

[19]   J. A. Tsanakas, and P. N. Botsaris, On the Detection of Hot Spots in Operating Photovoltaic Arrays through Thermal Image Analysis and a Simulation Model, Materials Evaluation 71 (4), 2013.

[20]   International Electrotechnical Commission, „IEC 60904-3, Photovoltaic devices - Part 3: Measurement principles for terrestrial photovoltaic (PV) solar devices with reference spectral irradiance," Geneva, Switzerland, 2019.

[21]   E. Duran, M. Piliougine, M. Sidrach-de Cardona, J. Galan, and J. Andujar, Different methods to obtain the i–v curve of pv modules: A review, 33rd IEEE Photovoltaic Specialists Conference, pp. 1–6, 2008, 2008.

[22]   Y. Zhu, and W. Xiao, „A comprehensive review of topologies for photovoltaic I–V curve tracer," *Solar Energy 196,* p. pp 346–357, 2020.

[23]   European Commission Joint Research Center Institute for Energy, „Guidelines for PV Power Measurement in PV Industry," 2010.

[24]   L. Dunn, M. Gostein, and K. Emery, "Comparison of Pyranometers vs. PV Reference Cells for Evaluation of PV Array Performance," in *38th IEEE Photovoltaic Specialists Conference*, Austin, USA, 2012.

[25]   M. Schweiger, and W. Herrmann, "Characterizing the Impact of Solar Spectral Irradiance on PV module output," in *44th IEEE Photovoltaic Specialists Conference*, 2017.

[26]   International Electrotechnical Commission, „IEC 60904-2, Photovoltaic devices - Part 2: Requirements for photovoltaic reference devices," Geneva, Switzerland, 2015.

[27]   International Electrotechnical Commission, „IEC 60904-1, Photovoltaic devices - Part 1: Measurement of photovoltaic current-voltage characteristics," Geneva, Switzerland, 2006.

[28] International Electrotechnical Commission, „IEC 60904-5, Photovoltaic devices - Part 5: Determination of the equivalent cell temperature (ECT) of photovoltaic (PV) devices by the open-circuit voltage," Geneva, Switzerland, 2011.

[29] International Electrotechnical Commission, „IEC 60891, Photovoltaic devices - Procedures for temperature and irradiance corrections to measured I-V characteristics," Geneva, Switzerland, 2009.

[30] G. Blaesser, and W. Zaaiman, "On-site power measurements on large-scale PV arrays," in *10th EUPVSEC*, Lisbon, Portugal, 1991.

[31] G. Blaesser, „PV system measurements and monitoring the European experience," *Solar Energy Materials and Solar Cells,* Bd. 47, pp. 167-176, 1997.

[32] International Electrotechnical Commission, „IEC 61829, Photovoltaic (PV) array - On-site measurement of current-voltage characteristics," Geneva, Switzerland, 2015.

[33] International Electrotechnical Commission, IEC 61724-1: Photovoltaic system performance monitoring – Guidelines for measurement, data exchange and analysis, Geneva, Switzerland, 2017.

[34] D.Ji, C. Zhang, M. Lv, Y. Ma, and N. Guan, "Photovoltaic Array Fault Detection by Automatic Reconfiguration," *energies,* vol. 10, p. 699, 2017.

[35] Joint Committee for Guides in Metrology (JCGM), „JCGM 100, Evaluation of measurement – Guide to the expression of uncertainty in measurement (GUM)," 2008.

[36] D. Dirnberger, J. Bartke, Andreas Steinhüser, K. Kiefer, and F. Neuberger, "Uncertainty of field I-V-curve measurements in large scale PV systems," in *EUPVSEC*, Valencia, Spain, 2010.

[37] E. Kopp, "I-V analysis of photovoltaic modules deployed outdoors at Tuscon electric power solar test yard," University of Arizona, Master thesis, Arizona, USA, 2012.

[38] W. Herrmann, D. Moldenhauer, and G. Köppe, Erzielbare Genauigkeiten für die Leistungsbemessung von PV-Modulen im Feld und im Labor, Cologne, Germany: 13. Workshop „Photovoltaik-Modultechnik", 2016.

[39] IEC 60904-9 Ed. 3, "Photovoltaic devices - Part 9: Classification of solar simulator characteristics", Geneva, Switzerland, 2020.

[40] IEC 61215-2, Terrestrial photovoltaic (PV) modules - Design qualification and type approval - Part 2: Test procedures, Geneva, Switzerland, 2016.

[41] F. P. Baumgartner, J. Haller, P. D. Polverini and G. Tzamalis, "Intercomparison of Pulsed Solar Simulator Measurements between the Mobile Flasher Bus and Stationary Calibration Laboratories," in *Proc. 26th Eur. Photovolt. Sol. Energy Conf. Exhib. (EUPVSEC)*, Hamburg, Germany, 2011.

[42] D. Schär, and F. P. Baumgartner, Spectral sensitivity analyses of tandem modules using standard flasher and dynamic LED backlight, Paris, France: in Proc. 28th Eur. Photovolt. Sol. Energy Conf. Exhib. (EUPVSEC), 2013.

[43] IEC 61730-2, Photovoltaic (PV) module safety qualification - Part 2: Requirements for testing, Geneva, Switzerland, 2016.

[44] [Online]. Available: http://snsppg.com/products/hipot-tester/solar-hipot-test-circuit/)..

[45] F. P. Baumgartner, T. Achtnich, N. Allet, B. Aeschbach, M. Pezzotti, F. Koch and C. Droz, "Swiss Mobile Flasher Bus," in *Proc. 24th Eur. Photovolt. Sol. Energy Conf. Exhib. (EUPVSEC)*, Hamburg, Germany, 2009.

[46] T. Achtnich, F. P. Baumgartner, N. Allet, M. Pezzotti, J. Haller and B. Aeschbach, "Swiss mobile flasher bus: progress and new measurements," in *Proc. 25th Eur. Photovolt. Sol. Energy Conf. Exhib. (EUPVSEC)*, Valencia, Spain, 2010.

[47] M. Bliss, F. Plyta, T. R. Betts and R. Gottschalg, "LEDs based characterisation of photovoltaic devices," in *International Conference on Energy Efficient LED Lighting and Solar Photovoltaic Systems Conference*, Kanpur, India, 2014.

[48] F. Plyta, B. V. Mihaylov, T. R. Betts and R. Gottschalg, "Optical design of a LED solar simulator and survey on its performance characterisation capability," in *Proceedings of the 8th Photovoltaic Science, Application and Technology (PVSAT)*, 2012.

[49] F. Plyta, T. R. Betts and R. Gottschalg, "Towards a fully LED-based solar simulator-spectral mismatch considerations," in *28th European Photovoltaic Solar Energy Conference and Exhibition*, Paris, France, 2013.

[50] F. P. Baumgartner and D. Schär, "Portable LED flasher with implemented bypass diode tester," in *29th Eur. Photovolt. Sol. Energy Conf. Exhib. (EUPVSEC)*, Amsterdam, The Netherlands, 2014.

[51] B. Jaeckel, B. Mihaylov, R. Gottschalg and J. Arp, "Smart PV module batch testing: reduction of performance measurement uncertainty by up to 50%," in *Proc. 33rd Eur. Photovolt. Sol. Energy Conf. Exhib. (EUPVSEC)*, Amsterdam, The Netherlands, 2017.

[52] J. Coello, L. Pèrez, F. Dominguez and M. Navarrete, "On-site quality control of photovoltaic modules with the PV MOBILE LAB," *Energy Procedia,* vol. 57, p. 89–98, 2014.

[53] S. Pandey, B. Jain, S. Jadhav and P. Pillai, "Quality Control of PV Plants with on-site Mobile PV Modules Test Laboratory," 2019. [Online]. Available: https://www.saurenergy.com/solar-energy-articles/quality-control. [Accessed 2020 12 10].

[54] I. Glover, „From farm to flash," *PV magazine,* pp. 60-65, Issue 06-2015.

[55] R. Knecht, F. P. Baumgartner, F. Carigiet, C. Frei, F. Beglinger, W. Zaaiman, D. Pavanello, M. Field, R. Galleano and T. Sample, "Field testing of portable LED flasher for nominal power measurements of PV-modules on-site," in *33rd Eur. Photovolt. Sol. Energy Conf. (EUPVSEC)*, Amsterdam, The Netherlands, 2017.

[56] S. Roest, "Webinar on PV module quality control and testing," 19 May 2020. [Online]. Available: https://eternalsunspire.com/webinar-pv-module-quality-control-and-testing/. [Accessed 2020 12 10].

[57] M. Köntges, S. Kurtz, C. Packard, U. Jahn, K. A. Berger, K. Kato, T. Friesen, H. Liu, M. Van Iseghem, J. Wohlgemuth, D. Miller, M. Kempe, F. Reil, N. Bogdanski, W. Herrmann, C. Buerhop-Lutz, G. Razongles and G. Friesen, "Review of Failures of Photovoltaic Modules: Report IEA-PVPS T13-01:2014," ISBN 978-3-906042-16-9, 2014.

[58] M. Köntges, G. Oreski, U. Jahn, M. Herz, P. Hacke, K. A. Weiss, G. Razongles, M. Paggi, D. Parlevliet, T. Tanahashi and R. H. French, Assessment of Photovoltaic Module Failures in the Field, Report IEA-PVPS T13-09:2017, ISBN 978-3-906042-54-1, 2017.

[59] E. Bamberger, *Modulcharakterisierung mit einem mobilen Testlabor,* Bern: 17. Nationale Photovoltaik-Tagung, 2019.

[60] MBJ Solutions GmbH, "MBJ Solar Module Judgment Criteria: Analysis criteria for solar module testing in Mobile Lab / Mobile PV-Testcenter," 2019. [Online]. Available: https://www.mbj-services.com/fileadmin/cont_services/downloads/MBJ_PV-Module_Judgement_Criteria_3.4.pdf. [Accessed 2020 12 10].

[61] SUPSI PVLab, "Qualitätsbewertung PV Module Kriterien zur Beurteilung fabrikneuer Module," [Online]. Available: https://www.supsi.ch/isaac/servizi/SUPSI-PVLab/Downloads.html. [Accessed 2020 12 10].

[62] E. Bamberger and C. Biba, "Zwei Jahre Erfahrung mit mobilem Photovoltaik-Testlabor," [Online]. Available: https://www.spf.ch/index.php?id=18344. [Accessed 2020 12 10].

[63] S. Dittmann, „Characterization of Bifacial PV Mini-Modules Using Front - and Double-Side Illumination," in *Proc. 35th Eur. Photovolt. Sol. Energy Conf. Exhib. (EUPVSEC)*, Brussels, Belgium, 2018.

[64] "Spectral measurements of the LED sun simulator performed at Anhalt Photovoltaic Performance and Liftime Laboratory (APOLLO)," [Online]. Available: www.hs-anhalt.de. [Accessed 18 02 2021].

[65] P. D. Burton and B. H. King, "Spectral Sensitivity of Simulated Photovoltaic Module Soiling for a Variety of Synthesized Soil Types," *IEEE Journal of Photovoltaics,* vol. 4, no. 3, May 2014.

[66] Compiled by partners in the Performance FP6 Integrated project, „Guideline for PV power measurement in industry , AITEUR 24359 EN," JRC Scientific and Technical Reports, 2010.

[67] E. Fokuhl, T. Naeem, A. Schmid, P. Gebhardt, T. Geipel and D. Philipp, "LeTID - A comparison of test methods on module level," in *Proc. 36th Eur. Photovolt. Sol. Energy Conf. Exhib. (EUPVSEC)*, Marseille, France, 2019.

[68] S. Dittmann, A. Virtuani, G. Friesen and F. Serrano, "Current-soaking and dark storage effects of polycrystalline thin film solar modules," in *IEEE 40th Photovoltaic Specialist Conference (PVSC)*, Denver, CO, 2014.

[69] Saur News Bureau, "MBJ Post Shipment and Post Installation Inspection Report," 21 Feb 2019. [Online]. Available: https://www.saurenergy.com/solar-energy-articles/mbj-post-shipment-and-post-installation-inspection-report. [Accessed 2020 12 10].

[70] D. King, B. Hansen and J. Kratochvil, "Dark current-voltage measurements on photovoltaic modules as a diagnostic or manufacturing tool," in *Conference Record of the Twenty Sixth IEEE Photovoltaic Specialists*, DOI: 10.1109/PVSC.1997.654286, 1997.

[71] K. Mertens, A. Arnds and M. Diehl, "Quick and Effective Plant Evaluation Using Dark-IV String Curves," in *Proceedings of 33st European Photovoltaic Solar Energy Conference*, Amsterdam, The Netherlands, 2017.

[72] T. Schlager, Messhardware zur Charakterisierung von Photovoltaikmodulen mittels Dunkelkennlinien-Messung, Vienna, Austria: University of Applied Science Vienna, 2017.

[73] B. Kubicek, T. Schlager and N. Severino, "Limitierungen bei der Hochrechnung von Dunkel- auf Hellkennlinien," in *PV Symposium Bad Staffelstein*, 2019.

[74] M. Teuber, "Anlagenevaluation mittels Data-Mining für Hell- und Dunkelkennlinien," in German, FH Bielefeld, Minden, Germany, 2019.

[75] M. Diel, "Measuring the dark IV curves of photovoltaic systems," 2017. [Online]. Available: https://photovoltaikbuero.de/en/pv-know-how-blog-en/measuring-the-dark-iv-curves-of-photovoltaic-systems/. [Accessed 2020 12 10].

[76] Chinese Society for Electrical Engineering (CSEE), T/CSEE 0160 Technical Specification for on-site energy efficiency testing and assessment of photovoltaic (PV) power plants, 2020.

[77] D. L. King, More "efficient" Method for Specifying and Monitoring PV system performance, 37th IEEE Photovoltaic Specialists Conference, pp. 219-224, 2011.

[78] X. J. Zou, F. F. Jiang, and H. T. Liu, Performance Analysis of Two PV plants in Different Geographical Environment, 3rd Annual International Conference on Sustainable Development, 2017.

[79] M. E. Orazem, and B. Tribollet, Electrochemical Impedance Spectroscopy, John Wiley and Sons Ltd, 2008.

[80] [Online]. Available: https://emazys.com/z200-pv-analyzer/.

[81] M. I. Oprea, S. V. Spataru, D. Sera, P. B. Poulsen, S. Thorsteinsson, R. Basu, A. R. Andersen, and K. H. B. Frederiksen, Detection of Potential Induced Degradation in c-Si PV Panels Using Electric Impedance Spectroscopy, in Proc. IEEE 43rd Photovoltaic Specialists Conference (PVSC), 2016.

[82] J. K. Symonowiez, N. Riedel, S. Thorsteinsson, D. Sera, and P. B. Poulsen, New method of silicon photovoltaic panel fault detection using impedance spectroscopy, 33rd European Photovoltaic Solar Energy Conference and Exhibition, 2017.

[83] [Online]. Available: https://emazys.com/.

[84] [Online]. Available: https://www.youtube.com/watch?v=TN4R7wcE6pw.

[85] S. Koch, T. Weber, C. Sobottka, A. Fladung, P. Clemens, and P. I. P. B. Ag, Outdoor Electroluminescence Imaging of Crystalline Photovoltaic Modules: Comparative Study between Manual Ground-Level Inspections and Drone-Based Aerial Surveys, Munich, Germany: 32nd European Photovoltaic Solar Energy Conference and Exhibition, 2016, p. 1736–1740.

[86] B. Doll et al., High-throughput, outdoor characterization of photovoltaic modules by moving electroluminescence measurements, Opt. Eng., vol. 58, no. 08, p. 1, August 2019.

[87] K. Mertens, A. Arnds, G. Behrens, and A. Domnik, LowCost-Outdoor-Electroluminescence: Significant Improvements of the Method, Munich, Germany: 32nd European Photovoltaic Solar Energy Conference and Exhibition, pp. 2081–2083, 2016.

[88] L. Stoicescu, M. Reuter, and J. H. Werner, Daysy: Luminescence Imaging of PV Modules in Daylight, Amsterdam, The Netherlands: 29th European Photovoltaic Solar Energy Conference and Exhibition, pp. 2553–2554, 2014.

[89] L. Stoicescu, M. Reuter, and J. H. Werner, Method and apparatus for testing photovoltaic modules, US9680412B2, 2017.

[90] J. Adams et al., Non-Stationary Outdoor EL-Measurements with a Fast and Highly Sensitive InGaAs Camera, Munich, Germany: 32nd European Photovoltaic Solar Energy Conference and Exhibition, pp. 1837-1841, 2016.

[91] T. J. Silverman, M. G. Deceglie, K. VanSant, S. Johnston, and I. Repins, Illuminated Outdoor Luminescence Imaging of Photovoltaic Modules, Washington, DC, USA: IEEE 44th Photovoltaic Specialist Conference (PVSC), pp. 3452–3455, 2017.

[92] B. G. A. dos Reis, S. Thorsteinsson, N. Riedel, P. Poulsen, and A. Thorseth, "Development of outdoor luminescence imaging for drone-based PV array inspection," 44th IEEE Photovoltaic Specialists Conference, p. 6, 2017.

[93] H. R. Parikh et al., „Enhancement of Electroluminescence images for fault detection in photovoltaic panels," IEEE 7th World Conference on Photovoltaic Energy Conversion (WCPEC), (Joint Conference of 45th IEEE PVSC, 28th PVSEC 34th EU PVSEC), pp. 0447–0452, 2018.

[94] B. G. A. dos Reis, and N. Riedel, "Luminescence Imaging Strategies for Drone-Based PV Array Inspection," Amsterdam, The Netherlands, 33rd European Photovoltaic Solar Energy Conference and Exhibition, pp. 2016–2020, 2017.

[95] T. Kropp, M. Berner, L. Stoicescu, and J. H. Werner, Self-Sourced Daylight Electroluminescence From Photovoltaic Modules, IEEE Journal of Photovoltaics, vol. 7, no. 5, pp. 1184–1189, September 2017.

[96] International Electrotechnical Commission, „IEC 60904-13: 2018 Photovoltaic devices –Part 13: Electroluminescence of photovoltaic modules," Geneva, Switzerland.

[97] A. M. Karimi, J. S. Fada, N. A. Parrilla, B. G. Pierce, M. Koyuturk, R. H. French, and J. L. Braid, Generalized and Mechanistic PV Module Performance Prediction From Computer Vision and Machine Learning on Electroluminescence Images, IEEE Journal of Photovoltaics, pp. 1–10, doi: 10.1109/JPHOTOV.2020.2973448., May 2020.

[98] A. M. Karimi, J. S. Fada, M. A. Hossain, S. Yang, T. J. Peshek, J. L. Braid, and R. H. French, "Automated Pipeline for Photovoltaic Module Electroluminescence Image Processing and Degradation Feature Classification," IEEE Journal of Photovoltaics, vol. 9, no. 5, pp. 1324–1335, doi: 10.1109/JPHOTOV.2019.2920732, September 2019.

[99] Carolina M. Whitaker, Benjamin G. Pierce, Ahmad Maroof Karimi, Roger H. French, and Jennifer L. Braid, "Types of PV Cell Cracks and Impacts on Electrical Performance," IEEE PVSC, Virtual, 2020.

[100] J. H. Wohlgemuth, Photovoltaic Module Reliability, Wiley, p. 22, 2020.

[101] „Guide for identifying cell defects in crystalline silicon pv modules by electroluminescence (el) imaging, SEMI Draft Document 6070E".

[102] NN, "PV09400 - SEMI PV94 - Guide for Identifying Cell Defects In Crystalline Silicon Photovoltaic (PV) Modules By Electroluminescence (EL) Imaging, SEMI [Online].," [Online]. Available: https://store-us.semi.org/products/pv09400-semi-pv94-guide-for-identifying-cell-defects-in-crystalline-silicon-pv-modules-by-electroluminescence-el-imaging. [Accessed 01 10 2020].

[103] J. S. Fada, N. R. Wheeler, D. Zabiyaka, N. Goel, T. J. Peshek, and R. H. French, "Democratizing an electroluminescence imaging apparatus and analytics project for widespread data acquisition in photovoltaic materials," Review of Scientific Instruments, vol. 87, no. 8, p. 085109, doi: 10.1063/1.4960180, August 2018.

[104] M. Navarrete et al., On-site inspection of PV modules using an internationally accredited PV mobile lab: A three-year experience operating worldwide, Hamburg, Germany: 31st European Photovoltaic Solar Energy Conference and Exhibition, 2015.

[105] "Solar Center: Mobile PV Test Center - MELI," [Online]. Available: https://www.solarzentrum-stuttgart.com/produkte/mobile-pv-test-center-meli/. [Accessed 2020 12 02].

[106] "Suncycle EL inspection system," [Online]. Available: https://www.suncycle.de/solaranlage-leistungen/mobiles-labor/. [Accessed 2020 12 02].

[107] A. M. Karimi, B. G. Pierce, J. S. Fada, N. A. Parrilla, R. H. French, and J. L. Braid, Package for PV Image Analysis and Machine Learning Modeling, https://pypi.org/project/pvimage/. [Accessed: 28-Feb-2020], 2020.

[108] I. Berardone, J. Lopez Garcia, M. Paggi, Analysis of electroluminescence and infrared thermal images of monocrystalline silicon photovoltaic modules after 20 years of outdoor use in a solar vehicle, Solar Energy, 173, pp. 478-486, 2018.

[109] K. Bedrich, M. Bliss, T. R. Betts, and R. Gottschalg, "Electroluminescence Imaging of PV Devices: Uncertainty due to Optical and Perspective Distortion," 31st European Photovoltaic Solar Energy Conference and Exhibition, pp. 1748–1752., 2015.

[110] C. Mantel et al., "Correcting for Perspective Distortion in Electroluminescence Images of Photovoltaic Panels," IEEE 7th World Conference on Photovoltaic Energy Conversion (WCPEC) (Joint Conference of 45th IEEE PVSC, 28th PVSEC 34th EU PVSEC), pp. 0433–0437, 2018.

[111] G. C. Eder, Y. Voronko, C. Hirschl, R. Ebner, G. Újvári, and W. Mühleisen, Non-destructive failure detection and visualization of artificially and naturally aged PV modules, Energies, vol. 11, no. 5, p. 1053, 2018.

[112] J. Schlothauer, C. Peter, C. Hirschl, G. Oreski, and B. Röder, Non-destructive monitoring of ethylene vinyl acetate crosslinking in PV-modules by luminescence spectroscopy, Journal of Polymer Research, vol. 24, no. 12, p. 233, 2017.

[113] G. C. Eder, Y. Voronko, P. Grillberger, B. Kubicek, and K. Knöbl, UV-Fluorescence measurements as tool for the detection of degradation effects in PV-modules, Vienna, Austria: Proceedings of the European Weathering Symposium EWS, pp. 205-214, 2017.

[114] F. J. Pern, Ethylene-vinyl acetate (EVA) encapsulants for photovoltaic modules: Degradation and discoloration mechanisms and formulation modifications for improved photostability, Angew. Makromol. Chem., vol. 252: 195-216, 1997.

[115] F. J. Pern, Factors that affect the EVA encapsulant discoloration rate upon accelerated exposure, Sol. Energy Mater. Sol. Cells, vol. 41–42, pp. 587–615, 1996.

[116] F. J. Pern, and S. H. Glick, Fluorescence analysis as a diagnostic tool for polymer encapsulation processing and degradation, AIP Conference Proceedings, vol. 306, p. 573, 1994.

[117] K. Grabmayer, G. M. Wallner, S. Beißmann, J. Schlothauer, R. Steffen, D. Nitsche, B. Röder, W. Buchberger, and R. W. Lang, Characterization of the aging behavior of polyethylene by photoluminescence spectroscopy, Polymer Degradation and Stability, pp. 28-36, 2014.

[118] J. Schlothauer, Evaluierung von EVA-Degradationsprozessen in Si-Photovoltaikmodulen mittels 2D-Lumineszenz, Phd Thesis, Humboldt University Berlin, Germany, p. Xviii, Figure 184 a, 2016.

[119] J. C. Schlothauer, K. Grabmayer, I. Hintersteiner, G. M. Wallner, and B. Röder, Non-destructive 2D-luminescence detection of EVA in aged PV modules: Correlation to calorimetric properties, additive distribution and a clue to aging parameters, Sol. Energy Mater. Sol. Cells, vol. 159, pp. 307–317, 2017.

[120] M. Köntges, S. Kajari-Schröder, and K. I., Cell Cracks Measured by UV Fluorescence in the Fields, 27th European Photovoltaic Solar Energy Conference, pp. 3033–3040, 2012.

[121] W. Mühleisen, G.C. Eder, Y. Voronko, K. Knöbl, M. Spielberger, H. Sonnleitner, R. Ebner, G. Uijvari, and C. Hirschl, Outdoor Detection and Visualization of Hailstorm Damages of Photovoltaic Plants, Renewable Energy 118, pp. 138-145, 2018.

[122] C. Hirschl, G.C. Eder, L. Neumaier, W. Mühleisen, Y. Voronko, R. Ebner, B. Kubicek, and K.A. Berger, Long term development of Photovoltaic module failures during accelerated ageing tests, 33th PV-SEC, pp. 1709-1712, 2017.

[123] Y. Lyu, J. H. Kim, and X. Gu, Fluorescence imaging on the cross-section of photovoltaic laminates aged under different UV intensities, IEEE 44th Photovoltaic Specialist Conference (PVSC), pp. 2844–2848, 2017.

[124] M. Köntges, S. Kajari-Schröder, and I. Kunze, Crack Statistic for Wafer-Based Silicon Solar Cell Modules in the Field Measured by UV Fluorescence, IEEE J. Photovoltaics, vol. 3, no. 1, pp. 95–101, 2013.

[125] I. Duerr, J. Bierbaum, J. Metzger, J. Richter, and D. Philipp, Silver Grid Finger Corrosion on Snail Track affected PV Modules – Investigation on Degradation Products and Mechanisms, Energy Procedia, vol. 98, pp. 74–85, 2016.

[126] P. Peng et al., Microscopy study of snail trail phenomenon on photovoltaic modules, Adv. R S C, no. 2, pp. 11359–11365, 2012.

[127] S. Meyer et al., Silver nanoparticles cause snail trails in photovoltaic modules, Sol. Energy Mater. Sol. Cells, vol. 121, pp. 171–175, 2014.

[128] C. Peike, L. Purschke, K.-A. Weiss, M. Kohl, and M. Kempe, Towards the origin of photochemical EVA discoloration, IEEE 39th Photovoltaic Specialists Conference (PVSC), pp. 1579–1584, 2013.

[129] A. Morlier, M. Siebert, I. Kunze, S. Blankemeyer, and M. Köntges, Ultraviolet fluorescence of ethylene-vinyl acetate in photovoltaic modules as estimation tool for yellowing and power loss, Proceedings of the IEEE 7th World Conference on photovoltaic Energy Conversion, Kona, Hawaii, USA, pp. 1597-1602, 2018.

[130] J. Schlothauer, S. Jungwirth, B. Röder, and M. Köhl, Fluorescence imaging- a powerful tool for the investigation of polymer degradation in PV modules, Photovoltaics International , vol. 10, pp. 149-154, 2010.

[131] C. Peike, P. Hülsmann, M. Blüml, P. Schmid, K.-A. Weiß, and M. Köhl, Impact of Permeation Properties and Backsheet-Encapsulant Interactions on the Reliability of PV Modules, ISRN Renew. Energy, vol. 2012, pp. 1–5, 2012.

[132] M. Köntges, A. Morlier, G. Eder, E. Fleis, B. Kubicek, and J. Lin, Review: Ultraviolet Fluorescence as Assessment Tool for Photovoltaic Modules, IEEE J. Photovoltaics, vol. 10, no. 2, pp. 1–18, 2020.

[133] S. Jungwirth, The influence of different back sheet materials on EVA degradation in photovoltaic modules investigated by luminescence detection, San Diego, CA, USA: Proc. SPIE Conf., vol. 7773, paper. 7773-11, 2010.

[134] A. Morlier, M. Siebert, I. Kunze, S. Blankemeyer, and M. Köntges, Influence of environmental conditions on UV fluorescence imaging in the field, Kona, Hawaii, USA: Proceedings of the IEEE 7th World Conference on photovoltaic Energy Conversion, pp. 1309-131, 2018.

[135] Y. Xi et al., Junction Temperature in Ultraviolet Light-Emitting Diodes, Jpn. J. Appl. Phys., vol. 44, no. 10, pp. 7260–7266, 2005.

[136] ICNIRP GUIDELINES on limits of exposure to ultraviolet radiation of wavelengths between 180nm and 400nm (International commission on non-ionizing radiation protection), HEALTH PHYSICS, vol. 87, no. 2, pp. 171-186, 2004.

[137] International air transportation authority, Lithium battery risk mitigation guidance for operators, 2nd Edition, 2016.

[138] B. Sartorius, D. Franke, and M. Schlak, Luminescence microscopy for quality control of material and processing, J. Cryst. Growth, vol. 83, no. 2, pp. 238–245, 1987.

[139] M. Baeumler, C. Fitz, U. Weinberg, J. Wagner, and W. Jantz, Luminescence imaging - a well-established technique to study material- and device-related problems, Mater. Sci. Eng. B-Solid State Mater. Adv. Technol., vol. 66, no. 1–3, pp. 131–140, 1999.

[140] T. Trupke, R. A. Bardos, M. C. Schubert, and W. Warta, Photoluminescence imaging of silicon wafers, Appl. Phys. Lett., vol. 89, no. 4, p. 044107, 2006.

[141] "UNSW," [Online]. Available: http://www2.pv.unsw.edu.au/videos/Thorsten-Trupke-15December2016/seminar.php. [Accessed 26 01 21].

[142] Solarzentrum Stuttgart GmbH, "DaySy Measurement Guide," 2019. [Online]. Available: https://www.solarzentrum-stuttgart.com/uploads/file/DaySy_Measurement_Guide_current.pdf. [Accessed 26 01 21].

[143] R. Bhoopathy, O. Kunz, M. Juhl, T. Trupke, and Z. Hameiri, Photoluminescence outdoor measurements of photovoltaic modules under full sunlight illumination, 27th International Photovoltaic Science and Engineering Conference, 2017.

[144] L. Stoicescu, M. Reuter, and J. H. Werner, DaySy Reliably Detects PID in Daylight, Munich: 32nd European PV Solar Energy Conference and Exhibition, 2016.

[145] M. Guada, Á. Moretón, S. Rodríguez-Conde, L. A. Sánchez, M. Martínez, M. Á. González, J. Jiménez, L. Pérez, V. Parra, and O. Martínez, "Daylight luminescence system for silicon solar panels based on a bias switching method," [Online]. Available: https://doi.org/10.1002/ese3.781. [Accessed 21 01 21].

[146] N. Bosco, and M. Springer , "Investigation of Failure Modes, Mechanisms and Driving Forces for Electrically Conductive Adhesives as Interconnects in PV Modules," [Online]. Available: https://www.eupvsec-proceedings.com/proceedings?paper=48987. [Accessed 21 01 21].

[147] PhD Thesis, and Liviu Stoicescu,, Bildgebende Messung der Lumineszenz von Photovoltaikanlagen unter Tageslicht, Munich, Germany: University of Stuttgart, Verlag Dr. Hut, 2018.

[148] R. Bhoopathy, O. Kunz, M. Juhl, T. Trupke, and Z. Hameiri, Outdoor photoluminescence imaging of photovoltaic modules with sunlight excitation, University Stuttgart, Germany: Verlag Dr. Hut München, Photovoltaics Res. Appl., vol. 26, no. 1, pp. 69–73, 2018.

[149] R. Bhoopathy, O. Kunz, M. Juhl, T. Trupke, and Z. Hameiri, "Outdoor photoluminescence imaging of solar panels by contactless switching: Technical considerations and applications," Photovoltaics Res. Appl., pp. 1–12, 2019.

[150] K. G. Bedrich, M. Bliss, T. R. Betts, and R. Gottschalg, Electroluminescence imaging of PV devices: Camera calibration and image correction, IEEE 43rd Photovoltaic Specialists Conference (PVSC), pp. 1532–1537, 2016.

[151] I. Zafirovska, M. K. Juhl, A. Ciesla, R. Evans, and T. Trupke, "Low temperature sensitivity of implied voltages from luminescence measured on crystalline silicon solar cells," Sol. Energy Mater. Sol. Cells, vol. 199, no. March, pp. 50–58, 2019.

[152] D. Jordan, Technology and Climate Trends in PV Module Degradation, 27th European Photovoltaic Solar Energy Conference and Exhibition, pp. 3118 – 3124, DOI: 10.4229/27thEUPVSEC2012-4DO.5.1, 2012.

[153] E. Wang, Failure mode evaluation of PV module via materials degradation approach, Energy Procedia, vol. 33, pp. 256 – 264, 2013.

[154] A. Omazic, G. Oreski, M. Halwachs, G. C. Eder, C. Hirschl, L. Neumaier, G. Pinter, and M. Erceg, Relation between degradation of polymeric components in crystalline silicon PV module and climatic conditions: A literature review, Solar Energy Materials and Solar Cells; 192, Pages 123-133; DOI: 10.1016/j.solmat.2018.12.027, 2019.

[155] W. Herrmann, Outdoor Weathering of PV Modules - Effects of Various Climates and Comparison with Accelerated Laboratory Testing, Photovoltaic Specialists Conference (PVSC), 37th IEEE 2011; pp. 2305 – 2311, DOI: 10.1109/PVSC.2011.6186415, 2011.

[156] G. C. Eder, Y. Voronko, S. Dimitriadis, K. Knöbl, G. Újvári, K. A. Berger, M. Halwachs, L. Neumaier, and C. Hirschl, Climate specific accelerated ageing tests & evaluation of ageing induced electrical, physical and chemical changes, Prog Photovolt Res Appl. 2018;1–16; DOI:10.1002/pip.3090, 2018.

[157] A. Czanderna, "Encapsulation of PV modules using ethylene vinyl acetate copolymer as a pottant: A critical review, Solar Energy Materials and Solar Cells 1996; 43(2), pp. 101 – 181," [Online]. Available: http://dx.doi.org/10.1016/0927-0248(95)00150-6. [Accessed 2020 12 10].

[158] Y. Voronko, G. C. Eder, M. Knausz, G. Oreski, T. Koch, and K. A. Berger, 2015, Correlation of the loss in photovoltaic module performance with the aging behaviour of the backsheets used, Prog. Photovolt: Res. Appl. 2015; DOI: 10.1002/pip.2580.

[159] W. Gambogi, The Role of Backsheet in Photovoltaic Module Performance and Durability, 26th European Photovoltaic Solar Energy Conference and Exhibition 2011; pp. 3325 – 3328, DOI: 10.4229/26thEUPVSEC2011-4AV.1.10.

[160] D. C. Jordan, T. J. Silverman, J. H. Wohlgemuth, S. R. Kurtz, and K. T. VanSant, April 2017, Photovoltaic failure and degradation modes, Prog Photovolt Res Appl, Vol. 25, pp. 318-326.

[161] D. C. Jordan, T. J. Silverman, B. Sekulic, and S. R. Kurtz, PV degradation curves: non-linearities and failure modes, Prog Photovolt Res Appl, vol. 25, pp. 583-591, 2017.

[162] L. Bokobza, "Review: Some Applications of Vibrational Spectroscopy for the Analysis of Polymers and Polymer Composites; Polymers 2019,11, 1159; DOI::10.3390/polym11071159," [Online]. Available: www.mdpi.com/journal/polymers. [Accessed 2020 12 10].

[163] "Chromacademy," [Online]. Available: https://www.chromacademy.com/lms/sco533/images/P1-electromagnetic-spectrum.jpg. [Accessed 04 12 2020].

[164] P. J. Larkin, Infrared and Raman Spectroscopy: Principles and Spectral Interpretation, Elsevier, ISBN: 978-0-12-386984-5 , 2011.

[165] F. Siebert, and P. Hildebrandt, Vibrational Spectroscopy for Life Science, Wiley-VCH, ISBN 978-3-527-40506-0, 2007.

[166] [Online]. Available: https://oceanoptics.com/nir-spectroscopy-unbound/. [Accessed 20 01 21].

[167] H. Siesler, Near-infrared spectroscopy of polymers, Makromolekulare Chemie. Macromolecular Symposia,52 (1), pp 113-129, 1991.

[168] R. A. Crocombe, "Portable Spectroscopy, Applied Spectroscopy Vol 72, Issue 12, Review Article," 2018. [Online]. Available: https://doi.org/10.1177/0003702818809719. [Accessed 2020 12 10].

[169] G. C. Eder, Y. Lin, Y. Voronko, and L. Spoljaric-Lukacic, "On-Site Identification of the Material Composition of PV Modules with Mobile Spectroscopic Devices, Energies 2020, 13(8), 1903," 2020. [Online]. Available: https://doi.org/10.3390/en13081903. [Accessed 2020 12 10].

[170] G. C. Eder, Y. Voronko, B. Kubitschek, and K. Knöbl, Fluorescence Spectroscopy and Imaging on aged polymeric PV Encapsulantes, 20th ESOPS, 09.2016 Dresden; DOI: 10.13140/RG.2.2.20827.36648, 2016.

[171] C. Peike, T. Kaltenbach, K. A. Weiß and M. Koehl, Non-destructive degradation analysis of encapsulants in PV modules by Raman Spectroscopy, Sol.Energy Mater.Sol.Cells 2011, 95(7), pp. 1686-1693, 2011.

[172] C. Peike, T. Kaltenbach, K. A. Weiß and M. Koehl, Indoor vs. outdoor aging: polymer degradation in PV modules investigated by Raman spectroscopy, Proc. SPIE 2012, 8472: 84720V, 2012.

[173] M. Köntges, A. Morlier, G. C. Eder, E. Fleiß, B. Kubicek, and J. Lin, Review: Ultraviolet Fluorescence as Assessment Tool for Photovoltaic Modules, IEEE J. Photovoltaics, Vol. 10, no. 2, pp. 1–18, 2020.

[174] H. Li, R. Kikuchi, M. Kumagai, T. Amano, H. Tang, J.-M. Lin, K. Fujiwara and N. Ogawa, Nondestructive estimation of strength deterioration in photovoltaic backsheets using a portable near infrared spectrometer, Sol. Energy Mater. Sol. Cells 2012, 101, pp. 166-169, DOI:10.1016/j.solmat.2012.01.017, 2012.

[175] B. S. Chernev, C. Hirschl, and G. C. Eder, Non-destructive determination of ethylene vinyl acetate crosslinking in PV modules by Raman Spectroscopy, Appl. Spectrosc. 2013, 67(11), pp. 1296-1301, 2013.

[176] "www.americanlaboratory.com/914-Application-Notes/138641-Handheld-and-Portable-FTIR-Spectrometers-for-the-Analysis-of-Materials-Taking-the-Lab-to-the-Sample/," [Online]. [Accessed 2020 12 10].

[177] "www.agilent.com/en/products/ftir/ftir-compact-portable-systems," [Online]. [Accessed 04 12 2020].

[178] [Online]. Available: www.oceanoptics.com/product. [Accessed 20 01 21].

[179] "www.htds.fr/en/analytical-sciences/molecular-sectroscopy/ftir-nir-spectrometer/portable-nir-spectrometer-microphazir-rx/," [Online]. [Accessed 04 12 2020].

[180] "www.analytik.co.uk/product/portable-vis-nir-spectroscopy-labspec/," [Online]. [Accessed 04 12 2020].

[181] A. J. Rein, and J. Seelenbinder, Portable FTIR Spectrometers for the Analysis of Materials: Taking the Lab to the Sample, American Laboratory, 2013.

[182] "BWtek," [Online]. Available: https://bwtek.com/technology/raman/. [Accessed 20 01 21].

[183] "Oceanoptics," [Online]. Available: www.oceanoptics.com/products-category/raman. [Accessed 20 01 21].

[184] "Bruker," [Online]. Available: www.bruker.com/de/products/infrared-near-infrared-and-raman-spectroscopy/raman/. [Accessed 20 01 21].

[185] G. C. Eder, Y. Voronko, G. Oreski, W. Mühleisen, M. Knausz, A. Omazic, A. Rainer, C. Hirschl, and H. Sonnleitner, Error analysis of aged modules with cracked polyamide backsheets, Solar Energy Materials & Solar Cells 203 (2019) 110194, DOI: 10.1016/j.solmat.2019.110194, 2019.

[186] Y. Lyu, A. Fairbrother, M. Gong, J. H. Kim, X. Gu, M. Kempe, S. Julien, K.-T. Wan, S. Napoli, A. Hauser, G. O'Brien, Y. Wang, R. French, L. Bruckman, and L. J. K. Boyce, "Impact of environmental variables on the degradation of photovoltaic components and perspectives for the reliability assessment methodology; Solar Energy 199 (2020) 425-436;," 2020. [Online]. Available: https://doi.org/10.1016/j.solener.2020.02.020. [Accessed 2020 12 10].

[187] G. Oreski, Eds.: H. E. Yang, R. French, and L. Bruckman, Durability and Reliability of Polymers and Other Materials in Photovoltaic Modules, Elsevier, 2019, pp. 135–140, ISBN:978-0-12-811545-9, 2019.

[188] International Organization for Standardization, DIN EN ISO 2858-1: Sampling procedures for inspection by attribures - Part 1: Sampling schemes indexed by acceptance quality limit (AQL) for lot-by-lot inspection, second edition, 1999.

ANNEX 1 – MEASUREMENT UNCERTAINTY ASSESSMENT ACCORDING TO JCGM 100:2008

The principles for measurement uncertainty assessment are defined in the guidance document JCGM 100:2008 "Evaluation of measurement – Guide to the expression of uncertainty in measurement (GUM)" [35], which was prepared by the Joint Committee for Guides in Metrology (JCGM).

If a variable X (i.e. P_{MAX}) has X_i independent uncertainty sources, the combined standard uncertainty u_C is given by to the formula

$$u_C = \sqrt{\sum_i (u_i)^2} \tag{3}$$

where u_i are the standard uncertainties of uncertainty sources X_i. Standard uncertainties are always related to 65% confidence level, which means that the true value lies with 65% probability in the confidence interval

$$[measured\ value - u_C, measured\ value + u_C] \tag{4}$$

For industrial applications, however, a higher confidence level of 95% is required. This transition is done by multiplication of u_C with the coverage factor k=2. This results in the expanded measurement uncertainty U:

$$U = k \cdot u_C \tag{5}$$

U: Expanded measurement uncertainty

u_C: Combined standard uncertainty

k: Coverage factor, k=2 for 95% confidence level

For a variable X two types of uncertainty source can be distinguished:

Type A uncertainties u_A: These are determined by statistical analysis or a series of observations. The standard uncertainty u_i of the uncertainty component X_i is given by the standard uncertainty of the mean value. Examples for type A uncertainties are the repeatability or the reproducibility of independent measurements.

Type B uncertainties u_B: These are based on estimations or assumptions according to the experience or best practice of the test lab. They may also include manufacturer specifications or calibrations results. In combination with type u_B uncertainty, a probability shape must be considered to calculate the standard uncertainty u_i

- For a Gaussian distribution, the standard uncertainty u_i is the provided or estimated uncertainty u_B divided by $\sqrt{2}$
- For rectangular shape, where all values have the same probability, the standard uncertainty u_i is the provided or estimated uncertainty u_B divided by $\sqrt{3}$

With this background, the working steps of measurement uncertainty analysis can be summarized as follows: a) Identification of uncertainty sources u_A or u_B, b) calculation of standard uncertainties u_i with consideration of probability shapes, c) calculation of the combined standard uncertainty u_C and expanded uncertainty U.

The document JCGM 100:2008 provides a standardized calculation sheet for expanded measurement uncertainty, which is shown in Table 35. In addition to the previous explanations, the sheet also contains so-called sensitivity factors s_i, which become relevant when the uncertainty contributions u_i are not expressed in the same units. This is not the case for I-V measurement, where uncertainties sources can be expressed either as percentage or°C. Then, all sensitivity components s_i are unity.

Table 35: Standardized calculation table for expanded measurement uncertainty according to JCGM 100:2008 [35].

Source of Uncertainty X_i	Type A or B	Uncertainty $S_p(X_i)$	Probability Shape	Division Factor	Standard Uncertainty $u(X_i)$	Sensitivity Coefficient s_i	Uncertainty Contribution u_i
			Combined standard uncertainty, $u_c = \sqrt{\sum_i (u_i)^2}$				
			Coverage factor k = 2 , level of confidence = 95%				
			Expanded uncertainty U = u_c* k				